Development of Bio-Voltaic Cells from plant extract electrolytes using different electrodes and investigation of their electrochemical performance

Ph.D. Thesis

Submitted by

Md. Afzol Hossain

Registration Number: 30

Session: 2017-2018

Re-registration Number: 34

Session: 2022-2023

Department of Chemistry

University of Dhaka

02 April, 2024

Development of Bio-Voltaic Cells from plant extract electrolytes using different electrodes and investigation of their electrochemical performance

Ph.D. Thesis

Submitted by

Md. Afzol Hossain

Registration No. 30
Session: 2017-2018.
Re-registration Number: 34
Session: 2022-2023

Supervisor

Dr. M. Emran Quayum
Professor
Department of Chemistry
University of Dhaka.

Joint-supervisor

Dr. Md. Kamrul Alam Khan
Vice chancellor
Bangamata Sheikh Fojilatunnesa Mujib Science & Technology University
Jamalpur.

Declaration

I hereby declare that this Ph.D. thesis entitled ***"Development of Bio-Voltaic Cells from plant extract electrolytes using different electrodes and investigation of their electrochemical performance"*** is based on my original research work which has been carried out between 27 December, 2017 to April, 2023 under the joint supervision of Dr. Md. Emran Quayum, Professor, Department of Chemistry, University of Dhaka and Dr. Md. Kamrul Alam Khan, Vice chancellor Bangamata Sheikh Fojilatunnesa Mujib Science & Technology University, Jamalpur. I also declare that it has not been previously and currently submitted anywhere for the award of any degree or diploma at this University or any other University.

Md. Afzol Hossain
Registration No. 30
Session: 2017-2018
Re-registration Number: 34
Session: 2022-2023

Date: 02 April, 2024.

Dedicated to

My father
Alhaj Md. Abdul Khalaque

and

Mother
Zibatun Nessa

Acknowledgement

First of all, I would like to express my sincere and full thanks to my creator, Allah for giving me the full ability to complete my doctoral research works smoothly and successfully.

Then I would like to express my sincere gratitude and cordial thanks to my supervisor Professor Dr. Md. Emran Quayum, Department of Chemistry, University of Dhaka for giving me the opportunity to do work in his laboratory and efficient guidance through the entire path of research.

I would also like to express my deep gratitude and heartfelt thanks to my Joint-Supervisor Professor Dr. Md. Kamrul Alam Khan, Vice chancellor, Bangamata Sheikh Fojilatunnesa Mujib Science & Technology University, Jamalpur for giving me the opportunity to do work in his laboratory and valuable discussion throughout my research period.

I sincerely thank all the respected teachers of the Department of Chemistry at University of Dhaka for their supports in many ways during my Ph.D. study.

I am also very much thankful to the Bose Centre for Advanced Studies and Research in Natural Sciences, University of Dhaka for prestigious fellowship for the study of doctoral research.

Finally, I wish to express my heartfelt gratitude to my parents and sisters for their prayers, emotional support and encouragement.

My final thanks goes to my offspring and beloved wife Jannatul Ferdous for her continuous mental support with endless inspiration.

Md. Afzol Hossain
Dr. Muhammad Shahidullah Hall
University of Dhaka, Bangladesh.
02 April, 2024.

রসায়ন বিভাগ
ঢাকা বিশ্ববিদ্যালয়
ঢাকা-১০০০, বাংলাদেশ
ফোন: ৮৮-০৯৬৬৬৯১১৪৬৩/৭১৩০/৭১৩১

DEPARTMENT OF CHEMISTRY
UNIVERSITY OF DHAKA
DHAKA-1000, BANGLADESH
Phone: 88-09666911463/7130/7131 (Off)
FAX: 880-2-55167810
E-mail: chairchemistry@du.ac.bd

To Whom it May Concern

This is to certify that **Md. Afzol Hosain**, Ph.D. student of Registration No.: 30, session: 2017-2018, and Re-registration No.: 34 Session: 2022-2023 has submitted thesis entitled ***"Development of Bio-Voltaic Cells from Plant Extract Electrolytes Using Different Electrodes and Investigation of Their Electrochemical Performance".*** This research work has been carried out by this student in the Physical Chemistry Research Laboratory of the Department of Chemistry, University of Dhaka under our direct supervision for the requirement of the doctoral degree (Doctoral of Philosophy) in Physical Chemistry. We further certify that no part of this thesis has been submitted to any other university or institute for any degree or diploma or any other award. All terms and conditions for the doctoral (Ph.D.) degree has been fulfilled by the candidate including two presentations of his research findings in the seminars held in the Department of Chemistry, University of Dhaka. We have gone through the final draft of the thesis and recommend its submission. The similarity index of the thesis has been checked in the Dhaka University Central Library. The Librarian, the Central Library and the Dean, Faculty of science accepted and certified the test result. It is in conformity with the regulation of this University and meets the accepted standard with respect to originality and quality.

Dr. M. Emran Quayum
Professor
Department of Chemistry
University of Dhaka

Prof. Dr. M. Emran Quayum
Supervisor
Department of Chemistry
University of Dhaka,
Dhaka-1000, Bangladesh.

Prof. Dr. Md. Kamrul Alam Khan
Joint-supervisor
Vice chancellor
Bangamata Sheikh Fojilatunnesa Mujib Science & Technology University
Jamalpur, Bangladesh.

Prof. Dr. Md. Kamrul Alam Khan
Vice-Chancellor
Bangamata Sheikh Fajilatunnesa
Mujib Science & Technology University,
Jamalpur, Bangladesh

ABSTRACT

In this research, bio-voltaic cell (BVC) has been developed using various types of electrodes and Arum Leaf (AL) scientific name *Colocasia esculenta* and Pathor Kuchi Leaf (PKL) scientific name *Briophyllum pinnatum* plant extract electrolytes. Various parameters such as open circuit voltage, V_{oc} (V), short circuit current, I_{sc} (A), power (W), voltage efficiency (η_v), voltage regulation (V_R), power efficiency (η_p), internal resistance (R_{int}), coulombic efficiency (η_Q %), self-discharge characteristics have been measured to check the performance of BVC. Gas Chromatography-Mass Spectrometry (GC-MS) has been carried out to know mainly which compounds of PKL and AL take part to produce electricity in BVC. Apart from this, various electrolytes effects such as, (i) AL living plant, (ii) PKL living plant, (iii) AL extract, (iv) PKL extract on different electrodes, like (i) Zn/Cu, (ii) Ag NPs adsorbed paper, (iii) Reduced Graphene Oxide (RGO) adsorbed paper electrode (iv) RGO-Ag NPs composite paper electrode on cell potential of the developed BVC have been studied to investigate the performance of BVC. In all cases, the effect of the addition of small quantity of secondary salt with electrolytes have been examined. In this study, effect of PKL and AL living plant as electrolyte in BVC has been investigated and it was found that PKL living plant shows better electrical performance than that of AL. The thickness and midrib area of PKL is more than that of AL and it was observed that as the exposed area of midrib of living plant increases, it can act as better electrolyte and show better performance in the developed BVC. As a result, open circuit voltage, V_{oc} (V), short circuit current, I_{sc} (A) and power (W) of BVC using PKL living plant were found to be higher than that of AL living plant. Similarly electrical performance of BVC developed using different electrodes and PKL and AL extract electrolytes have been investigated. Secondary salt plays an important rule to improve the performance of BVC in presence of AL and PKL plant extract electrolytes. When the performance of BVC reduces to a margin level, addition of a small quantity of the secondary salt helps to increase the performance of open circuit voltage, V_{oc} (V), short circuit current, I_{sc} (A) and power (W) of BVC. Moreover, Ag NPs have been synthesized from both PKL and AL and BVC is constructed using this NPs to examine the power generation performance. The performance of BVC changes with changing the size of NPs. The smaller the particle size the higher is the performance of BVC. The size of NPs synthesized from PKL is smaller than that of NPs obtained from AL. Hence, the performance of Ag NPs from PKL is higher than that of AL in BVC. The formation of Ag NPs has been characterized by using X-Ray Diffraction (XRD), UV–visible spectroscopy, Fourier Transforms Infrared (FT-IR), Energy Dispersion X-ray spectroscopy (EDX), and Field Emission Scanning Electron Microscopy (FESEM). It has been observed that Ag NPs play a decisive role in improving open circuit voltage, short circuit current, and thus enhance the power generation of BVC. The highest open circuit voltage (V_{oc}) of 0.45 (V) has been found for the constructed BVC using AL extract and the highest value of V_{oc} has been found to be 0.92 (V) for the developed BVC using PKL extract. The value of V_{oc} is found to be 1.10 (V) when small quantity of secondary salt is added with AL extract and V_{oc} value is found to be 1.34 (V) when a small quantity of secondary salt is added with PKL extract electrolyte. The open circuit voltage (V_{oc}) of 1.28 (V) has been found when BVC is constructed using Ag NPs adsorbed paper electrode with AL extract and V_{oc} value of 1.41 (V) is observed when BVC is developed using Ag NPs adsorbed paper electrode with PKL extract electrolyte. However, maximum open circuit voltage (V_{oc}) of 1.51 (V) has been found for the BVC developed using secondary salt diluted AL extract and Ag NPs adsorbed paper electrode and a maximum open circuit voltage (V_{oc}) of 1.63 (V) has been found for the BVC developed using secondary salt diluted PKL extract and Ag NPs adsorbed paper electrode.

Moreover, the highest short circuit current, (I_{sc}) of 110 (mA) has been found for BVC developed using AL extract and the highest I_{sc} is found to be 260 (mA) when PKL extract electrolyte is used in BVC. Beside this, I_{sc} value of 450 (mA) has been found using secondary salt with AL extract electrolyte and I_{sc} value of 545 (mA) has been found using PKL extract electrolyte in BVC. I_{sc} value of 820 (mA) has been found using Ag NPs with AL extract and I_{sc} value of 915 (mA) is found when PKL extract electrolyte is used with Ag NPs in BVC. However, maximum I_{sc} of 960 (mA) and 981 (mA) have respectively been found for the developed BVC using secondary salt diluted AL extract and PKL extract with Ag NPs adsorbed paper electrodes. Power, $P_{max} = V_{oc} \times I_{sc}$ (W) of the developed BVC cell also increases similarly. In addition, chemically synthesized RGO has been prepared by modified Hummers' method which has been deposited on the surface of cellulose paper. This RGO adsorbed cellulose paper has been applied in BVC as electrode. Thus, RGO and AgNPs deposited on cellulose paper have been mixed together to construct a highly conductive RGO/AgNPs hybrid electrode for BVC. In this research, attempts have been taken to investigate the effect of AL and PKL extract electrolytes with Zn/Cu ($1cm^2$) electrode, Zn/ RGO absorbed paper electrode, Zn/ RGO wrapped Ag NPs composite paper electrode to construct BVC and to examine which BVC can generate enough electricity for the longest period. It is observed that, the highest open circuit voltage (V_{oc}) 0.95 (V) has been found using Zn/Cu (1 cm^2) electrode with AL extract and that of 1.00 (V) has been found using Zn/Cu (1 cm^2) electrode with PKL extract in BVC. Apart from this when BVC is constructed using Zn/ RGO (2 h) electrode with AL electrolyte, a V_{oc} of 0.99 (V) has been found and when BVC is developed using Zn/ RGO (2 h) electrode with PKL extract electrolyte a (V_{oc}) value of 1.20 (V) is observed. The BVC constructed using Zn/ RGO (24 h) wrapped Ag NPs with PKL extract exhibit higher value of V_{oc} of 1.34 (V) than that of BVC developed using Zn/ RGO (24 h) wrapped Ag NPs with AL extract (V_{oc} value of 1.21 V). Again, the highest short circuit current, (I_{sc}) of 110 (mA) has been found for BVC constructed using Zn/Cu (1 cm^2) electrode with AL extract and I_{sc} of 178 (mA) has been observed for BVC developed using Zn/Cu (1 cm^2) electrode with PKL extract.

Beside this, I_{sc} of 215 (mA) has been found for BVC constructed using Zn/ RGO (2 h) electrode with AL electrolyte and I_{sc} value of 210 mA is found when BVC is developed using Zn/ RGO (2 h) electrode with PKL extract electrolyte. A short circuit current, (I_{sc}) of 297 mA has been found using Zn/ RGO (24 h) electrode with AL electrolyte and I_{sc} of 320 mA has been observed when BVC is made using Zn/ RGO (24 h) electrode with PKL electrolyte. On the other hand, 346 (mA) has been found when the cell is made by using Zn/ RGO (2 h) wrapped Ag NPs with AL extract and I_{sc} of 410 (mA) has been found for the cell of Zn/ RGO (2 h) wrapped Ag NPs and PKL extract electrolyte. However, maximum short circuit current, (I_{sc}) of 423 mA has been found for the cell made of Zn/ RGO (24 h) wrapped Ag NPs with AL extract and $I_{sc\ of}$ 496 (mA) is found when the cell is made using Zn/ RGO (24 h) wrapped Ag NPs with PKL extract electrolyte. Power, $P_{max} = V_{oc} \times I_{sc}$ (W) also increases similarly. The developed BVC has been compared with Traditional Voltaic Cell (TVC) using various types of electrodes and electrolytes and it is observed that BVC shows better performance for longer time than that of TVC. The highest longevity of open circuit voltage, V_{oc} (V) of TVC is 470 minutes whereas BVC is 1090 minutes. The highest longevity of short circuit current, I_{sc} (A) of TVC is 320 minutes and for BVC I_{sc} last for 1090 minutes. Again, the highest longevity of power of TVC is 320 minutes while that of BVC is 1090 minutes using same parameters. Because, the strength of H_2SO_4 runs out within 320 minutes but strength of plant extract electrolytes does not run out up to 1090 minutes. This developed BVC is able to produce enough electricity to energize a few LED bulbs and to run a ceiling fan.

Finally, from this study, it is possible to design a 1 KW mini power plant using different electrodes and AL and PKL extract electrolytes with an affordable price. This mini power plant can be a source of power generation and may be utilized for distributing electricity, where the nationwide grid is out of reach.

List of Publications

1. **Md Afzol Hossain**, Md Emran Quayum, K.A. Khan, "The significant impact of green synthesized silver nanoparticles on a bio-voltaic cell for electricity generation" Energy Systems (Springer Nature), under review, 2024.

2. **Md Afzol Hossain**, Bithi Paul, K.A. Khan, Monika Paul, M.A. Mamun, Md Emran Quayum, "Green synthesis and characterization of silver nanoparticles by using Bryophyllum pinnatum and the evaluation of its power generation activities on bio-electrochemical cell" Materials Chemistry and Physics, (elsevier) 282 (2022) 125943, https://doi.org/10.1016/j.matchemphys.2022.125943

Contents

List of Figures

List of Tables

Abbreviations and Symbols

BVC	: Bio-Voltaic Cell
PKL	: Pthor Kuchi Leaf
BPL	: Briophyllum Pinnatum Leaf
AL	: Arum Leaf
CE	: Colocasia Esculenta
Ag NPs	: Silver Nanoparticles
GO	: Grphene Oxide
RGO	: Reduced Grphene Oxide
I_{sc}	: Short Circuit Current
V_{oc}	: Open Circuit Voltage
P_{max}	: Maximum Power
I_L	: Load Current
V_L	: Load Voltage
P_{out}	: Load Power
UV	: Ultra Violet
XRD	: X-Ray Diffraction
FT-IR	: Fourier Transforms Infrared Ray
EDX	: Energy Dispersion X-ray
FESEM	: Field Emission Scanning Electron Microscopy
FCC	: Face Centered Cubic
η_v	: Voltage Efficiency
V_R	: Voltage Regulation
η_p	: Power Efficiency
TVC	: Traditional Voltaic Cell
R_{int}	: Internal Resistance
η_Q	: Columbic Efficiency
GC-MS	: Gas Chromatography-Mass Spectrometry
MW	: Mega Watt
KW	: Kilo Watt
SERC	: Solar Energy Research Center
SPR	: Surface Plasmon Resonance
DI	: Deionized Water
mM	: milli Molar
KeV	: Kiloelectron Volt

V_{NL}	: Voltage no load
R_L	: resistance of the load connected
Q_{output}	: Output Charge
Ω	: Internal Resistance
FWHM	: Full Width at Half Maximum
AAS	: Atomic Absorption Spectroscopy
A	: Ampere
mA	: milli Ampere
NM	: Nano Meter
V	: Volt

Chapter 1

INTRODUCTION

Chapter 1: Introduction

1.1 General Introduction

The sources of traditional energy are very inadequate in the globe which are going to be finished in immediate future, which motivates the researchers to explore the alternate source of energy [1]. For such continuous exploration, we have selected completely a new type of sources in the plant kingdom such as Arum Leaf (AL) scientific name *Colocasia esculenta* and PKL (Pathor kuchi leaf) scientific name *Briophyllum pinnatum (BPL)* which will deliver energy to the rabble in the off grid areas who are not finding electricity at all [2]. In this fact, BPL and AL has been used to produce electricity for real exploitation at the off grid regions in the glob [3,4]. On the other hand, this research aimed to synthesize silver nanoparticles (Ag NPs) by using PKL and AL extract and explore the electrical performance of Ag NPs in BVC for power production systems. The chemical constituents of PKL and AL have been studied by Gas Chromatography-Mass Spectrometry (GC-MS) by many researchers [5,6,7]. PKL and AL contain many active bio-molecular compounds such as flavonoids, triterpenes, organic acids, alkaloids, glycosides, steroids, tannins and minerals [5-9]. Among these, flavonoid compounds play a more active role in transforming metal ions to metal nanoparticles through bio-reduction [10]. Some flavonoid group compounds were identified in PKL and AL including quercetin and kaempferol as well as a few flavone glycosides [9]. Moreover the outstanding medicinal accomplishments of BPL and AL, the extract of this plant was used as electrolyte to produce electricity by BPL and AL extract based BVC [11, 12, 13]. In this study, the reduction of Ag^{+} to Ag^{0} atom was conducted by the existing functional group of PKL and AL extract through the formation of Ag NPs, and the power development of PKL and AL extract-based electrochemical cells by using Ag NPs has been studied for the first time. A comparative study has been implemented with and without Ag NPs for a PKL and AL bio-electrochemical cell. Various electrical parameters of the cells have been studied and Ag NPs applied to the development of power production are observed. After implying Ag NPs on bio-electrochemical cells, the open circuit voltage, short circuit current and power have been increased with the variation of time. As a result, the power production of the designated cells has been enriched significantly. Besides this, another material called Graphene has been established as electrode, whose resources are many and show highly stable electrochemical performances [14-18]. Chemically manufactured Graphene Oxide (GO) holds active groups that countenance a diversity of inorganic nanomaterials to be deposited on its surface of cellulose paper [19-21]. Hence, GO Nano sheet have been combined with Ag NPs and reduced them more to extremely conductive RGO/Ag hybrid electrode for BVC. More significantly, the stability could be greatly amplified for the effectively meticulous redox of Ag NPs by wrapping RGO all over the place cellulose paper.

GO Nano sheet was produced by the modified Hummers' technique which is also mentioned in aforementioned publications [22, 23]. Finally, this research deals with comparative investigation applying AL and PKL extract electrolyte with Zn/Cu (1cm^2) electrode, Zn/2 (h) RGO absorbed paper electrode, Zn/24(h) RGO absorbed paper electrode, Zn/2 (h) RGO wrapped Ag Nano composite paper electrode and Zn/24(h) RGO wrapped Ag Nano composite paper electrode electrochemical cell which would generate enough electricity for the longest period. This would be possible to fabricate a mini power plant by any person using this procedure wit reasonable price in the rustic areas, whereas the nationwide grid is out of range and can be a hopeful issue in the case of rural progress by distributing electricity.

1.1.1 Background

Bangladesh is a country of approximately 180 million people. The demand of electricity is increasing day by day among the local people as well as in the commercial and industrial sector. But it is still quite a long way to go to fulfill the demand. A proper solution is yet to be found. Gap between supply and demand for electricity is around 1500 MW. Despite the government's remarkable progress in fulfilling the demand, natural gas and biomass energy are the main source of energy in Bangladesh. But these sources are reducing day by day. Under this condition, Bangladesh is highly supposed to explore various renewable energy resource options. Renewable energy policy of Bangladesh set a target of generating 5% of power from renewable source by 2015, 10% by 2020 and 15% by 2025 [24, 25]. But this target has yet been fulfilled. Recently Afzol Hossain and his coworkers have developed this method adding AL, NPs, RGO and NPs-RGO nano-composite to enrich electricity production. This new method is able to produce enough electricity to energize a few LED bulbs and to run a ceiling fan. Finally, Large scale electricity even 1 KW power can be produced using this method.

1.1.2 Scientific Classification of Bryophyllum Pinnatum [26]

Figure 1.1: Briophyllum Pinnatum Plant

Kingdom : Plantae
Division : Angiosperms
Class : Eudicots
Order : Saxifragales
Family : Crassulaceae
Genus : Bryophyllum
Species : B. pinnatum
Origin : Native to Madagascar and southern Africa.

1.1.3 Scientific Classification of Arum

Synonym : Species arum colocasia
Kingdom : Plantae
Phylum : Tracheophyta
Class : Liliopsida
Order : Alismatales
Family : Araceae
Genus : Colocasia
Species : Colocasia esculenta

Figure 1.2: Arum Leaf

1.1.3.1 PKL and AL Living Plant Energy

The sources of traditional energy are very limited in the world which would run out in the immediate future. That is why researchers are searching another sources of energy [28]. In this case, renewable energy may play an active rule to face the energy crisis after finishing traditional energy sources. Researchers have explored and discussed various types of renewable energy sources [4, 29-34]. As a perpetuation of such exploration, we have found absolutely a new type of sources which are the living plant named *Colocasia esculenta* (CE) or AL and PKL which will provide energy to the people to use in their practical life. When electrode is inserted into plants, fluctuation of electrical signals (electrical surge) are formed [34, 35]. Generally, this reaction only makes small modifications in membrane conduction or ion distribution along with channels of electrical movement [36,37]. According to the paper, written by Fensom et. al. [38] claims that motion of ions in living plant tissue will increase the conduction with each different size and own rate by giving electrochemical gradient. On the other hand, the active resistance of apoplast along with the midrib of the living plant leaf is contrariwise proportional to the thickness of leaf [39].

1.1.4 Nanoparticles

The particles having the size of 100 nm or less in at least one dimension are considered as nanoparticles. After making nanoparticles, the surface chemistry and various properties is remarkably changed from the existing materials which increase their areas of application. The most widely field of application is in the biomedical sector. Beside this in contemporary years, nanomaterials have prolonged a lot of demands because of their extraordinary electrical, optical and magnetic properties [40]. Nano crystalline materials are synthesized by various techniques, amongst them green synthesis of nanoparticles have fascinated a significant curiosity to the

researchers as it is environment approachable, cost effective and facile. It is demonstrated to have its unique properties than its bulk due to huge surface to volume quotient [41]. These materials have attracted significance due to their extraordinary surface range and enhanced reactive sites. The application of nanoparticles in BPL and AL electricity production system has not been studied yet. In this study, the described results concerning green synthesis nanoparticles produced from BPL and AL extract as a reducing agent, have been studied to generate electricity for practical utilizations.

1.1.5 Ag Nanoparticle from PKL

Since the past few decades, nanomaterials have been widely studied due to their unique properties and the versatile applications in various fields such as electronics, optical, bio-imaging, biosensor, medicines, cancer therapeutics, targeted drug delivery, agriculture, food industry, textile, renewable energy, water treatment, materials science, biotechnology [42–49]. Among all the nanomaterials, noble metal nanoparticles (e.g.; platinum, gold, silver) are being extensively used in interdisciplinary fields, such as physical, chemical, industrial, and biomedical applications [47,50]. Besides this, the metal nanoparticles show one of the most significant characteristics of Surface Plasmon Resonance (SPR) which allows them to exhibit unique optical properties [51]. Various structure of nanostructures and tiny particle sizes with a large surface-to-volume ratio are of great interest, leading to startling differences between the chemical and physical phenomenon of nanoparticles [52, 53]. Furthermore, the behavior of nanoparticles are fluctuate with various synthesis approaches and relay on the size, shape, and morphology varieties of nanoparticles [46,51].Over the few years, the auspicious antibacterial and anticancer actions of Ag NPs made it a potential field to the researchers for wide investigations of silver nanostructures [50,54]. On the other hand the significant Nano medicinal activities of Ag NPs have enormous applications like nonlinear optics, selective coating for solar energy absorption, intercalation materials for electrical batteries as optical receptors, catalyst in chemical reactions, antibacterial materials, and good electrical conductors [51, 55, 56]. Furthermore, the applications of Ag NPs have been developed rapidly due to their remarkable influences on agriculture, food industries, water treatments, textile industries, targeted drug delivery [52, 53]. Recently, various chemical synthesis procedure of silver nanoparticles are informed in the literature where commercially available reducing agents like sodium borohydride, ascorbic acid, trisodium citrate, and polyols have been used to reduce silver ions from the precursor solution [57]. Nonetheless, most chemical and physical extraction methods are time-consuming and costly. They may also have detrimental effects on the environment due to the toxicity of chemicals and the troubles of removing them from NPs [53, 57, 58]. Environ friendly, cost-effective synthesis methods of NPs are now a extreme interest of the researchers. As a result, there has been an improved importance on introducing the plant extract mediated synthesis (green synthesis) methods of NPs to reduce the chemical waste from the environment, which

promotes non-toxic, natural, economical, and ecofriendly reducing and capping agents during the synthesis process [51]. Maximum parts of plant such as leaves, roots, seeds, latex, bark can be used to isolate the NPs, which are available in nature. Functional groups are present in plants helps to reduce silver ions to silver nanoparticles [59]. Plant and fruit extracts application help to eliminate the residuals toxic compounds from the isolated NPs that can speed up the usage of NPs in medicinal applications [53]. Plant extract contains various important compounds (e.g., polyphenols, ascorbic acids, flavonoids, terpenoids, alkaloids, enzymes, amino acids, ascorbic acid, caffeine, linalool, and proteins), which able to play a vital role in the reaction mechanism of metal ion reduction from precursor solution and NPs can be captured by the bio-molecules [59,60]. From the last few years, various studies of green synthesis of silver NPs have been described for the favorable anticancer and antibacterial activities such as Plant extracts of Sesbania grandiflora [61], Rubus glaucusBenth [62], Alpinia calcarate [63], Thymbra Spicata [64], Aloe vera leaves [57], and Artocarpus heterophyllus [65]. The use of L. acapulcensis extract is established as the proper antimicrobial activities of Ag NPs [60], and silver NPs using with Neem leaf (Azadirachta indica) extract has also been studied [66]. Green synthesized Ag NPs have extensively been investigated for their antibacterial, anticancer actions. However, the applications of green synthesized NPs in electricity production still require further investigations. This research targeted to synthesize Ag NPs by by PKL extract and explore the electrical activities of Ag NPs on bio-electrochemical cells for power production systems.

1.1.6 Ag Nanoparticle from AL

Over this decade, green synthesis has been one of the most exciting methods of synthesizing nanomaterials. Various plant extracts such as A. ciniformis [67], Vitas vinifera [68], Blumea eriantha DC [69], Crocus Haussknechtii Boiss [70], Peganum harmala [71], Veronica amygdalina [72], Salvia hispanica L. seeds [73] have been reported to synthesis the semiconductor oxide and metal NPs (Ag, Au, ZnO, CuO, TiO_2 etc) as the reducing agent for the remarkable antibacterial and anticancer activities. The simplicity of the synthesis process has made this method very popular in the research community. The active functional groups of bio compounds exist in the different parts of plants (polyphenols, ascorbic acids, flavonoids, terpenoids, alkaloids, enzymes, amino acids, caffeine, linalool, proteins) play an important role to reduce metals ion to metals NPs [77–80]. In this report, Colocasisa.esculenta or AL extract was used to synthesize the silver nanoparticles (Ag NPs) by the green synthesis process. Colocasia.esculenta is a familiar plant available in the tropical regions, especially in Bangladesh and India. The local name of this plant is ‘kochu’, and the English name of this plant leaf is called AL. The important biomolecular compounds, including flavonoids, steroids, ascorbic acid, thiamine, riboflavin, niacin, carbohydrates, and fats, are available in Colocasia.esculenta leaves, which are responsible for the bioreduction of NPs [81, 82, 83]. Different structures of nanomaterials such as Ag, Au, ZnO, CuO,

and TiO_2 are the most common nanoparticles which have widely been synthesized by the green method for the last decade to be used in pharmaceutical applications (e.g.; targeted drug delivery, tumor therapeutic, cancer therapeutic, antifungal, antibacterial, and Nano medicines) [68,74]. Among these, Ag NPs have drawn significant attention due to their multidimensional uses in physical, chemical, industrial, agricultural, and biomedical applications [75, 76]. Besides the antibacterial activities of green synthesized Ag NP, it has a significant influence on electrochemical cells as a catalyst to integrate the electrical performances. Nowadays, various plant extracts (vegetables and fruits) have been used as the electrolyte solution in an electrochemical cell to generate electricity, and such a plant extract electrolyte-based cell is called by the name of bio-electrochemical cell [84–88]. To develop the bio-electrochemical cell, different kinds of plant exacts, fruits, and vegetable extract (such as Bryophyllum pinnatum leaf, Aloe Vera, Tomato, and Lemon) are generally used as an electrolyte solution of the electrochemical cell instead of chemical electrolyte. In this study, a novel bio-electrochemical cell is developed to generate electricity and Ag NPs have been used to integrate the electrical performances of the cell. Four types of low-cost and portable bio-electrochemical cells have been designed by varying the electrolyte solution. Different electrical parameters have been examined to understand the impact of nanoparticles on cells. Comparative electrical performances were recorded to monitors the role of Ag NPs on electricity generation. The short circuit current, (I_{sc}) and open circuit voltage, (V_{oc}) were recorded for all cells with the time duration and it was found that both the voltage and current were changing by varying the electrolyte solution of cells. The power and capacity of all bio-electrochemical cells were calculated and it is noted that after using Ag NPs in the electrolyte solution, the power and capacity of cell have been significantly integrated. This novel mini bio-electrochemical cell power plant can be constructed by any person or even school-going students at an affordable price. Hence, this innovative renewable power plant may open a new era for low-cost electricity generation.

1.1.7 Graphene Oxide (GO) and Reduced Graphene Oxide (RGO)

Graphene is 2-dimensional (2D) thin sheet of sp^2 hybridized carbon atoms in a honeycomb configuration. It has various anticipated behaviors for example extraordinary mechanical power [89], electrical conductivity power [90], molecular obstruction facilities [91] and other significant behavior. That's why, it have been the vision of numerous research exertions to integrate graphene into polymers to formate polymer-based nanocomposites [92-95]. Nonetheless, the application of pristine graphene have shown to be exciting because of interesting bottom-up synthesis [96], less solubility [97] and agglomeration properties in solution because of van der Waals force [90]. Graphene can be isolated from graphite or any other source of carbon applying top-down method. Beside this modified Hummers' method is famous for synthesis of reduced graphene oxide (RGO). Graphene oxide (GO) can be prepared by oxidizing of graphite. GO contains hydroxyl (-OH),

carbonyl (=CO), carboxylic acid (-COOH) and further oxygen-based functional groups [98]. Beside this easy synthesis process, these oxygenated functional groups are liable for many helps over graphene as well as higher solubility [90]. Moreover, GO can be preserved by a numeral of methods to isolate reduced graphene oxide (RGO) [99]. Graphene Quantum Dots (GQDs) which is another class of graphene has exceptional edge effects of graphene. GO, RGO, GQDs are graphene derivatives which have ideal material behavior and dispersibility in polymer mediums [100,101].Those have many applications such as packaging [100], safety for sensitive electronic devices [102] or even corrosion-resistant materials [103,104]. Recently for excellent electrical conductivity of RGO (Reduced Graphene Oxide) it can be applied as electrode after adsorbing or wrapping on cellulose paper [105].

1.2 Objectives of the Research

Bangladesh is a developing country. The supply of electricity is very essential for the development of country. But we have scarcity of electricity. This deficiency of electricity is a obstacle to development. The progress of this country is subject to how much energy it can produce, use and consume for the future generation. About 85% electricity is produced from traditional source.There is 1500 MW gap between supply and demand of electricity in our country. In this circumstances, Bangladesh is bound to explore various renewable energy resource options. Renewable energy policy of Bangladesh sets a target of generating 5% of power from renewable source by 2015 and 10% by 2020 and 15% by 2025 [24]. It is high time we took the necessary steps to search the alternating energy source including renewable energy sources. In this perspective, the electricity generation from biomass will be very much available if necessary technology is developed. Electricity generation from Pathor Kuchi Leaf (PKL) and Arum Leaf (AL) is an additional source of renewable energy. It's developed in Bangladesh and it has boundless benefits over other renewable resources as well. PKL and AL electricity can be produced anywhere, anytime, any places without any complexity. Moreover, it can provide electricity directly from the system which is very convenient and cheap. Maximum people in Bangladesh live in rural zones and most of them are poor. For the alleviation of poverty, supplying energy is very important. This is a massive challenge for the government of Bangladesh to fulfil the future demand of electricity especially in rural zones. PKL and AL electricity can be a great source to meet up the demand in rural areas. Beside this, Ag NPs and RGO are significantly applied in PKL and AL bio-electrochemical cell so that it can be generated commercially. Especially main vision of our works to supply electricity at the coastal areas, islands, i.e. the off-grid areas of Bangladesh where providing electricity from grid is economically inefficient.

The specific objectives of the research are given below:

(i) To design a new type of BVC
(ii) To generate electricity from green plants (eco–friendly)
(iii) To compare cost analysis
(iv) To study the impact of different electrodes and electrolytes in BVC and TVC for power production
(v) To study the performance of difference RGO based paper electrodes in BVC

1.3 Present Work

AL has been collected from Dhaka University campus and PKL from Jagannath University campus. Then PKL and AL extract were prepared to use as electrolyte. Bio-Voltaic Cell is prepared using various size of battery boxes and five type of electrode such as Zn/Cu (1 cm^2) electrode, Zn/(2 h) RGO adsorbed paper electrode, Zn/(24 h) RGO adsorbed paper electrode, Zn/(2 h) RGO wrapped Ag Nano composite paper electrode and Zn/(24 h) RGO wrapped Ag Nano composite paper electrode. Secondary salt is applied to enhance the power performance of the BVC. Ag NPs are synthesized from PKL and AL and applied in BVC to enhance power. On the contrary, reduced graphene oxide is prepared using modified Hummers' method and adsorbed on cellulose paper to fabricate new types electrode and this electrodes finally has been applied in BVC to reduce cost. The outline of present work is as below:

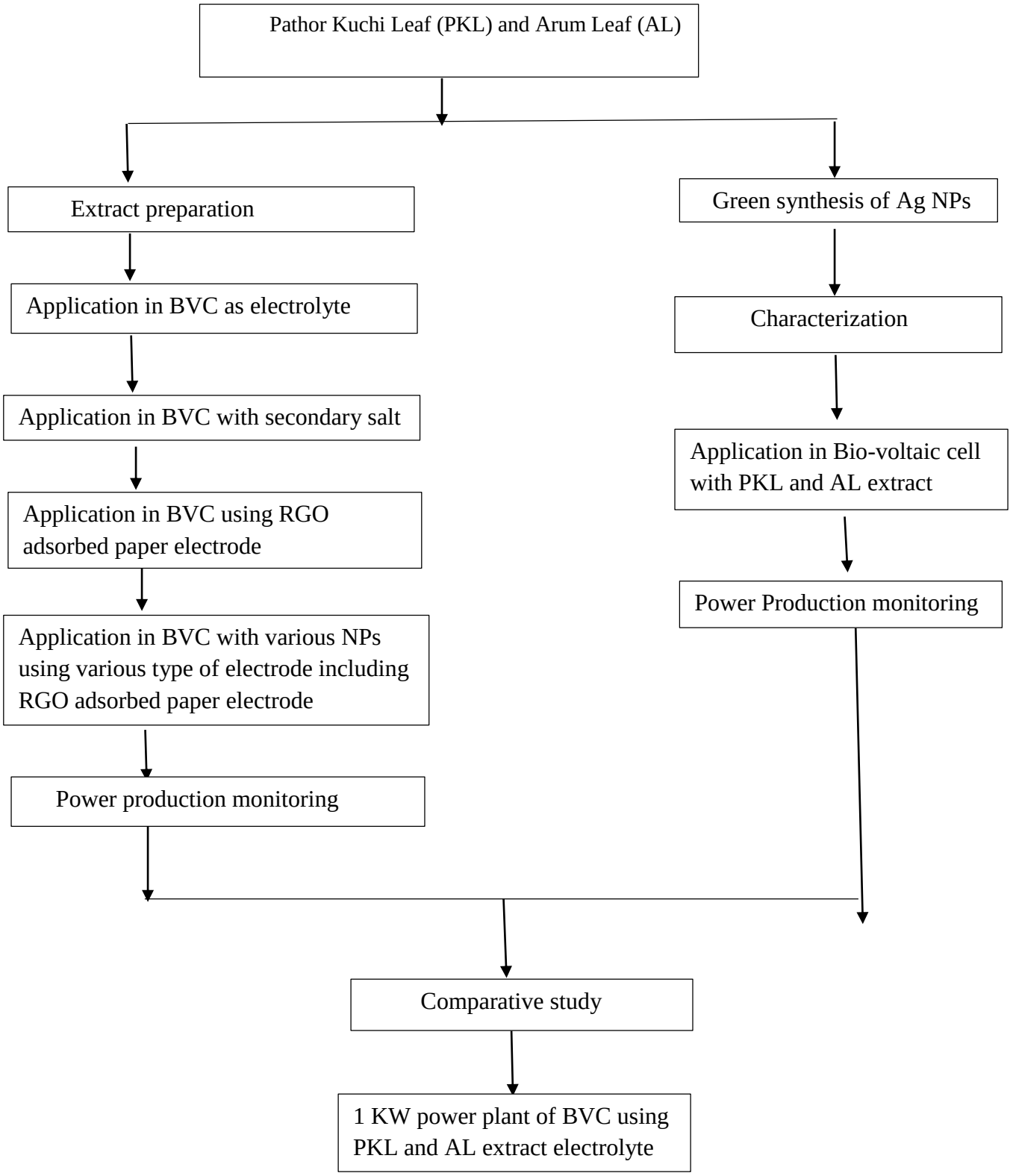

Figure 1.3: Outline of the present study

Finally, 1 KW micro power plant has been developed for practical utilization. The loads are 2 street lights, 1 tube light, 1 ceiling fan, 1 table fan, 2 LED lights and one LED indicator light etc which are also set up on the stand [Fig. 4]. There is a circuit board also one circuit breaker is also set up there on the stand. The people who are living at the off-grid zones and are not able to use computer in their areas, this work will help them to access to the electricity for Wi-Fi connections.

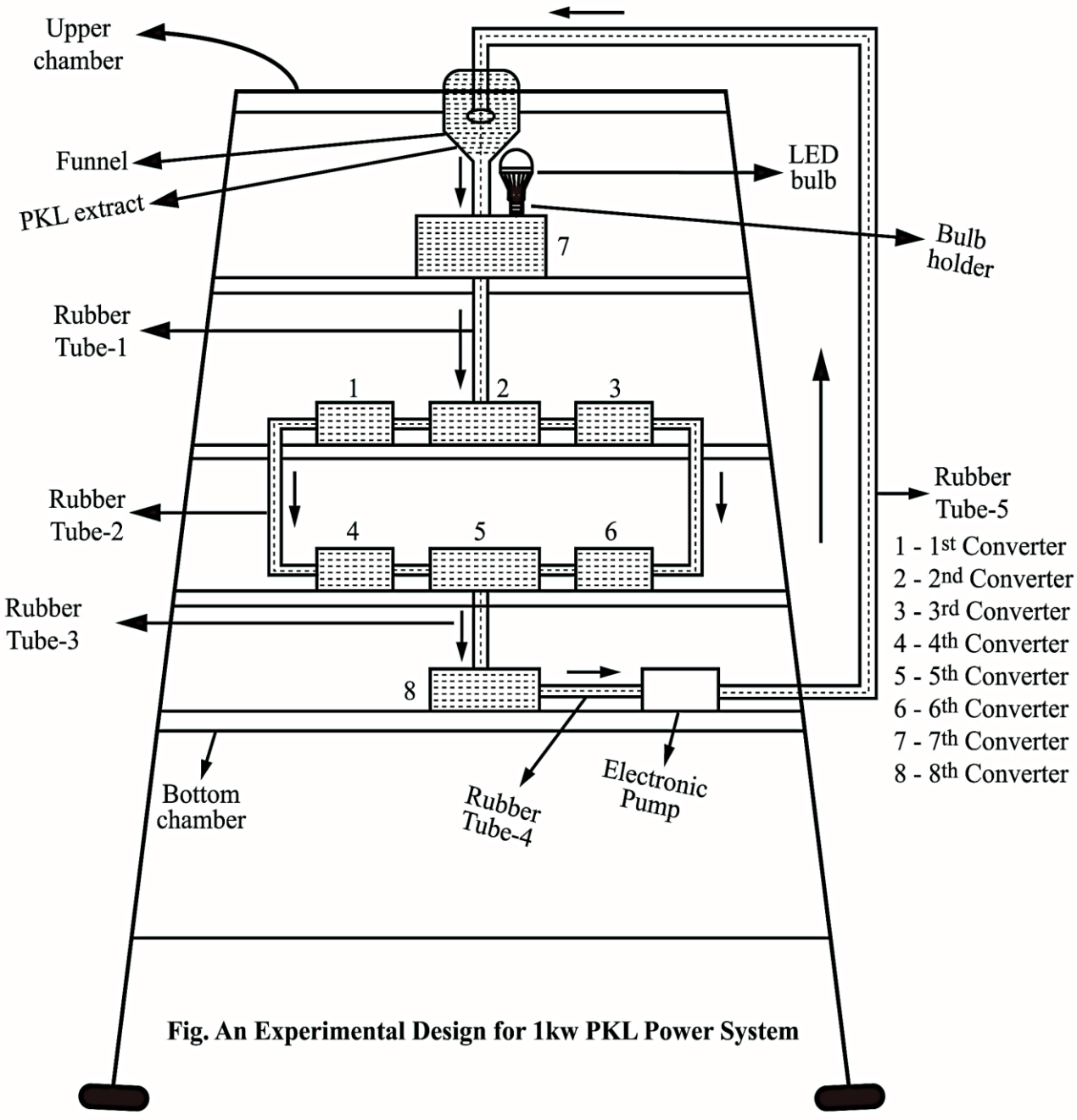

Fig. An Experimental Design for 1kw PKL Power System

Figure 1.4: An experimental design of 1KW PKL/AL Power Plant

1.4 Review of Literature

Alessandro Volta described the first electrochemical battery in 1800. The Daniell cell, discovred in 1836 by British chemist John Frederic Daniell, was the first practical source of electricity. Although, available capacity of all batteries drops with decreasing temperature.

Welsh physicist and barrister William Grove wrote about the improvement of his first crude fuel cells in 1938. He used a combination of sheet iron, copper and porcelain plates and a solution of sulphate of copper and dilute acid. In 1939, British engineer Francis Thomas Bacon effectively developed a 5 KW stationary fuel cell. W. Thomas Grubb, a chemist working for the General Electric Company (GE), further improved the original fuel cell project by using a sulphonated polystyrene ion-exchange membrane as the electrolyte after sixteen years. Later in 1959, Bacon and his co-workers demonstrated a practical five-kilowatt unit capable of powering a welding machine. Finally the first hydrogen fuel cell automobile was developed by Roger Billings in 1991. In 2002, Yet-Ming Chiang and his group at MIT exhibited a substantial development in the performance of lithium batteries by enhancing the material's conductivity by doping it with aluminium, niobium and zirconium. The particular mechanism causing the proliferation became the subject of widespread debate. During 2004, Chiang once more improved the performance by employing iron (III) phosphate particles of less than 100 nanometers in diameter. This reduced particle density almost one hundredfold, increased the positive electrode's surface area and improved capability and performance. Commercialization led to a fast growth in the market for advanced capacity LIBs, as well as a patent infringement battle between Chiang and Good enough. In 2007, researched at Stanford University discovered a nanowire battery. A nanowire battery uses to increase the surface area of one or both of its electrodes. Two designs, variants of the lithium-ion battery has been proclaimed, although neither is commercially accessible. Both replace the traditional graphite anode. One uses silicon, while the other uses germanium. Researchers at Nissan have established at lithium-ion battery in 2009 using a lithium nickel manganese cobalt oxide cathode (NMC). The new battery will offer twice the energy density. Scientists at Massachusetts Institute of Technology made Nano ball batteries that are intensify charge rates 100 times in 2009. They are capable of a 10 second re-charge of a cell phone battery and a 5 minute re-charges of an electric car battery. The cathode is composed of Nano sized balls of lithium iron phosphate

As of 2009 a new technique of electricity production based on BPL was established at Solar Energy Research Center, Department of Physics, Jagannath University, Dhaka, Bangladesh [25]. As a extension, community BPL electricity generation system [105], Performance of PKL electricity and its uses in Bangladesh [106], Development of portable PKL lantern [107], Performance study on PKL electricity for using DC fan [108], PKL electricity for switching on the television and radio [109], performance study of hybrid SPV and BPL electricity production and storage for

practical application in Bangladesh [110], organic electricity generation, storage and utilization by PKL cell [111], Studies on Bryophyllum pinnatum Leaf (BPL) and solar photovoltaic electricity generation [112], demonstrating of a biomass energy based power generation plant and its features in evaluation with other plants [113], Performance analysis of PKL electricity module [114], A study on low power generation from PKL for practical utilization in Bangladesh [115], Electricity Generation from BPL-an innovative approach for both physicist and chemist [116], A study on internal resistance of the PKL Cell [117], A new approach of increasing the power output of PKL Cell [118], BPL is an eternal source of renewable electrical energy for future world [119], Studies on discharge characteristics and temperature effect of PKL Cell [120], A comparative learning on BPL, Aloe Vera, Lemon and Tomato extract for electricity production [121], A study of performance investigation of BPL electricity production parameters: An experimental analysis on voltage regulation, capacity and energy efficiency of BPL cell [122], Studies on electrochemistry for PKL Power System [123], Studies on energy efficiency for PKL power system in Bangladesh [124], Examination on parameters performance of Zn/Cu electrodes of BPL, AVL, Tomato and Lemon extract based electrochemical cells: A relative study [125], Experimental characterization and identification of cell parameters in a BPL electrochemical device [126], PKL electrochemical cell: physics and chemistry [127], Studies on performance Parameters of a practical transformer for various utilizations, microsystem technologies [128], performance evaluation of PKL electricity for use in television and radio [129], A performance analysis of product ion and reactant ion during BPL electricity generation [130], PKL electricity - The role of physics [131], Leaf and vegetative extract electrochemical cells - In comparative research for capacity study [132], Prospects of PKL electricity [133], Effect of pH of the PKL extract during electricity production [134], A study on current density for PKL electrochemical cell [135], Electrochemistry of green Ag nanoparticles modified electrode surface [136], Development of a LED lamp using ginger extract for practical utilization [137], energy competence and sustainability in outdoor lighting - A bet for the forthcoming energy efficiency and sustainable lighting [138], voltage collecting from fresh leaves of air plant, climbing spinach, mint, spinach and indian pennywort for practical exploitation [139], A study on PKL electrochemical cell for three different conditions [140], A study on development of PKL power [141], Green separation of magnetite (Fe_3O_4) nanoparticles using azadirachta indica leaf extract and their characterization [142], A study on light traps for attracting and killing the insects applying BPL electricity [143], A study on electrochemical characterizations of Bryophyllum pinnatum Leaf (BPL) Electricity [144], Applications of PKL electricity for use in DC instruments [145], 3R economy of a PKL electrochemical cell [146], PKL backup LED bulb- an alternative source of electricity during load shading [147], electrochemical conversion of CO_2 into useful chemicals and PKL electricity [148], An examination of energy density for BPL, Aloe Vera, Myrobalan, Lemon, and Tomato electrochemical cell [149], Comparative Studies of V_L, I_L, and P_L from different vegetative and fruits electrochemical cells [150], Electricity generation using soil and living PKL tree [151] have been studied.

Chapter 2

EXPERIMENTAL

Chapter 2 Experimental

2.1 Materials

Arum Leaf (AL) scientifically known as *Colocasia esculenta (C. esculenta)* was collected from Dhaka University campus and PKL (Pathor Kuchi Leaf) scientifically known as *Briophyllum pinnatum (B. pinnatum)* was from Jagannath University campus. Thomas Baker Cellulose Filter Paper (whatman 41 and 42), model name and number: TBF-P-040-110-1110-3. Natural Flake Graphite (NFG) was purchased from LOBA Chemie India having a mean size of 60 mesh and purity of 98%, Sulfuric acid (H_2SO_4), potassium permanganate ($KMnO_4$), phosphorous pent oxide (P_2O_5) and hydrogen peroxide (H_2O_2) were procured from Merck India. De-ionized water was used throughout the experiments whenever it was needed. Silver nitrate ($AgNO_3$) purity of 98.99%, sodium borohydride ($NaHB_4$,) purity of 98.99%, were purchased from D.F. Goldsmith-Producer & distributers of precious metals, USA and Graphene oxide (GO) was purchased from Sigma Aldrich purity of 999.99%,USA. Disodium hydrogen phosphate (Na_2HPO_4) were obtained from Shanghai Aladin Biochemical Technology Co., Ltd. China.

All above reagents and chemicals applied in this study were analytical grade and used without further purification

2.2 Instrumentation

Ampere-Volt-Ohm Meter (AVOM); model no. CD 800A 4000 counts, Sanwa Digital Multimeter, Sanwa Electric Instrument Co. Ltd., Tokyo, Japan. Atomic Absorption Spectrophotometer (AAS), Shimadzu, Japan and UV Visible spectrometer; UV—1650 PC, Shimadzu, Japan. Analysis of different electro active metals Cu (II), Zn (II) in extract was analyzed by using Atomic Absorption Spectrophotometer (AAS), Shimadzu, Japan. pH meter; PHS—25, LIDA Instrument, USA. Field Emission Scanning Electron Microscopy (FESEM) images JSM-7610 F equipped with an energy dispersion X-ray spectroscopy (EDX) attachment at 15 KeV. X-ray diffraction instrument, Rigaku Ultima IV 2036E202. FT-IR spectrophotometer, IRPrestige-21, Shimadzu, Japan. GCMS, QP – 2010 SE Shimadzu, Japan. JSE Magnetic Stirrer, IndiaMART and Centrifuge machine, JT&CLAND, Shanghai.

2.3 Energy harvesting from living PKL/AL plant

In this study 1:1 Zn/Cu electrode has been used to harvest energy from PKL/AL living plant. Here the performance of PKL/AL living plant has also been investigated by increasing number of electrode pair, changing the geometry of electrode and changing the embedded area of electrode. Moreover, we have investigated open circuit voltage (V_{oc}), short circuit current (I_{sc}) and maximum

power (P_{max}) with the variation of time. This research will help to find several ways to harvest living plant energy and utilizing in real life.

Figure 2.1: Energy harvesting from PKL/AL plant

2.4 Pathor Kuchi Leaf (PKL)/ Arum Leaf (AL) extract preparation

There are two types of electrolyte such as PKL and AL extract including various NPs have been applied in bio-voltaic cell. PKL/AL are taken at first then it has been chopped. Thereafter it has been blended in presence of water (1:1) by a hand blender machine [152]. As a result, 60% of extract has been prepared. Then it has been filtrate. This extract has been applied in bio-voltaic cell to generate electricity. Once a mixture is prepared for generating electricity. It serves the purpose for 6 months constantly. On the contrary, remaining 40% extract can be applied after 6 months. Besides this process, produced byproduct can be applied as bio-fertilizer.

Figure 2.2: PKL and AL extract preparation

2.5 Electrode Preparation

There are five types of electrode applied in bio-voltaic cell such as Zn/Cu, Zn/ RGO (2 h) absorbed paper electrode, Zn/ RGO (24 h) absorbed paper electrode, Zn/ RGO (2 h) adsorbed and Ag NPs wrapped paper electrode and Zn/ RGO (24 h) adsorbed and Ag NPs wrapped paper electrode.

Table 2.1: Various types of cell

No.	**Types of electrodes**
1.	Zn/Cu (1 cm^2)
2.	Zn/ RGO (2 h) absorbed paper electrode
3.	Zn/ RGO (24 h) absorbed paper electrode
4.	Zn/ RGO (2 h) absorbed paper electrode + Ag NPs from PKL/AL
5.	Zn/ RGO (24 h) absorbed paper electrode + Ag NPs from PKL/AL

25.1 Metal Electrode Preparation

E-Cu58 Copper foil have been purchased from Jiangsu Xiguan Metal Product Co. Ltd. China and Zinc sheet from Ing Co. Ltd. Japan. Then it has been scissored to prepare electrode. Various parameters of electrode have been prepared for various types of electrode.

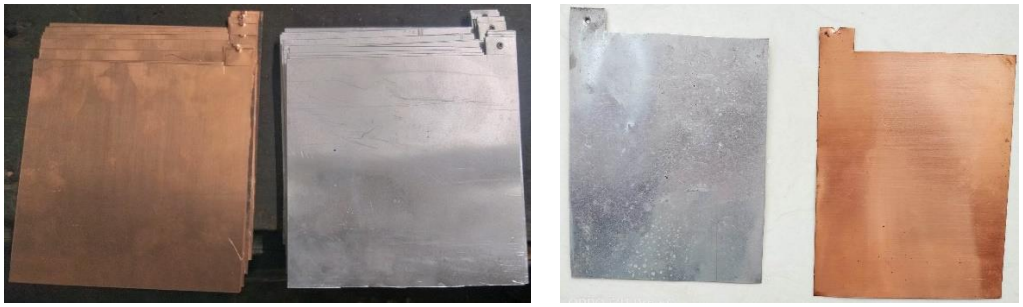

Figure 2.3: Various parameters of electrode for bio-voltaic cell

2.5.2 Reduced Graphene Oxide (RGO) Preparation

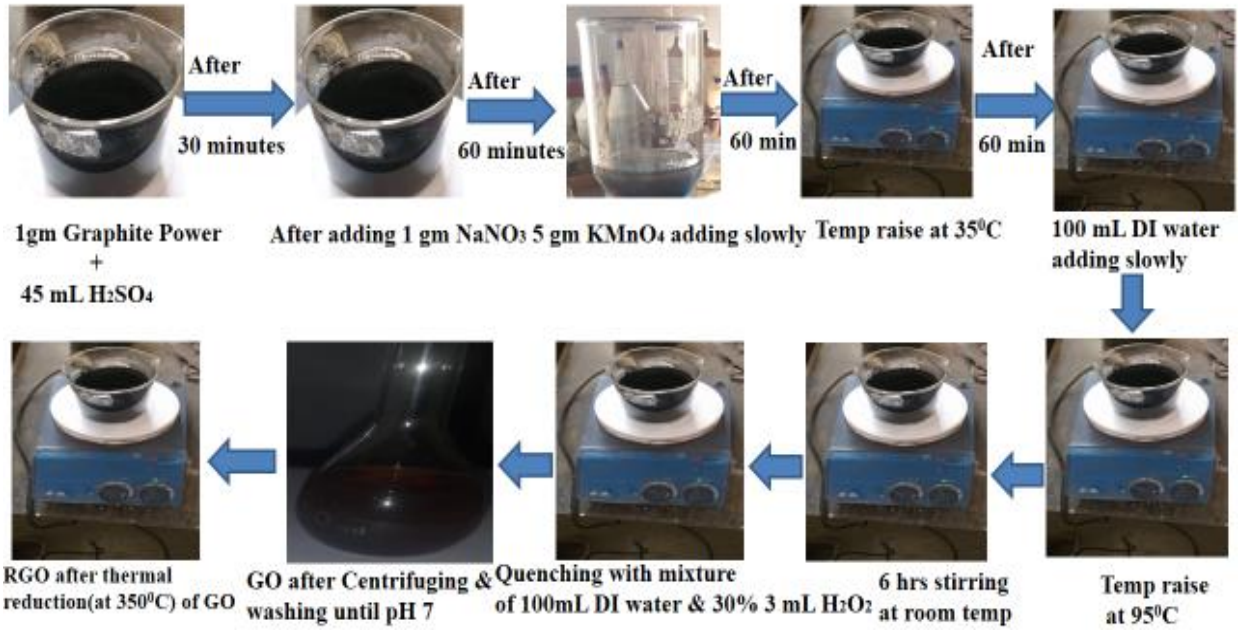

Figure 2.4: Preparation of reduced Graphene Oxide (RGO) using modified Hummers' method

RGO has been prepared using modified Hummers' method. At first, 1gm graphite powder with 45 mL H_2SO_4 is taken in beaker. After 30 minutes 1gm $NaNO_3$ has been added. After 60 minutes 5gm $KMnO_4$ has been added slowly then temperature raised at 35℃ using magnetic stirrer with hot pot for mixing. After 60 minutes 100 mL DI water was added slowly then temperature raised at 95℃ then 6 hours stirred at room temperature. Afterwards, quenched with mixture of 100 mL DI water and 30% 3 mL H_2O_2. After centrifuging and washing up to pH 7, graphene oxide (GO) has been prepared. Finally, after thermal reducing at 350℃ of GO reduced graphene oxide has been prepared.

2.5.3 RGO adsorbed paper electrode preparation

Four types of RGO adsorbed paper electrode have been prepared.

(a) At first, RGO has been adsorbed on cellulose paper using auto suction pump. After 2 hours adsorption it turns into brown colour then it is made as electrode according to specific measurement. Finally this electrode is applied in cell in the substitute of Cu with Zn electrode.

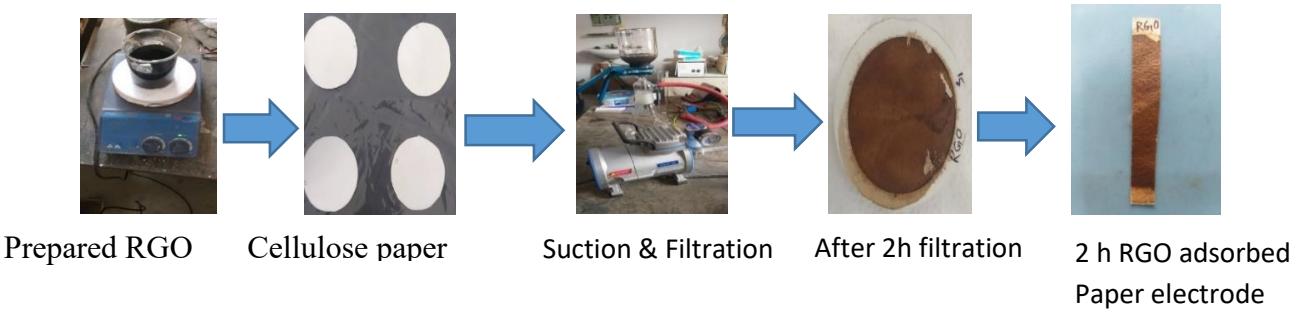

Figure 2.5: Preparation of RGO adsorbed paper electrode for two hours

(b) Prepared two hours RGO adsorbing paper electrode is kept under Ag NPs solution then it forms RGO-Ag Nano composite paper electrode. Finally, RGO-Ag Nano composite paper electrode is applied on cell in the substitute of Cu with Zn electrode.

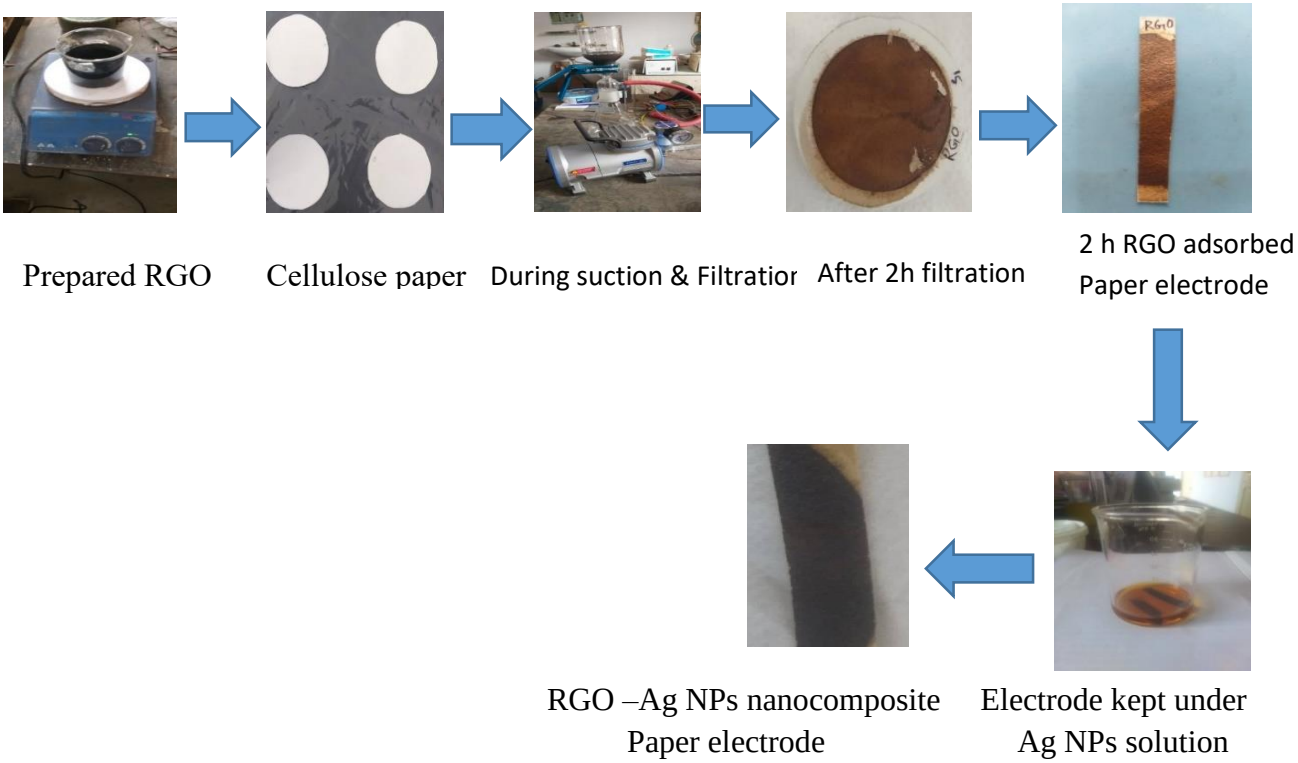

Figure 2.6: preparation of Ag NPs wrapped RGO adsorbed paper electrode for (2 h)

(c) On the other hand, when RGO 48 hours is adsorbed on cellulose paper, it turns into blackish colour. Then it is made as electrode according to specific measurement. Finally, it is applied in cell with Zn electrode.

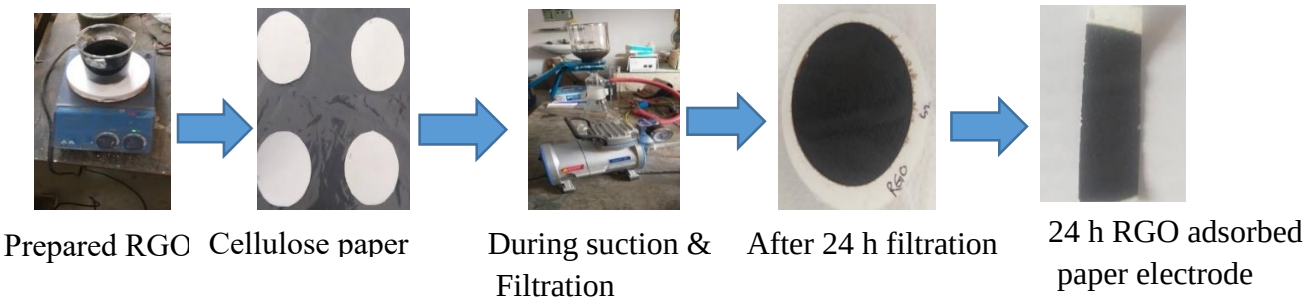

Figure 2.7: Preparation of RGO adsorbed paper electrode for (24 h)

(d) Prepared 48 hours adsorbed paper electrode is kept under Ag NPs solution. Then it forms RGO-Ag Nano composite electrode. Then it turns into deep black colour. Finally RGO-Ag Nano composite paper electrode is applied on cell with Zn electrode.

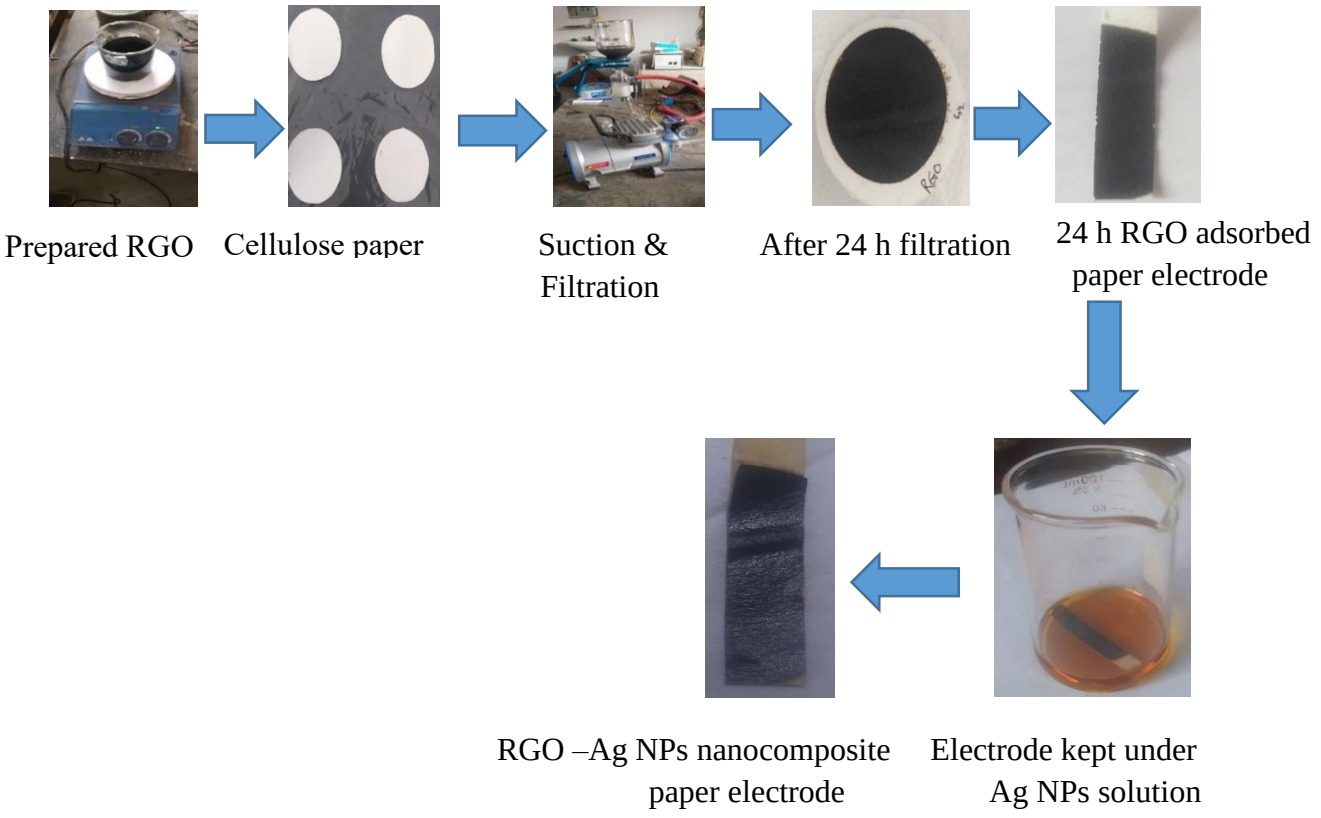

Figure 2.8: Preparation of Ag NPs wrapped RGO adsorbed paper electrode for (24 h)

2.6 Synthesis of Ag Nanoparticle from Pathor Kuchi Leaf

20g fresh *B. pinnatum* is picked from Jagannath University area, then washed by Deionized (DI) water and chopped to make a paste. Thereafter, 100 mL DI water is added to the leaves paste. During the pest preparation pH value was 5.5 then heated at 60 to 70^0C for an hour with nonstop magnetic stirrer. The solution from PKL pest is then kept onto magnetic stirrer for a while to make it cool. When temperature downs at room temperature, the solution is filtered twice with Whatman41 and Whatman 42 filter paper to remove residual solids. Finally, the PKL extract solution is kept in refrigerator at 3 to 4 ^{0}C to prepare Ag NPs.

On the contrary, pure (99.98%) $AgNO_3$ precursor is applied in this experiment to synthesis Ag NPs which are purchased from Sigma Aldrich. 1.0mM of 45 mL $AgNO_3$ solution is prepared then 100mL solution is taken onto a conical flask and 5 mL PKL extract which is prepared and stored in refrigerator is added drop wise into the above $AgNO_3$ solution. After shaking wisely the mixture is kept in dark chamber. Then the colorless mixture turns into yellow to brown within three or four hours. After two days, it is finally formed a dark-brown color solution with some black sediments at the bottom of the flask, which indicates the development of Ag NPs.

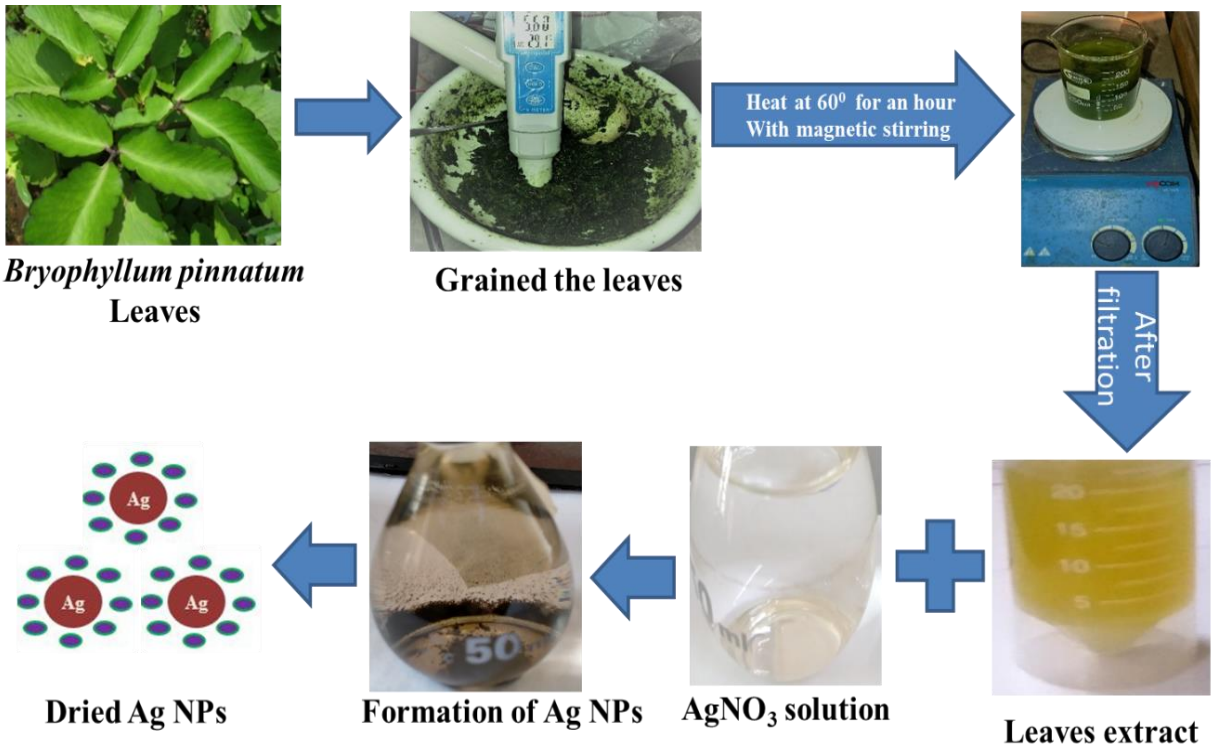

Figure 2.9: Steps diagram of green synthesis of AgNPs using *B. pinnatum* extract

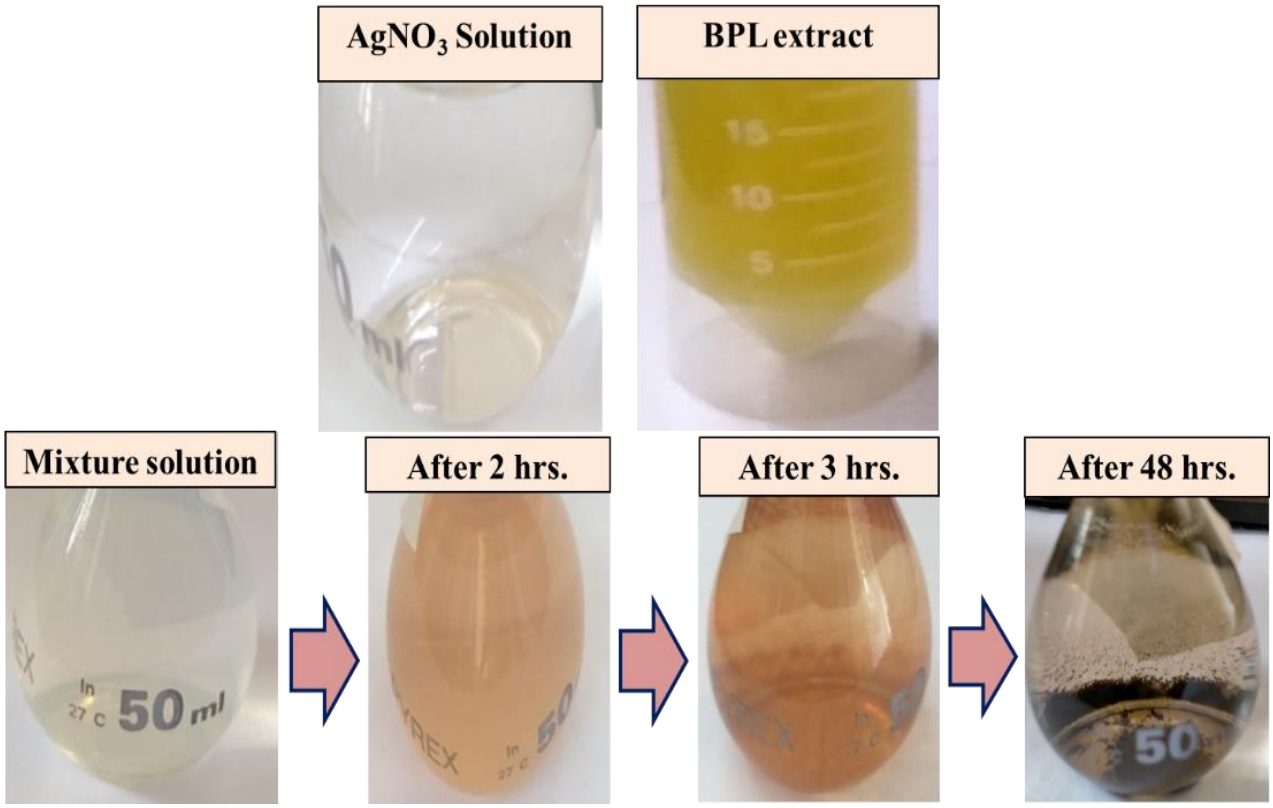

Figure 2.10: Schematic diagram of colour changes throughout the fromation of Ag NPs.

2.7 Synthesis of Ag Nanoparticle from Arum Leaf (AL)

C.esculenta leaves/AL were collected from Dhaka University campus, Bangladesh. 20g of leaves were taken and appropriately washed with pure water to remove the unwanted particles. Thereafter, the leaves were washed with Deionized (DI) water three times and chopped to blend to make a fine paste. 100 mL of deionized water were mixed with leaves paste and placed on a hot plate at 60℃ for one hour. The hot solution was kept aside to cool. The solution was filtered twice with Whatman41 and Whatman42 filter paper then the filtrated extract solution was kept in a refrigerator at 4℃ before use. A pure $AgNO_3$ precursor purchased from Sigma Aldrich has been used in this experiment. Then 5 mL AL extract solution was added to the 1mM 45 mL $AgNO_3$. After an hour, the color of mixture had been changing that was observed. The colorless mixture solution was becoming brownish with the time, which indicated the formation of Ag NPs. To complete the reduction of Ag^+ to Ag0 the solution was kept at room temperature for the next couple of days in a dark chamber. The color change from light yellow to dark brown affirms the reduction of Ag^+ and the formation of Ag NPs. The fabrication steps are shown in Figure 2.11.

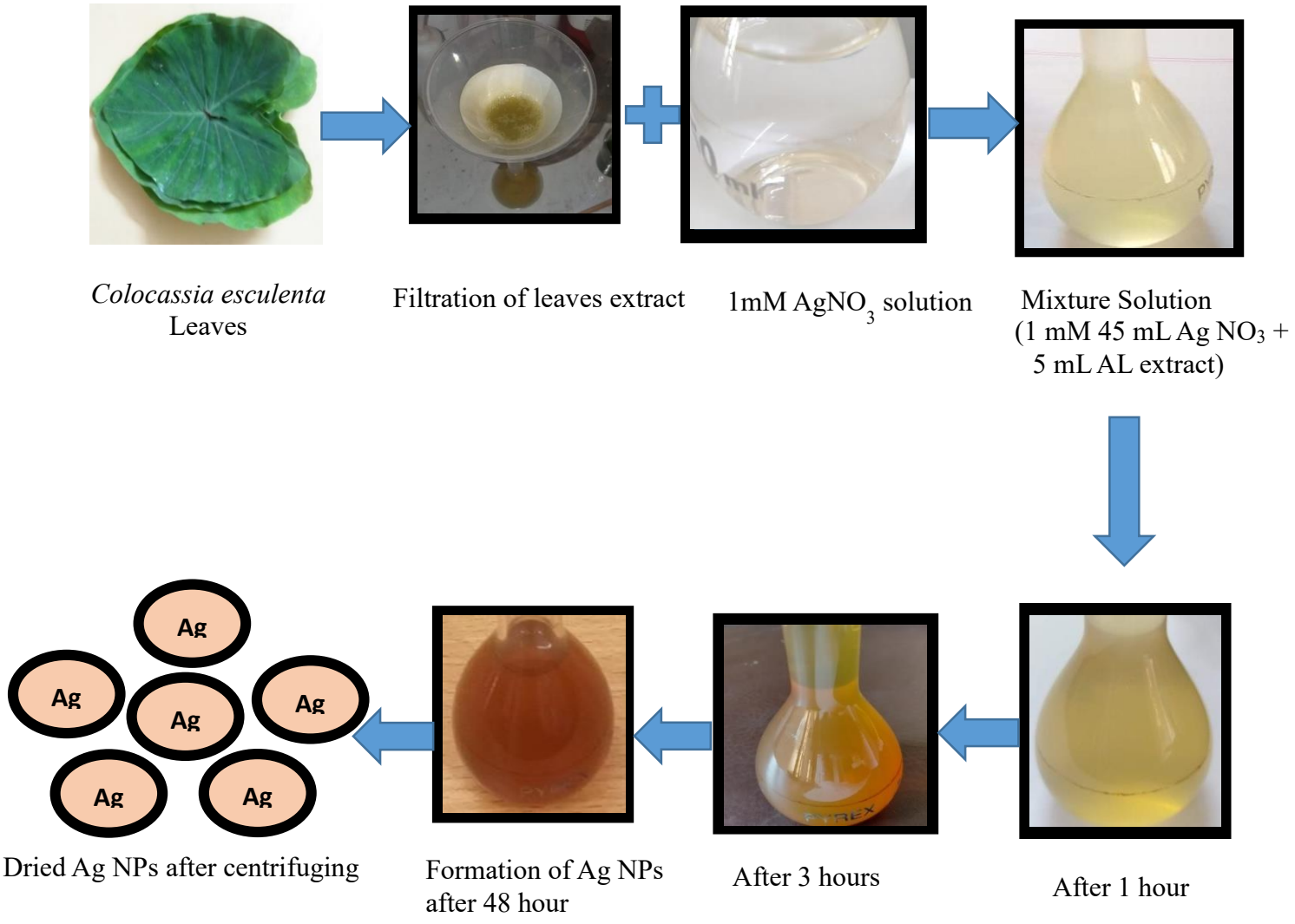

Figure 2.11: Schematic diagram for preparation of Ag NPs using AL extract

2.8 GC-MS Analysis of PKL Extract

The constituents of the PKLare analyzed by GC/MS analysing. The Acetone extract of the leaves of PKL on GC/MS analysis reveals eight peaks indicating the presence of eight compounds in the plant leaves as shown in the figure 3.13.

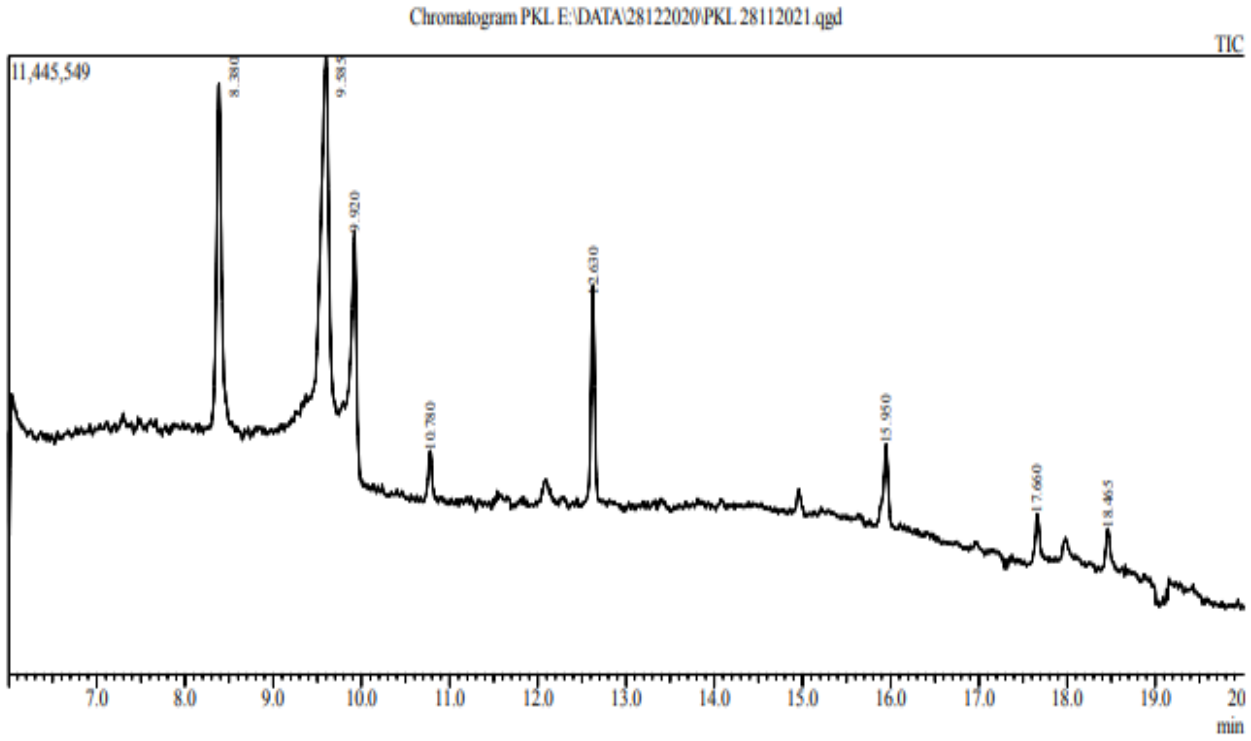

Figure 3.12: Gas Chromatogram of the leaf essential oil of PKL.

The retention time, molecular weight, and percentage constituents of the compounds are shown in Table 3.2. The compounds of the essential oil are Acetate (20.722%), 3-Hexamine (28.088%),2-Propanone, 1-cyclopentyl- (12.398%),Pent-3-yne (7.742%), 2,5-Furandion, dihydro-3-methylene- (25.843%), 5-Decen-1-ol, acetate, (E)- (1.536%), Benzofuran, 2,3-dihydro- (2.025%), and 2-Furanone, 3,4-dihydroxxytetrahydro (1.646%).

Table 2.2: Chemical compositions of *B. pinnatum* extract

SL No.	Compounds	Retention Time (min)	Molecular weight (m/z)	Conc.
1	Acetate <butyl->	8.383	56.00	20.722 %
2	3-Hexanamine	9.596	72.00	28.088 %
3	2-Propanone, 1-cyclopentyl-	9.920	59.00	12.398 %
4	Pent-3-yne <1-hydroxy->	10.772	54.00	7.742 %
5	2,5-Furandione, dihydro-3-methylene-	12.625	68.00	25.843 %
6	5-Decen-1-ol, acetate, (E)-	15.950	81.00	1.536 %
7	Benzofuran, 2,3-dihydro-	17.661	120.00	2.025 %
8	2-Furanone, 3,4-dihydroxytetrahydro	18.460	55.00	1.646 %

2.9 Electrochemical cell Preparation

Eight types of electrochemical cell have been prepared in this experiment. Four types of cell hane been prepared using Zn/Cu and four types of cell prepared using Zn/RGO adsorbed paper electrode. On the contrary, electrolyte density and electrode parameter have been changed during experiment. Secondary salt has been applied to amplify the performance of extract electrolyte. Beside this, Ag NPs have been applied to form Ag – RGO Nano composite so that RGO adsorbed paper electrode can transport electron rapidly.

2.9.1 PKL/AL cell preparation

When only one pair of electrode like one electrode used as anode and other electrode used as cathode has been submerged in BVC, it is PKL/AL cell. Here, Zn electrode has been applied as anode and Cu electrode as cathode to construct this cell. Because of applying plant extract as electrolyte this cell is called bio-voltaic cell (BVC). Four types of bio-voltaic cell have been prepared in this experiment: (a) Cell using only Zn/Cu electrode with PKL/AL extract electrolyte (b) Cell using only Zn/Cu electrode with secondary salt mixed PKL/AL extract electrolyte (c) Cell

using only Zn/ Ag NPs coted Cu with PKL/AL electrolyte (d) Cell using only Zn/Ag NPs coted Cu with secondary salt mixed PKL/AL electrolyte. The performance of PKL/AL cell depends on

- Concentration of the PKL/AL extract electrolyte
- Parameter of the electrodes
- Space between the two electrodes
- The constituent elements of the electrodes
- The volume of the PKL/AL extract
- The temperature of the PKL/AL extract
- The age of the PKL/AL
- PH of the PKL/AL extract
- Absorptivity of the electrodes
- Adsorptivity of the electrodes
- Thickness of the electrodes
- Purity of the electrodes

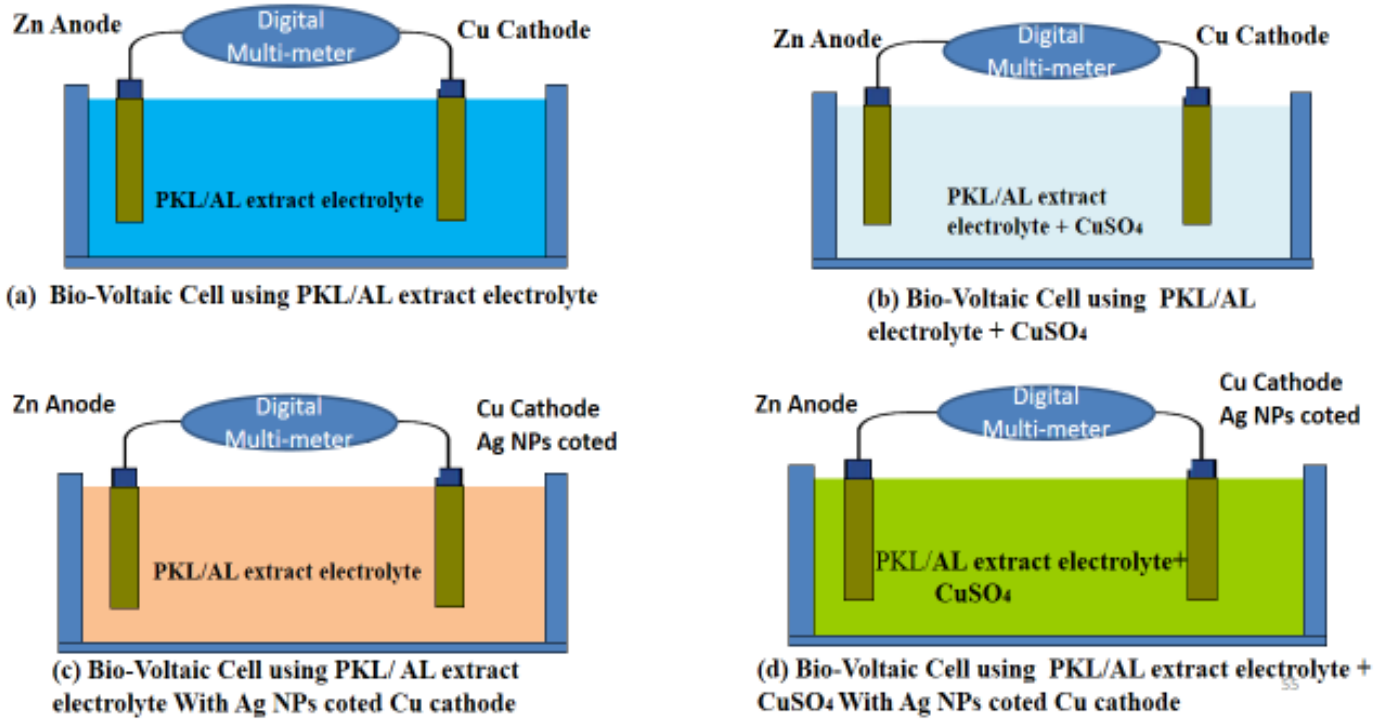

Figure 2.13: Various types of PKL/AL cell using various electrode and electrolyte

2.9.2 PKL/AL module cell preparation

To construct PKL/AL module cell some instruction have been followed.

- PKL/AL extract = 500 mL (PKL /AL: H_2O = 1:1)
- Anode = Zinc (Zn)
- Cathode = Copper (Cu)
- No. of Anode = 12
- No. of Cathode = 12
- Thickness of anode = 0.71 mm
- Thickness of cathode = 0.17 mm
- Mass of anode = 27.71 gm
- Mass of cathode = 6.77 gm
- Area of each anode immersed in extract (A_i) =73.34 cm^2
- Area of each cathode immersed in extract (A_i) =80.7 cm^2
- Distance between anode & cathode = 8 cm
- Volume of cell = 1000 mL
- Concentration of extract = (X-Y)/Z

Where,

X = Weight for fresh leaves before blending,

Y = Weight of the fresh leaves after blending (g) and

Z = Weight of water after filtration (g)

Figure 2.14: PKL/AL module cell

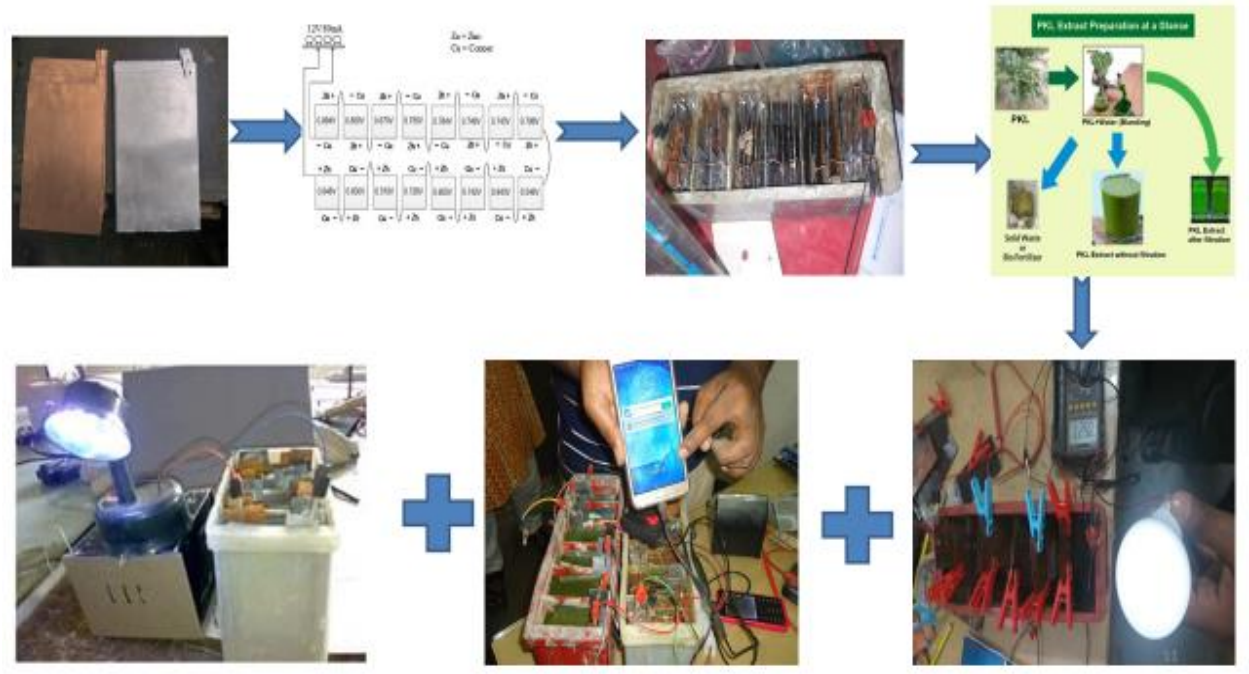

Figure 2.15: Schematic diagram for preparation of PKL/AL module cell

2.9.3 PKL/AL panel cell preparation

To construct PKL/AL panel cell, at first some module cell has been prepared. Then all of modules are connected by parallel. Finally, PKL/AL panel cell has been prepared. As a result, the performance of cell that means voltage, current, power has increased remarkably.

Figure 2.16: PKL/AL panel cell

2.9.4 PKL/AL 1KW power plant fabrication

Figure 2.17: Fabrication of an experimental setup of a 1 KW PKL power production from the PKL/AL extract

It has been designed and fabricated with 6 insulated boxes (figure 2.16) which are available in the local market of Bangladesh. The Copper and Zinc plates are set-up in the boxes scientifically with parallel and series combinations. The plates Zn and Cu are parallel in connection with each boxes and the boxes are connected in series connection with each other for getting required current, voltages and power [153-159]. The boxes are set up in a standalone chamber. There is a small insulated box filled up with Zn and Cu plates including with LED lantern on the top of the chamber. There is also a small insulated box filled up with Zn and Cu plates under the bottom of the chamber.

Figure 2.18: Front side experimental setup of a 1 KW PKL /AL power plant

Figure 2.18 shows the fabrication of the 1KW PKL power production system. It is fabricated based on the design of the PKL/AL power system. Here it is shown through the converter-1, converter-2, converter-3, converter-4, converter-5, converter-6, converter-7 and converter-8. It is also shown that, there are two street lights= 600W, two LED lights =60 W, one ceiling fan = 80 W, one table

fan = 30 W, one tube light = 40 W and oneself operated electric pump = 50 W which carry PKL/AL extract forcibly from the converter-8 to the converter-7 (red color). The light is used at the converter-7 as an indicator of the 1KW PKL/AL power system. The total power is used in the system = 860 W, which is around 80% of the source. It is mentioned that the output power should be 80% of the source power [160-165].

Figure 2.19: Left side 1 KW PKL power plant

It is shown (figure 2.18) in the left side of the 1 KW PKL micro power plant where there is a control board consisting of a circuit breaker, some switches and two LED lights. The total circuit of the 1KW PKL/AL micro power plant is controlled by the switches and the circuit board.

2.9.5 Electrochemical cell preparation using Zn/RGO adsorbed paper Electrode

To reduce the cost of bio-voltaic cell construction; RGO adsorbed paper electrode has been applied. RGO adsorbed paper electrode has been applied in bio-voltaic cell in the substitute of Cu. RGO adsorbed paper electrode price is ¼ times less than Cu electrode. This type of paper electrode is also lighter than Cu electrode.

2.9.5.1 Zn/(2 h) RGO adsorbed paper electrode cell preparation

At first prepared RGO has been adsorbed on cellulose paper using auto suction pump. After 2 hours adsorption it turns into brown colour. When Cellulose paper has adsorbed RGO for two hours, it is sized according to the measurement of substituted Cu. Thereafter, Zn acts as anode and 2 hours RGO adsorbed paper electrode acts as cathode in the bio-voltaic cell. As a result, Zn/2 h RGO adsorbed paper electrode cell have been prepared.

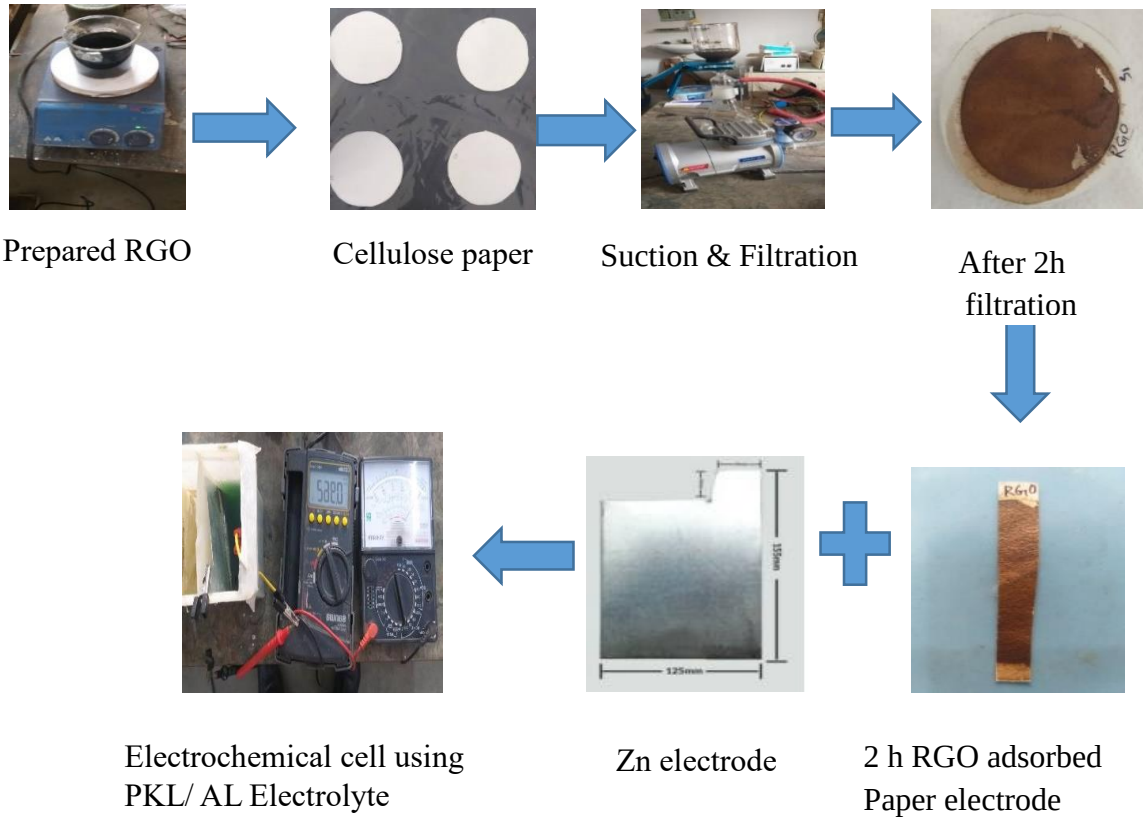

Figure 2.20: Schematic diagram for preparation of Zn and 2 hours RGO adsorbed paper electrode cell using PKL/AL electrolyte

2.9.5.2 Zn/ RGO (2 h) adsorbed and Ag NPs wrapped Nano composite paper electrode cell preparation

At first prepared RGO has been adsorbed on cellulose paper using auto suction pump. After 2 hours adsorption it turns into brown colour. Then prepared two hours RGO adsorbed paper electrode is kept under Ag NPs solution. Then it forms RGO-Ag Nano composite paper electrode. This RGO-Ag Nano composite paper electrode is sized according to the measurement of substituted Cu electrode. Thereafter. Zn acts as anode and RGO (2 h) – Ag Nano composite paper electrode acts as cathode in the bio-voltaic cell. Finally, RGO-Ag Nano composite paper electrode has been applied in bio-voltaic cell with Zn electrode. As a result, Zn/ RGO (2 h) –Ag Nano composite paper electrode cell has been prepared.

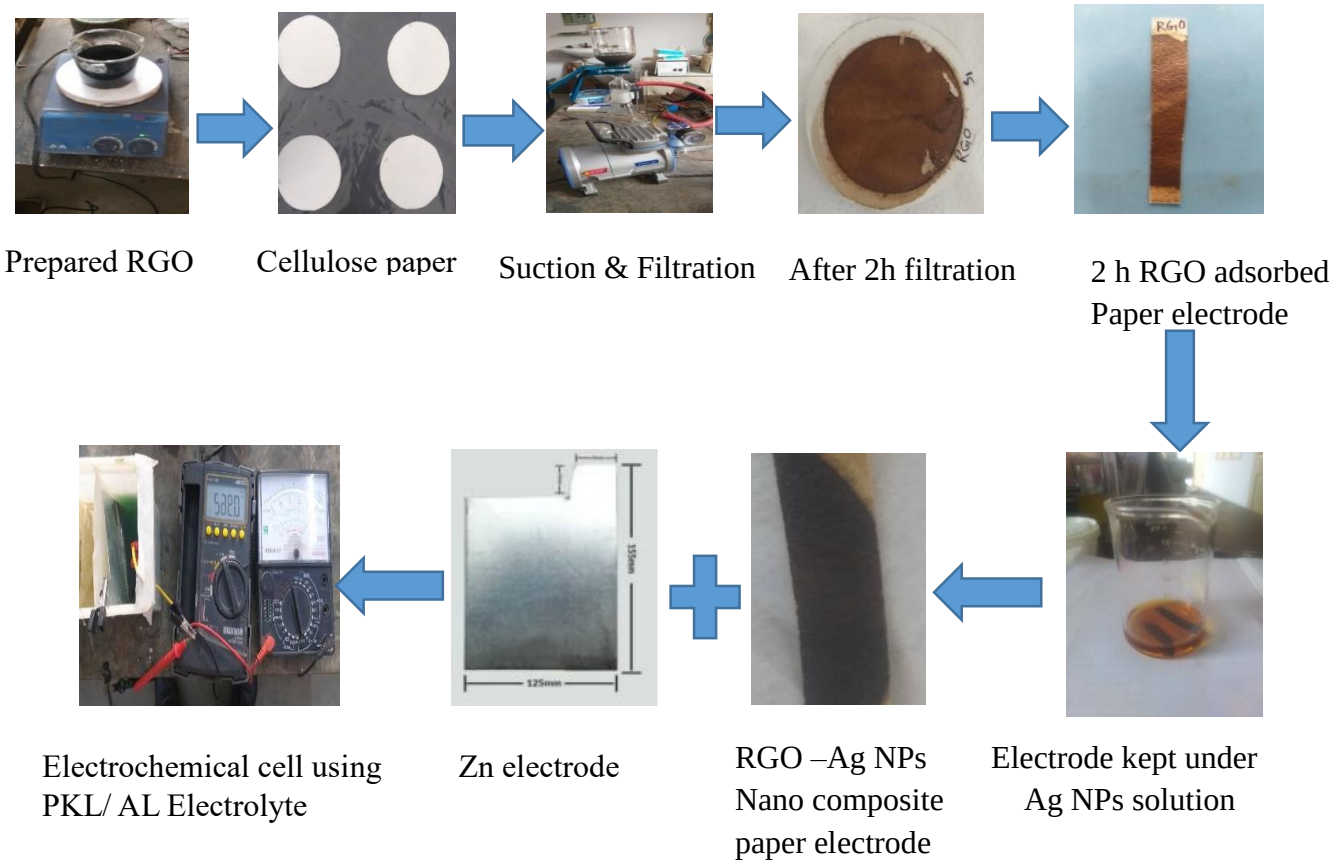

Figure 2.21: Schematic diagram for preparation Zn and RGO (2 h) – Ag NPs Nano composite paper electrode cell using PKL/AL electrolyte

2.9.5.3 Zn/24 (h) RGO adsorbed paper electrode cell preparation

At first prepared RGO has been adsorbed on cellulose paper using auto suction pump. After 24 hours adsorption it turns into blackish colour. When Cellulose paper adsorbs RGO for 24 hours, it is sized according to the measurement of substituted Cu. Thereafter, Zn acts as anode and 24 hours RGO adsorbed paper electrode acts as cathode in the bio-voltaic cell. As a result, Zn/24 (h) RGO adsorbed paper electrode cell has been prepared.

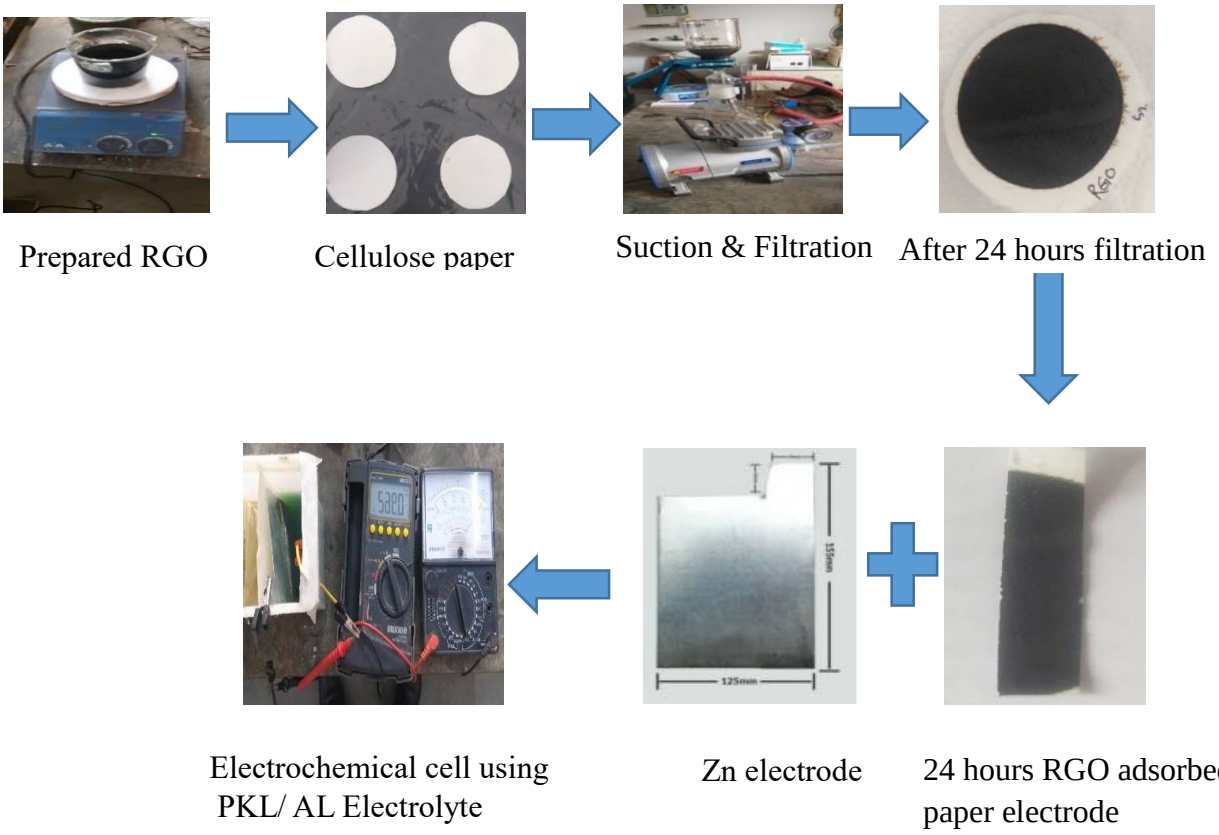

Figure 2.22: Schematic diagram for preparation Zn and 24 hours RGO adsorbed paper electrode cell using PKL/AL electrolyte

2.9.5.4 Zn/ RGO (24 h) adsorbed and Ag NPs wrapped Nano composite paper electrode cell preparation

At first prepared RGO has been adsorbed on Cellulose paper using auto suction pump. After 24 hours adsorption it turns into blackish colour. Then prepared 24 hours RGO adsorbed paper electrode is kept under Ag NPs solution. Then it forms RGO-Ag Nano composite paper electrode. This RGO-Ag Nano composite paper electrode has been sized according to the measurement of substituted Cu. Thereafter, Zn acts as anode and RGO (24 h) adsorbed and Ag NPs wrapped Nano composite paper electrode acts as cathode in the bio-voltaic cell. Finally, RGO-Ag Nano composite paper electrode has been applied on cell with Zn electrode. As a result, Zn/ RGO (24 h) adsorbed and Ag NPs Nano composite paper electrode cell has been prepared.

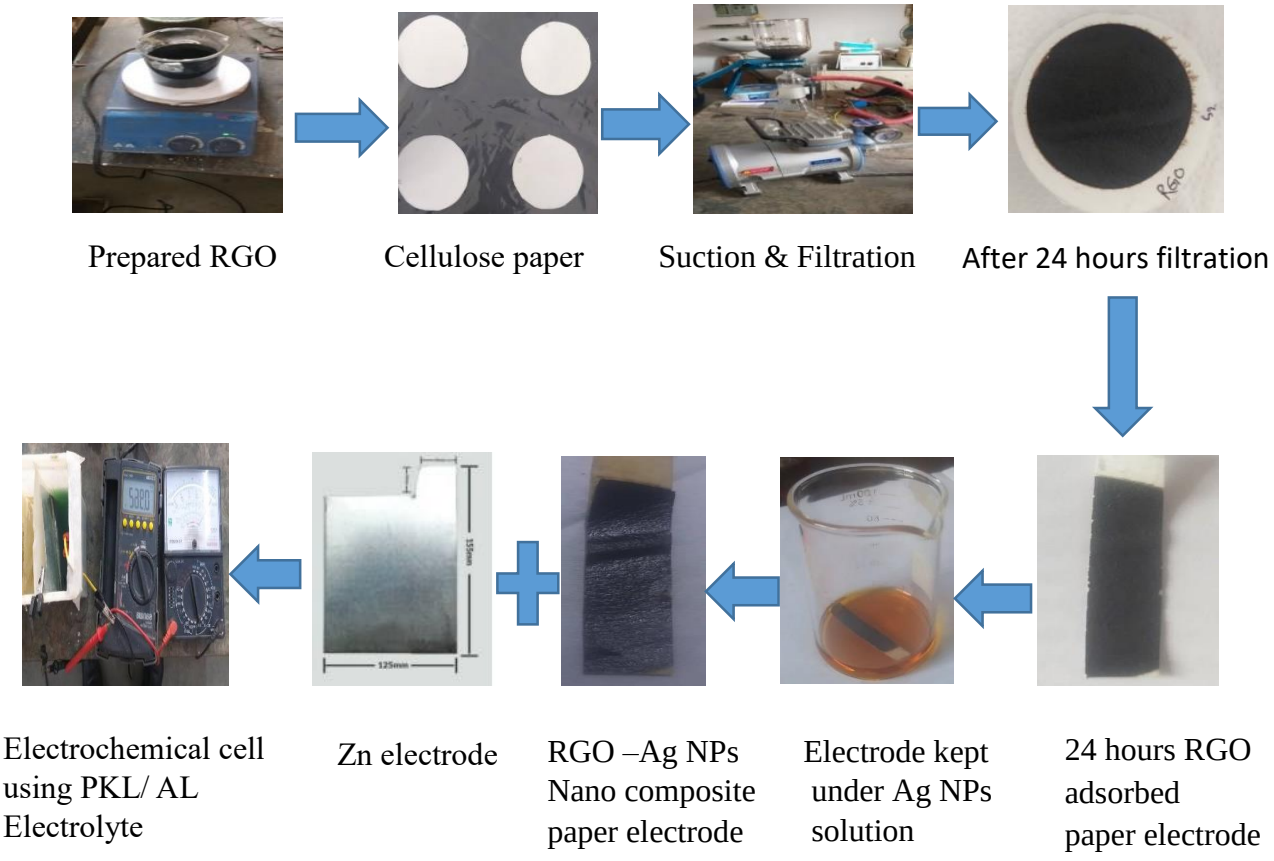

Figure 2.23: Schematic diagram for preparation Zn and RGO (24 h) – Ag NPs Nano composite paper electrode cell using PKL/AL electrolyte

2.10 UV- Visible Spectra Analysis

Green synthesized Ag NPs have been probed by using the UV–Vis spectrometer (UV-2102, China), and the spectra of reaction solution (10 times diluted) have been measured in the range of (200 nm–800 nm). The outline of UV- Visible spectra analysis of Ag NPs from PKL/AL is as below:

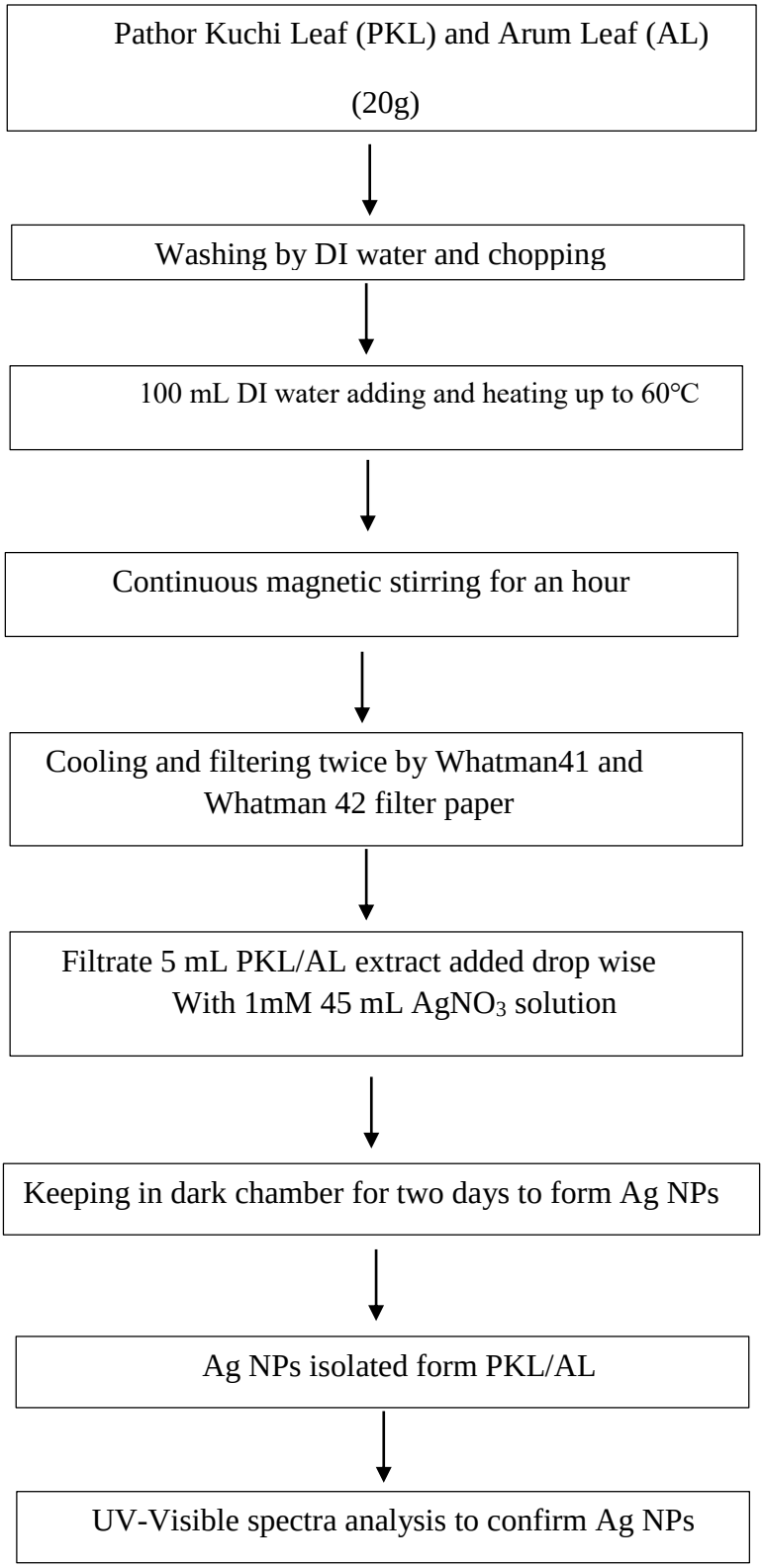

Figure 2.24: Outline of UV- Visible spectra analysis of Ag NPs from PKL/AL

2.11 X-ray Diffraction (XRD) Analysis

The crystalline phase of Ag NPs has been investigated by the Rigaku (Ultima IV 2036E202) X-ray diffraction instrument. The CuKα radiation (λ = 1.5405 Å) source has been used for the XRD measurements in different range of 2θ angle (20°- 80°). The outline of X-ray Diffraction (XRD) analysis of Ag NPs from PKL/AL is as below:

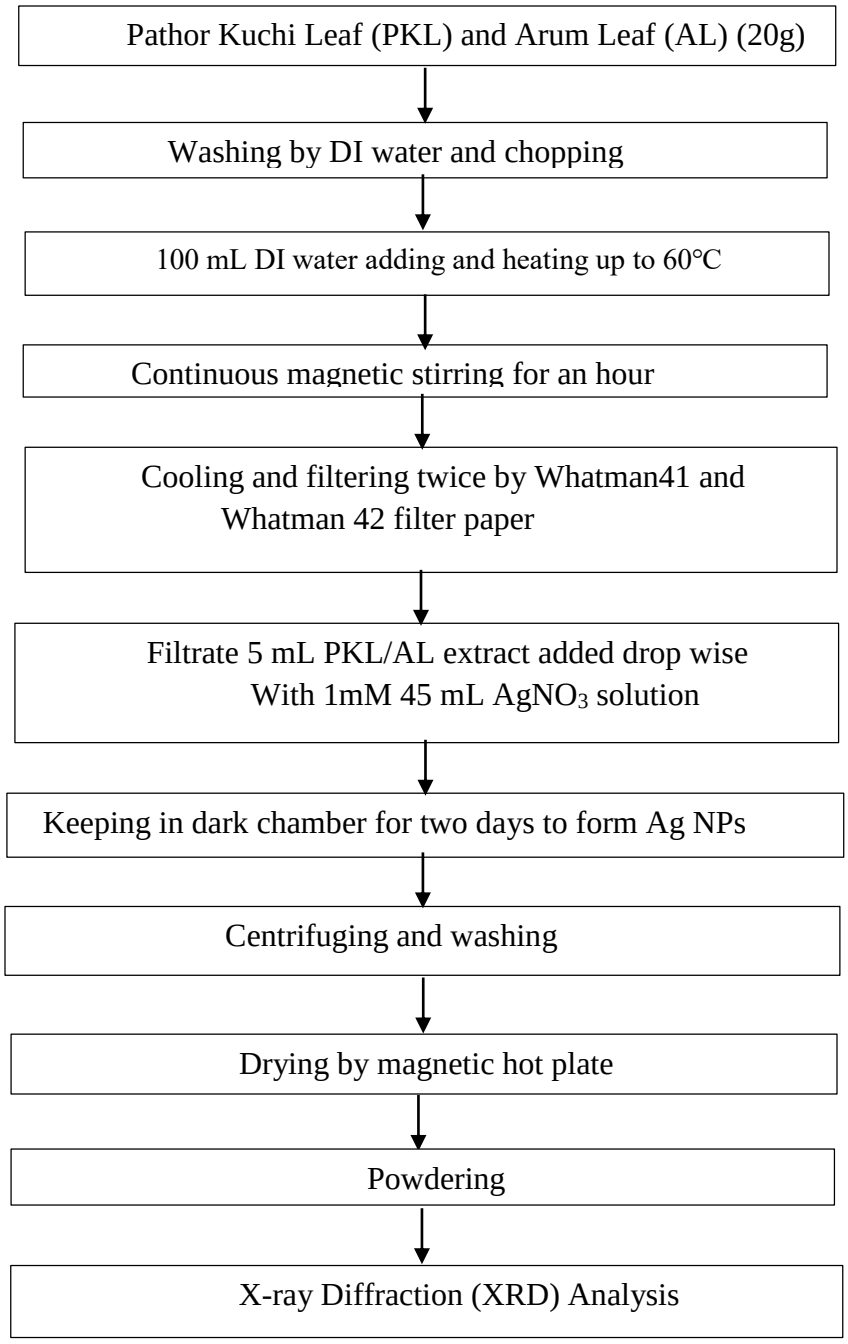

Figure 2.25: Outline of X-ray Diffraction (XRD) analysis of Ag NPs from PKL/AL

2.12 FTIR Analysis

Fourier Transform Infrared (FTIR) measurements of PKL/AL extract mediated Ag NPs have been conducted by using the Shimadzu (IRPrestige-21) FT-IR spectrophotometer. The outline of Fourier Transform Infrared (FTIR) measurements analysis of Ag NPs from PKL/AL as below:

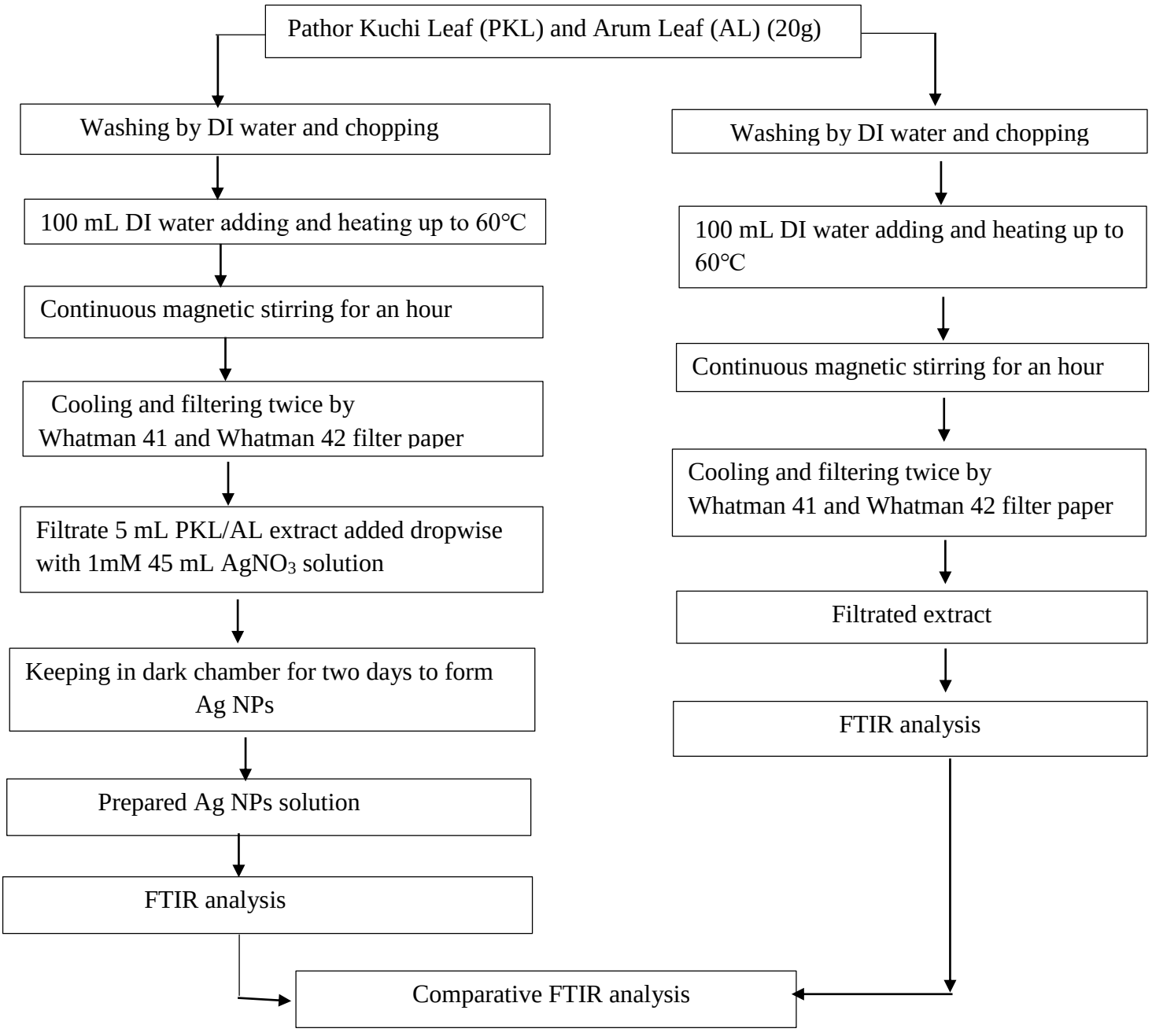

Figure 2.26: Outline of FTIR analysis of Ag NPs from PKL/AL

2.13 FESEM Analysis

The morphology of silver nanoparticles from PKL/AL has been analyzed using the Field Emission Scanning Electron Microscopy (FESEM) images JSM-7610F equipped with an energy dispersion X-ray spectroscopy (EDX) attachment at 15 KeV. Before taking the FESEM images, Ag NPs have been inserted in JEC-3000FC auto fine platinum coater for 10 seconds. The outline of Field Emission Scanning Electron Microscopy (FESEM) analysis of Ag NPs from PKL/AL is as below:

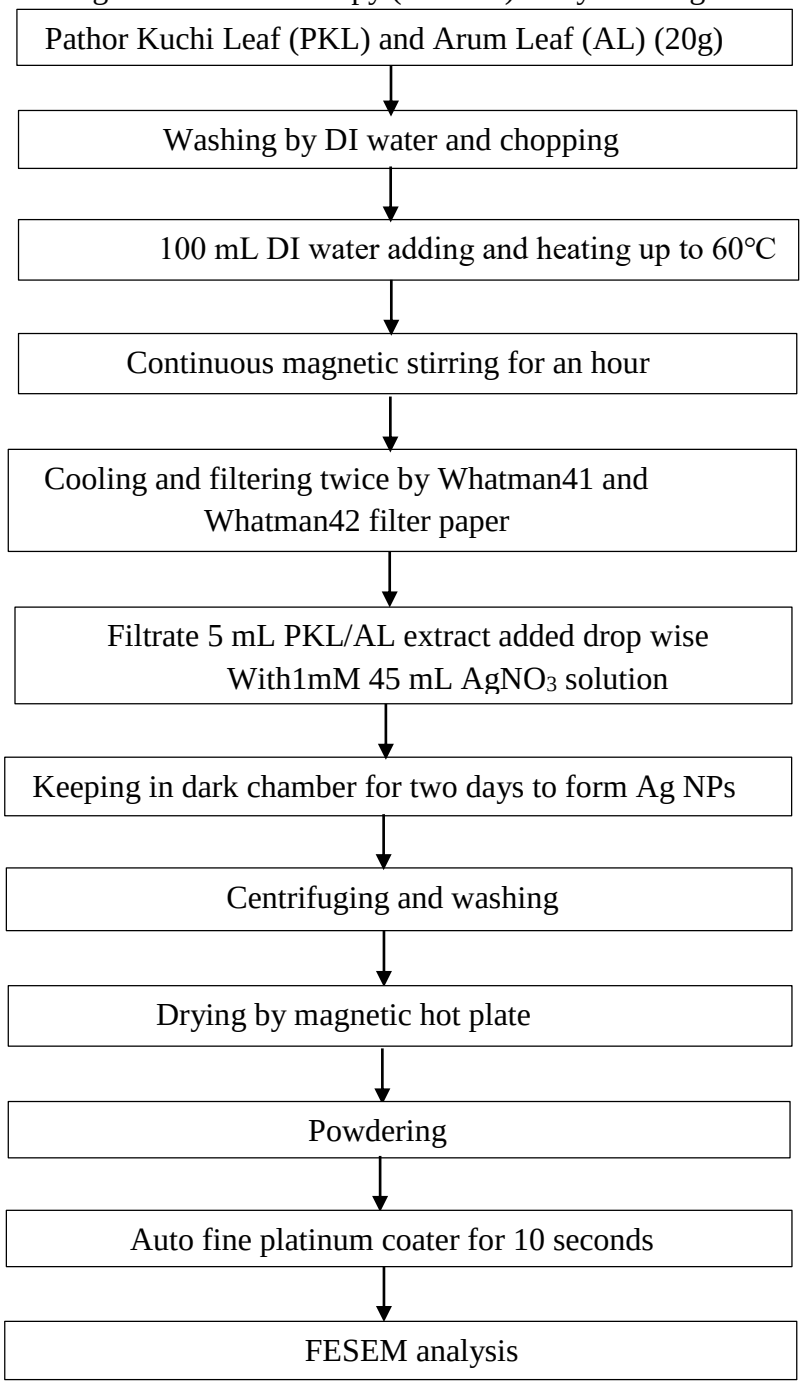

Figure 2.27: Outline of FESEM analysis of Ag NPs from PKL/AL

2.14 GC-MS Analysis

The Gas-chromatography analysis of PKL/AL has been performed GCMS QP – 2010 SE SHIMADZU, JAPAN with the helium gas carrier at 1.00 mL/min and the injection temperature was 200 ◦C. The outline of Field Emission Scanning Electron Microscopy (FESEM) analysis of Ag NPs from PKL/AL is as below:

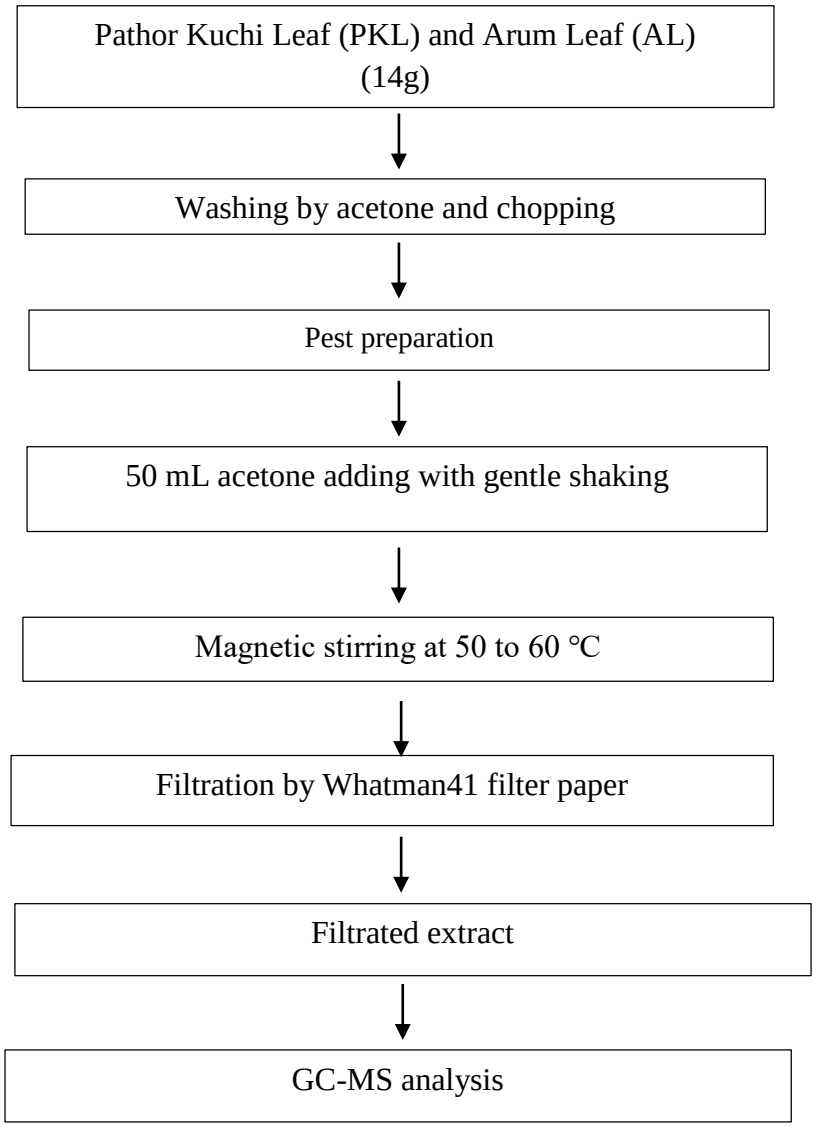

Figure 2.28: Outline of GC-MS analysis of Ag NPs from PKL/AL

2.15 Chemical Analysis

2.15.1 Chemical component in AL

Colocsia esculenta leaves or Arum leaves contains calcium oxalate, fibers, minerals, starch and vitamin A, B, C etc [166]. But from phytochemical investigation of AL, there are three compounds found in AL which play an important role to flow electron. [167]. such as figure 2.29(a): Apigenin figure 2.29(b): Luteolin and figure 2.29(c): Anthocyanins. Most of the compounds are phenolic and show resonance. As a result, during resonance those compounds can donate proton. These protons help to flow electron by reduction process.

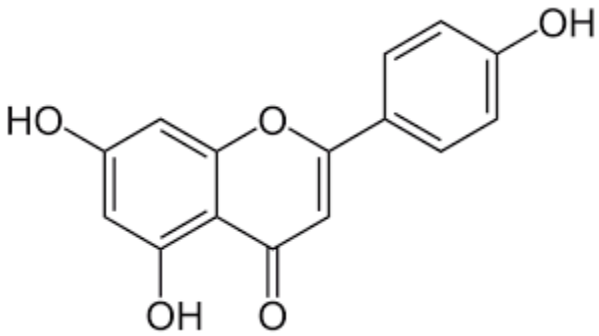

Figure (a): Apigenin

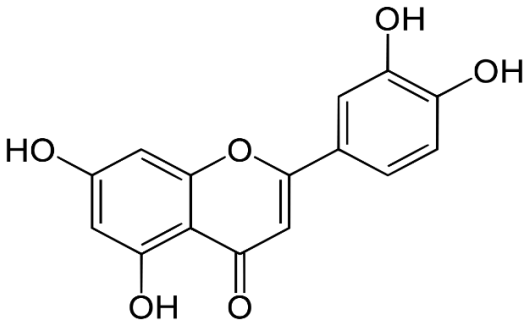

Figure (b): Luteolin

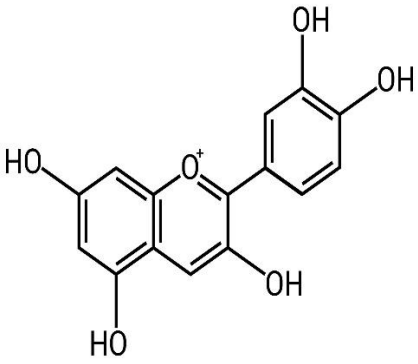

Figure (c): Anthocyanin

Figure 2.29: Main compound in AL (a): Apigenin (b): Luteolin (c): Anthocyanin

2.15.2 Chemical component in PKL

There are many organic acid, mineral, flavonoids and vitamins which have been found from GC-MS result analysis of PKL (Described in 3.17). Especially, citric acid, iso-citric acid and malic acid are main acetic ingredients which donate proton in electrolyte. As a result, transport number including current and voltage increases during cell reaction.

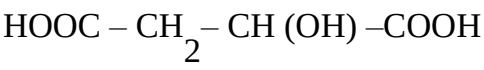

Figure 2.30(a): Malic acid

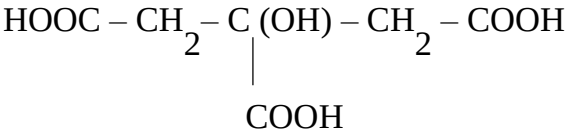

Figure 2.30(b): Citric acid

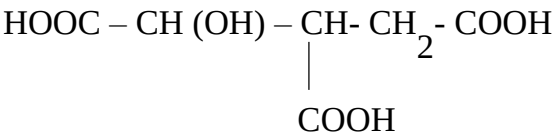

Figure 2.30(c): Iso-citric acid

Figure 2.30: Chemical component of PKL

2.16 Voltage Efficiency (η_v)

The Voltaic Efficiency of a cell is the ratio between the maximum voltage of load and open circuit voltage i.e. no-load voltage.

That is, Voltaic Efficiency, $(\eta_{v\,\%}) = \frac{VL}{Vmax} \times 100\%$ ……(2.6)

Here, the Vmax is the voltage without any load (V_{NL}) and V_L is the voltage with load.

2.16.1 Experimental set-up of Voltage Efficiency (η_v)

In this study, filament bulb of resistance 2Ω in both type of cells was added. A voltmeter was connected in parallel to the load or the filament bulb to give the value of load voltage. Another voltmeter was also used to measure the terminal voltage when the load was disconnected from both cells. At first the load voltage of each cell was taken and then the no-load voltage or the open circuit voltage. There after data was taken by a short time interval in both type of cells.

2.17 Voltage Regulation (V_R) Analysis

Voltage sags or swells are caused by the disturbances or faults in power systems. The input voltage fluctuation also affects the output voltage. Voltage regulation is the change of voltage from full loaded to no loaded condition. When there is no load connected then the terminal voltage is equal to the generated voltage. But when load is connected then the terminal voltage becomes less than the no loaded condition [65]. This voltage drop is due to the internal resistance or impedance of the system. An ideal voltage source has zero internal impedance. But practically internal impedance is one. Once a load current is drawn there will be a voltage drop across the source of internal impedance and then the terminal voltage will therefore drop. The higher the load current, the higher the voltage drops. This phenomenon is expressed as voltage regulation. In electrical power system the voltage regulation is the percentage of voltage difference between no load and load voltages.

Mathematically,

Voltage Regulation, $V_R = \frac{\text{No Load Volatge} - \text{Load Voltage}}{\text{Load Voltage}}$

Usually it is expressed as %.

Voltage Regulation in % $V_R = \frac{VNL-VL}{VL} \times 100\%$ ……..(2.7)

Where, V_R = Voltage Regulation, V_{NL} = No load Voltage, V_L = Load Voltage.

2.17.1 Experimental set-up of Voltage Regulation (V_R) Analysis

This experiment was also set as voltaic efficiency experiments. At first the filament bulb of resistance 2Ω in both type of cells was added. A voltmeter was connected in parallel to the load or the filament bulb to give the value of load voltage. Another voltmeter was also used to measure the terminal voltage when the load was disconnected from both cells. At first the load voltage of each cell was taken and then the no-load voltage or the open circuit voltage. There after data was taken by a short time interval in both type of cells.

2.18 Power Efficiency (η_p)

The power supplied to electrical equipment is not all converted into useful power. Usually, some power is wasted. The ability of an electrical component to convert power into a useful output is defined in terms of power efficiency [68-170]. The symbol for power efficiency is η.

$$\text{Power Efficiency, } \eta_p = \frac{Power\ output}{Power\ input} \times 100\% \quad \text{.....(2.8)}$$

2.19 Internal Resistance (R_{int}) Analysis

When currents flows from an electrochemical cell then electrons are transferred externally from the negative electrode to the positive electrode. If the load current is very small then the terminal voltage under load may not be noticeably different from the open-circuit output voltage. When the load current is large then the terminal voltage falls below the open-circuit voltage level. If the load current is made too large then the cell terminal voltage falls to near zero. Because the chemical action cannot occur fast enough to replace the charges removed from the electrodes. The maximum current taken from a voltage cell without a substantial drop in output voltage is proportional to the surface area of the electrodes and to the composition of the electrolyte. During supplying current if terminal voltage drop of an each cell then certain internal resistance occurred. On the other hand a practical electrical power source which is a linear electric circuit represent as an ideal voltage source in series with an impedance. This resistance is termed the internal resistance of the source. When the power source delivers current then the measured voltage output is lower than the no-load voltage and this difference is the voltage drop. This voltage drop occurred because of internal resistance. The internal resistance found more or less in all kinds of electrical sources [171].The internal resistance of an electrochemical is dependent on the specific cell's size, chemical properties, age, temperature and the discharge current. It has an electronic component due to the resistivity of the cell's component materials and an ionic component due to electrochemical factors such as electrolyte conductivity, ion mobility, and electrode surface area. The internal resistance of a battery can be calculated from its open circuit voltage, voltage on-load, and the load resistance:

$$\text{Rin} = \left(\frac{VNL}{VL} - 1\right) \times R_L \quad \text{.....(2.9)}$$

Where Rint is the internal resistance, V_{NL} is the no load voltage, V_L is the full load voltage and R_L is the resistance of the load connected to that cell.

2.20 Columbic Efficiency of Cell (η_Q %)

The columbic efficiency is the ratio of the charge obtained to the total charge supplied by the anode [172], i.e.

$\eta_{Q\%} = \frac{Qoutput}{Qinput} \times 100\%$

$= \frac{Q\ obtained}{Qsupplied} \times 100\%$ ………………………………………………………………(2.10)

If the life time of the cell becomes t, with an outer circuit connection, and the current measured by the ammeter is I.

Then the output charge, $Q_{output} = It$……………………………………………………..(2.11)

Again, the source of electron is the anode where electron produces by the oxidation reaction on the metal used as anode. Thus with reaction the weight of the anode reduces with time. If the weight of the anode used is = W_1, and the weight after time t is = W_2,

The weight lost = $W_1 - W_2$

= x g

Again the molecular weight of the metal used as anode is M, and the oxidation number is n. Then the reaction taking place on the anode can be represented as

$A \rightarrow An+ + ne^-$

Where, A represents anode. Thus, one mole metal will produce n mole electron.

So, M gm. metal anode (A) will supply n mole electron.

X gm. metal anode will supply = $\frac{n.x}{M}$ mole electron

$= \frac{n.x.NA}{M}$ electron

$= \frac{n,x,NA}{M} \times 1.6 \times 10^{-19}$ coulomb charge

$= \frac{n \times F}{M}$ coulomb charge

Where, F = 1 Faraday.

That is x gm anode by decaying under oxidation process supply $\frac{n \times F}{M}$ coulomb charge.

So, the input charge $Q_{input} = \frac{n \times F}{M}$ coulomb charge ……(2.12)

From Equations-(2.10), (2.11) and (2.12) we get,

$\eta_{Q\%} = \frac{Qoutput}{Qinput} \times 100\%$

$= \frac{It}{\frac{n \times F}{M}} \times 100\%$

$= \frac{MIt}{n \times F} \times 100\%$

So, columbic efficiency $\eta_{Q\%} = \frac{MIt}{n \times F} \times 100\%$ …….... (2.13)

So, by putting the values of the quantities in equation-(2.13) we can calculate the columbic efficiency.

2.21 Self-discharge Characteristics of Cell

A cell subjected to self-discharge during operation. Self-discharge is caused by parasitic reactions, such as corrosion. That occur even when the cell is not in use. Thus, the chemical energy may slowly decrease with time. The self-discharge rate also depends on the temperature. The self-discharge state is more spontaneous thermodynamically. The rate of self-discharge of the voltaic cell is fairly rapid when no external load is applied. Further energy loss may occur due to electrolyte consuming. But the rate of self-discharge can be reduced significantly by incorporating certain design features [173].

Typical self-discharge rates for common rechargeable cells are given below: [174]
Nickel Cadmium 10% per month
Nickel Metal Hydride 30% per month
Lithium 5% to 10% per month
NiMH batteries 1.25% per month
Nickel Cadmium 10% per month

2.21.1 Experimental Set-up

In this study, six zinc plates as anode and six copper plates as cathode. The surface area of each electrodes were uniform. The increasing the plates number means increasing the surface area of each plates. The electrodes were immersed 120 mm deep in the PKL/AL extract in a rectangular container. This depth was kept fixed throughout this experiment. A filament bulb of 2Ω was connected between the anode and cathode. The two leads of a voltmeter and an ammeter were

connected to the two electrodes to measure the open circuit voltage and short circuit current and a pH meter was immersed at the upper part of the container to get the pH value continuously. In this experiment the PKL/AL in the extract was 85.308%, water was 14.214% and $CuSO_4$ $5H_2O$ was 0.4739% approximately. The gap between the electrodes was 5 mm and corresponding load-current and pH readings were taken for several times. Here we used a term named "Cycle" which is the number of uses of same extract for several periods. Cycle-1 means newly made extract was used for the study. When the pH of the extract becomes 7 then the extract transfer from the cell to another container. After some days this used extract was taken in the cell to second time experiment for further study known as Cycle-2 investigation. Thus this experiment was continued for Cycle-3.

2.22 Effect of Secondary Salt

In this study, the space between the electrodes has been kept constant at 5 mm by placing a plastic separator to hold them. An electric balance has been used to measure the mass of secondary salt ($CuSO_4.5H_2O$). At first, 1000 (g) PKL/AL extract has been taken where PKL/AL and water ratio is 1:1. Then the extract has been poured in cell and data have been collected i.e. open circuit voltage and short circuit current have been measured using two digital multi-meters. After that 5 (g) $CuSO_4.5H_2O$ has been added in the cell and mixed this secondary salt with glass rod. At that moment second reading has been taken. As a results, voltage and current have increased. Again, more 5 (g) $CuSO_4.5H_2O$ has been added in the cell and shake with glass rod then third reading has been taken. As a result, performance of cell has increased from previous state. Finally, this experiment shows that addition of secondary salt gradually performance of BVC increases gradually.

2.23 Effect of Reduced Graphene Oxide (RGO) Adsorbed Paper electrode

For excellent electrical conductivity of RGO (Reduced Graphene Oxide) it can be applied as electrode by adsorbing or wrapping on cellulose paper [175]. Here, whatman 41 and 42 filter paper has been applied to adsorb RGO. Beside this, when RGO adsorbed paper electrode is wrapped by green synthesized Ag NPs then electrical conductivity increases abruptly. Because, Ag NPs have more electrochemical performance with various electrolyte [176]. As a result, RGO- Ag Nano composite has attained superior energy as well as power density. On the other hand, more adsorbed RGO-Ag Nano composite has showed enhanced electrical conductivity and also reached nonlinear current voltage characteristics. [176].This current voltage characteristics varied with the variation electrolyte such as Arum Leaf (AL) and Pathor Kuchi Leaf (PKL) electrolyte.

2.24 Effect ROG-Ag Nano composite Adsorbed Paper Electrode

Prepared RGO using modified Hummers' method play an important rule to enrich conductivity of electrode. When RGO is adsorbed on cellulose paper, then cellulose paper can be used as electrode in the substitute of Cu electrode with Zn electrode in bio-voltaic cell. On the other hand, when RGO adsorbed paper electrode has been kept under Ag NPs solution then it forms RGO-Ag Nano composite. As a result, conductivity of electrode enriches abruptly from existing state. That's why voltage, current and power performance enrich from existing state. Using this procedure cost can be reduced to fabricate the bio-voltaic cell.

2.25 How to act Ag NPs on RGO

When RGO adsorbed paper electrode is kept under Ag NPs solution, Ag NPs are wrapped on RGO adsorbed paper electrode. As a result, RGO-Ag nanocomposit is formed. [175]. For excellent conductivity power of RGO, voltage, current and power have been significantly improved from previous condition.

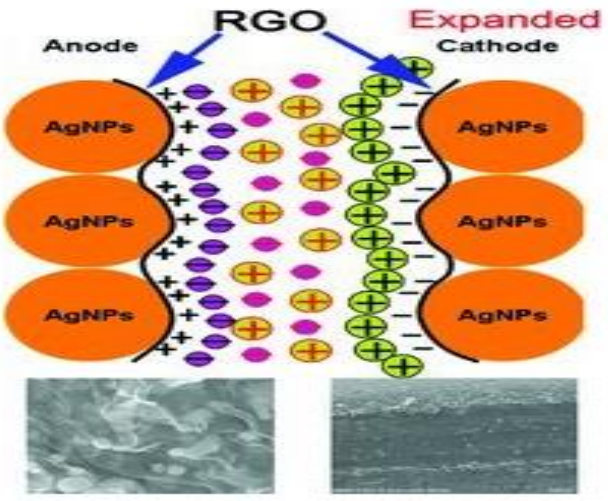

Figure 2.31: RGO-AgNPs nanocomposit [175]

2.26 Cost Analysis

Generally a 6V cell consists of 12 copper plates and 18 zinc plates. The average area of these electrodes is 10426 mm^2 or 1.04 cm^2 approximately. So, the total area of zinc and copper plate in a 6V cell is approximately 18.72 cm^2 and 12.48 cm^2 and the weight of 18 zinc plates is 750 (g) and for copper is 350 (g) approximately. These electrodes have been set in a blank plastic battery box. The total cost of building a cell like this will be,

Cost of 1Kg Zinc = 250TK

Cost of 1Kg Copper = 1000TK

So, the cost of 750 (g) 18 zinc plates is 187.5TK and 350 (g) or 12 copper plates is 350TK.

The price of plastic box is 150TK. Rubber separator and electric wires only 50TK only. So, total price of a single cell will not be greater than 750TK. To construct 10 similar kind of cell will cost 7500 TK-9000TK. The electrolyte or PKL/AL extract is free because it can cultivate or available in local area. So, only 9000TK will be the cost of a 50W PKL/AL mini power plant. This 50W power source can run 5-15 LED bulbs or other electrical components. This cells can work well up to 1year. Only by changing zinc plates and washing the copper plates we can use again these cells.

On the contrary, to fabricate TVC single cell around 1200 TK required. Because, the price of H_2SO_4 (98%), is 30,000TK per ton currently.

Chapter 3

RESULTS and DISCUSSION

Chapter 3: Results and Discussion

3.1 Effect of AL living plant in bio-voltaic cell (BVC)

Three parameters such as open circuit voltage, V_{oc} (V), short circuit current, Isc (A) and power, $P_{max} = V_{oc} \times I_{sc}$ (W) are measured to check the performance to develop BVC using Zn, Cu electrode and AL living plant. The area of the Zn plate was 7.14 cm^2, 5.06 cm^2 and 6.5 cm^2 for leaf 1, 2 and 3 respectively and the area of Cu plate was 9.6 cm^2, 5.76 cm^2 and 6.5 cm^2 for leaf 1, 2 and 3 respectively. Embedded average area of three Zn is 3.57 cm^2 and three Cu is 2.53 cm^2.

3.1.1 Open circuit voltage, V_{oc} (V) of bio-voltaic cell (BVC) using AL living plant

An experimental investigation of open circuit voltage, V_{oc} (V) from living AL plant has studied and given below-

Figure 3.1: Measuring voltage from living AL plant

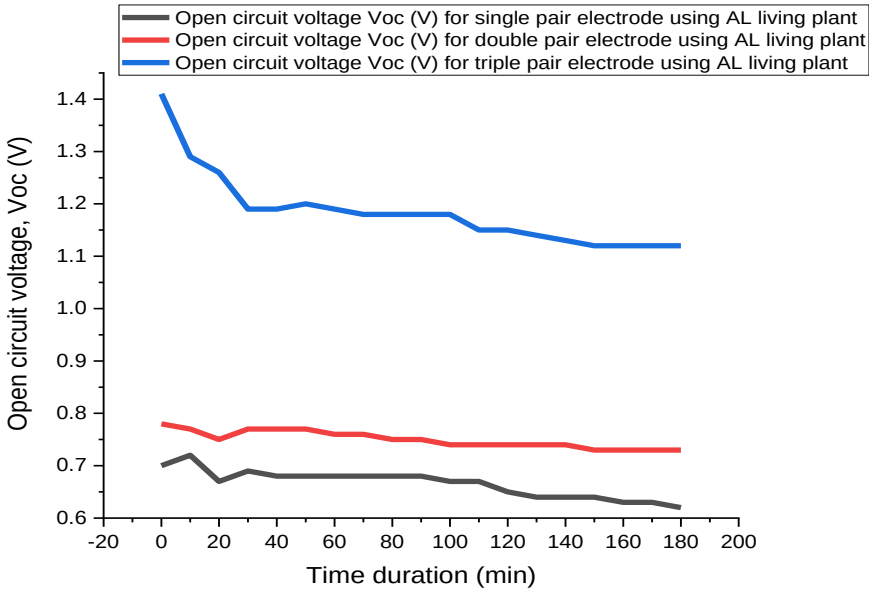

Figure 3.2: Variation of V_{oc} (volt) with time (min) in different pair of AL leaves.

The figure 3.2 shows the open circuit voltage, V_{oc} (V) of BVC using double and triple pair electrctrode. The BVC using triple electrode pair shows better performer than that of double electrode pair. As the exposed area of midrib of living plant increases, the electrolyte area increases. As a result open circuit voltage (V_{oc}) of BVC increases which is consistent wih the published result [236].

The figure 3.2 also shows that at first open circuit voltage (V_{oc}) of triple pair electrctrode decreased rapidly from 1.4 volt to 1.17 volt covering 25 minutes. Then decreased very slowly and almost linearly up to 1.14 volt. Beside this open circuit voltage (V_{oc}) of double pair electrctrode did not decreased abruptly. On the otherhand, open circuit voltage (V_{oc}) of single pair electrctrode fluctuate i.e. at first increased 0.1 volt then decreased and finally was almost linearly decreased. We can conclude from the information that, with the increasing electrode pair of leaf, the voltage of BVC increased.

3.1.2 Short circuit current, I_{sc} (A) of BVC using AL living plant

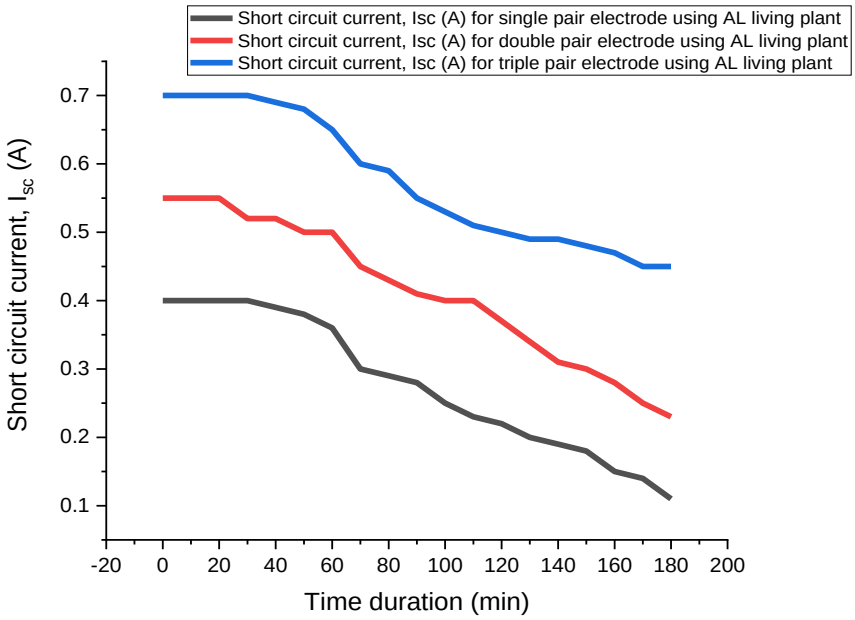

Figure 3.3: Variation of I_{sc} (A) with time (min) in different pair of AL leaves

The figure 3.3 shows the short circuit current, I_{sc} (A) of BVC using double and triple pair electrctrode. The BVC using tripe electrode pairs are better performer than the short circuit current, I_{sc} (A) of double electrode pair with AL living plant electrolyte. As the exposed area of midrib of living plant increases, the flow of electron increases. As a result the developed BVC shows better performance which is consistent wih the published result [236, 237].

The figure 3.3 also shows that short circuit current, I_{sc} (A) of triple pair is 0.15 (A) greater than double pair in BVC. When, embedded area of Zn 5.06 cm^2 and embedded area of Cu 5.76 cm^2. The % of current, I_{sc} (A) variation using double pair (0.4-0.23)/0.23 = 0.73 % and the % of current, I_{sc} (A) variation using triple pair (0.7-0.43)/0.43 = 0.62%.

3.1.3 Power (W) of BVC using AL living plant

Figure 3.4: Measuring power in AL leaves

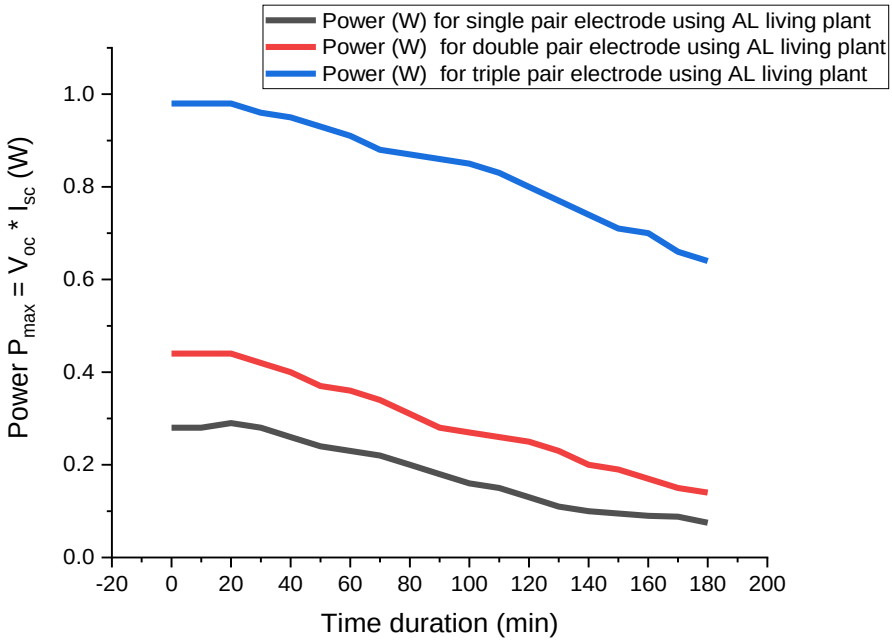

Figure 3.5: Variation of power (W) with time (min) in different pair of AL leaves.

The figure 3.5 shows that the power (W) of BVC using double and triple pair electrctrode.The BVC using tripe electrode pairs are also better performer than double electrode pair. Because,

when open circuit voltage (V_{oc}) and short circuit current, Isc (A) increase than power increase automatically [236, 237].

The figure 3.5 also shows that the power (W) of trriple electrode pair is 0.57 (W) greater than double electrode pair in BVC using AL living plant electrolyte when embedded area of Zn 5.06 cm^2 and embedded area of Cu 5.76 cm^2. The % of power (W) variation using double pair (0.43-0.15)/0.15 = 1.86 % and the % of power (W) variation using triple pair (0.90-0.63)/0.63 = 0.27%.

3.2 Effect of PKL living plant in BVC

To study the performance of PKL living plant, here also measured three parameters of BVC such as open circuit voltage, V_{oc} (V), short circuit current, I_{sc} (A) and power, $P_{max} = V_{oc} \times I_{sc}$ (W) using Zn and Cu electrode and PKL living plant as electrolyte. The area of the Zn plate 7.14 cm^2 , 5.06 cm^2 and 6.5 cm^2 for leaf 1,2 and 3 respectively and the area of Cu plate 9.6 cm^2, 5.76 cm^2 and 6.5 cm^2 for leaf 1,2 and 3 respectively. Embedded average area of three Zn is 3.57 cm^2 and three Cu is 2.53 cm^2.

3.2.1 Open circuit voltage, V_{oc} (V) of BVC using PKL living plant

The open circuit voltage, V_{oc} (V) have been measured from PKL living plant as below:

Figure 3.6: Measuring voltage and current from PKL leaves

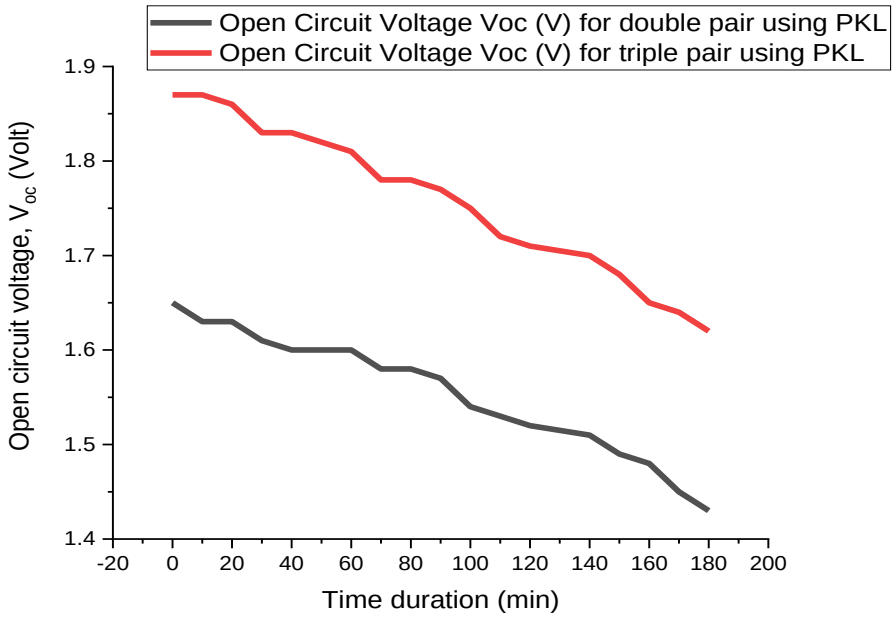

Figure 3.7: Variation of V_{oc} (volt) with time (min) in different pair of PKL leaves.

The figure 3.7 shows the open circuit voltage, V_{oc} (V) of BVC using double and triple pair electrctrode. The BVC using tripe electrode pair are better performer than double electrode pair using PKL living plant electrolyte. As the exposed area of midrib of living plant increases, the electrolyte area increases. As a result open circuit voltage, V_{oc} (V) of BVC increases which is consistent wih the published result [236,237,238].

The figure 3.7 also shows that open circuit voltage, V_{oc} (volt) of tripe electrode pair is 0.21 (W) greater than double pair electrctrode using PKL living plant as electrolyte in BVC when embedded area of Zn 5.06 cm^2 and embedded area of Cu 5.76 cm^2. The % of voltage, V_{oc} (V) variation using double pair electrode (1.65-1.43)/1.43 = 0.15% and the % of voltage, V_{oc} (V) variation using triple pair electrode (1.87-1.62)/1.62 = 0.40%.

3.2.2 Short circuit current, I_{sc} (A) of BVC using PKL living plant

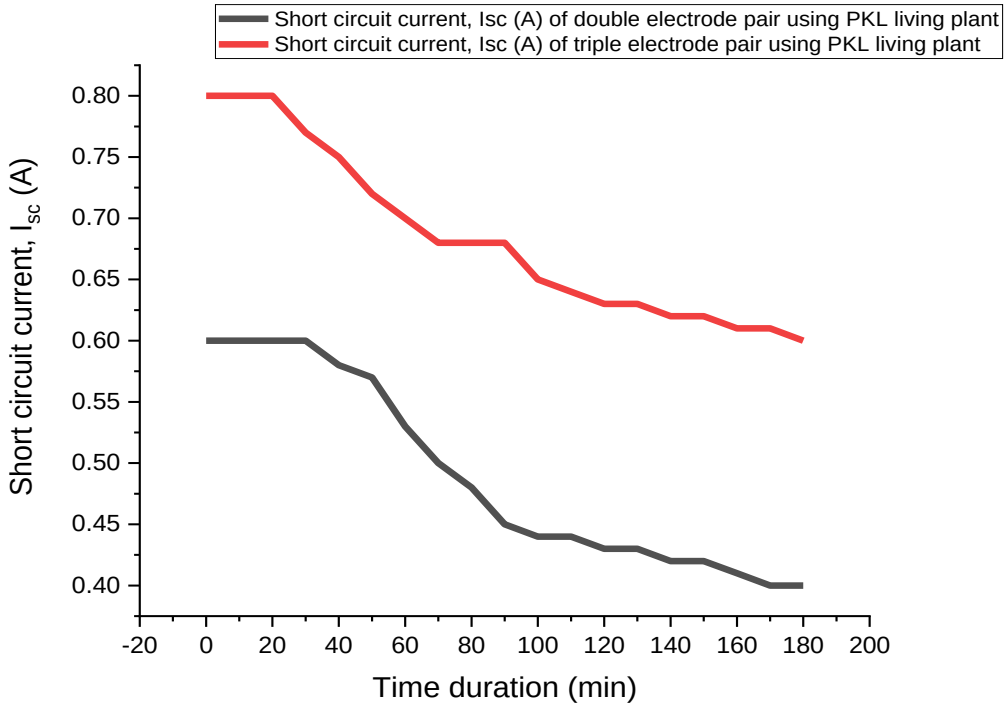

Figure 3.8: Variation of I_{sc} (A) with time (min) in different pair of PKL leaves

The figure 3.8 shows the short circuit current, I_{sc} (A) of BVC using double and triple pair electrctrode. The BVC using tripe electrode pairs are better performer than the short circuit current, I_{sc} (A) of double electrode pair with PKL living plant electrolyte. As the exposed area of midrib of living plant increases, the flow of electron increases. As a result the developed BVC using triple electrode pair shows better performance which is consistent wih the published result [236, 237,238].

The figure 3.8 also shows that short circuit current, I_{sc} (A) of triple pair is 0.20 (A) greater than double pair in BVC. When, embedded area of Zn 5.06 cm^2 and embedded area of Cu 5.76 cm^2. The % of current, I_{sc} (A) variation using double pair electrode (0.60-0.40)/0.40 = 0.33 % and the % of current, I_{sc} (A) variation using triple pair (0.8-0.60)/0.60 = 0.33%.

3.2.3 Power (W) of BVC using PKL living plant

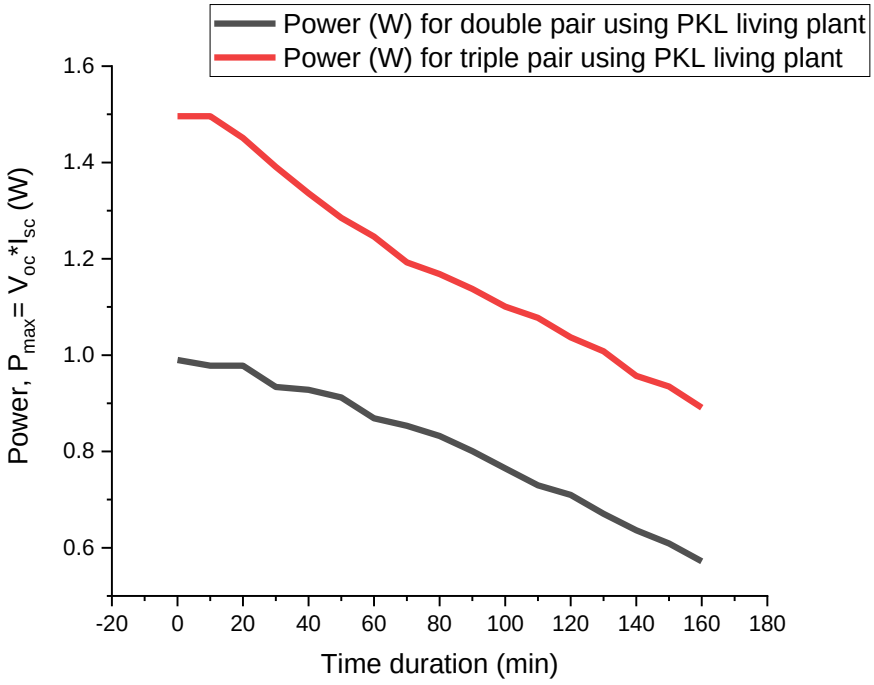

Figure 3.9: Variation of power (W) with time (min) in different pair of PKL leaves.

The figure 3.9 shows that the power (W) of BVC using double and triple pair electrctrode.The BVC using tripe electrode pairs are also better performer than double electrode pair using PKL living plant electrolyte. Because, when open circuit voltage (V_{oc}) and short circuit current, I_{sc} (A) increase than power increase automatically [236, 237,238].

The figure 3.9 also shows that the power (W) of trriple electrode pair is 0.50 (W) greater than double electrode pair in BVC using PKL living plant electrolyte when embedded area of Zn 5.06 cm^2 and embedded area of Cu 5.76 cm^2. The % of power (W) variation using double pair electrode (0.99-0.572)/0.572 = 0.73 % and the % of power (W) variation using triple pair electrode (1.496-0.891)/0.891 = 0.68%.

3.3 Comparative performance of BVC using PKL and AL living Plant

Table 3.1: Comparative performance of BVC using PKL and AL living Plant

No.	Performance parameters of BVC	Type of plant leaf used	Highest magnitude of measured parameters	
			Double pair electrode	Tripe pair electrode
1	Open circuit voltage, V_{oc} (V)	AL	0.78	1.4
		PKL	1.65	1.87
2	Short circuit current, I_{sc} (mA)	AL	0.55	0.7
		PKL	0.60	0.80
3	Power, $P_{max} = V_{oc} \times I_{sc}$ (W)	AL	0.43	0.99
		PKL	1.00	1.50

It is clear from the above table 3.1 that BVC developed using PKL living plant showed better performance than that of the cell developed using AL living plant. As the expose area of midrive of living plant increases, the developed bio-voltaic cell (BVC) showed better performance which is the consistent with the published result [236].

3.4 Effect of PKL extract in bio-voltaic cell

Parameters such as open circuit voltage, short circuit current, load voltage, load current, voltage regulation, internal resistance and power are measured to check the performance analysis of PKL bio-voltaic cell, which are described below:

3.4.1 Open circuit voltouage, V_{oc} (V) of BVC using PKL extract

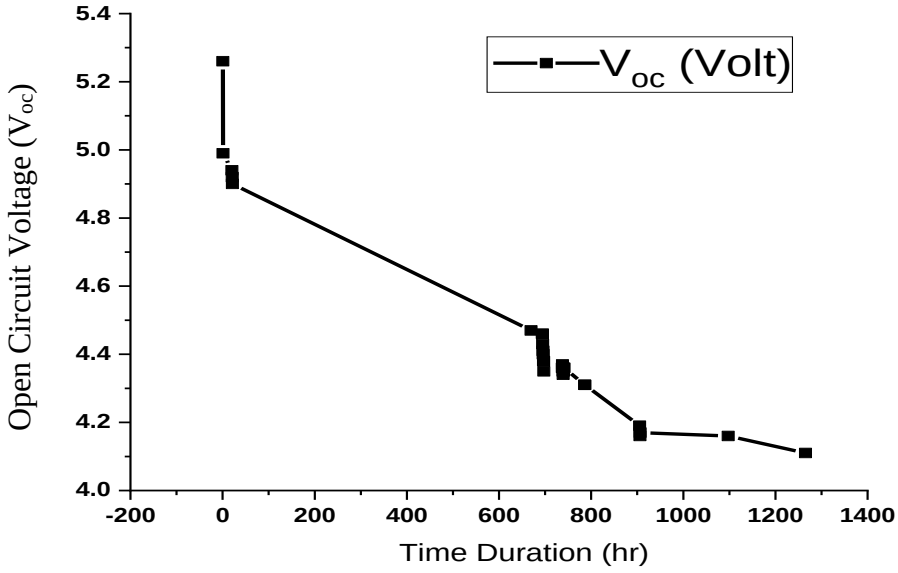

Figure 3.10: Variation of V_{oc} (V) with time duration (hr)

The figure 3.10 shows the open circuit voltage, V_{oc} (V) of BVC using PKL extract electrolyte. At first open circuit voltage, V_{oc} (V) reduced rapidly. Because, the independent function time duration range was very high with the dependent function open circuit voltage (V_{oc}) Volt range was very low. That is why from the graph it is shown the open circuit voltage (V_{oc}) Volt decreases very fast. That means, only 0.3 Volt reduced covering 50 hours.

The figure 3.10 also shows that at first open circuit voltage (V_{oc}) rapidly decreases from 5.30 (V) to 5.00 (V) within 50.00 hour. Then it decreases from 5.00 (V) to 4.90 (V) within very short time. But it steadily decreases from 4.90 (V) to 4.40 (V) covering 700 hours. Again, it abruptly decreases from 4.40 (V) to 4.30 (V) and it changes from 4.30 (V) to 4.10 (V) in a steady way. Finally it changes very slowly from 4.10 (V) to 4.05 (V).

3.4.2 Short circuit current, I_{sc} (A) of BVC using PKL extract

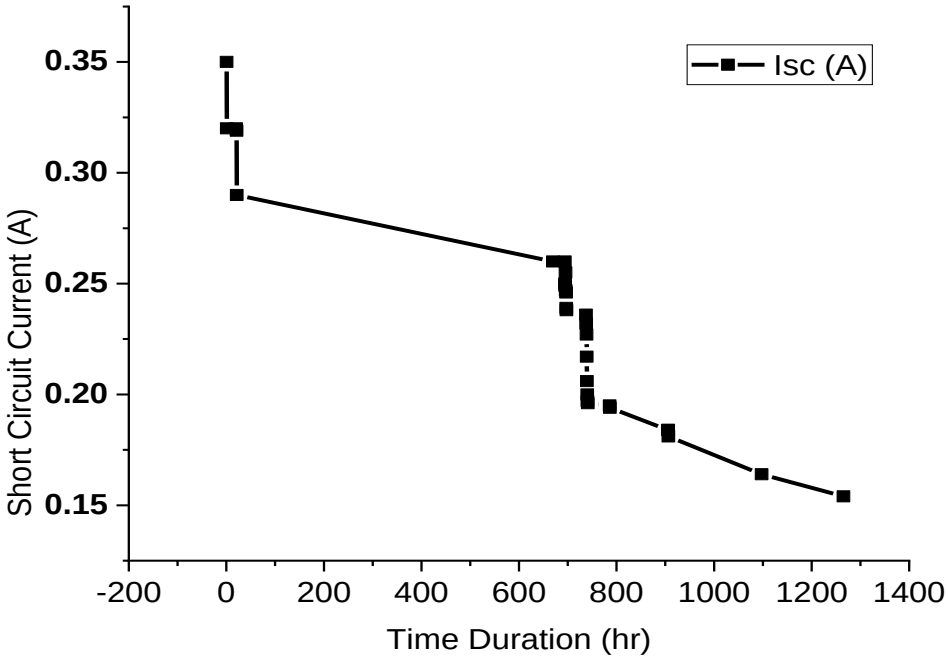

Figure 3.11: Variation of I_{sc} (A) with time duration (hr)

The figure 3.11 shows the short circuit current, I_{sc} (A) of BVC using PKL extract electrolyte. At first short circuit current, I_{sc} (A) reduced rapidly. Because, the independent function time duration range was also very high with the dependent function short circuit current, I_{sc} (A) range was very low. That is why from the graph it is shown the short circuit current, I_{sc} (A) decreases very fast. That means, only 2.97 (A) reduced covering 39 hours.

The figure 3.11 also shows that the short circuit current falls down sharply into two phases; from 0.35 (A) to 0.325 (A) and from 0.325 (A) to 0.280 (A) respectively within 21.5 hours. Then it steadily decreases from 0.28 (A) to 0.26 (A). Then again it falls down sharply into to phases; from 0.26 (A) to 0.23 (A) and from 0.23 (A) to 0.17 (A) respectively. Finally it changes steadily from 0.17 (A) to 0.14 (A).

3.4.3 Power (W) of BVC using PKL extract

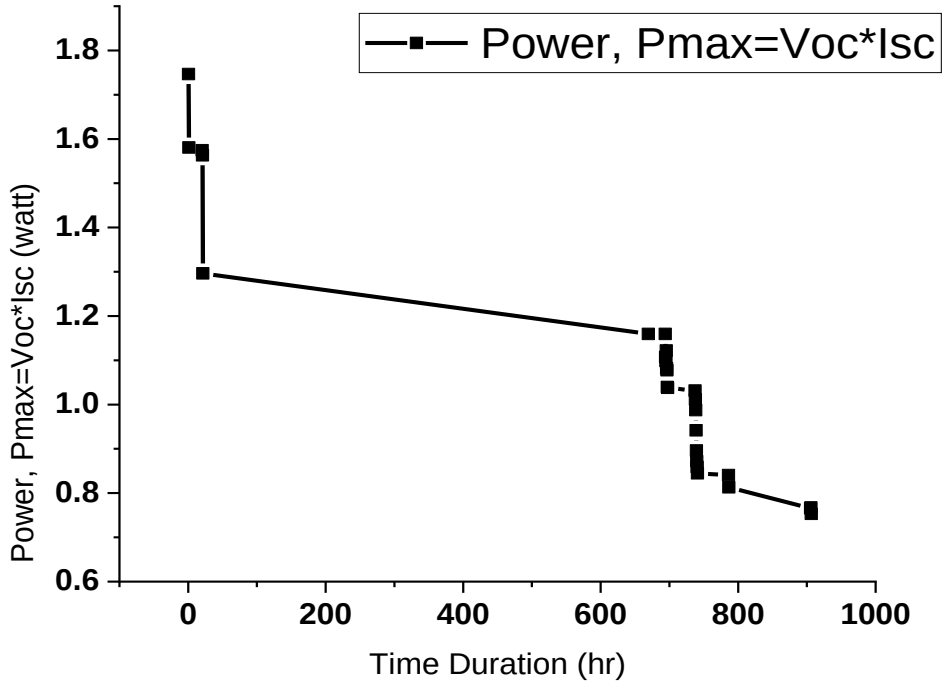

Figure 3.12: variation of power (W) with time (hr) using PKL extract electrolyte

The figure 3.12 shows the power $P_{max} = V_{oc} \times I_{sc}$ (W) of BVC using PKL extract electrolyte. At first power $P_{max} = V_{oc} \times I_{sc}$ (W) reduced rapidly. Because, when open circuit voltage, V_{oc} (V) and short circuit current, I_{sc} (A) reduced gradually then power $P_{max} = V_{oc} \times I_{sc}$ (W) reduced automatically. That is why from the graph it is shown the power $P_{max} = V_{oc} \times I_{sc}$ (W) decreases very fast. That means, only 0.18 (W) reduced covering 40 hours.

The figure 3.12 also shows that power $P_{max} = V_{oc} \times I_{sc}$ (W) falls down sharply into two phases; from 1.75 (W) to 1.60 (W) and from 1.60 (W) to 1.30 (W) respectively within 21.5 hours. Then it steadily decreases from 1.30 (W) to 1.10 (W). Then again it falls down sharply into two phases; from 1.10 (W) to 1.00 (W) and from 1.00 (W) to 0.75 (W) respectively. Finally it changes steadily from 0.75 (W) to 0.50 (W).

3.4.4 Load voltage, V_L (V) of BVC using PKL extract

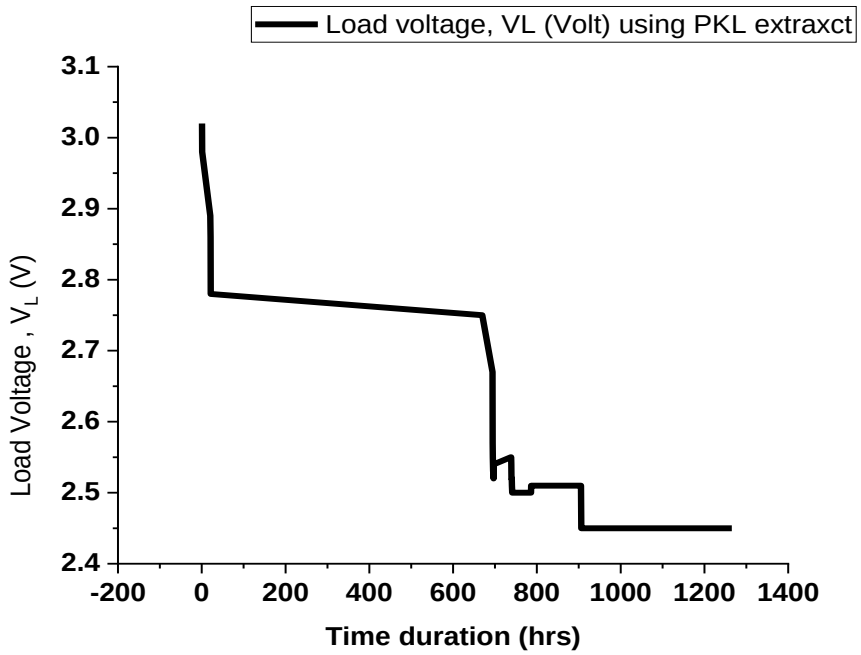

Figure 3.13: Variation of load voltage (V_L) with time duration (hr)

The figure 3.13 shows the load voltage, V_L (V) of BVC using PKL extract electrolyte. Here also load voltage, V_L (V) reduced rapidly. Because, at primary stage concentration of PKL extract electrolyte reduced rapidly. That is why load voltage, V_L (V) reduced sharply which is consistent with the published result [13].

The figure 3.13 also shows that at first load voltage, V_L (V) rapidly decreases from 3.40 (V) to 2.82 (V) within 10.00 hour. Then it decreases from 2.82 (V) to 2.88 (V) very slowly. Again it rapidly decreases from 2.88 (V) to 2.50 (V) covering only 10 hours. Then it fluctuate three times covering 200 hours. Finally it changes very steadily from 2.55 (V) to 2.56 (V) covering 400 hours.

3.4.5 Load current, I_L (A) of BVC using PKL extract

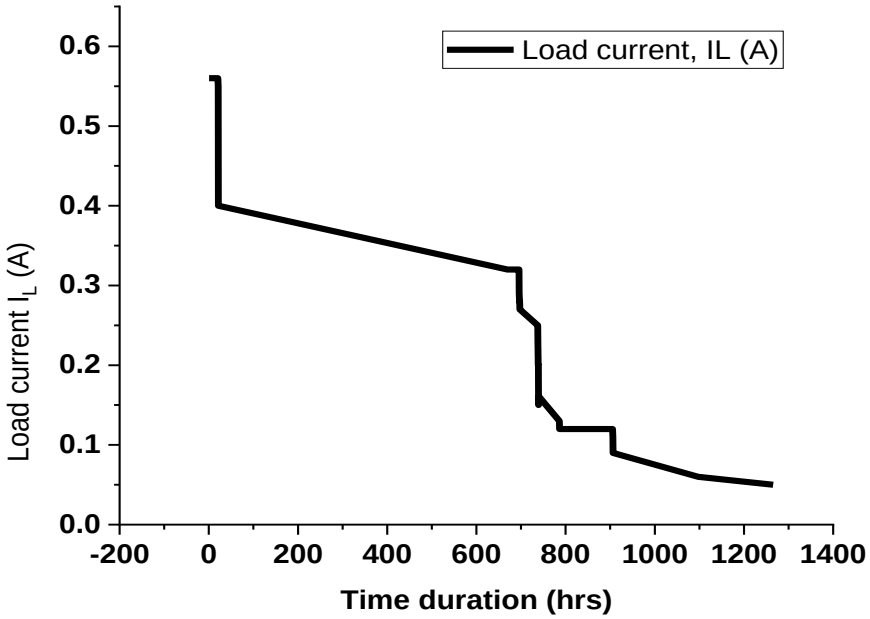

Figure 3.14: Variation of load current, I_L (A) with time duration (hour)

The figure 3.14 shows the the load current, I_L (A) of BVC using PKL extract electrolyte. The load current, I_L (A) reduced rapidly. Because, at primary stage concentration of PKL extract electrolyte reduced rapidly. That is why load current, I_L (A) reduced sharply which is consistent with the published result [13].

The figure 3.14 also shows that at first load current (I_L) rapidly decreases from 5.50 (A) to 4.00 (A) within 10.00 hour. Then it decreases from 4.00 (A) to 3.00 (A) very slowly covering 640 hours. Again it rapidly decreases from 3.00 (A) to 1.00 (A) covering only 70 hours. Then it fluctuate three times covering 210 hours. Finally it changes very steadily from 1.00 (A) to 0.51 (A) covering 410 hours.

3.4.6 Voltage regulation (V_R) of BVC using PKL extract

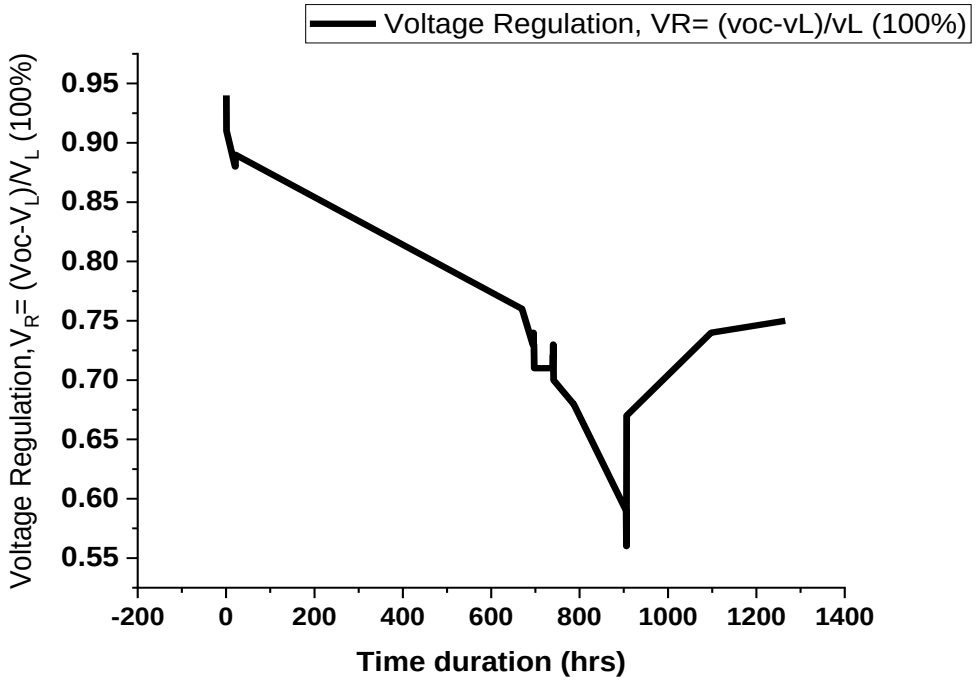

Figure 3.15: Variation of voltage regulation (V_R**)** with time duration (hr)

The figure 3.15 shows the voltage regulation (V_R**)** of BVC using PKL extract electrolyte. At first voltage regulation reduced up to 0.55 then fluctuate and increased up to 0.75. Because voltage regulation is the change of voltage from full loaded to no loaded condition. When there is no load connected then the terminal voltage is equal to the generated voltage. But when load is connected then the terminal voltage becomes less than the no loaded condition [65]. This voltage drop is due to the internal resistance or impedance of the system.

The figure 3.15 also shows that at first voltage regulation (V_R) rapidly decreases from 0.94 to 0.87 within 15.00 hour. Then it decreases from 0.87 to 0.75 very slowly covering 615 hours. Again it rapidly decreases from 0.75 to 0.70 covering only 20 hours. Then it was almost constant 35 hours. Then it's decreases very rapidly from 0.72 to 0.55. Finally voltage regulation (V_R) increased very rapidly from 0.55 to 0.65 within 5 hours. Then steadily increased 0.65 to 0.75.

3.4.7 Internal resistance (Ω) of BVC using PKL extract

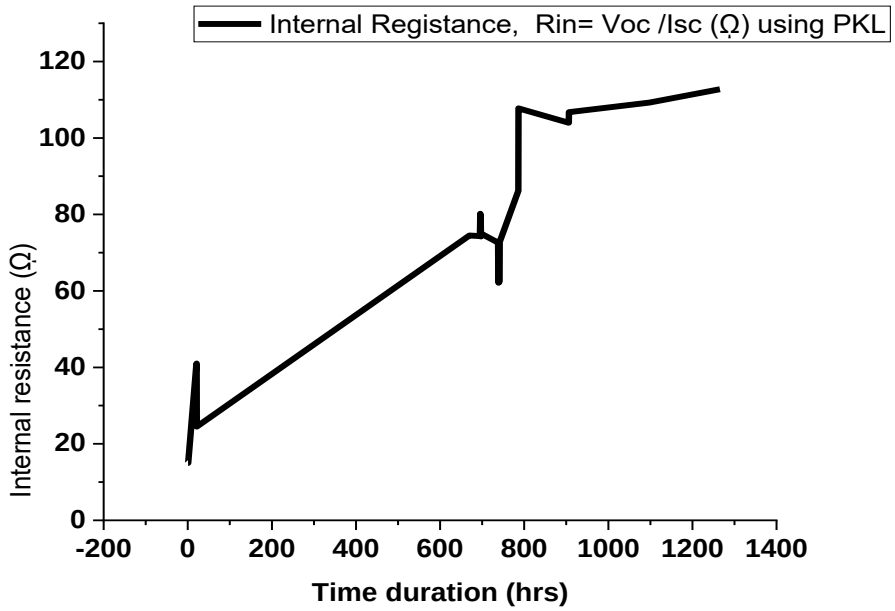

Figure 3.16: Variation of internal resistance (Ω) with time duration (hr)

The figure 3.16 shows the internal resistance (Ω) of BVC using PKL extract electrolyte. The internal resistance found more or less in all kinds of electrical sources [171].The internal resistance of an electrochemical cell is dependent on the specific cell's size, chemical properties, age, temperature and the discharge current. It has an electronic component due to the resistivity of the cell's component materials and an ionic component due to electrochemical factors such as electrolyte conductivity, ion mobility, and electrode surface area. The internal resistance of a battery can be calculated from its open circuit voltage, voltage on-load, and the load resistance:

$$R_{in} = \left(\frac{VNL}{VL} - 1\right) \times R_L$$

Where R_{in} is the internal resistance, V_{NL} is the no load voltage, V_L is the full load voltage and R_L is the resistance of the load connected to that cell.

The figure 3.16 also shows that at first Internal resistance (Ω) rapidly increases from 15 (Ω) to 40 (Ω) within 1.00 hour. Then it sharply decreases from 40 (Ω) to 22 (Ω) covering 0.5 hours. Again it gradually increases from 22 (Ω) to 80 (Ω) covering 648.5 hours. Then it was turned from 80 (Ω) to 62 (Ω) within 45 hours. Again its increases very rapidly from 62 (Ω) to 110 (Ω) within 22 hours. Finally internal resistance (Ω) increased very slowly from 110 (Ω) to 115 (Ω) covering 500 hours.

3.4.8 Load power (W) of BVC using PKL extract

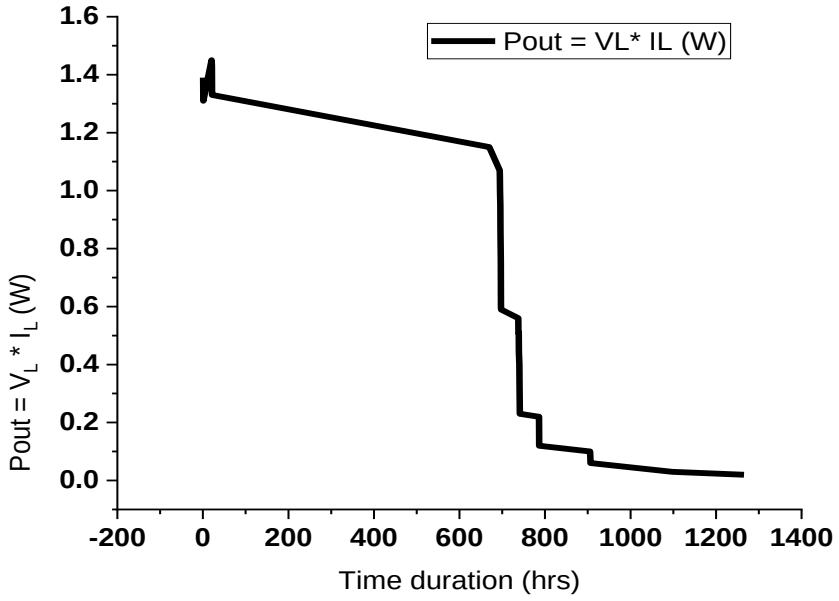

Figure 3.17: Variation of load power, P_{out} (W) with time duration (hr)

The figure 3.17 shows the load power, $P_{out} = V_L \times I_L$ (W) of BVC using PKL extract electrolyte. At first load power, $P_{out} = V_L \times I_L$ (W) has fluctuated then reduced gradually there after reduced rapidly. As the load voltage, V_L (V) and load current I_L (A) reduced, the load power, $P_{out} = V_L \times I_L$ (W) reduced which is consistent with the published result [13].

The figure 3.17 also shows that at first power, $P_{out} = V_L \times I_L$ (W) fluctuate within 2 hours. Then decreases very steadily from 1.30 (W) to 1.10 (W) covering 648 hour. Then it decreases very rapidly from 1.10 (W) to 0.57 (W) within 30 minutes. Again it turn and decreases slowly from 0.57 (W) to 0.50 (W) covering only 10 hours. Then it fluctuate and decrease three times from 0.50 (W) to 0.10 (W) covering 210 hours. Finally it changes very slowly from 0.10 (W) to 0.02 (W) covering 490 hours.

3.4.9 Effect of adding 250 mL more PKL extract with previous PKL extract in BVC

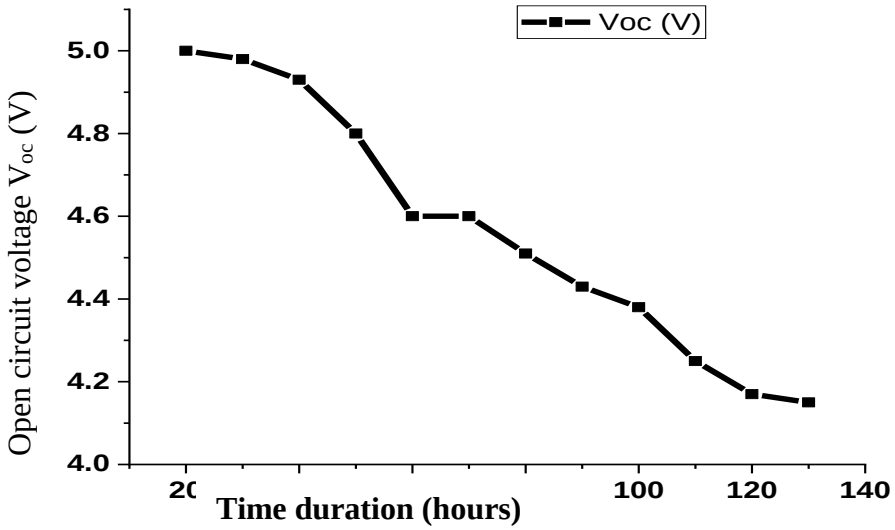

Figure 3.18: Variation of V_{oc} (V) with time duration (hr)

The figure 3.18 shows that, after adding more extract with previous extract open circuit voltage, V_{oc} (V) has increased. Because of adding more extract with previous extract electrolyte has gained more organic acid. As a result, open circuit voltage, V_{oc} (V), short circuit current, I_{sc} (A) and power $P_{max} = V_{oc} \times I_{sc}$ (W) has increased which is consistent with the published result [4].

The figure 3.18 also shows that after adding new extract with existing extract then open circuit voltage upgrades up to 5.00 (V) from previous 4.05 (V). Here, the graph shows that open circuit voltage (V) steadily decreases from 5.00 (V) to 4.60 (V). Then it remains unchanged. Then again it starts to decrease steadily from 4.60 (V) to 4.10 (V).

3.5 Effect of secondary salt in PKL extract BVC

3.5.1 Effect on open circuit voltage, V_{oc} (V) of PKL extract BVC

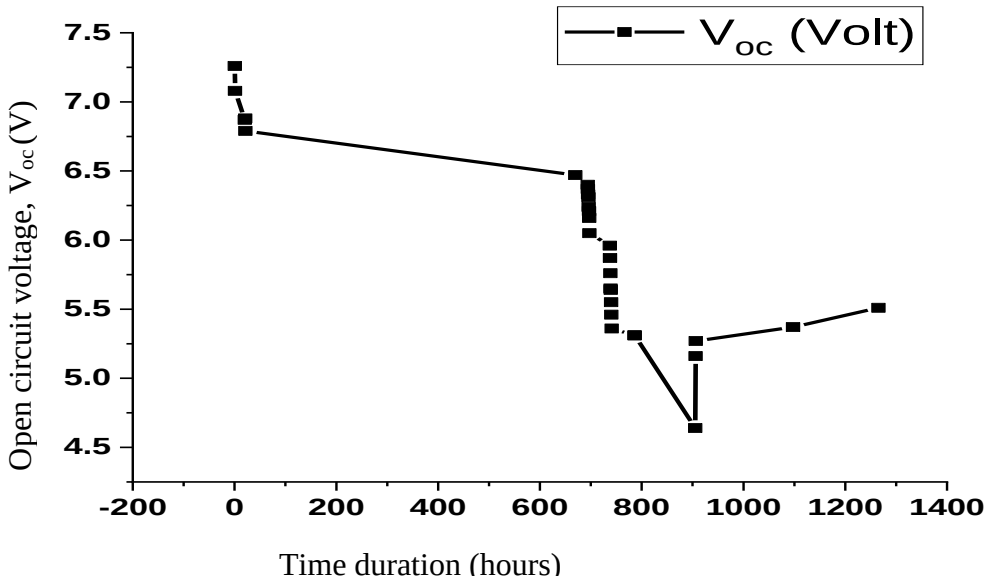

Figure 3.19: Effect of secondary salt on V_{oc} (V) with time duration (hr).

The figure 3.19 shows the effect of secondary salt on open circuit voltage, V_{oc} (V) of BVC using PKL extract electrolyte. Without applying secondary salt open circuit voltage, V_{oc} (V) decreased gradually. But, when secondary salt applied on the cell then open circuit voltage, V_{oc} (V) as well as performance of cell increased from existing state. Because, secondary salt supply Cu^{2+} in electrolyte. As a result, lnQ_c reduced as well as E_{cell} increased which is consistent with the published result [231].

The figure 3.19 also shows that at first open circuit voltage, V_{oc} (V) rapidly decreases from 7.25 (V) to 6.75 (V) within 30 hour. Then it decreases very slowly from 6.75 (V) to 6.50 (V) covering 635 hours. Again it rapidly decreases from 6.50 (V) to 6.00 (V) covering only 10 hours. Then it turned three times and decreased from 6.00 (V) to 4.6 (V) within 250 hours. At this moment secondary salt added. Because of adding secondary salt voltage upgraded from 4.6 (V) to 5.25 (V) within 30 minutes. Then it's gradually increased from 5.25 (V) to 5.50 (V) covering 500 hours.

3.5.2 Effect on power (W) of PKL extract BVC

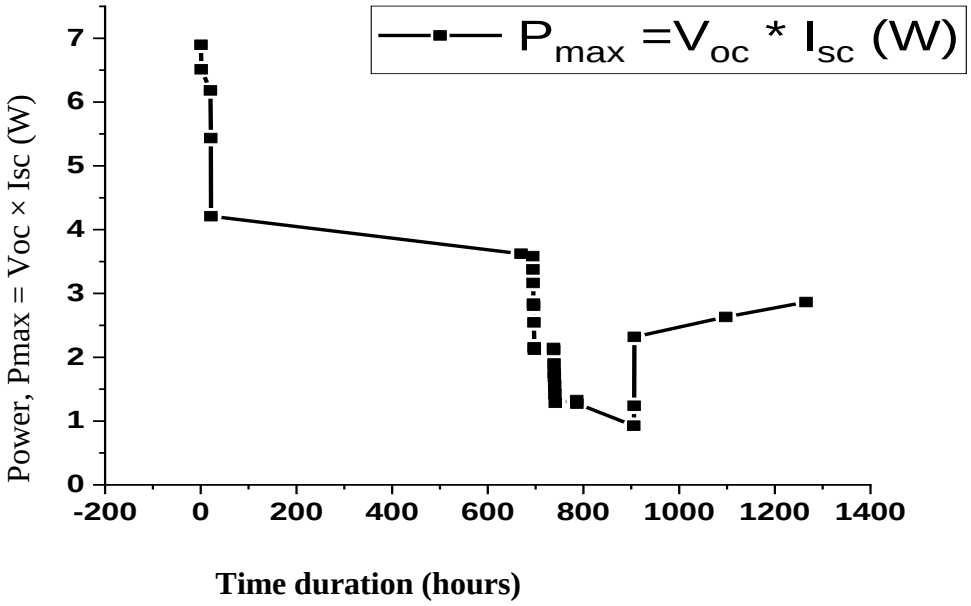

Figure 3.20: Effect of secondary salt on power (W) with time duration (hr)

The figure 3.20 shows the effect of secondary salt on power (W) of BVC using PKL extract electrolyte. Without applying secondary salt power, $P_{max} = V_{oc} \times I_{sc}$ (W) decreased. But, when secondary salt applied on cell then power of cell increased from existing state. Because, secondary salt supply Cu^{2+} in electrolyte. As a result, open circuit voltage, V_{oc} (V) and short circuit current, I_{sc} (A) increased as well as power, $P_{max} = V_{oc} \times I_{sc}$ increased which is consistent with the published result [231].

The graph also shows that at first power, $P_{max} = V_{oc} \times I_{sc}$ (W) rapidly decreases from 6.90 W to 4.20 W within 20 hour. Then it decreases very slowly from 4.20 W to 3.70 W covering 660 hours. Again it rapidly decreases from 3.70 W to 2.00 W covering only 10 hours. Then it turned four times and decreased from 2.00 W to 0.66 V within 140 hours. At this moment secondary salt added. Because of adding secondary salt power, $P_{max} = V_{oc} \times I_{sc}$ (W) upgraded from 0.66 W to 2.40 W within 35 minutes. Then it's gradually increased from 2.40 W V to 2.90 W covering 500 hours.

3.6 Effect of Ag NPs in PKL extract BVC

3.6.1 Characterization of bio-synthesized Ag NPs

3.6.1.1 UV-visible spectra analysis

The bio reduction of $AgNO_3$ solution to Ag nanoparticles was also confirmed by the UV-vis spectroscopy [UV-2102, China]. Generally, Ag NPs reveals the maximum UV-visible absorption in the range of (400 nm-500 nm) due to the surface Plasmon resonance which depends on the size of the Ag NPs [177,178]. Absorption at lower band indicates the smaller particle size whereas higher absorption band affirms the lager nanoparticles [179]. The *d*-band electrons of Ag NPs are uplifted by the absorbing the incident radiat\ion to higher electronic states in the *sp*-band which is the main reason of fluorescence [180]. A surface Plasmon resonance absorption band is appeared due to the combined vibration of free electrons of metal nanoparticles in resonance with exposed light [181]. Ag NPs emits light between (400-700) nm varies with particle size, shape, morphology, and solvents [182,183]. Figure 6 shows the UV- visible spectra of $AgNO_3$ solution, *B. pinnatum* extract, and synthesized Ag NPs.

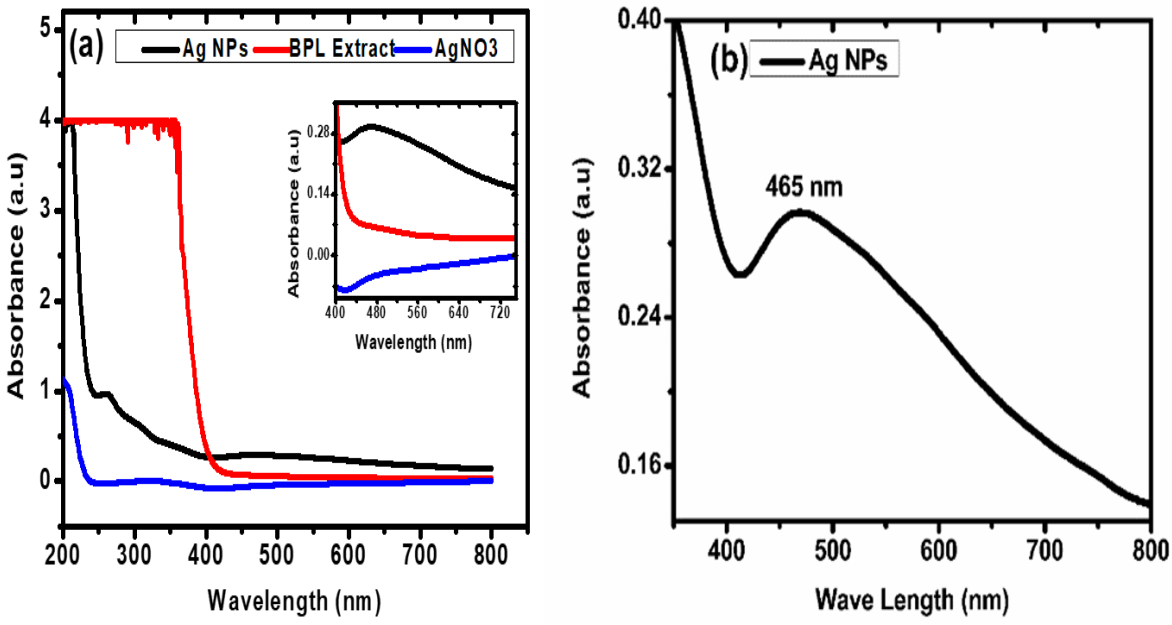

Figure 3.21: UV-vis spectra of (a) Ag NPs, PKL Extract, and $AgNO_3$ (b) Ag NPs

The maximum absorption is observed with a strong broad peak at around 465 nm [Figure 3.25 (b)] due to the conversion of Ag^+ to Ag^0 which is related to the surface plasmon absorption of Ag NPs [184]. The absorption peak at the higher wavelength near or above 400 nm is originated due to the

larger particle size (around 40 nm) [185,186]. Moreover, color change of the solution is occurred for the radiation absorption in the visible region of the electromagnetic spectrum due to the localized surface plasmon of silver nanoparticles [187,188]. During the synthesis process addition of *B. pinnatum* extract to $AgNO_3$ solution led to changes the color of solution to dark-brown visually observed, which indicates the formation of Ag^0 from the $AgNO_3$ solution. The free electrons of Ag NPs yield a surface resonance absorption band due to the mutual vibration of electrons in resonance with light wave [189]. Hence, it is easy to explain that the reducing agent of plant exact played an important role to oxidation of Ag and the color changes of mixture solution along with the wide absorption peak at around 465 nm indicate the formation of Ag NPs.

3.6.1.2 Structural analysis of Ag NPs by XRD

The XRD measurements carried out in the Bragg-Brentano geometry to investigate the crystal structure of as prepared Ag NPs. Powder samples of Ag NPs were subjected to the XRD measurement and figure 4 shows the XRD pattern of Ag NPs. The XRD data reveals diffraction peaks at around 38.12^0, 46.26^0, 64.56^0, and 77.36^0 that confirm the formation of face-centered cubic (FCC) silver nanoparticles which corresponds to (111), (200), (220), and (311) planes respectively [182,190–199].

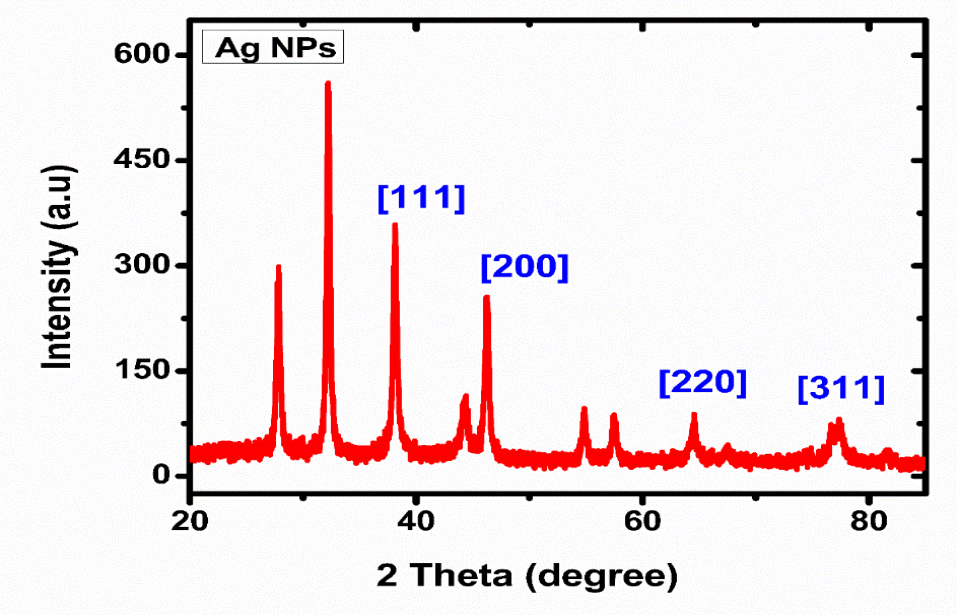

Figure 3.22: XRD pattern of green synthesized Ag NPs

An intense peak at 32.15 is may be appeared for the cubic structure to of AgK_3 [195]. Some of other undefined peaks are also found in the XRD pattern those may be attributed due to the crystallization of bio-organic phase existed in the *B. pinnatum* extract on the surface of green synthesized Ag NPs [200,201]. The XRD pattern demonstrates naturally crystalline Ag NPs

formed by the *B. pinnatum* extract reducing agent and capped with organic bio-molecular compounds on the surface of NPs. The average crystal size of Ag NPs is calculated from the XRD data using Debye-Scherrer formula,

$$D=0.89\lambda/\beta\cos\theta$$

Where, λ is the X-ray wavelength (λ = 1.54056 Å), θ is Bragg's diffraction angle, and β is the full width at half maximum (FWHM) [199,202,203]. The calculated average crystal size of the green synthesized Ag NPs is found ~18 nm.

3.6.1.3 Fourier transformed infrared spectroscopy (FT-IR) analysis

Different functional groups (like flavonoids, polysaccharides, polyphenols, and triterpenoids) of bio-chemical compounds presence in plants extract are responsible for the reduction process of metal nanoparticles from the precursor salt solution [204]. The reduction and the capping of nanoparticles may strongly associate due to the stretching, wagging, and bending vibrations of these functional groups. Possible functional groups which are responsible for the reducing, capping, and efficiently stabilizing of *B. pinnatum* extract mediated Ag NPs were investigated by the FT-IR analysis. The FT-IR spectra revealed from the aqueous *Bryophyllum pinnatum* leaves extract and green synthesized Ag NPs are shown in figure 5.

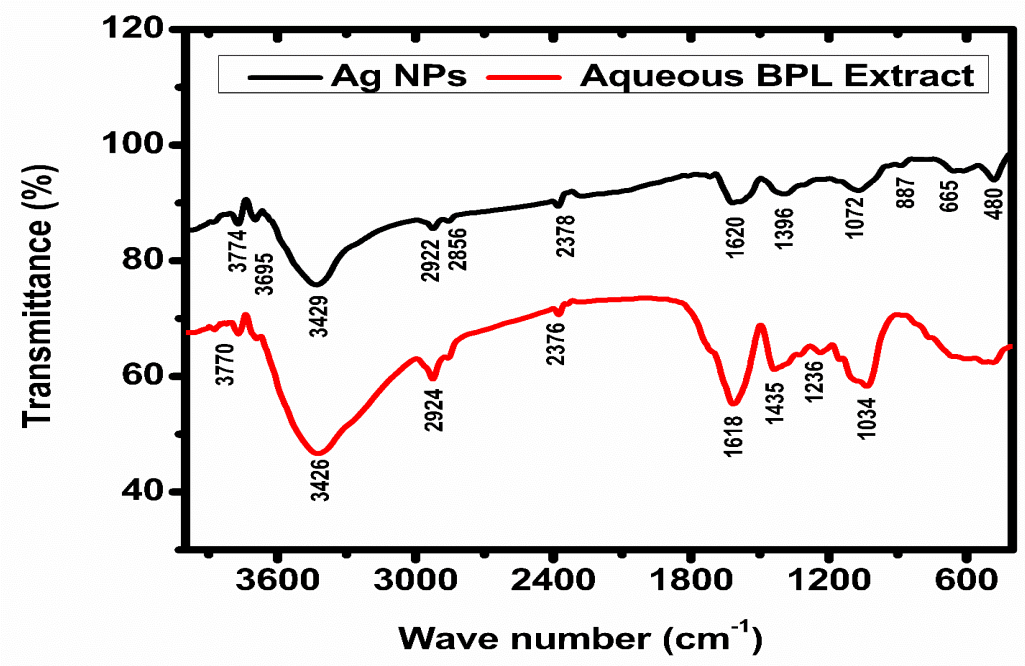

Figure 3.23: FT-IR spectrum of Ag NPs and aqueous *B. pinnatum* Extract

In the spectrum of *B. pinnatum* extract, three prominent peaks were appeared at the wave number values of around 3426 cm^{-1}, 1618 cm^{-1}, and 1034 cm^{-1} are corresponding the stretching vibration

bands of -OH, −C=O, and C-O-C respectively [205,206]. There are some weak peaks also found at around 3770 cm^{-1}, 2924 cm^{-1}, 2376 cm^{-1}, 1435 cm^{-1}, and 1236 cm^{-1} and these peaks are obtained due to the starching vibration bands of -OH, C-H, C≡C, C-H of amine, C-OH respectively [205,206]. Apart from these peaks, few weak signals are found at around 3693 cm^{-1}, 2854 cm^{-1}, 887 cm^{-1}, 665 cm^{-1} which can be originated to the stretching of -OH, alkynes, and N-H of amide group respectively [204–206]. The functional groups may be evolved due to the large number of bio-molecules, like flavones, alkaloids, etc presented in the aqueous leaves extract which can be acted as the reducing and capping agents [205, 224, 225]. The FT-IR spectra of Ag NPs showed almost similar functional groups with some shifting wave numbers due to stretching and bending vibrations of molecular bands which were existed in the plant extract. The similar functional groups, presented in the green synthesized Ag NPs are signifying the encapsulation of Ag NPs with bio-molecules of *B. pinnatum* extract.

In the FT-IR spectra of Ag NPs, all peaks of corresponding functional groups present in the extract were found with the shifting wavenumbers due to the interaction between plant extract and Ag NPs. The FT-IR spectra of Ag NPs revealed several peaks at around 3774 cm^{-1}, 3695.61 cm^{-1}, 3429.43 cm^{-1}, 2922 cm^{-1}, 2856cm^{-1}, 2378 cm^{-1}, 1620 cm^{-1}, 1396cm^{-1}, 1072 cm^{-1}, 887cm^{-1}, 665cm^{-1}, and 480 cm^{-1}. These shifts indicated that Ag NPs may be interacted with the biomolecules such as alcohols, phenols, alkaloids, tannins, terpenes and terpenoids during the reduction, capping and stabilizing processes [196, 226, 227]. The bio-molecules may be attached with Ag NPs during the reduction process of Ag+, alongside capping and stabilization of the Ag NPs.

The peak at around 3774 cm^{-1} may be associated for the stretching vibration of both amide and –OH bond [205,206] whereas the peak at around 3695 cm^{-1} is appeared due to the stretching of -OH [206, 228, 229]. A significant peak at 3429 cm^{-1} is commonly assigned due to -OH stretching of water, H-bonded, alcohol and phenol as functional group [196,201,204-207]. Another two peaks at around 2922 cm^{-1} and 2856 $cm^{-1}$are associated due to the stretching vibration of C-H and alkynes (flavonoids) and the most importantly those strong functional groups were referred as reducing as well as capping agents during the synthesis of metal nanoparticles [198,205,206,208-210]. Moreover, the active band of bio molecular functional groups indicate that the surface of Ag NPs may be coated with the protein layer [198, 230]. The peaks at around 2378 cm^{-1} was appeared due to the stretching vibration of C≡C and a sharp peak at 1620 cm^{-1} may be associated due to the stretching oscillation of −C=O and C-H bands [205,211]. The bending vibration of O-H and CH_3 bond may be responsible for the peak at around 1396 cm^{-1} [196,204]. Another sharp peak at around 1072 cm^{-1} is originated due to the stretching vibrations of O-C and C-N bond of aliphatic amines [205,204,208]. This sharp band indicated the presence of flavanones which are generally absorbed by the surface of metal nanoparticles [189, 222]. The peaks at around 665 $cm^{-1}$and 887 cm^{-1} are appeared due to the N-H stretching of amide group [204, 221, 223], the wagging of N-H primary and secondary amines [208, 214-217]. Moreover, an additional peak at around 480 cm^{-1} is found for the spectrum of Ag NPs which may be appeared due to the O-Si-O stretching, the ring-opening vibration, and deforming oscillations of silica [189,212].

Eventually, it can ascertained that the reduction of Ag^{+} to Ag^{0} from the $AgNO_3$ solution may be attributed due to the presence of flavonoids in plant extract because flavonoids compounds play an important role as the reducing agent to the formation of metal nanoparticles from metal ions [189, 218]. The details of functional groups, appearing on Ag NPs which may be acted as the reducing, capping and stabilizing agents are summarized in table-1.

Table 3.2: Summary of FTIR interpretation of *B. pinnatum* extract mediated Ag NPs

Peak position of Ag NPs (cm^{-1})	Functional groups	References
3774	stretching vibration of amide and –OH bond	[205,206]
3695	stretching of -OH	[206]
3429	-OH stretching of water, H-bonded, alcohol and phenol as functional group	[204,206,207,208,210,212]
2922	stretching vibration of C-H and alkynes (flavonoids)	[198,205,206,208,214]
2856	stretching vibration of C-H and alkynes (flavonoids)	[205,206,208,214]
2378	stretching vibration of C≡C and −C=O bonds respectively	[205]
1620	stretching vibration −C=O and C-H bands	[205,211]
1396	bending of O-H	[204]
1072	stretching vibrations of O-C and C-N bond of aliphatic amines	[204,205,208]
887	N-H stretching of amide group	[204]
665	wagging of N-H primary and secondary amines	[208]
480	O-Si-O stretching, the ring-opening, and deforming oscillations of silica	[189,212]

3.6.1.4 Field emission scanning electron microscopy (FESEM) and EDX analysis

Figure 7(a,b) represent high resolution FESEM image of Ag NPs with different scale. From the FESEM images the spherical nanoparticles are clearly observed and the average particle size to be found in-between 35-40 nm. The particle size and the morphology of metallic nanoparticles may depend on the concentration rate of the capping and stabilizing agents present in the plant extract [213, 219]. EDX data confirm the concentration of Ag NPs with other residuals elements those may be appeared from the environment as well as capping elements from extract. Figure 7c showed the EDX data of green synthesized Ag NPs.

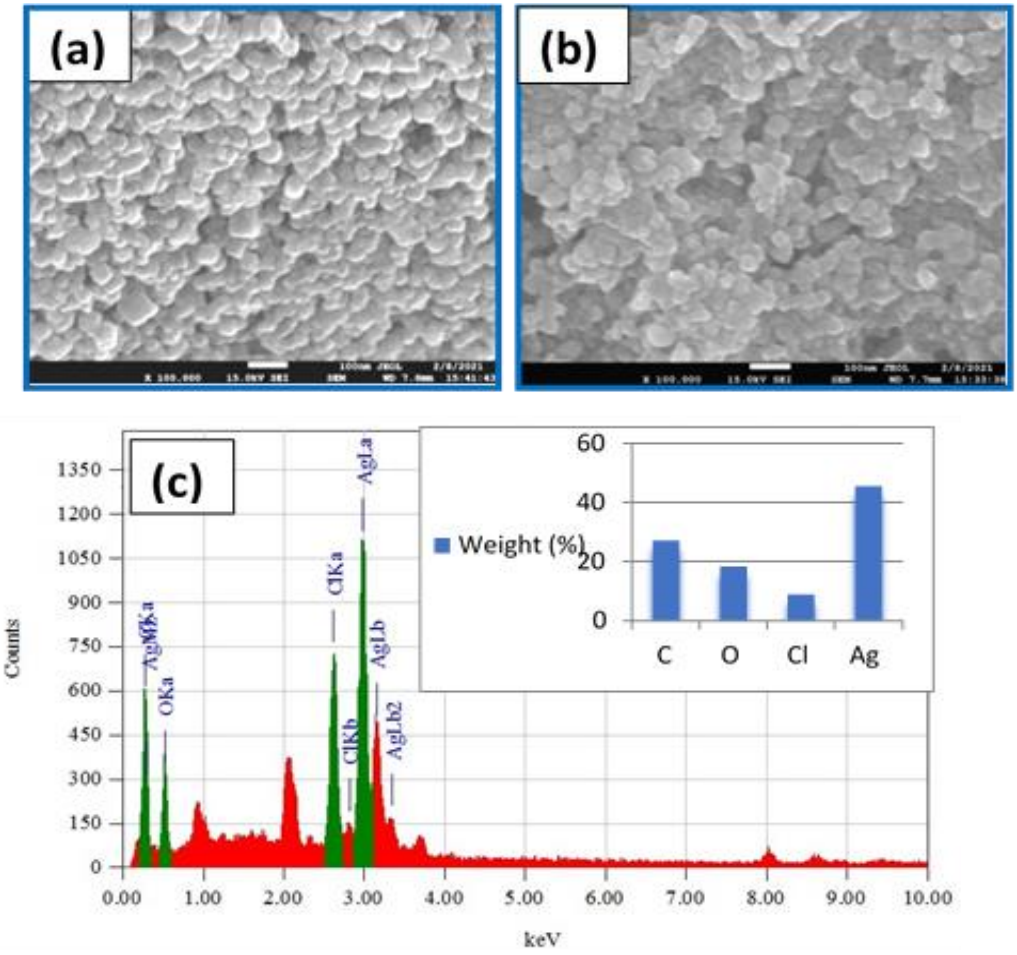

Figure 3.24: (a,b) FESEM images of Ag NPs in different scale and (c) EDX data of Ag NPs

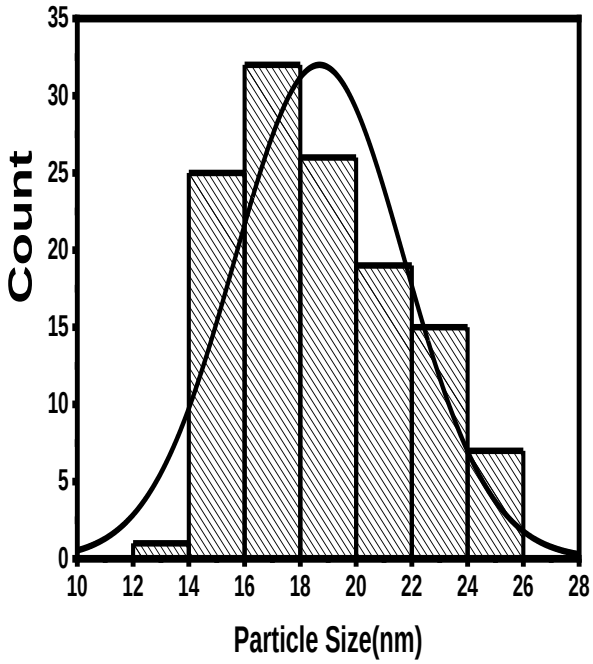

Figure 3.25: Particle size histogram of green synthesized silver nanoparticles.

3.6.2 Effect of Ag NPs in power generation activities of PKL extract BVC

The green synthesized Ag NPs have been applied in the bio-electrochemical cell to understand the impact of NPs on the power development system. Three types of bio-electrochemical cells were designated to perform the electrical analysis of Ag NPs. Figure 3.28 represents the impact of Ag NPs on three bio-electrochemical cells.

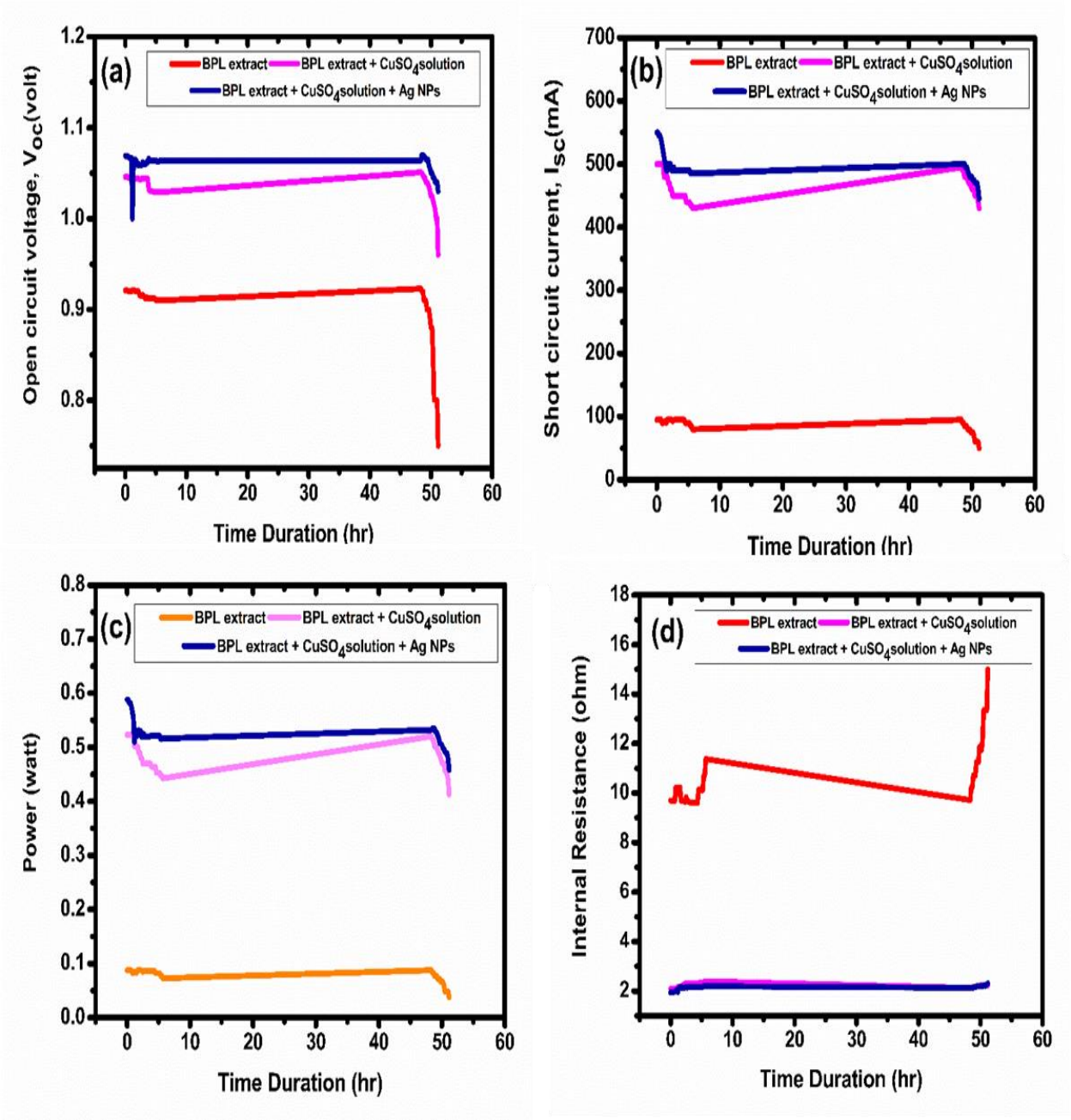

Figure 3.26: Electrical activities of *B. pinnatum* bio-electrochemical cells (a) open circuit voltage (b) short circuit current (c) power, and (d) internal resistance.

Figure 3.26a shows the open circuit voltage with the variation of time duration for different cases. It is shown that the open circuit voltages for case 1 are higher than the other two cases of case 2 and case 3. It is very interesting to say that the voltage for case 1 was almost steady up to 50h whereas the open circuit voltage for case 2 was less than case 3. It is clearly shown that the open circuit voltage for case 3 is less than the other two cases but the change of voltage was almost

constant up to 50 h for all the cases. The maximum voltage for first case is 1.07 volt and the minimum is1.03 volt.

For case 2 the maximum is 1.046 voltage and minimum are 0.96 volt and for only *B. pinnatum* extract [case 1] maximum open circuit voltage is 0.921 volt and minimum 0.75 volt. The difference of maximum open circuit voltage between first and second cases is 0.024 volt. The difference of open circuit voltage between first and third cases is 0.149 volt and the difference of open circuit voltage between second and third cases is 0.125 volt. The results showed that the greater difference was found between case 1 and case 3 that is 0.149 volt which claims the importance of nanoparticles in the open circuit voltage generation on bio-electrochemical cell.

Figure 3.26b shows the short circuit current with variation of time duration for different cases. It is clearly shown that the short circuit current of case 1 is higher than case 2 and case 3. It is also very interesting to say that case 1 gives the maximum short circuit current (600 mA) compare with other two cases and it remained same for 50 h. The minimum value of short circuit current for case 1 is 445 mA which is also greater than case 2 (430 mA) and case 3 (50 mA). Hence, it is evidently shown that the presence of Ag NPs can play very import role to increase the supply of short circuit current with the time duration on the *B. pinnatum* bio-electrochemical cell.

Figure 3.26c shows the calculated power of the cells with the time duration. For the case1 the maximum power is to be calculated 0.642 watt and the minimum value of power is 0.457 watt. For the case 2 and case 3 the highest power is found at 0.575 watt and 0.087 watt respectively and the lowest power for both cases are at 0.412watt, 0.035 watt respectively. It is surprisingly noticeable that after applying the Ag NPs on *B. pinnatum* bio-electrochemical cell, the maximum power is found which is also stable for next 50 h. Finally, the power for case 1 is started to decrease after 50 h but the minimum value is found at 0.458 watt which is even greater than the lowest values of other two cases.

Figure 3.26d represents the internal resistance for all three cases. The internal resistance for only *B. pinnatum* extract bio-electrochemical cell is found higher than the two other cases. After using the secondary solution $CuSO_4$ for case 2 and Ag NPs on case 1, the internal resistance rapidly decreased and the lowest internal resistance is found for case 1 which allows the more current the bio-electrochemical cell.

Table 2 represents the values of average open circuit voltage, short circuit current, power, and internal energy for all of three bio-electrochemical cells. Figure 9 also represents the summary of average open circuit voltage, short circuit current, power, and internal resistance of bio-electrochemical cell.

Table 3.3: Average electrical performances of *B. pinnatum* bio-electrochemical cells

Name of the case	Average open circuit voltage (volt)	Average short circuit current (A)	Average power (watt)	Average internal resistance (ohm)
Case 1	1.059	0.494	0.524	2.144
Case 2	1.035	0.463	0.480	2.234
Case 3	0.899	0.086	0.078	10.537

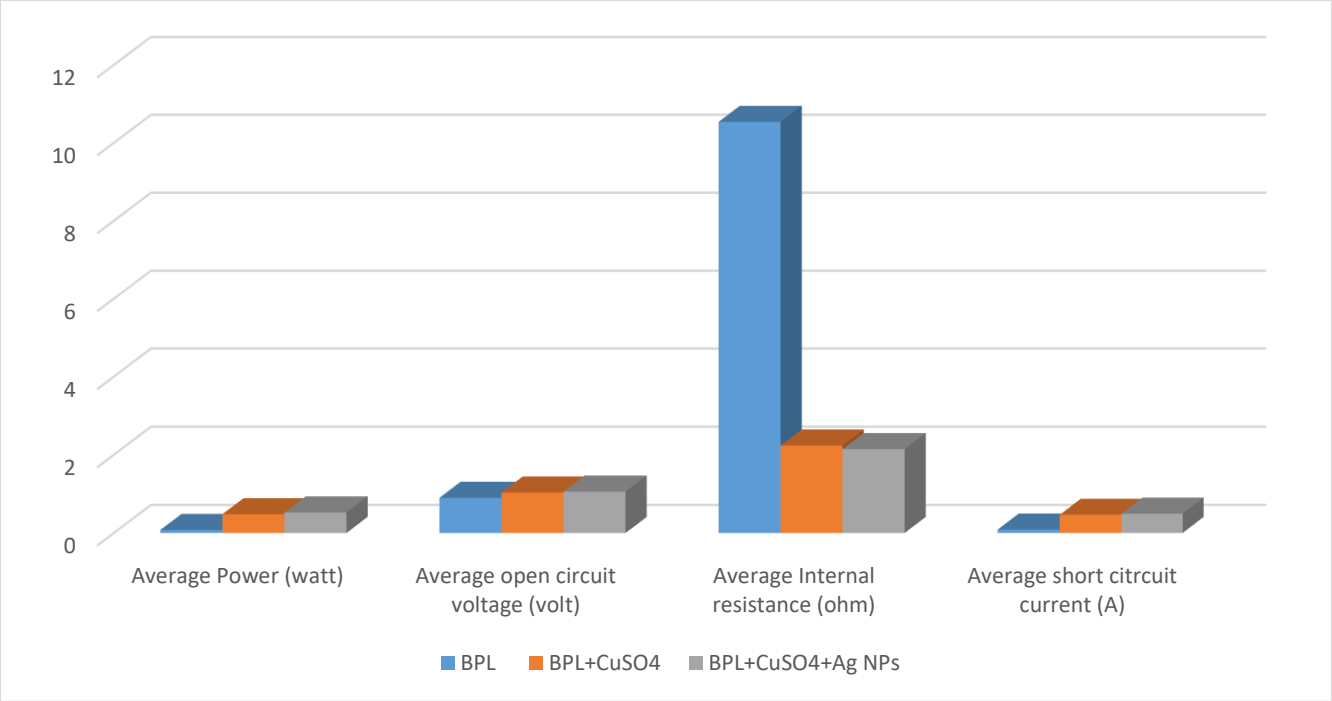

Figure 3.27: Average electrical performances of *B. pinnatum* bio-electrochemical cells.

After applying the Ag NPs on the cell, the open circuit voltage and short circuit current are rapidly increased. As a result, the power of the *B. pinnatum* bio-electrochemical cell is significantly increased. On the other hand, the internal resistance of the cell was found around 10.5 Ω for only *B. pinnatum* extract and it is surprisingly dropped at around 2.2Ω for (*B. pinnatum* +$CuSO_4$ solution) bio-electrochemical cell and the resistance increased at 2.1Ω after adding NPs in cell. In a nutshell, the influences of Ag NPs in the bio-electrochemical cell are remarkable for the future power development applications.

3.7 Effect of AL extract in BVC

Electricity generation from AL extract using various electrode in BVC have been studied very carefully.Various organic compound; especially Apigenin, Luteonin, Anthocyanidin and Cyanidin -3- glucoside [177] are present in AL extract. All of existing compounds in AL are phenolic compounds and form resonance structure. As a result hydrogen ion (H^+) release from compounds and pH range lie between 4.50 to 5.75. In this BVC Zn use as anode and Cu used as cathode. AL extract used as electrolyte. Using secondary salt ($CuSO_4$ $5H_2O$), various NPs and RGO adsorbed paper electrode; voltage, current and power can be increased from existing state.

3.7.1 Open circuit voltage, V_{oc} (V) of BVC using AL extract

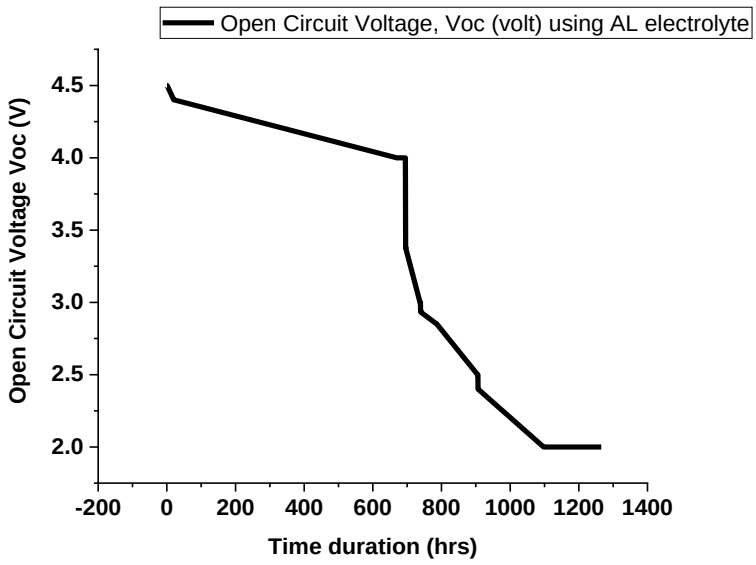

Figure 3.28: Variation of V_{oc} (V) with time duration (hr)

The figure 3.28 shows the open circuit voltage, V_{oc} (V) of BVC using AL extract electrolyte. At first open circuit voltage, V_{oc} (V) rapidly decrease for a while. Because, the independent function time duration range was very high with the dependent function open circuit voltage, V_{oc} (V) range was very low. That is why from the graph it is shown the open circuit voltage, V_{oc} (V) decreases very fast. That means, only 0.2 Volt reduced covering 45 hours.

The figure 3.28 also shows that at first open circuit voltage, V_{oc} (V) rapidly decreases from 4.54 (V) to 4.3 (V) within 10 hour. Then it decreases from 4.3 (V) to 4.00 (V) very slowly. But it abruptly decreases from 4.00 (V) to 3.00 (V) covering 100 hours. Again, it slowly decreases from 3.00 (V) to 2.50 (V) and it changes from 2.51 (V) to 2.00 (V) in a steady way. Finally it changes almost constantly from 2.00 (V) to 2.10 (V).

3.7.2 Short circuit current, I_{sc} (A) of BVC using AL extract

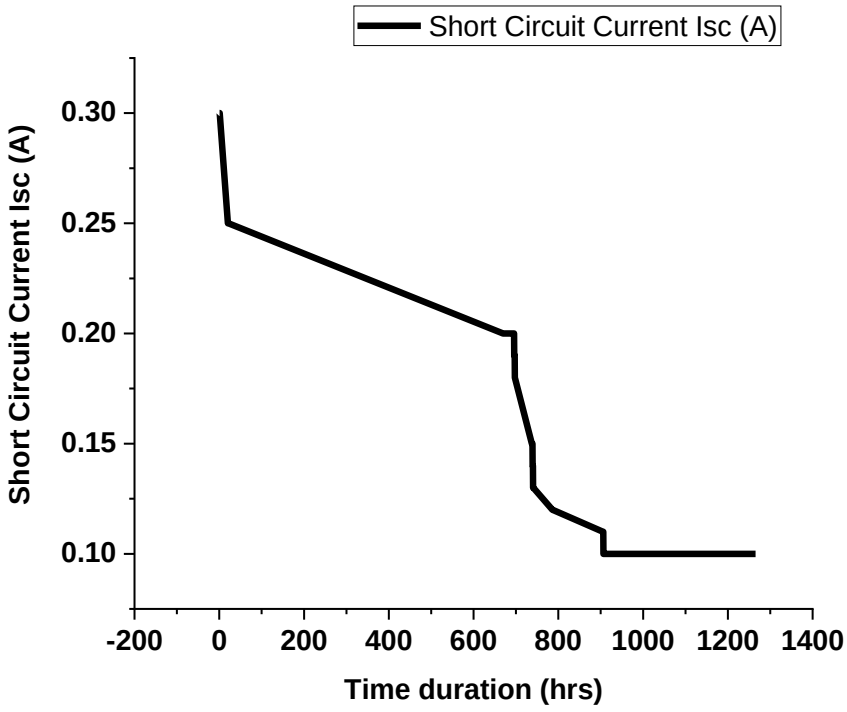

Figure 3.29: Variation of I_{sc} (A) with time duration (hr).

The figure 3.29 shows the short circuit current, I_{sc} (A) of BVC using AL extract electrolyte. At first short circuit current, I_{sc} (A) rapidly decrease for a while. Because, the independent function time duration range was very high with the dependent function short circuit current, I_{sc} (A) range was very low. That is why from the graph it is shown the short circuit current, I_{sc} (A) decreases very fast. That means, only 0.75 (A) reduced covering 48 hours.

The figure 3.29 also shows that short circuit current falls down sharply into four phases. At first from 0.30 (A) to 0.25 (A) decrease very sharply within10 hours then it decrease very slowly from 0.25 (A) to 0.20 (A) very slowly within 700 hours. Then it decreases very fast from 0.20 (A) to 0.14 (A). Then again it falls down sharply into two phases; from 0.14 (A) to 0.12 (A) and from 0.12 (A) to 0.10 (A) respectively. Finally it changes very steadily from 0.10 (A).

3.7.3 Power (W) of BVC using AL extract

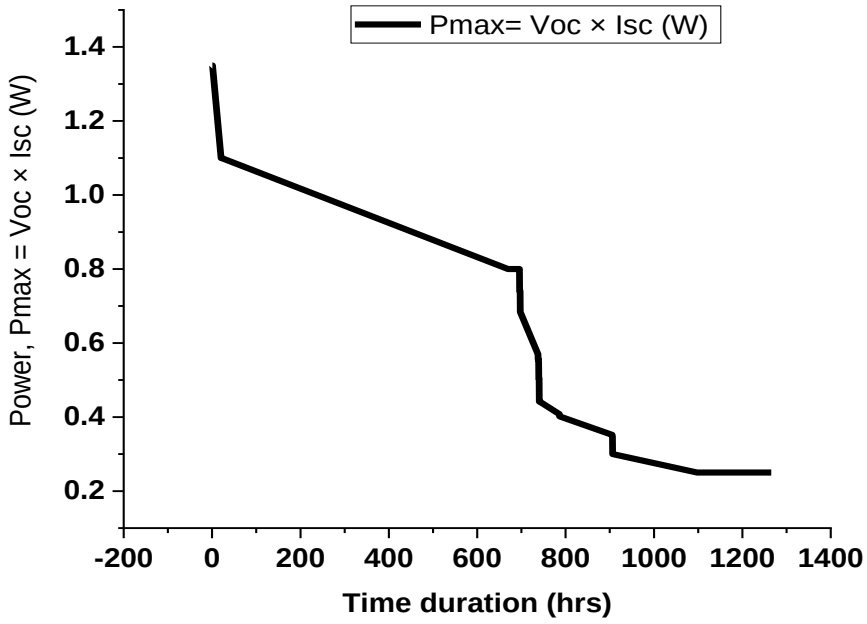

Figure 3.30: Variation of power (W) with time duration (hr)

The figure 3.30 shows the power $P_{max} = V_{oc} \times I_{sc}$ (W) of BVC using AL extract electrolyte. At first power $P_{max} = V_{oc} \times I_{sc}$ (W) reduced rapidly. Because, when open circuit voltage, V_{oc} (V) and short circuit current, I_{sc} (A) reduced gradually then power $P_{max} = V_{oc} \times I_{sc}$ (W) reduced automatically. That is why from the graph it is shown that the power $P_{max} = V_{oc} \times I_{sc}$ (W) decreases very fast. That means, only 0.16 (W) reduced covering 42 hours.

The figure 3.30 also shows that power $P_{max} = V_{oc} \times I_{sc}$ (W) falls down sharply from 1.35 (W) to 1.15 (W) within 20 hours. Then it steadily decreases from 1.15 (W) to 0.80 (W) covering 680 hours. Then again it falls down sharply into three phases; from 0.80 (W) to 0.43 (watt) and from 0.43 (W) to 0.33 (W) and 0.33 (W) to 0.29 (W) respectively within 200 hours. Finally it changes very steadily from 0.29 (W) to 0.520 (W) covering 478 hours.

3.8 Effect of Ag NPs in AL extract BVC

Silver nanoparticles have been applied in the BVC using Arum Leaf (AL) extract electrolyte and the impact of nanoparticles has been monitored. Four types of BVC have been designated with four different bio-electrolyte solutions. Figure 3.31 shows the comparative analysis of electrical parameters for all cells. The open-circuit voltage, short circuit current, power and internal resistance of four cells are shown in Figure 3.31 (a, b, c, d).

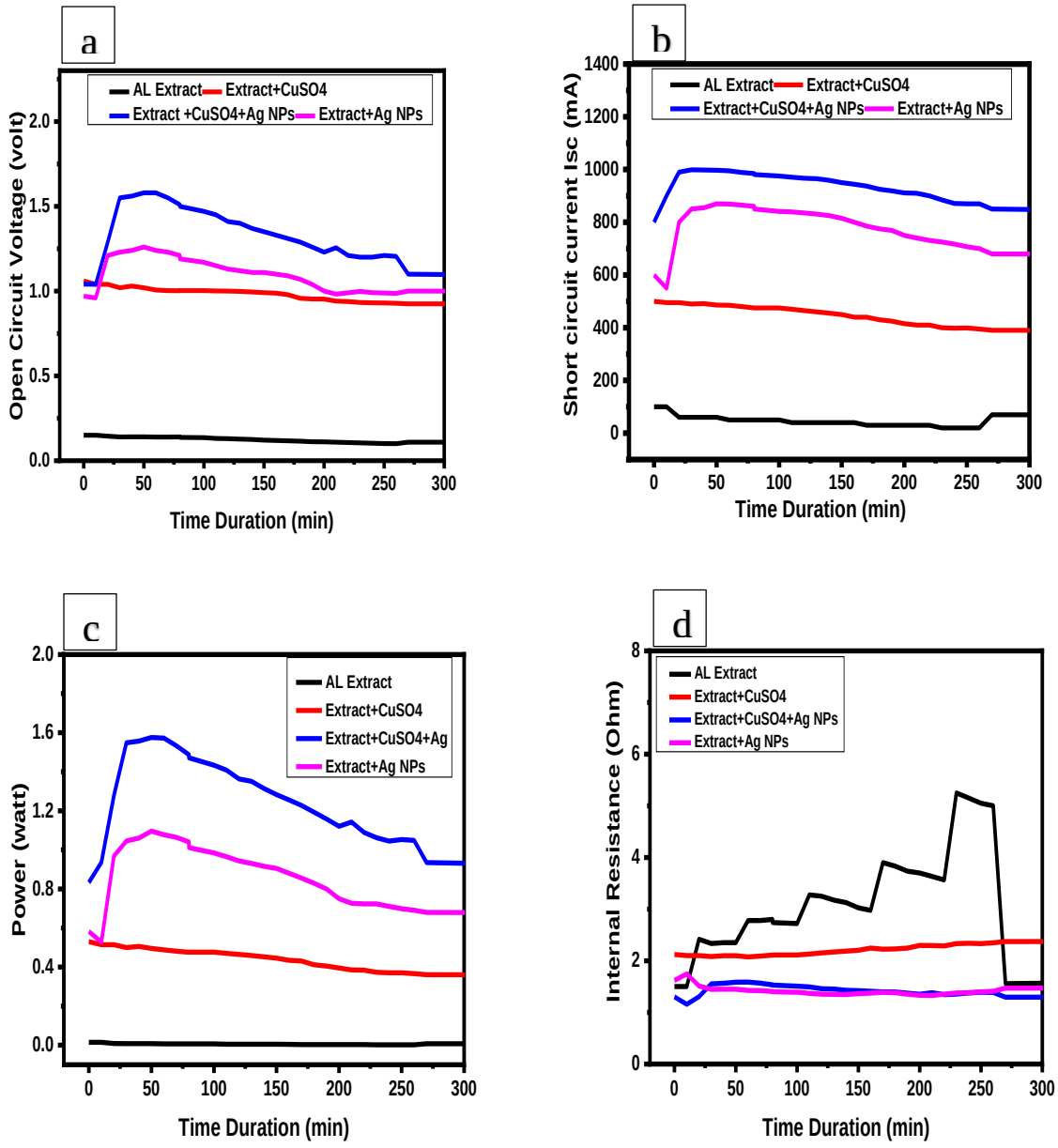

Figure 3.31. Comparative analysis of (a) open-circuit voltage, (b) short circuit current, (c) power, and (d) internal resistance of four bio-electrochemical cells.

The open circuit voltage and short circuit current were significantly increased after using Ag NPs to extract electrolytes. The lowest values of voltage and current were found for only plant extract electrolyte-based cells. After using $CuSO_4$ with extract, the electrical parameters were increased due to the secondary salt effect. Moreover, the current and voltage were surprisingly increased after using silver nanoparticles in bio-electrolyte and the maximum electrical performances were recorded for this case. Since the current and voltage were dramatically enhanced in the presence of nanoparticles. The highest power and the lowest internal resistance were calculated for this cell. Table 3.4 shows the average electrical parameters for four types of cells.

Table 3.4: The average power and capacity for different electrolyte-based BVC

Electrolyte of cell	Average power (Watt)	Average capacity (AH)
Extract	0.0024	0.0803
Extract + $CuSO_4$	0.4379	0.9619
Extract + Ag NPs	0.6224	1.7208
Extract + CuSO4+ Ag NPs	0.7024	2.0630

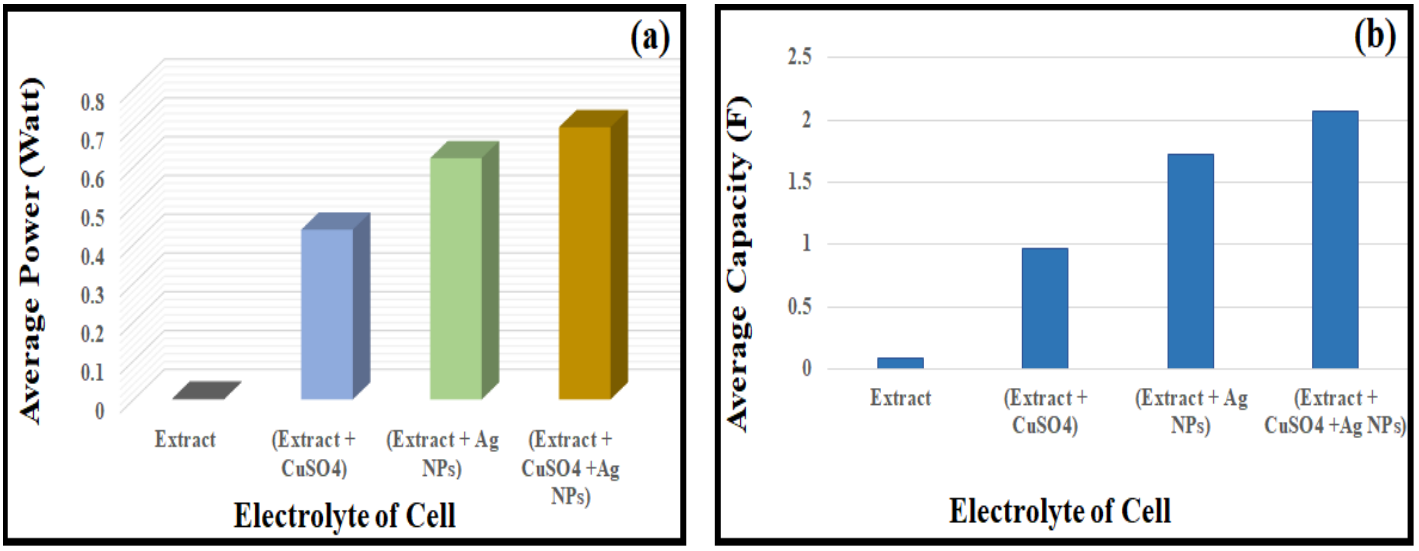

Figure 3.32: (a) Average power and (b) average capacity of four different electrolyte based bio-electrochemical cells.

Figure 3.32 represents the average power and the average capacity of four bio-electrochemical cells. Only AL extract electrolyte-based bio-electrochemical cell shows the minimum power and capacity and the maximum power and capacity were recorded for the (AL extract + $CuSO_4$ + Ag NPs) bio-electrolyte based cell. It is also noticeable that the (AL extract + Ag NPs) electrolyte-based cell showed the second-highest power and capacity among four cells which are even more significant than the (AL extract + $CuSO_4$) electrolyte-based cell. Hence, it is clearly demonstrated that the impact of Ag NPs on electrolyte solution is more effective than the secondary salt ($CuSO_4$) effect.

3.9 Comparative performance of BVC using AL and PKL NPs

Table 3.5: Comparative performance of BVC using various electrode including Ag NPs

Type of electrode	**Types of electrolytes**	**Types of performance parameter of BVC and highest magnitude**		
		Open circuit voltage, V_{oc} (V)	**Short circuit current, I_{sc} (mA)**	**Power, P_{max} = $V_{oc} \times I_{sc}$ (W)**
Zn/Cu (10 cm^2)	AL extract	0.45 V	110 mA	0.05 W
	PKL extract	0.92 V	260 mA	0.24 W
	AL extract + $CuSO_4$	1.10 V	450 mA	0.49 W
	PKL extract + $CuSO_4$	1.34 V	545 mA	0.73 W
	AL extract + Ag NPs	1.28 V	820 mA	1.05 W
	PKL extract + Ag NPs	1.41 V	915 mA	1.30 W
	AL extract + $CuSO_4$ + Ag NPs	1.51 V	960 mA	1.45 W
	PKL extract + $CuSO_4$ + Ag NPs	1.63 V	981 mA	1.60

It is clear from the above table 3.5 that BVC developed using Zn/Cu electrode and PKL extract + $CuSO_4$ + Ag NPs electrolyte showed better performance than that of the cell developed using (i) PKL extract (ii) PKL extract + $CuSO_4$ (iii) PKL extract + Ag NPs and (i) AL extract (ii) AL extract + $CuSO_4$ (iii) AL extract + Ag NPs (iv) AL extract + $CuSO_4$ + Ag NPs as electrolyte and Zn/Cu electrode. As the expose area of $CuSO_4$ and Ag NPs with PKL extract as electrolyte and Zn/Cu electrode increases, the developed bio-voltaic cell (BVC) showed better performance which is the consistent with the published result [220].

3.10 Effect of RGO in AL extract BVC

Three parameters such as open circuit voltage, V_{oc} (V), short circuit current, I_{sc} (mA) and power, $P_{max}= V_{oc} \times I_{sc}$ (W) are measured to check the performance analysing of BVC using five types of electrode such as Zn/Cu (1 cm^2), Zn/RGO (2 h), Zn/RGO (24 h), Zn/RGO (2 h) wrapped Ag NPs and Zn/RGO (24 h) wrapped Ag NPs two types of electrolyte such as PKL and AL electrolyte.

3.10.1 Effect on V_{oc} (V) of BVC using Zn/Cu (1 cm^2) and Zn/ RGO (2 h) electrode with AL electrolyte

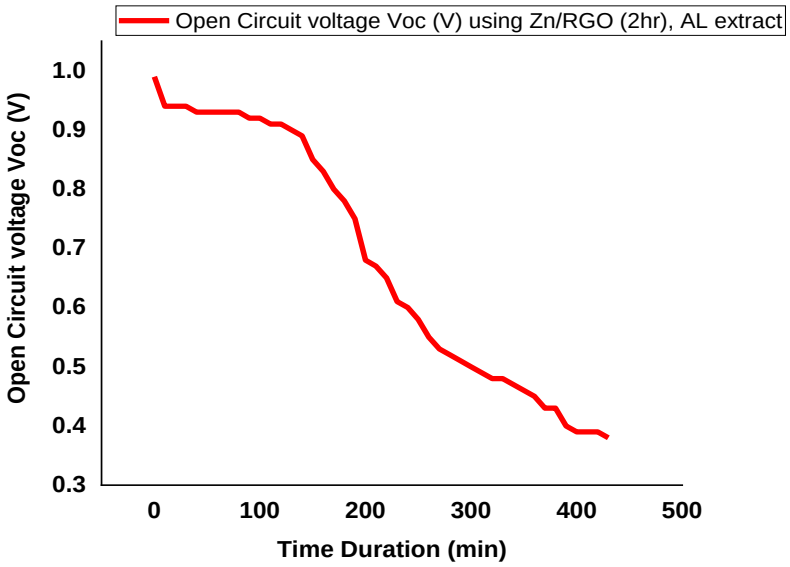

Figure 3.33: Varuation of V_{oc} (V) with time (min) using Zn/ RGO (2 h) electrode and AL electrolyte

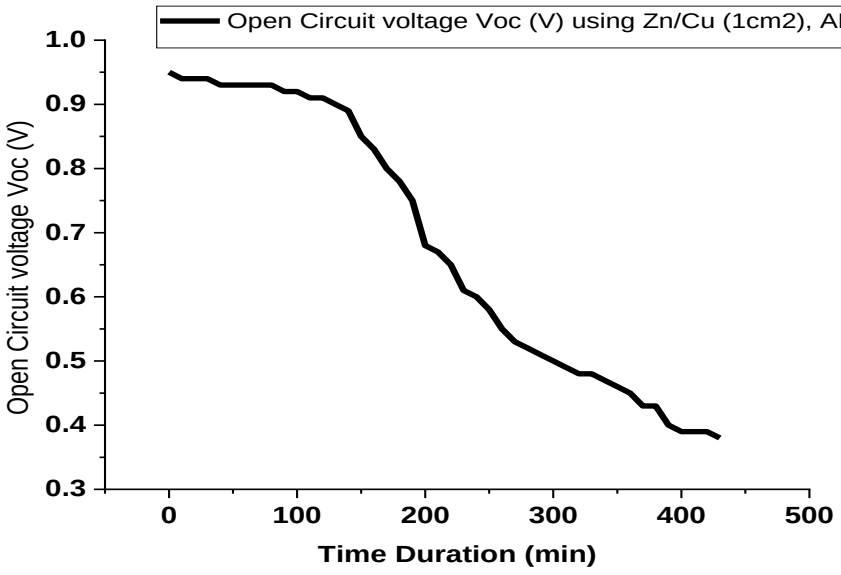

Figure 3.34: Variation of V_{oc} (V) with time (min) using Zn/Cu (1 cm^2) electrode and AL electrolyte

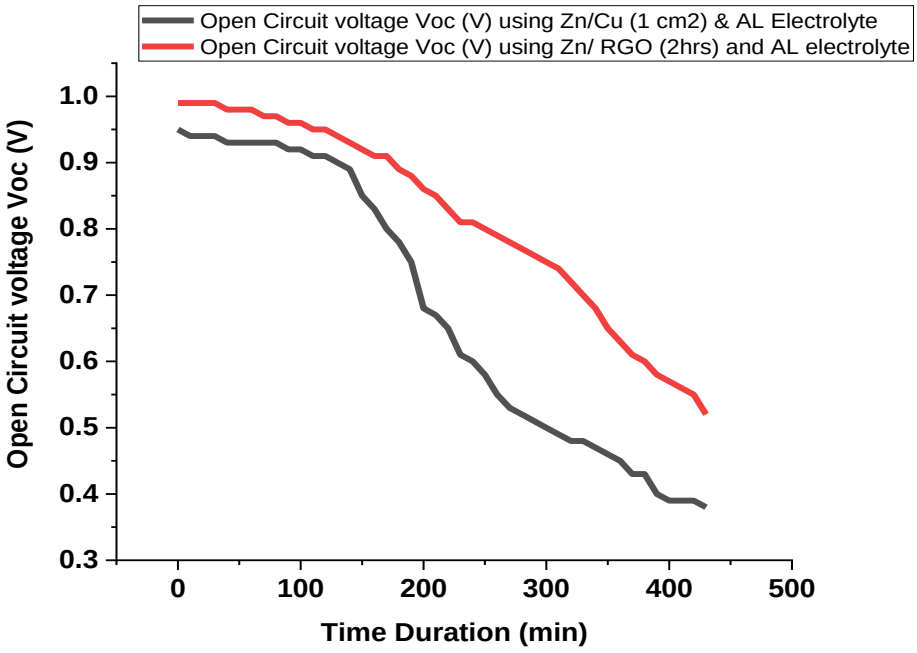

Figure 3.35: Variation of V_{oc} (V) with time (min) between Zn/Cu (1 cm^2) & Zn/ RGO (2 h) electrode using AL electrolyte

The figure 3.35 shows the open circuit voltage, V_{oc} (V) of BVC using Zn/Cu (1 cm^2) and Zn/ RGO (2 h) electrode with AL electrolyte. The open circuit voltage, V_{oc} (V) of BVC using Zn/ RGO (2 h) electrode is better performer than Zn/Cu (1 cm^2) electrode. Because, electrical conductivity of RGO is better than Cu which is consistent with the published result [99].

The figure 3.35 also shows the performance of open circuit voltage, V_{oc} (V) using Zn/ RGO (2 h) electrode with AL electrolyte. The figure 3.34 shows performance open circuit voltage, V_{oc} (V) using Zn/Cu (1 cm^2) electrode with AL electrolyte. The figure 3.35 also shows that performance of open circuit voltage V_{oc} (V) using Zn/ RGO (2 h) electrode is 0.4 V greater than Zn/Cu (1 cm^2) electrode with AL electrolyte.

3.10.2 Effect on I_{sc} (mA) of BVC using Zn/Cu (1 cm^2) and Zn/ RGO (2 h) electrode with AL electrolyte

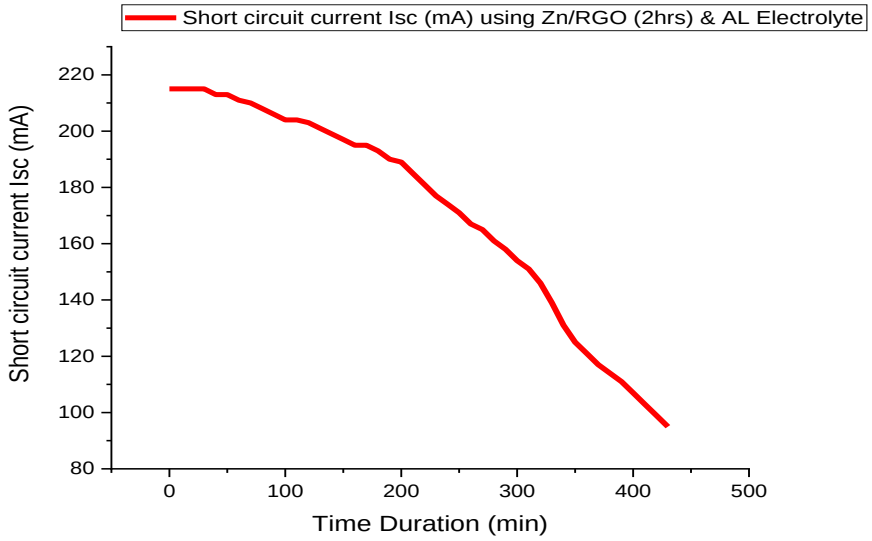

Figure 3.36: Variation of I_{sc} (mA) with time (min) using Zn/ RGO (2 h) electrode and AL electrolyte

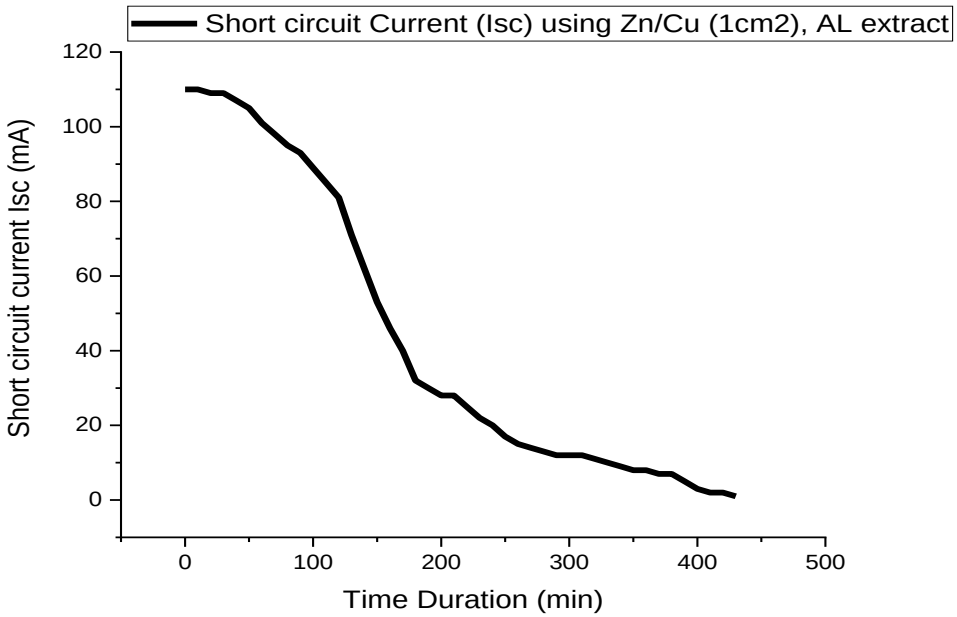

Figure 3.37: Variation of I_{sc} (mA) with time (min) using Zn/Cu (1 cm^2) electrode and AL electrolyte

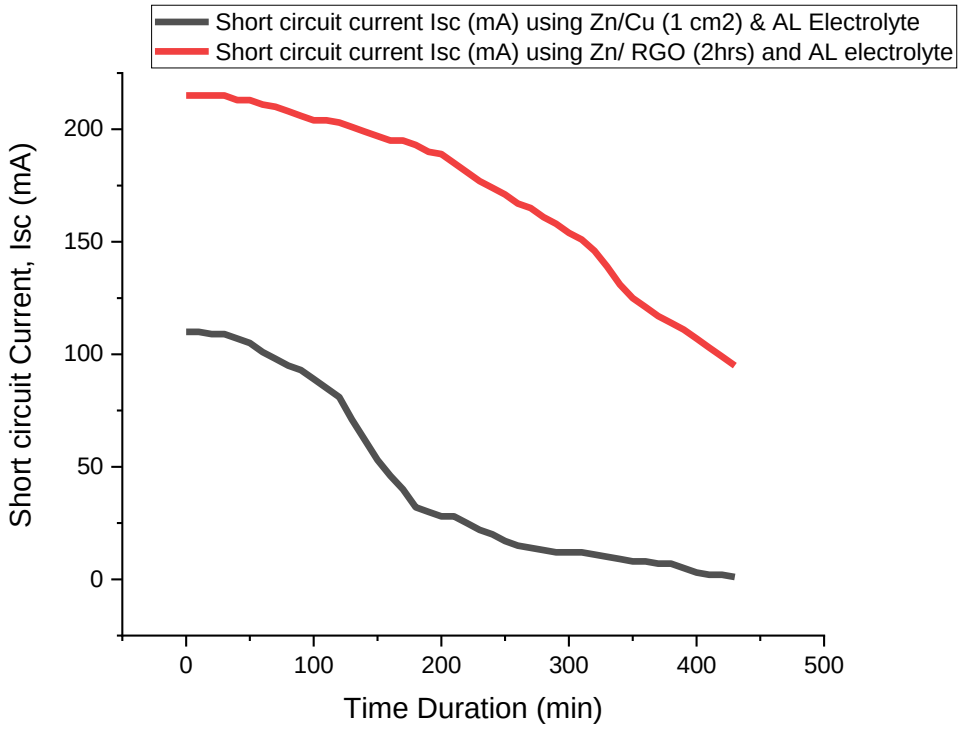

Figure 3.38: Variation of I_{sc} (mA) with time (min) between Zn/Cu (1 cm^2) and Zn/ RGO (2 h) electrode using AL electrolyte.

The figure 3.38 shows the short circuit current, I_{sc} (mA) of BVC using Zn/Cu (1 cm^2) and Zn/ RGO (2 h) lectrode with AL electrolyte. The short circuit current, I_{sc} (mA) of BVC using Zn/ RGO (2 h) electrode is better performer than Zn/Cu (1 cm^2) electrode. Because, electrical conductivity of RGO is better than Cu which is consistent with the published result [99].

The figure 3.36 also shows the performance of short circuit current, I_{sc} (mA) using Zn/ RGO (2 h) electrode with AL electrolyte. The figure 3.37 shows performance short circuit current, I_{sc} (mA) using Zn/Cu (1 cm^2) with AL electrolyte. The figure 3.38 also shows that short circuit current, Isc (mA) of Zn/ RGO (2 h) electrode is 105 mA greater than Zn/Cu (1 cm^2) electrode using AL electrolyte.

3.10.3 Effict on power (W) of BVC using Zn/Cu (1 cm^2) and Zn/ RGO (2 h) electrode with AL electrolyte

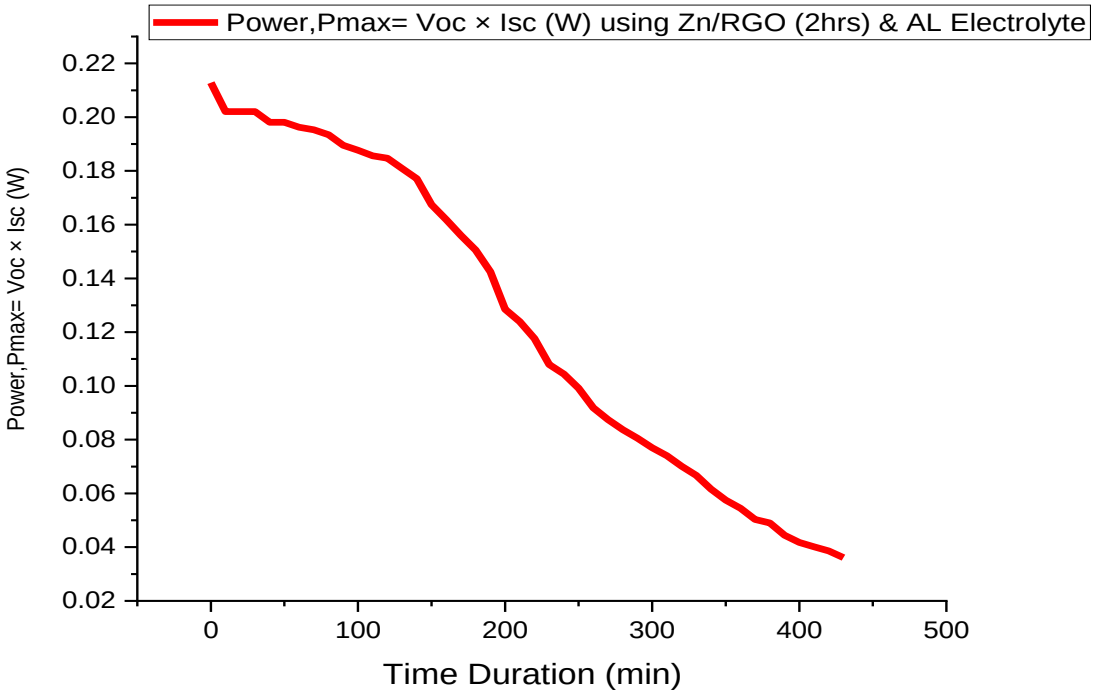

Figure 3.39: Variation of power (W) with time (min) using Zn/ RGO (2 h) electrode and AL electrolyte

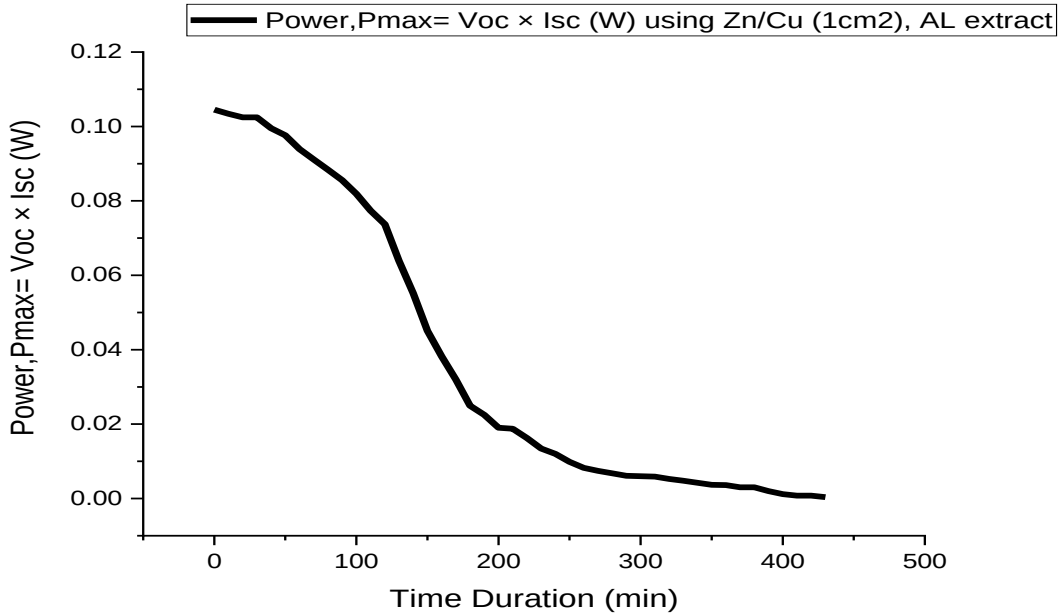

Figure 3.40: Variation of Power, $P_{max} = V_{oc} \times I_{sc}$ (W) with time (min) using Zn/Cu (1 cm^2) electrode and AL electrolyte

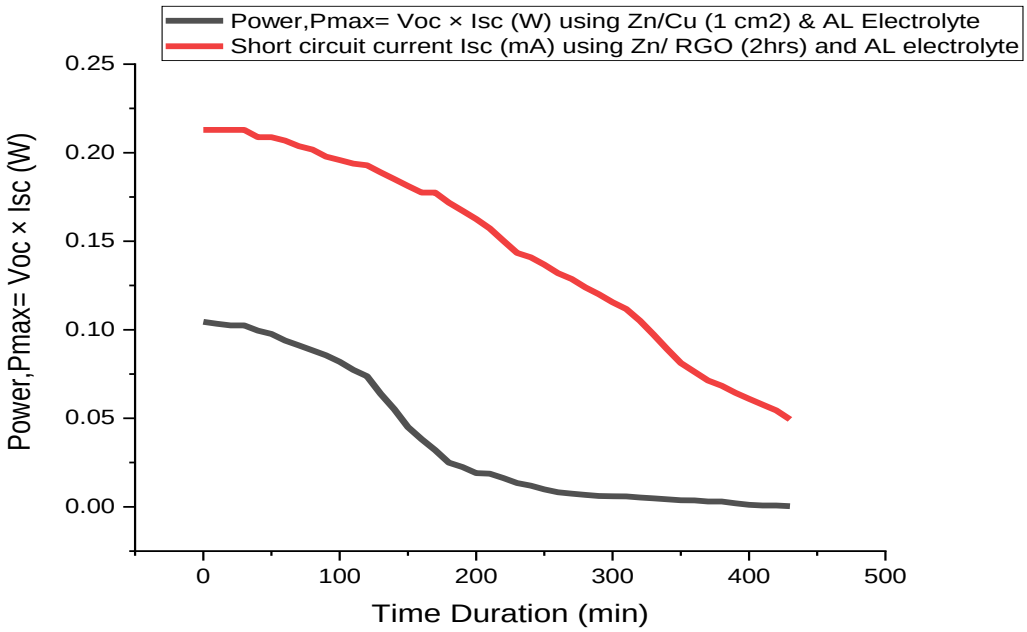

Figure 3.41: Variation of power, $P_{max}= V_{oc} \times I_{sc}$ (W) with time (min) between Zn/Cu (1 cm^2) & Zn/ RGO (2 h) electrode using AL electrolyte

The figure 3.41 shows the power, $P_{max}= V_{oc} \times I_{sc}$ (W) of BVC using Zn/Cu (1 cm^2) and Zn/ RGO (2 h) lectrode with AL electrolyte. The power, $P_{max}= V_{oc} \times I_{sc}$ (W) of BVC using Zn/ RGO (2 h) electrode is better performer than Zn/Cu (1 cm^2) electrode. Because, open circuit voltage, V_{oc} (V) and short circuit current, I_{sc} of Zn/ RGO (2 h) electrode is higher than Zn/Cu (1 cm^2). As a result power, $P_{max}= V_{oc} \times I_{sc}$ (W) of Zn/ RGO (2 h) is better than Zn/Cu (1 cm^2) which is consistent with the published result [99].

The figure 3.39 shows the power $P_{max}= V_{oc} \times I_{sc}$ (W) using Zn/ RGO (2 h) electrode with AL electrolyte. The figure 3.40 shows the power, $P_{max}= V_{oc} \times I_{sc}$ (W) of Zn/Cu (1 cm^2) electrode with AL electrolyte. The figure 3.41 also shows that power, $P_{max}= V_{oc} \times I_{sc}$ (W) using Zn/ RGO (2 h) electrode is 0.11W greater than Zn/Cu (1 cm^2) electrode with AL electrolyte.

3.10.4 Comparative study of Zn/Cu (1 cm^2) and Zn/RGO (2 h) electrode performance in BVC with AL electrolyte

Table-3.6: Comparative study of Zn/Cu (1 cm^2) and Zn/RGO (2 h) electrode performance in BVC with AL electrolyte

No.	Performance parameters of BVC	Type of electrolyte	Type of electrodes and highest magnitude	
			Zn/Cu (1 cm^2)	Zn/ RGO (2 h)
1	Open circuit voltage, V_{oc} (V)	AL	0.95 V	0.99 V
2	Short circuit current, I_{sc} (mA)	AL	110 mA	215 mA
3	Power, $P_{max}= V_{oc} \times I_{sc}$ (W)	AL	0.10 W	0.21 W

It is clear from the above table 3.6 that BVC developed using Zn/ RGO (2 h) electrode and AL extract electrolyte showed better performance than that of the BVC developed using Zn/Cu (1 cm^2) electrode and AL extract electrolyte. Because, electrical conductivity of RGO adsorbed paper electrode is better than Cu electrode which is the consistent with the published result [99].

3.10.5 Effect on V_{oc} (V) of BVC using Zn/Cu (1 cm^2), Zn/ RGO (2 h) and Zn/ RGO (24 h) electrode with AL electrolyte

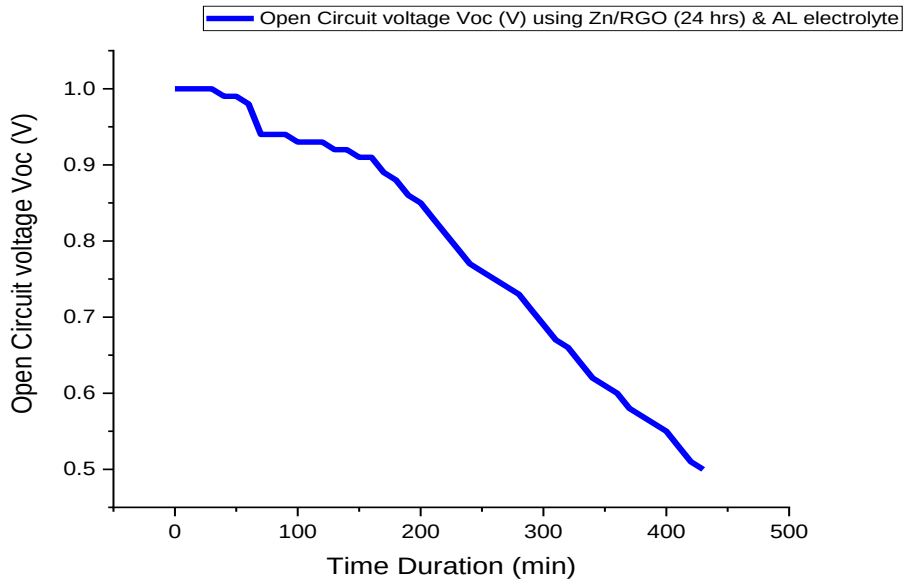

Figure 3.42: Variation of V_{oc} (V) with time (min) using Zn/ RGO (24 h) electrode and AL electrolyte

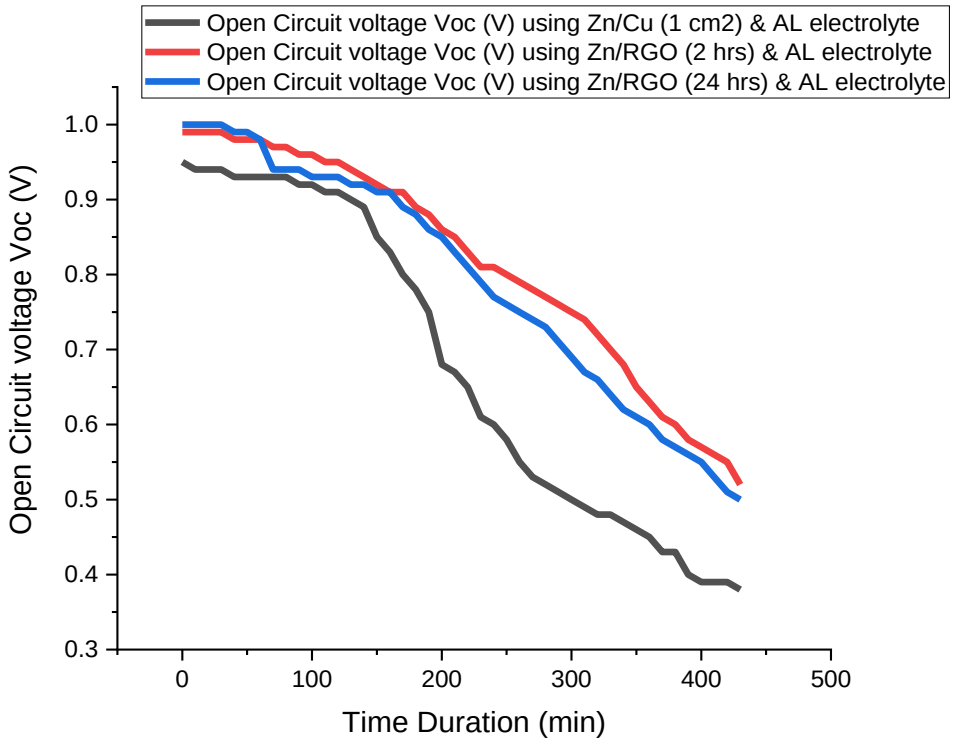

Figure 3.43: Variation of V_{oc} (V) with time (min) among Zn/Cu (1 cm^2), Zn/ RGO (2 h) & Zn/ RGO (24 h) electrode using AL electrolyte

The figure 3.43 shows the open circuit voltage, V_{oc} (V) of BVC using Zn/Cu (1 cm^2), Zn/ RGO (2 h) and Zn/ RGO (24 h) electrode with AL electrolyte. The open circuit voltage, V_{oc} (V) of BVC using Zn/ RGO (24 h) electrode is better performer than Zn/Cu (1 cm^2) and Zn/ RGO (2 h) electrode. Because, electrical conductivity of Zn/ RGO (24 h) is better than Zn/Cu (1 cm^2), Zn/ RGO (2 h) electrode which is consistent with the published result [99].

The figure 3.42 also shows the open circuit voltage, V_{oc} (V) of BVC using Zn/ RGO (24 h) electrode with AL electrolyte. The figure 3.43 shows the comparative open circuit voltage V_{oc} (V) among Zn/Cu (1 cm^2), Zn/ RGO (2 h) & Zn/ RGO (24 h) electrode of BVC using AL electrolyte. The figure 3.43 also shows that open circuit voltage V_{oc} (V) using Zn/ RGO (24 h) electrode is 0.1 (V) greater than Zn/ RGO (2 h) electrode and 0.5 (V) greater than Zn/Cu (1 cm^2) electrode with AL electrolyte.

3.10.6 Effect on I_{sc} (mA) of BVC using Zn/Cu (1 cm^2), Zn/ RGO (2 h) and Zn/ RGO (24 h) electrode with AL electrolyte

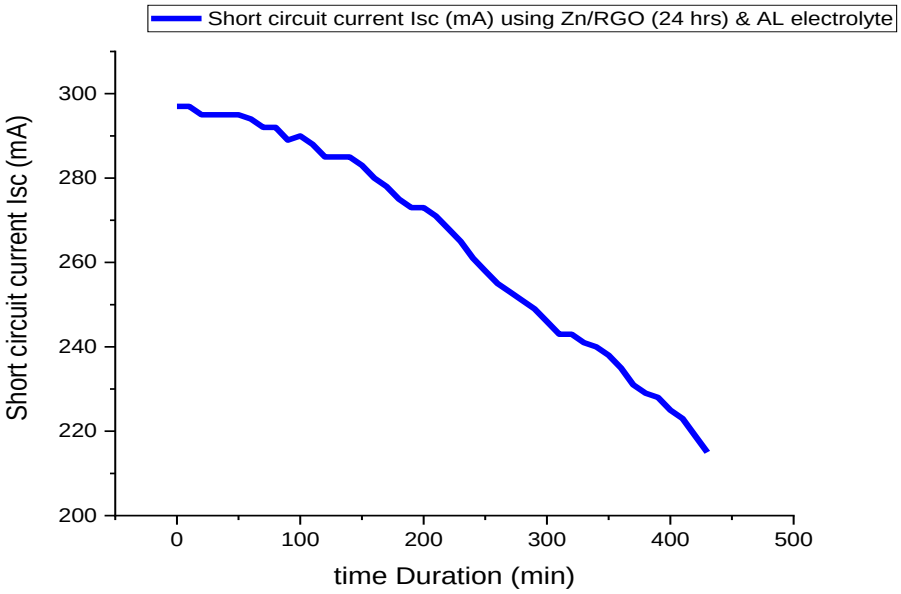

Figure 3.44: Variation of I_{sc} (mA) with time (min) using Zn/ RGO (24 h) electrode and AL electrolyte

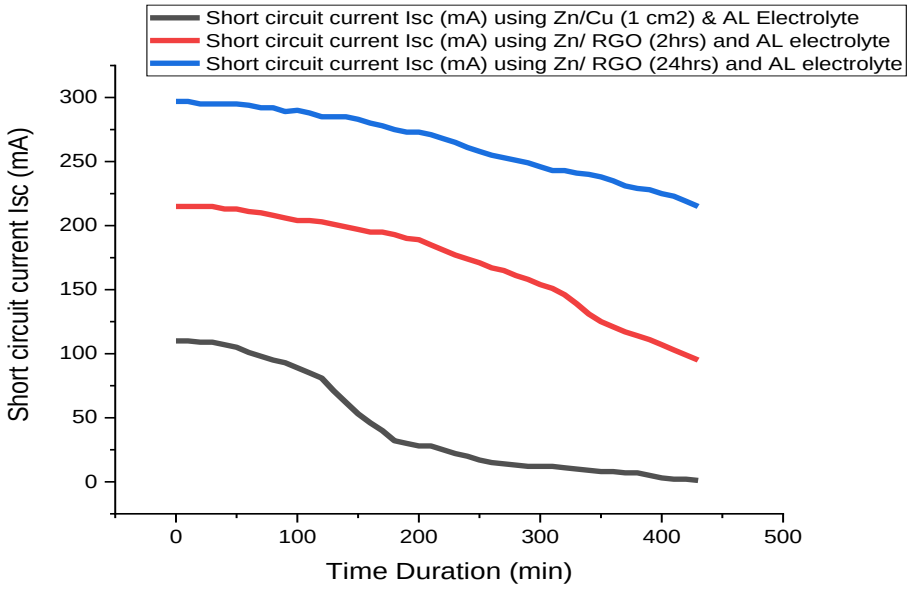

Figure 3.45: Variation of I_{sc} (mA) among Zn/Cu (1 cm^2), Zn/ RGO (2 h) & Zn/ RGO (24 h) electrode with time (min) using AL electrolyte

The figure 3.45 shows the short circuit current, I_{sc} (mA) of BVC using Zn/Cu (1 cm^2), Zn/ RGO (2 h) and Zn/ RGO (24 h) electrode with AL electrolyte. The short circuit current, I_{sc} (mA) of BVC using Zn/ RGO (24 h) electrode is better performer than Zn/Cu (1 cm^2) and Zn/ RGO (2 h) electrode. Because, electrical conductivity of Zn/ RGO (24 h) is better than Zn/Cu (1 cm^2), Zn/ RGO (2 h) electrode which is consistent with the published result [99].
The figure 3.44 also shows the short circuit current, I_{sc} (mA) using Zn/ RGO (24 h) electrode with AL electrolyte. The figure 3.45 shows the comparative performance of short circuit current (I_{sc}) among Zn/Cu (1 cm^2), Zn/ RGO (2 h) and Zn/RGO (24 h) electrode using AL electrolyte. The figure 3.45 also shows that performance of short circuit current I_{sc} (mA) using Zn/ RGO (24 h) electrode is 82 mA greater than Zn/ RGO (2 h) electrode and 187 mA greater than Zn/Cu (1 cm^2) electrode with AL electrolyte.

3.10.7 Effect on power (W) of BVC using Zn/Cu (1 cm^2), Zn/ RGO (2 h) and Zn/ RGO (24 h) electrode with AL electrolyte

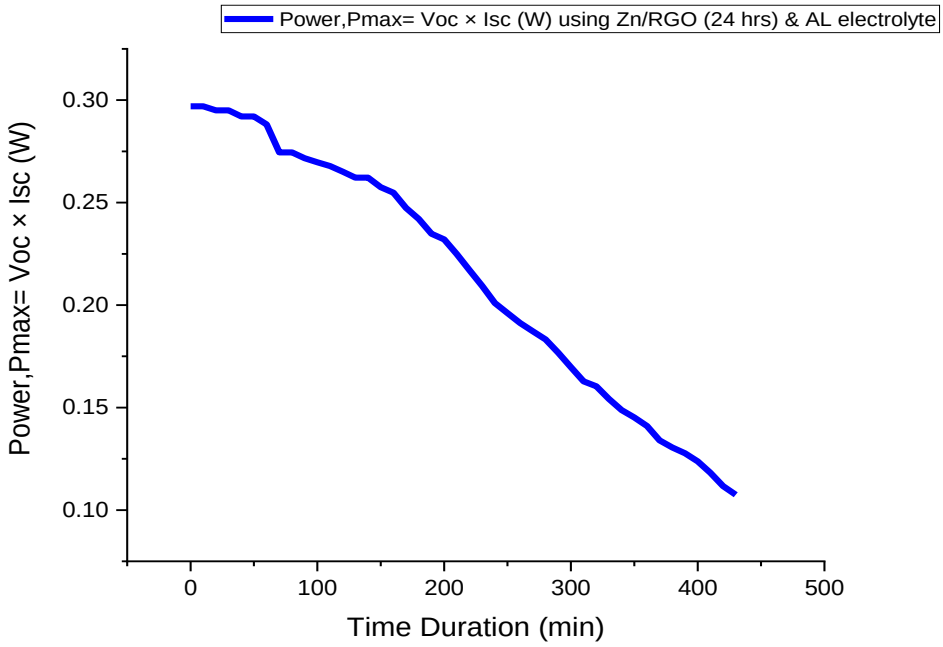

Figure 3.46: Variation of Power, $P_{max}= V_{oc} \times I_{sc}$ (W) with time (min) using Zn/ RGO (24 h) electrode and AL electrolyte

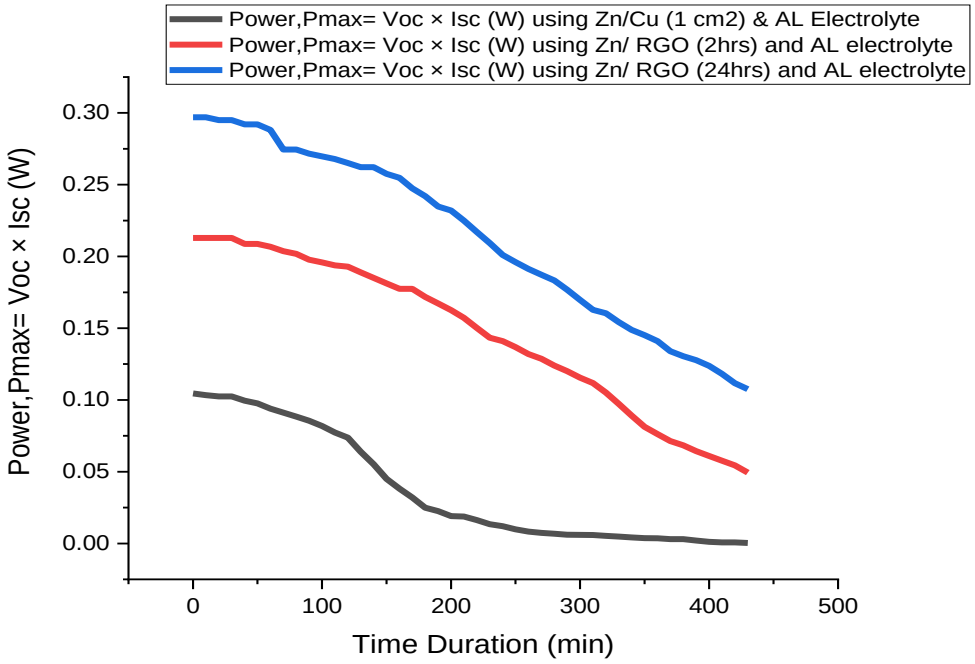

Figure 3.47: Variation of power, $P_{max}= V_{oc} \times I_{sc}$ (W) with time (min) among Zn/Cu (1 cm^2), Zn/ RGO (2 h) & Zn/ RGO (24 h) electrode using AL electrolyte.

The figure 3.47 shows the power, $P_{max}= V_{oc} \times I_{sc}$ (W) of BVC using Zn/Cu (1 cm^2), Zn/ RGO (2 h) and Zn/ RGO (24 h) electrode with AL electrolyte. The power, $P_{max}= V_{oc} \times I_{sc}$ (W) of BVC using Zn/ RGO (24 h) electrode is better performer than Zn/Cu (1 cm^2) and Zn/ RGO (2 h) electrode. Because, electrical conductivity of Zn/ RGO (24 h) is better than Zn/Cu (1 cm^2), Zn/ RGO (2 h) electrode. As a result open circuit voltage, V_{oc} (V) and short circuit current, I_{sc} (mA) as well as power, $P_{max}= V_{oc} \times I_{sc}$ (W) of Zn/ RGO (24 h) electrode are higher which is consistent with the published result [99].

The figure 3.46 also shows the performance of power, $P_{max}= V_{oc} \times I_{sc}$ (W) using Zn/ RGO (24 h) electrode with AL electrolyte. The figure 3.47 shows the comparative of power, $P_{max}= V_{oc} \times I_{sc}$ (W) among Zn/Cu (1 cm^2), Zn/ RGO (2 h) & Zn/RGO (24 h) electrode using AL electrolyte. The figure 3.57 also shows that power, $P_{max}= V_{oc} \times I_{sc}$ (W) of Zn/ RGO (24 h) electrode is 0.8 W greater than Zn/ RGO (2 h) electrode and 0.19 W greater than Zn/Cu (1 cm^2) electrode with AL electrolyte.

3.10.8 Comparative study of Zn/Cu (1 cm^2), Zn/RGO (2 h) and Zn/RGO (24 h) electrode performance in BVC with AL electrolyte

Table-3.7: Comparative performance of BVC using Zn/Cu (1 cm^2), Zn/RGO (2 h) and Zn/RGO (24 h) with AL electrolyte

No.	Performance parameters of BVC	Type of electrolyte	Type of electrodes and highest magnitude		
			Zn/Cu (1 cm^2)	Zn/ RGO (2 h)	Zn/ RGO (24 h)
1	Open circuit voltage, V_{oc} (V)	AL	0.95 V	0.99 V	1.00 V
2	Short circuit current, I_{sc} (mA)	AL	110 mA	215 mA	297 mA
3	Power, $P_{max}= V_{oc} \times I_{sc}$ (W)	AL	0.10 W	0.21 W	0.29 W

It is clear from the above table 3.7 that BVC developed using Zn/ RGO (24 h) electrode and AL extract electrolyte showed better performance than that of the BVC developed using Zn/Cu (1 cm^2) and Zn/ RGO (2 h) electrode and AL extract electrolyte. Because, electrical conductivity of 24 hours RGO adsorbed paper electrode is better than Cu and 2 hours RGO adsorbed paper electrode which is the consistent with the published result [99].

3.11 Effect of RGO-Ag nanocomposite in AL extract BVC

3.11.1 Effect of Zn/RGO (2 h)-Ag nanocomposite electrode on V_{oc} (V) in AL extract BVC

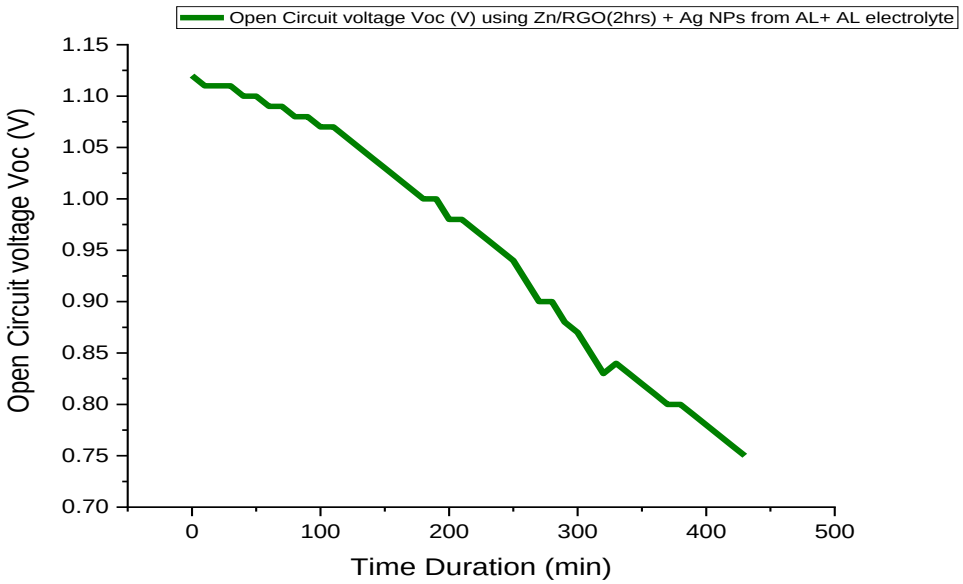

Figure 3.48: Variation of V_{oc} (V) with time (min) using Zn/ RGO (2 h) wrapped Ag NPs and AL electrolyte

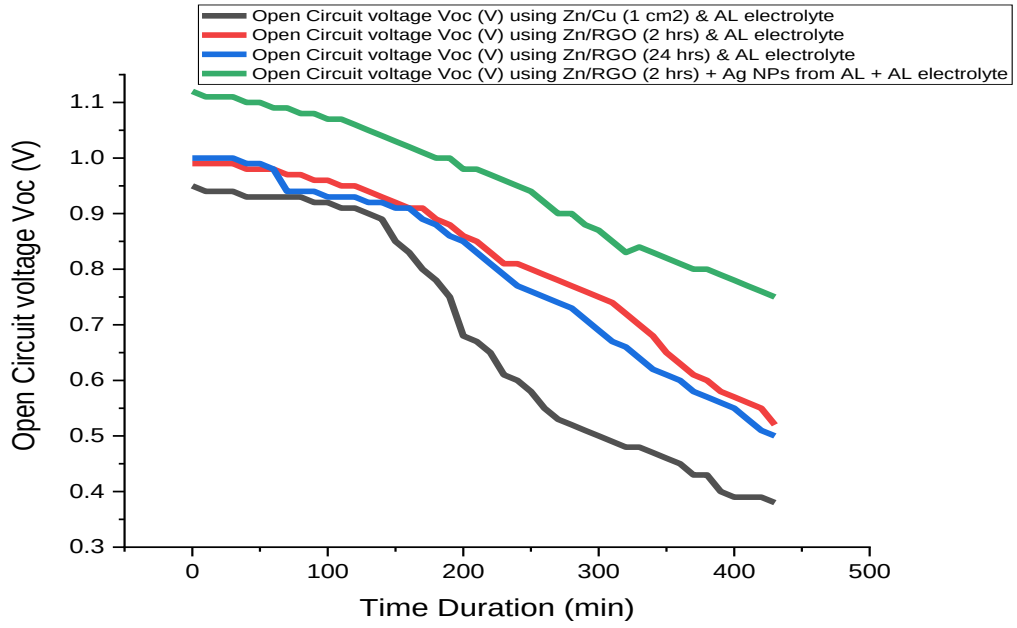

Figure 3.49: Variation of V_{oc} (V) with time (min) among Zn/Cu (1 cm^2), Zn/ RGO (2 h), Zn/ RGO (24 h) and Zn/ RGO (2 h) wrapped Ag NPs electrode using AL electrolyte

The figure 3.49 shows the open circuit voltage, V_{oc} (V) of BVC using Zn/Cu (1 cm^2), Zn/ RGO (2 h), Zn/ RGO (24 h) and Zn/ RGO (2 h) wrapped Ag NPs electrode electrode with AL electrolyte. The open circuit voltage, V_{oc} (V) of BVC using Zn/ RGO (2 h) wrapped Ag NPs electrode is better performer than Zn/Cu (1 cm^2), Zn/ RGO (2 h) and Zn/ RGO (24 h) electrode. Because, electrical conductivity of Zn/ RGO (2 h) wrapped Ag NPs electrode is better than Zn/Cu (1 cm^2), Zn/ RGO (2 h) and Zn/ RGO (24 h) electrode which is consistent with the published result [175].

The figure 3.48 also shows the performance of open circuit voltage, V_{oc} (V) using Zn/ RGO (2 h) wrapped Ag NPs electrode with AL electrolyte. The figure 3.49 shows the comparative open circuit voltage, V_{oc} (V) among Zn/Cu (1 cm^2), Zn/ RGO (2 h), Zn/ RGO (24 h) and Zn/ RGO (2 h) wrapped Ag NPs electrode using AL electrolyte. The figure 3.49 also shows that open circuit voltage V_{oc} (V) using Zn/ RGO (2 h) wrapped Ag NPs electrode is 0.12 (V) greater than Zn/ RGO (24 h) electrode, 0.13 (V) greater than Zn/ RGO (2 h) electrode and 0.17 (V) greater than Zn/Cu (1 cm^2) electrode with AL electrolyte.

3.11.2 Effect of Zn/RGO (2 h)-Ag nanocomposite electrode on I_{sc} (mA) in AL extract BVC

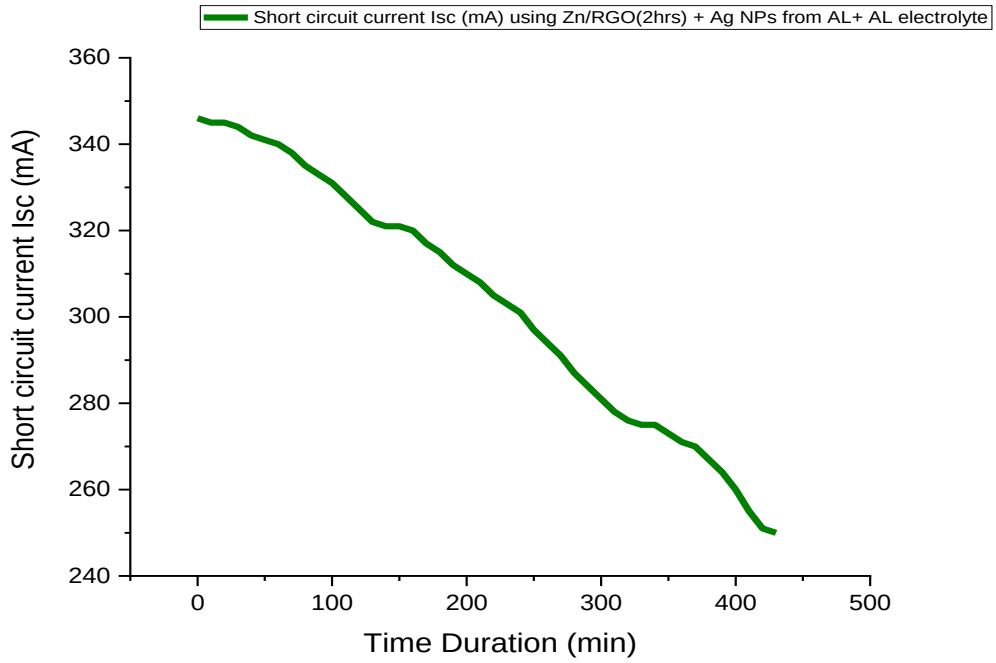

Figure 3.50: Variation of I_{sc} (mA) with time (min) using Zn/ RGO (2 h) wrapped Ag NPs electrode & AL electrolyte

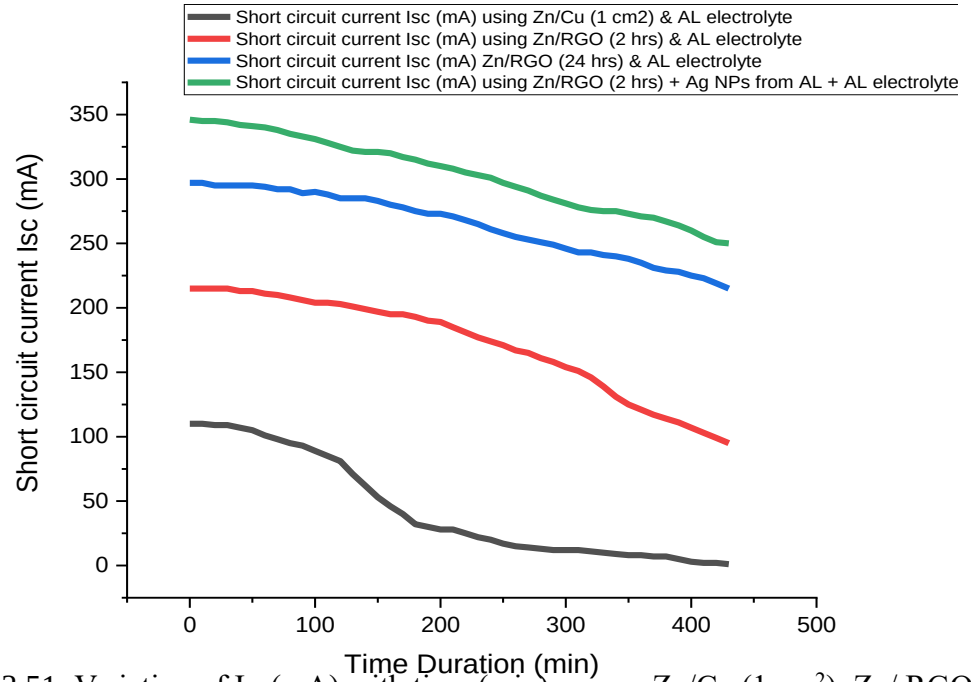

Figure 3.51: Variation of I_{sc} (mA) with time (min) among Zn/Cu (1 cm^2), Zn/ RGO (2 h), Zn/ RGO (24 h) and Zn/ RGO (2 h) wrapped Ag NPs electrode using AL electrolyte

The figure 3.51 shows the short circuit current, I_{sc} (mA) of BVC using Zn/Cu (1 cm^2), Zn/ RGO (2 h), Zn/ RGO (24 h) and Zn/ RGO (2 h) wrapped Ag NPs electrode electrode with AL electrolyte. The short circuit current, I_{sc} (mA) of BVC using Zn/ RGO (2 h) wrapped Ag NPs electrode is better performer than Zn/Cu (1 cm^2), Zn/ RGO (2 h) and Zn/ RGO (24 h) electrode. Because, electrical conductivity of Zn/ RGO (2 h) wrapped Ag NPs electrode is better than Zn/Cu (1 cm^2), Zn/ RGO (2 h) and Zn/ RGO (24 h) electrode which is consistent with the published result [175].

The figure 3.50 indicates the performance of short circuit current, I_{sc} (mA) using Zn/ RGO (2 h) wrapped Ag NPs electrode with AL electrolyte. The figure 3.51 shows the comparative short circuit current, I_{sc} (mA) among Zn/Cu (1 cm^2), Zn/ RGO (2 h), Zn/ RGO (24 h) and Zn/ RGO (2 h) wrapped Ag NPs electrode using AL electrolyte. The figure 3.51 also shows the short circuit current, I_{sc} (mA) using Zn/ RGO (2 h) wrapped Ag NPs electrode is 49 mA greater than Zn/ RGO (24 h) electrode, 131 mA greater than Zn/ RGO (2 h) electrode and 236 mA greater than Zn/Cu (1 cm^2) electrode with AL electrolyte.

3.11.3 Effect of Zn/RGO (2 h)-Ag nanocomposite electrode on power (W) in AL extract BVC

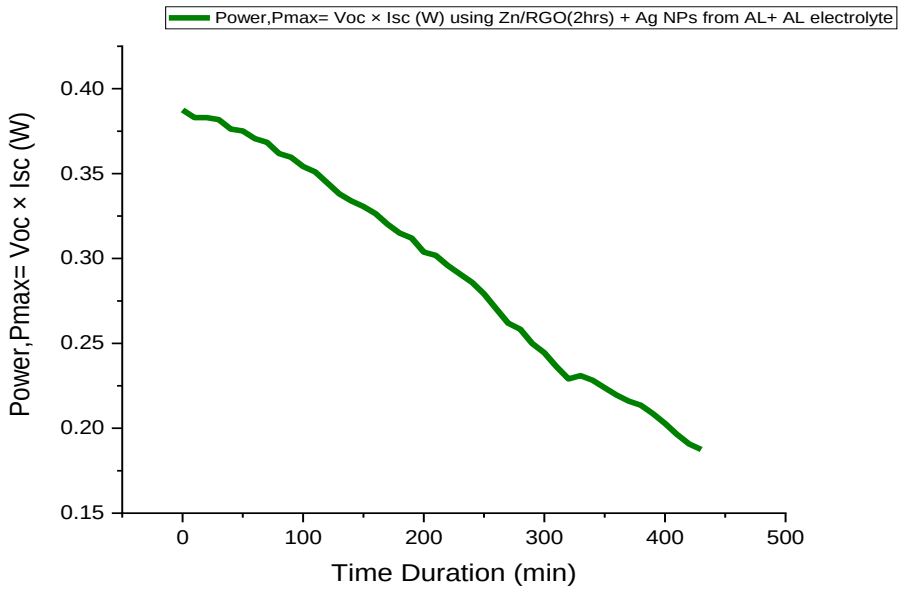

Figure 3.52: Variation of Power, $p_{max}= V_{oc} \times I_{sc}$ (W) with time (min) using Zn/ RGO (2 h) wrapped Ag NPs electrode and AL electrolyte

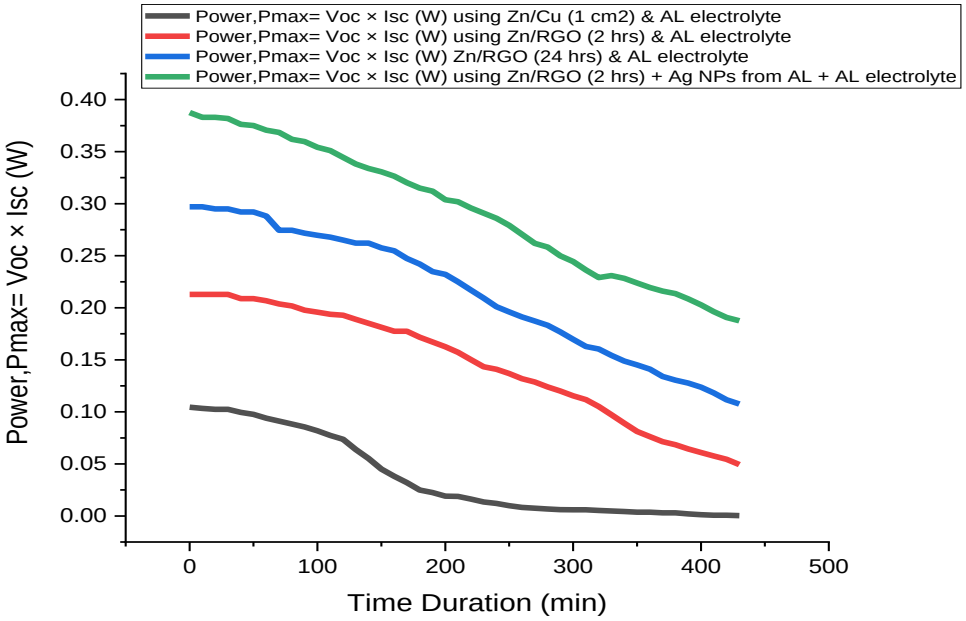

Figure 3.53: Variation of power, $P_{max}= V_{oc} \times I_{sc}$ (W) with time (min) among Zn/Cu (1 cm^2), Zn/ RGO (2 h), Zn/ RGO (24 h) & Zn/ RGO (2 h) wrapped Ag NPs electrode and AL electrolyte

The figure 3.53 shows the power, $P_{max}= V_{oc} \times I_{sc}$ (W) of BVC using Zn/Cu (1 cm^2), Zn/ RGO (2 h), Zn/ RGO (24 h) and Zn/ RGO (2 h) wrapped Ag NPs electrode electrode with AL electrolyte. The power, $P_{max}= V_{oc} \times I_{sc}$ (W) of BVC using Zn/ RGO (2 h) wrapped Ag NPs electrode is better performer than Zn/Cu (1 cm^2), Zn/ RGO (2 h) and Zn/ RGO (24 h) electrode. Because, electrical conductivity of Zn/ RGO (2 h) wrapped Ag NPs electrode is better than Zn/Cu (1 cm^2), Zn/ RGO (2 h) and Zn/ RGO (24 h) electrode which is consistent with the published result [175].

The figure 3.52 shows the power, $P_{max}= V_{oc} \times I_{sc}$ (W) of BVC using Zn/ RGO (2 h) wrapped Ag NPs electrode with AL electrolyte. The figure 3.53 shows the comparative power, $P_{max}= V_{oc} \times I_{sc}$ (W) of BVC among Zn/Cu (1 cm^2), Zn/ RGO (2 h), Zn/ RGO (24 h) and Zn/ RGO (2 h) wrapped Ag NPs electrode using AL electrolyte. The figure 3.53 also shows that power, $P_{max}= V_{oc} \times I_{sc}$ (W) of BVC using Zn/ RGO (2 h) wrapped Ag NPs electrode is 0.09 W greater than Zn/ RGO (24 h) electrode, 0.17 W greater than Zn/ RGO (2 h) and 0.28 W greater than Zn/Cu (1 cm^2) electrode with AL electrolyte.

3.11.4 Comparative study of Zn/Cu (1 cm^2), Zn/RGO (2 h), Zn/RGO (24 h) and Zn/RGO (2 h) wrapped Ag NPs electrode performance in BVC with AL electrolyte

Table-3.8: Comparative performance of BVC using Zn/Cu (1 cm^2), Zn/RGO (2 h), Zn/RGO (24 h) and Zn/RGO (2 h) wrapped Ag NPs with AL electrolyte

No.	Performance parameters of BVC	Type of electrolyte	Type of electrodes and highest magnitude			
			Zn/Cu (1 cm^2)	Zn/ RGO (2 h)	Zn/ RGO (24 h)	Zn/ RGO (2 h) wrapped Ag NPs
1	Open circuit voltage, V_{oc} (V)	AL	0.95 V	0.99 V	1.00 V	1.12 V
2	Short circuit current, I_{sc} (mA)	AL	110 mA	215 mA	297 mA	346 mA
3	Power, $P_{max}= V_{oc} \times I_{sc}$ (W)	AL	0.10 W	0.21 W	0.29 W	0.38752 W

It is clear from the above table 3.8 that BVC developed using Zn/ RGO (2 h) wrapped Ag NPs electrode and AL extract electrolyte showed better performance than that of the BVC developed using Zn/Cu (1 cm^2), Zn/ RGO (2 h) and Zn/ RGO (24 h) electrode and AL extract electrolyte. Because, electrical conductivity of Ag NPs wrapped 2 hours RGO adsorbed paper electrode is better than Cu, 2 hours RGO adsorbed paper electrode and 24 hours RGO adsorbed paper electrode which is the consistent with the published result [99,175].

3.11.5 Effect of Zn/RGO (24 h)-Ag nanocomposite electrode on V_{oc} (V) in AL extract BVC

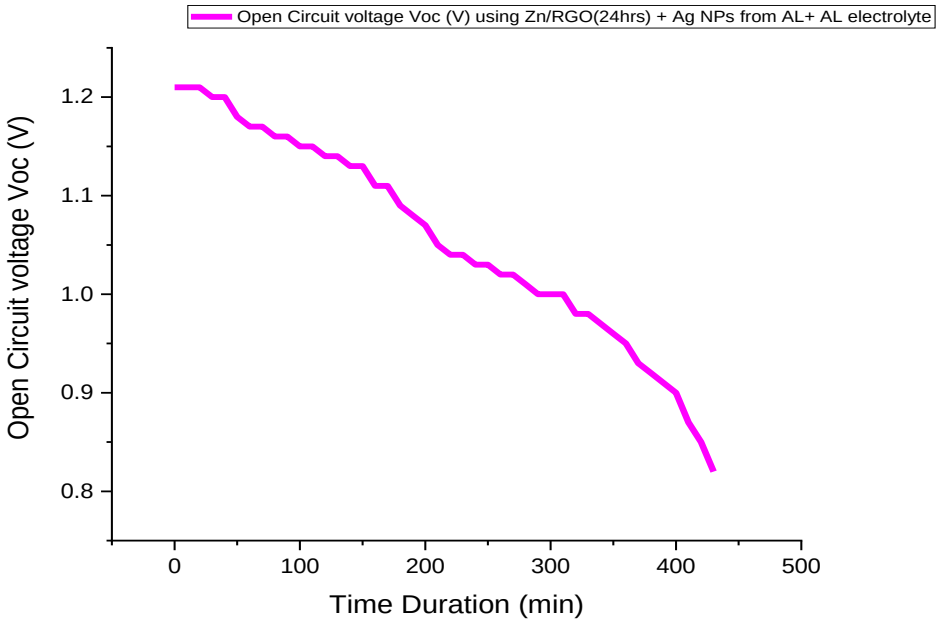

Figure 3.54: Variation of V_{oc} (V) with time (min) using Zn/ RGO (24 h) wrapped Ag NPs electrode and AL electrolyte

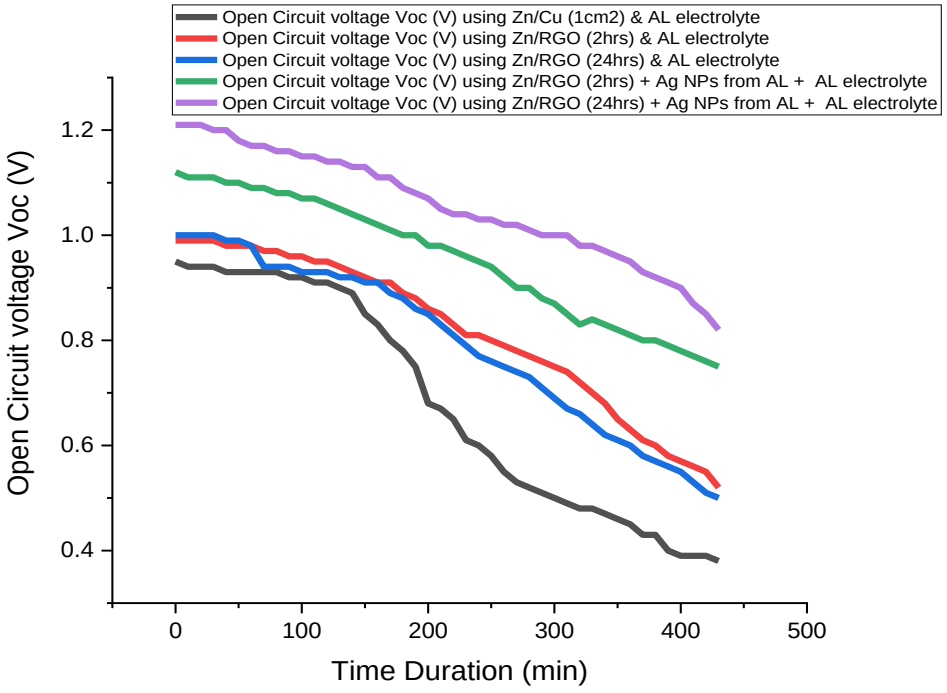

Figure 3.55: variation of V_{oc} (V) with time (min) among Zn/Cu (1 cm^2), Zn/ RGO (2 h), Zn/ RGO (24 h), Zn/ RGO (2 h) wrapped Ag NPs & Zn/ RGO (24 h) wrapped Ag NPs electrode and AL electrolyte

The figure 3.55 shows that open circuit voltage, V_{oc} (V) of BVC using Zn/Cu (1 cm^2), Zn/ RGO (2 h), Zn/ RGO (24 h), Zn/ RGO (2 h) wrapped Ag NPs and Zn/ RGO (24 h) wrapped Ag NPs electrode with AL electrolyte. The open circuit voltage, V_{oc} (V) of BVC using Zn/ RGO (24 h) wrapped Ag NPs electrode is better performer than Zn/Cu (1 cm^2), Zn/ RGO (2 h), Zn/ RGO (24 h) and Zn/ RGO (2 h) wrapped Ag NPs electrode. The electrical conductivity of Zn/ RGO (24 h) wrapped Ag NPs electrode is better performer than Zn/Cu (1 cm^2), Zn/ RGO (2 h), Zn/ RGO (24 h) and Zn/ RGO (2 h) wrapped Ag NPs electrode. Because, the more the time takes to form RGO and Ag NPs nanocomposite the more the electrical conductivity increases which is the consistent with the published result [175]. As a result Zn/ RGO (24 h) wrapped Ag NPs electrode is better performer than Zn/Cu (1 cm^2), Zn/ RGO (2 h), Zn/ RGO (24 h) and Zn/ RGO (2 h) wrapped Ag NPs electrode.

The figure 3.54 also shows the open circuit voltage, V_{oc} (V) using Zn/ RGO (24 h) wrapped Ag NPs electrode with AL electrolyte. The figure 3.55 shows the comparative open circuit voltage, V_{oc} (V) among Zn/Cu (1 cm^2), Zn/ RGO (2 h), Zn/ RGO (24 h), Zn/ RGO (2 h) wrapped Ag NPs and Zn/ RGO (24 h) wrapped Ag NPs electrode using AL electrolyte. The figure 3.55 also shows the open circuit voltage (V) using Zn/ RGO (24 h) wrapped Ag NPs electrode is 0.09 (V) greater than Zn/ RGO (2 h) wrapped Ag NPs, 0.21 (V) greater than Zn/ RGO (24 h) electrode, 0.22 (V) greater than Zn/ RGO (2 h) and 0.26 (V) greater than Zn/Cu (1 cm^2) electrode with AL electrolyte.

3.11.6 Effect of Zn/RGO (24 h)-Ag nanocomposite electrode on I_{sc} (mA) in AL extract BVC

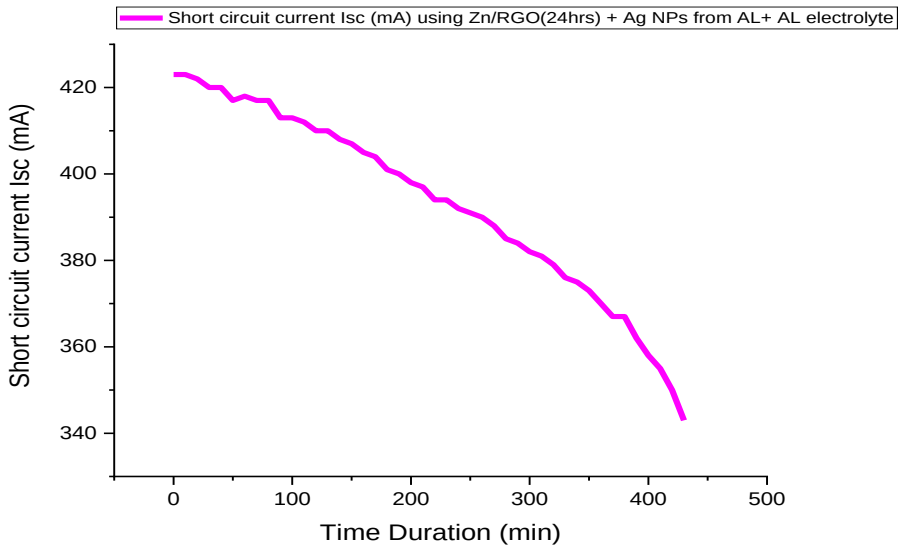

Figure 3.56: Variation of I_{sc} (mA) with time (min) using Zn/ RGO (24 h) wrapped AgNPs electrode and AL electrolyte.

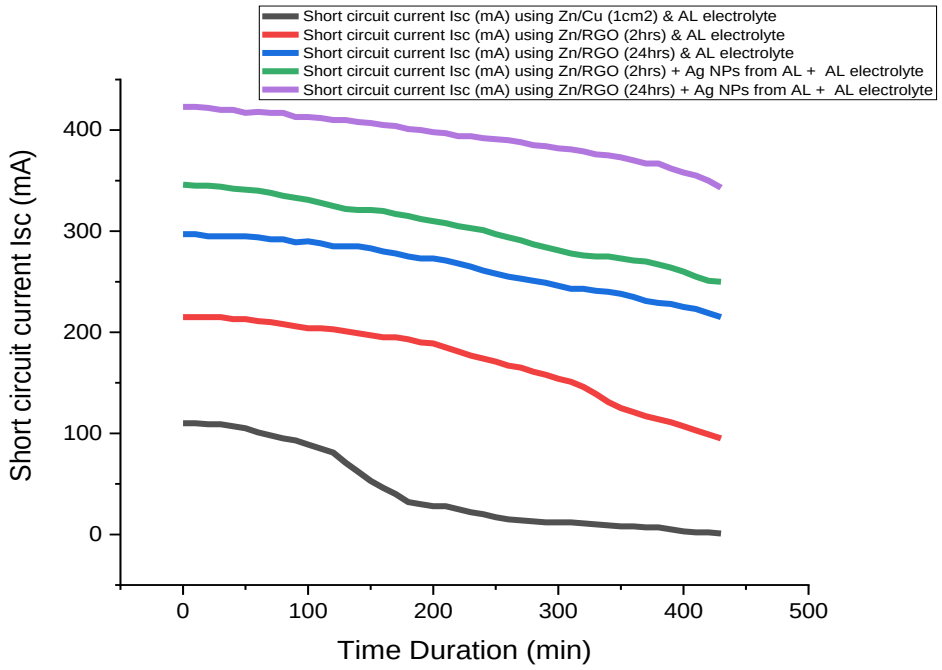

Figure 3.57: Variation of I_{sc} (mA) with time (min) among Zn/Cu (1 cm^2), Zn/ RGO (2 h), Zn/ RGO (24 h), Zn/ RGO (2 h) wrapped Ag NPs & Zn/ RGO (24 h) wrapped Ag NPs electrode and AL electrolyte

The figure 3.57 shows the short circuit current, I_{sc} (mA) of BVC using Zn/Cu (1 cm^2), Zn/ RGO (2 h), Zn/ RGO (24 h), Zn/ RGO (2 h) wrapped Ag NPs and Zn/ RGO (24 h) wrapped Ag NPs electrode with AL electrolyte. The short circuit current, I_{sc} (mA) of BVC using Zn/ RGO (24 h) wrapped Ag NPs electrode is better performer than Zn/Cu (1 cm^2), Zn/ RGO (2 h), Zn/ RGO (24 h) and Zn/ RGO (2 h) wrapped Ag NPs electrode. The electrical conductivity of Zn/ RGO (24 h) wrapped Ag NPs electrode is better performer than Zn/Cu (1 cm^2), Zn/ RGO (2 h), Zn/ RGO (24 h) and Zn/ RGO (2 h) wrapped Ag NPs electrode. Because, the more the time takes to form RGO and Ag NPs nanocomposite the more the electrical conductivity increases which is the consistent with the published result [175]. As a result Zn/ RGO (24 h) wrapped Ag NPs electrode is better than Zn/Cu (1 cm^2), Zn/ RGO (2 h), Zn/ RGO (24 h) and Zn/ RGO (2 h) wrapped Ag NPs electrode.

The figure 3.56 shows the performance of short circuit current, I_{sc} (mA) using Zn/ RGO (24 h) wrapped Ag NPs electrode with AL electrolyte. The figure 3.57 shows the comparative short circuit current, I_{sc} (mA) among Zn/Cu (1 cm^2), Zn/ RGO (2 h), Zn/ RGO (24 h), Zn/ RGO (2 h) wrapped Ag NPs and Zn/ RGO (24 h) wrapped Ag NPs electrode using AL electrolyte. The figure 3.57 also shows that the short circuit current, I_{sc} (mA) using Zn/ RGO (24 h) wrapped Ag NPs electrode is 77 mA greater than Zn/ RGO (2 h) wrapped Ag NPs, 126 mA greater than Zn/ RGO (24 h) electrode, 208 mA greater than Zn/ RGO (2 h) and 313 mA greater than Zn/Cu (1 cm^2) electrode with AL electrolyte.

3.11.7 Effect of Zn/RGO (24 h)-Ag nanocomposite electrode on power (W) in AL extract BVC

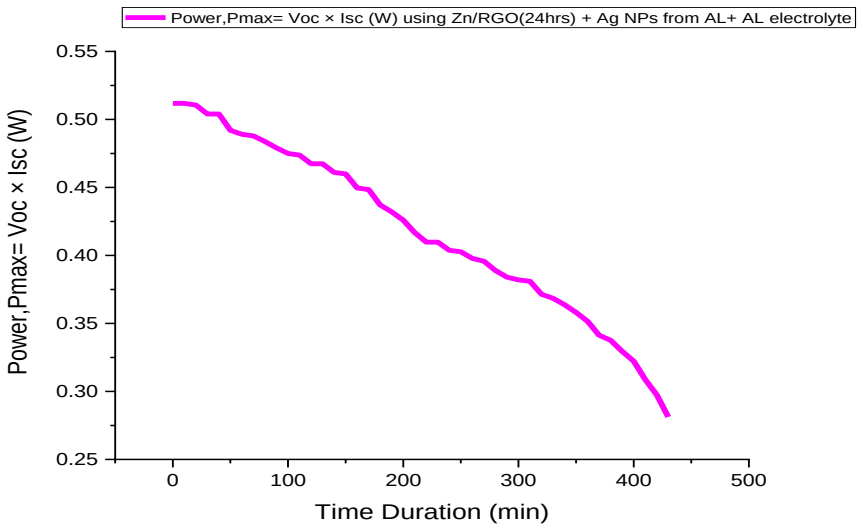

Figure 3.58: Variation of Power, $P_{max}= V_{oc} \times I_{sc}$ (W) with time (min) using Zn/ RGO (24 h) wrapped Ag NPs electrode and AL electrolyte.

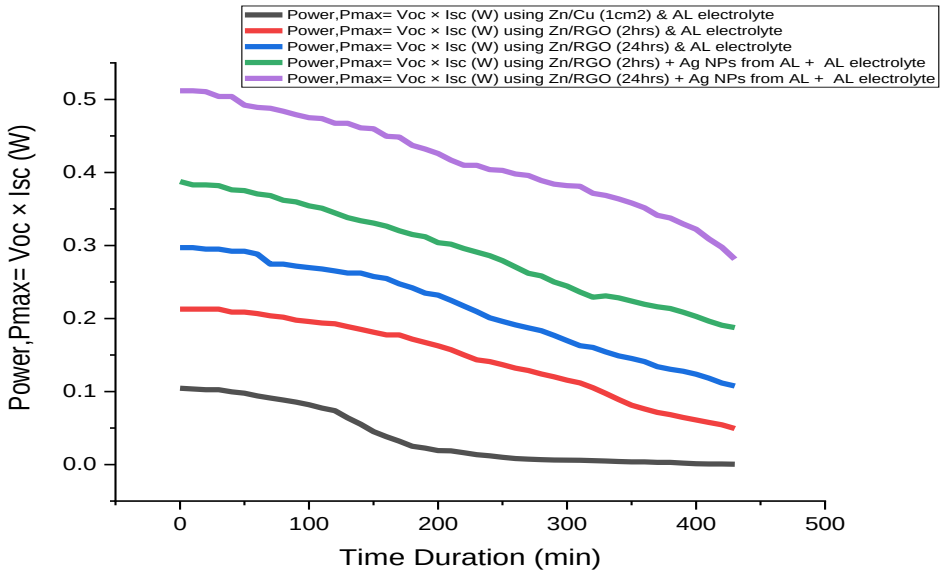

Figure 3.59: Variation of power (W) with time (min) among Zn/Cu (1 cm^2), Zn/ RGO (2 h), Zn/ RGO (24 h), Zn/ RGO (2 h) wrapped Ag NPs & Zn/ RGO (24 h) wrapped Ag NPs using AL electrolyte

The figure 3.59 shows the power, $P_{max}= V_{oc} \times I_{sc}$ (W) of BVC using Zn/Cu (1 cm^2), Zn/ RGO (2 h), Zn/ RGO (24 h), Zn/ RGO (2 h) wrapped Ag NPs and Zn/ RGO (24 h) wrapped Ag NPs electrode with AL electrolyte. The power, $P_{max}= V_{oc} \times I_{sc}$ (W) of BVC using Zn/ RGO (24 h) wrapped Ag NPs electrode is better performer than Zn/Cu (1 cm^2), Zn/ RGO (2 h), Zn/ RGO (24 h) and Zn/ RGO (2 h) wrapped Ag NPs electrode. The electrical conductivity of Zn/ RGO (24 h)

wrapped Ag NPs electrode is higher than Zn/Cu (1 cm^2), Zn/ RGO (2 h), Zn/ RGO (24 h) and Zn/ RGO (2 h) wrapped Ag NPs electrode. Because, the more the time takes to form RGO and Ag NPs nanocomposite the more open circuit voltage, V_{oc} (V), short circuit current, I_{sc} (mA) as well as power, $P_{max}= V_{oc} \times I_{sc}$ (W) increases which is the consistent with the published result [175]. As a result power, $P_{max}= V_{oc} \times I_{sc}$ (W) of Zn/ RGO (24 h) wrapped Ag NPs electrode is better than Zn/Cu (1 cm^2), Zn/ RGO (2 h), Zn/ RGO (24 h) and Zn/ RGO (2 h) wrapped Ag NPs electrode.

The figure 3.58 indicates the performance of power, $P_{max}= V_{oc} \times I_{sc}$ (W) using Zn/ RGO (24 h) wrapped Ag NPs electrode with AL electrolyte. The figure 3.59 shows the comparative power, $P_{max} = V_{oc} \times I_{sc}$ (W) of BVC among Zn/Cu (1 cm^2), Zn/ RGO (2 h), Zn/ RGO (24 h), Zn/ RGO (2 h) wrapped Ag NPs and Zn/ RGO (24 h) wrapped Ag NPs electrode using AL electrolyte. The figure 3.59 also shows the power, $P_{max}= V_{oc} \times I_{sc}$ (W) using Zn/ RGO (24 h) wrapped Ag NPs electrode is 0.124 W greater than Zn/ RGO (2 h) wrapped Ag NPs, 0.214 W greater than Zn/ RGO (24 h) electrode, 0.299 W greater than Zn/ RGO (2 h) and 0.407 W greater than Zn/Cu (1 cm^2) electrode with AL electrolyte.

3.11.8 Comparative study of Zn/Cu (1 cm^2), Zn/RGO (2 h), Zn/RGO (24 h), Zn/RGO (2 h) wrapped Ag NPs and Zn/RGO (24 h) wrapped Ag NPs electrode performance in BVC with AL electrolyte

Table-3.9: Comparative performance of BVC using Zn/Cu (1 cm^2), Zn/RGO (2 h), Zn/RGO (24 h), Zn/RGO (2 h) wrapped Ag NPs and Zn/RGO (24 h) wrapped Ag NPs electrode with AL electrolyte

No.	Performance parameters of BVC	Type of electrolyte	Type of electrodes and highest magnitude				
			Zn/Cu (1 cm^2)	Zn/ RGO (2 h)	Zn/ RGO (24 h)	Zn/ RGO (2 h) wrapped Ag NPs	Zn/ RGO (24 h) wrapped Ag NPs
1	Open circuit voltage, V_{oc} (V)	AL	0.95 V	0.99 V	1.00 V	1.12 V	1.21 V
2	Short circuit current, I_{sc} (mA)	AL	110 mA	215 mA	297 mA	346 mA	423 mA
3	Power, $P_{max}= V_{oc} \times I_{sc}$ (W)	AL	0.10 W	0.21 W	0.29 W	0.38752 W	0.51183 W

It is clear from the above table 3.9 that BVC developed using Zn/ RGO (24 h) wrapped Ag NPs electrode and AL extract electrolyte showed better performance than that of the BVC developed

using Zn/Cu (1 cm^2), Zn/ RGO (2 h), Zn/ RGO (24 h) and Zn/ RGO (2 h) wrapped Ag NPs electrode and AL extract electrolyte. Because, electrical conductivity of Ag NPs wrapped 24 hours RGO adsorbed paper electrode is better than Cu, 2 hours RGO adsorbed paper electrode, 24 hours RGO adsorbed paper electrode and Zn/ RGO (2 h) wrapped Ag NPs which is the consistent with the published result [99,175].

3.12 Effect of RGO in PKL extract BVC

Three parameters such as open circuit voltage, V_{oc} (V), short circuit current, I_{sc} (mA) and power, $P_{max}= V_{oc} \times I_{sc}$ (W) are also measured to check the performance of BVC using five types of electrode such as Zn/Cu (1 cm^2), Zn/RGO (2 h), Zn/RGO (24 h), Zn/RGO (2 h) wrapped Ag NPs and Zn/RGO (24 h) wrapped Ag NPs with two type of electrolyte such as PKL and AL electrolyte.

3.12.1 Effect on V_{oc} (V) of BVC using Zn/Cu (1 cm^2) and Zn/ RGO (2 h) electrode with PKL electrolyte

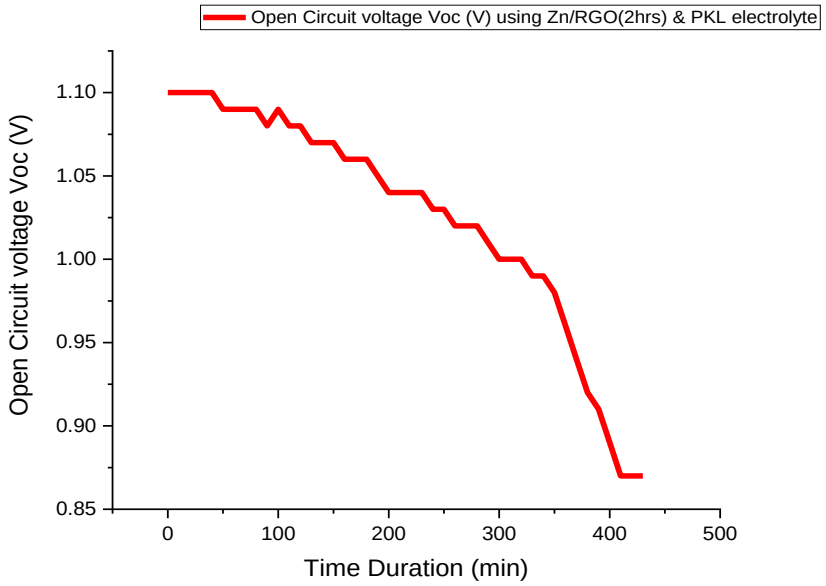

Figure 3.60: Variation of V_{oc} (V) with time (min) using Zn/ RGO (2 h) electrode and PKL electrolyte

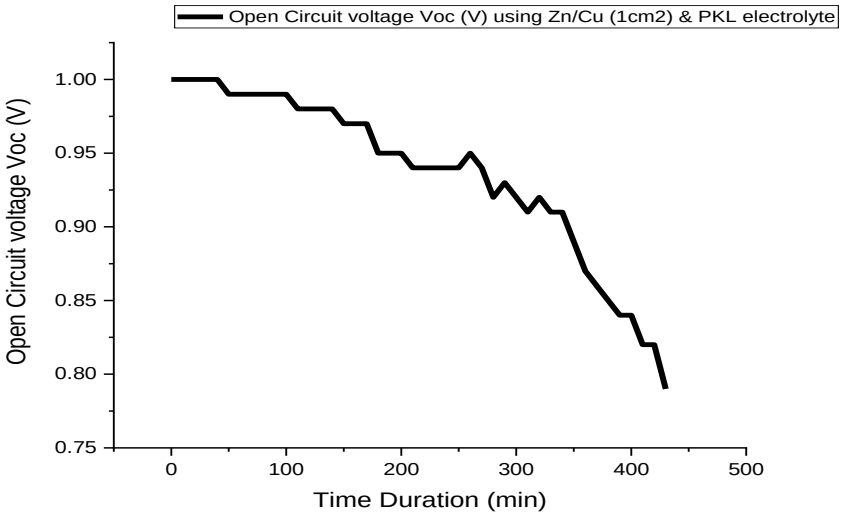

Figure 3.61: Variation of V_{oc} (V) with time (min) using Zn/Cu (1 cm^2) electrode and PKL electrolyte.

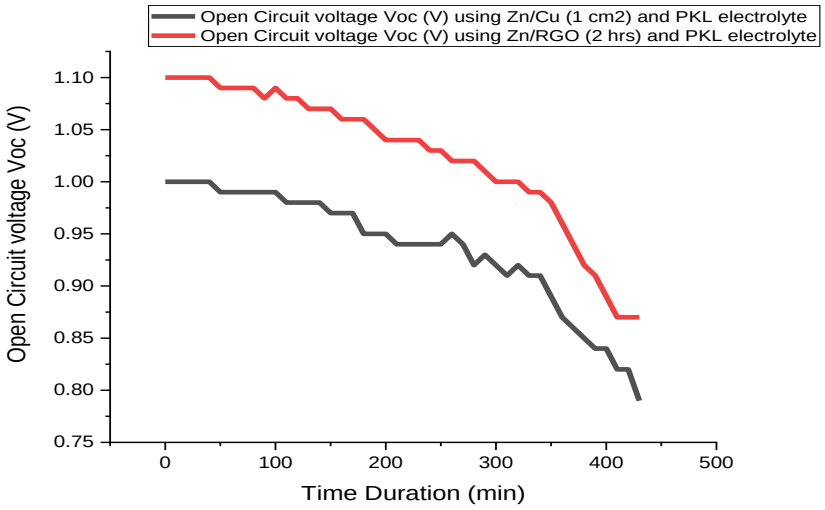

Figure 3.62: Variation of V_{oc} (V) with time (min) between Zn/Cu (1 cm^2) and Zn/ RGO (2 h) electrode using PKL electrolyte

The figure 3.62 shows the open circuit voltage, V_{oc} (V) of BVC using Zn/Cu (1 cm^2) and Zn/ RGO (2 h) electrode with PKL electrolyte. The open circuit voltage, V_{oc} (V) of BVC using Zn/ RGO (2 h) electrode is better performer than Zn/Cu (1 cm^2) electrode. Because, electrical conductivity of RGO is better than Cu which is consistent with the published result [99].

The figure 3.60 shows the open circuit voltage V_{oc} (V) of BVC using Zn/ RGO (2 h) electrode with PKL electrolyte.The figure 3.61 shows the open circuit voltage, V_{oc} (V) using Zn/Cu (1 cm^2) electrode with PKL electrolyte. The figure 3.62 shows the open circuit voltage, V_{oc} (V) using Zn/Cu (1 cm^2) and Zn/ RGO (2 h) electrode with PKL electrolyte. The figure 3.62 also shows that Zn/ RGO (2 h) electrode is 0.1 (V) greater than Zn/Cu (1 cm^2) electrode with PKL electrolyte.

3.12.2 Effect on I_{sc} (mA) of BVC using Zn/Cu (1 cm^2) and Zn/ RGO (2 h) electrode with PKL electrolyte

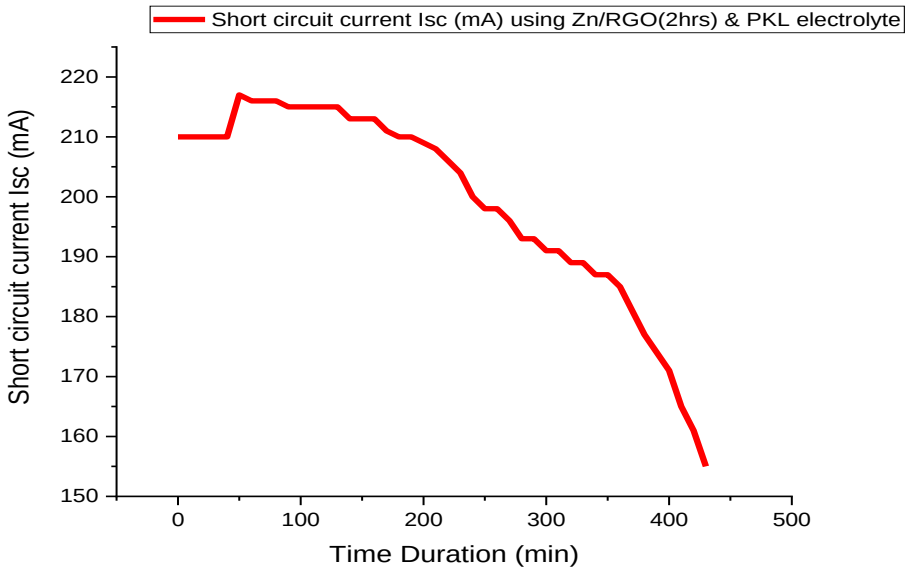

Figure 3.63: Variation of Isc (mA) with time (min) using Zn/ RGO (2 h) PKL electrolyte

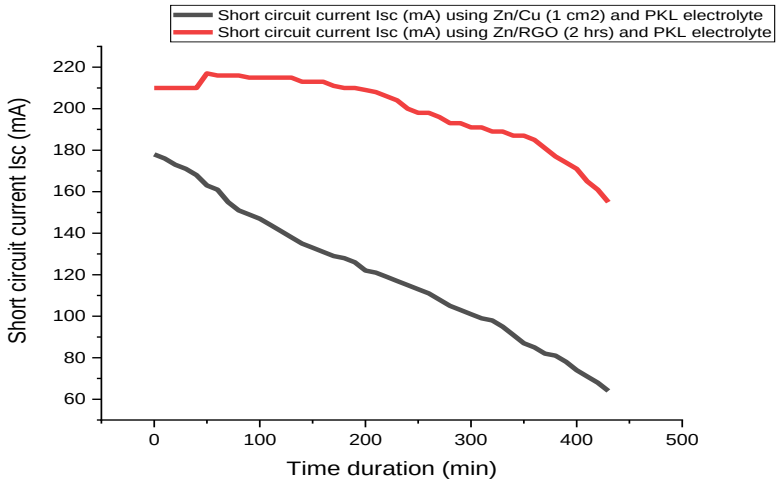

Figure 3.64: Variation of Isc (mA) with time (min) between Zn/Cu (1 cm^2) and Zn/ RGO (2 h) electrode using PKL electrolyte

The figure 3.64 shows the short circuit current, I_{sc} (mA) of BVC using Zn/Cu (1 cm^2) and Zn/ RGO (2 h) electrode with PKL electrolyte. The short circuit current, I_{sc} (mA) of BVC using Zn/ RGO (2 h) electrode is better performer than Zn/Cu (1 cm^2) electrode. Because, electrical conductivity of RGO is better than Cu which is consistent with the published result [99].

The figure 3.63 shows the short circuit current, I_{sc} (mA) of BVC using Zn/ RGO (2 h) electrode using PKL electrolyte. The figure 3.64 also shows the short circuit current, I_{sc} (mA) of BVC using Zn/ RGO (2 h) electrode is 32 (mA) greater than Zn/Cu (1 cm^2) electrode with PKL electrolyte.

3.12.3 Effect on power (W) of BVC using Zn/Cu (1 cm^2) and Zn/ RGO (2 h) electrode with PKL electrolyte

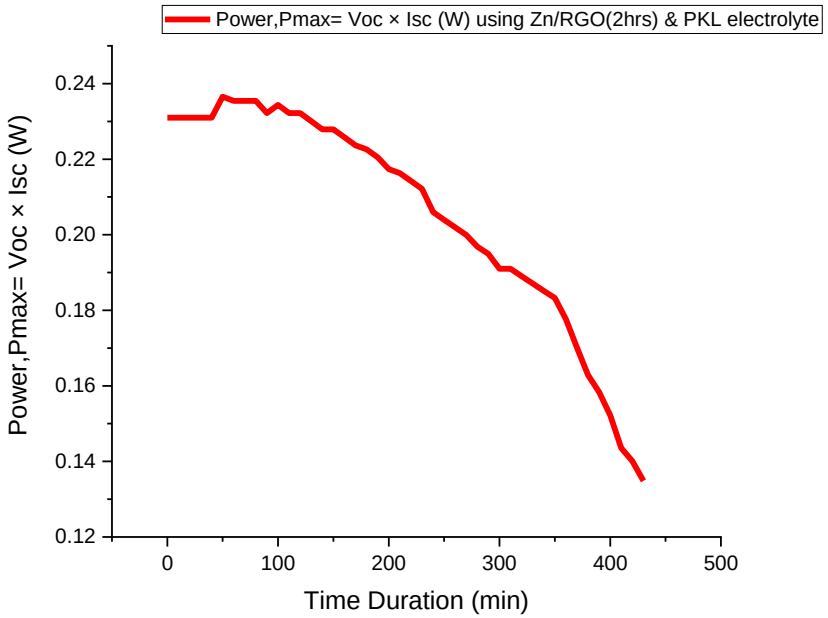

Figure 3.65: Variation of power (W) with time (min) using Zn/ RGO (2 h) electrode and PKL electrolyte

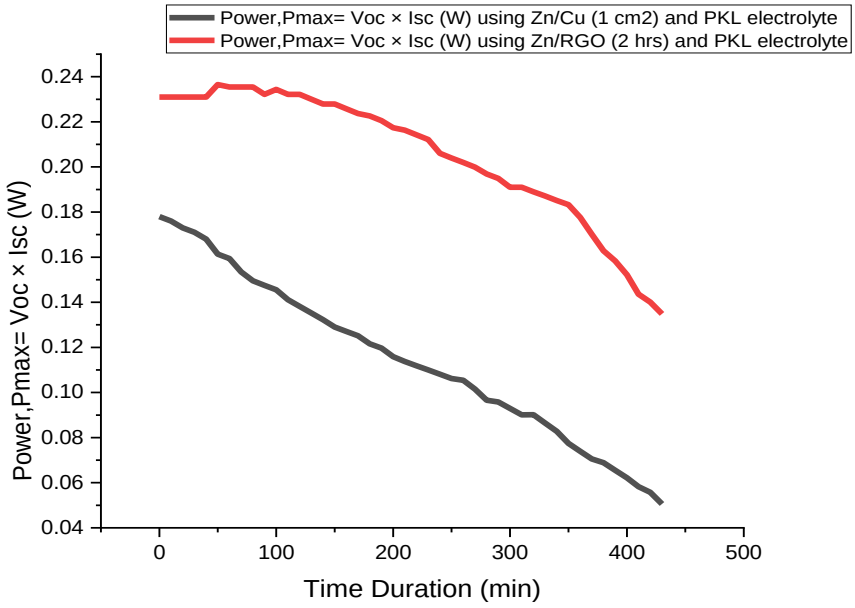

Figure 3.66: Variation of power (W) with time (min) between Zn/Cu (1 cm^2) and Zn/ RGO (2 h) electrode using PKL electrolyte

The figure 3.66 shows the power, $P_{max}= V_{oc} \times I_{sc}$ (W) of BVC using Zn/Cu (1 cm^2) and Zn/ RGO (2 h) lectrode with PKL electrolyte. The power, $P_{max}= V_{oc} \times I_{sc}$ (W) of BVC using Zn/ RGO (2 h) electrode is better performer than Zn/Cu (1 cm^2) electrode. Because, open circuit voltage, V_{oc} (V)

and short circuit current, I_{sc} of Zn/ RGO (2 h) electrode is higher than Zn/Cu (1 cm^2). As a result power, $P_{max}= V_{oc} \times I_{sc}$ (W) of Zn/ RGO (2 h) is better performer than Zn/Cu (1 cm^2) which is consistent with the published result [99].

The figure 3.65 also shows the power $P_{max}= V_{oc} \times I_{sc}$ (W) of BVC using Zn/ RGO (2 h) electrode using PKL electrolyte. The figure 3.66 shows that performance of power, $P_{max}= V_{oc} \times I_{sc}$ (W) using Zn/ RGO (2 h) electrode is 0.053 (W) greater than Zn/Cu (1 cm^2) electrode with PKL electrolyte.

3.12.4 Comparative study of Zn/Cu (1 cm^2) and Zn/RGO (2 h) electrode performance in BVC with PKL electrolyte

Table-3.10: Comparative performance of BVC using Zn/Cu (1 cm^2) and Zn/RGO (2 h) with PKL electrolyte

No.	Performance parameters of BVC	Type of electrolyte	Type of electrodes and highest magnitude	
			Zn/Cu (1 cm^2)	Zn/ RGO (2 h)
1	Open circuit voltage, V_{oc} (V)	PKL	1.00 V	1.10 V
2	Short circuit current, I_{sc} (mA)	PKL	178 mA	210 mA
3	Power, $P_{max}= V_{oc} \times I_{sc}$ (W)	PKL	0.178 W	0.231 W

It is clear from the above table 3.10 that BVC developed using Zn/ RGO (2 h) electrode and PKL extract electrolyte showed better performance than that of the BVC developed using Zn/Cu (1 cm^2) electrode and PKL extract electrolyte. Because, electrical conductivity of RGO adsorbed paper electrode is better than Cu electrode which is the consistent with the published result [99].

3.12.5 Effect on V_{oc} (V) of BVC using Zn/Cu (1 cm^2), Zn/ RGO (2 h) and Zn/ RGO (24 h) electrode with PKL electrolyte

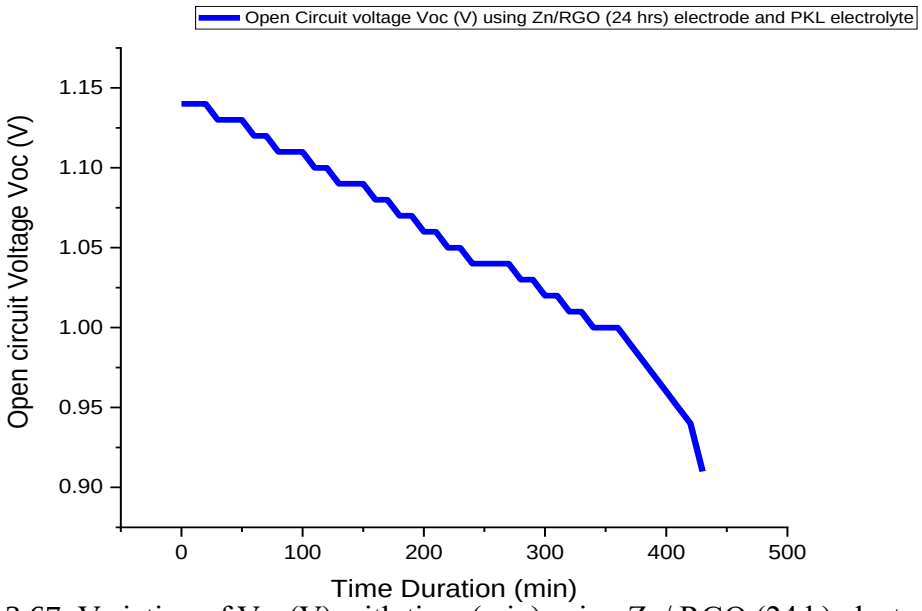

Figure 3.67: Variation of V_{oc} (V) with time (min) using Zn/ RGO (24 h) electrode and PKL electrolyte

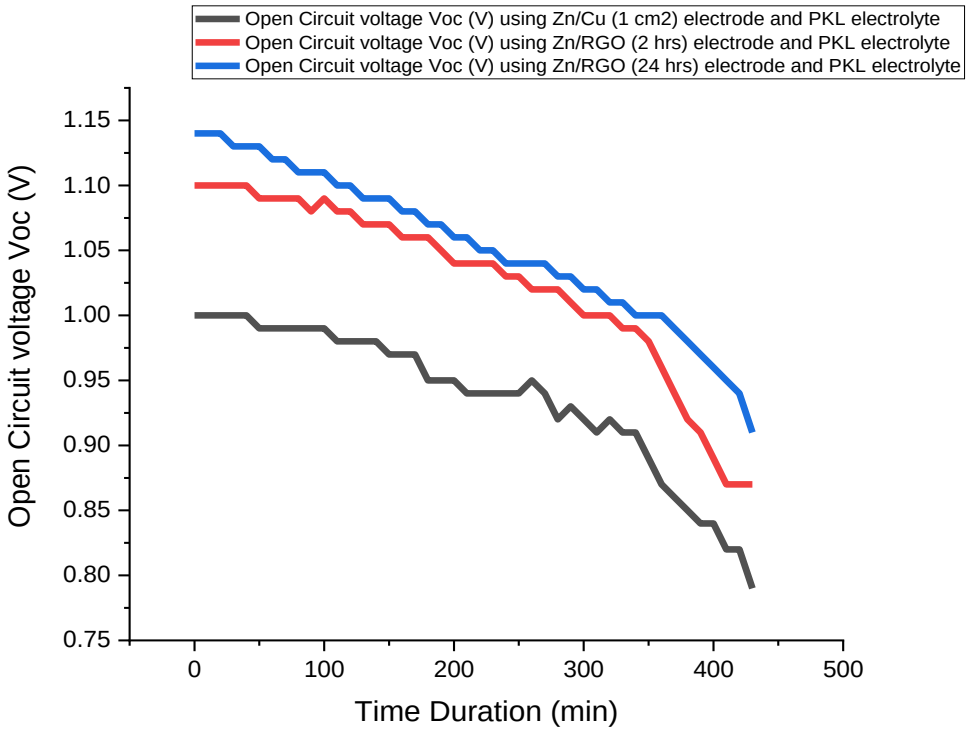

Figure 3.68: Variation of V_{oc} (V) with time (min) between Zn/Cu (1 cm^2), Zn/ RGO (2 h) and Zn/ RGO (24 h) electrode using PKL electrolyte

The figure 3.68 shows the open circuit voltage, V_{oc} (V) of BVC using Zn/Cu (1 cm^2), Zn/ RGO (2 h) and Zn/ RGO (24 h) electrode with PKL electrolyte. The open circuit voltage, V_{oc} (V) of BVC using Zn/ RGO (24 h) electrode is better performer than Zn/Cu (1 cm^2) and Zn/ RGO (2 h) electrode. Because, electrical conductivity of Zn/ RGO (24 h) is better than Zn/Cu (1 cm^2), Zn/ RGO (2 h) electrode which is consistent with the published result [99].

The figure 3.67 shows the open circuit voltage, V_{oc} (V) using Zn/ RGO (24 h) electrode with PKL electrolyte. The figure 3.68 shows the comparative performance of open circuit voltage V_{oc} (V) among Zn/Cu (1 cm^2), Zn/ RGO (2 h) & Zn/ RGO (24 h) electrode using PKL electrolyte. The figure 3.68 also shows that performance open circuit voltage V_{oc} (V) using Zn/ RGO (24 h) electrode is 0.10 V greater than Zn/ RGO (2 h) electrode and 0.14 V greater than Zn/Cu (1 cm^2) electrode with PKL electrolyte.

3.12.6 Effect on I_{sc} (mA) of BVC using Zn/Cu (1 cm^2), Zn/ RGO (2 h) and Zn/ RGO (24 h) electrode with PKL electrolyte

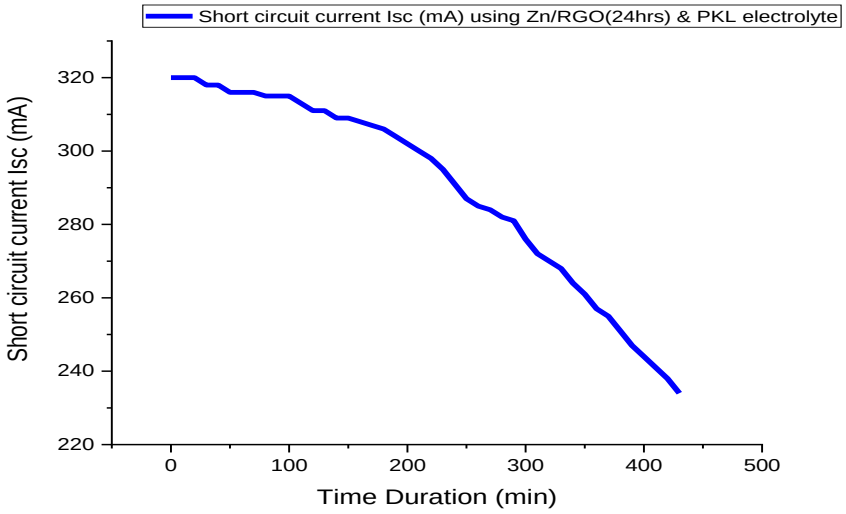

Figure 3.69: Variation of Isc (mA) with time (min) using Zn/ RGO (24 h) electrode and PKL electrolyte

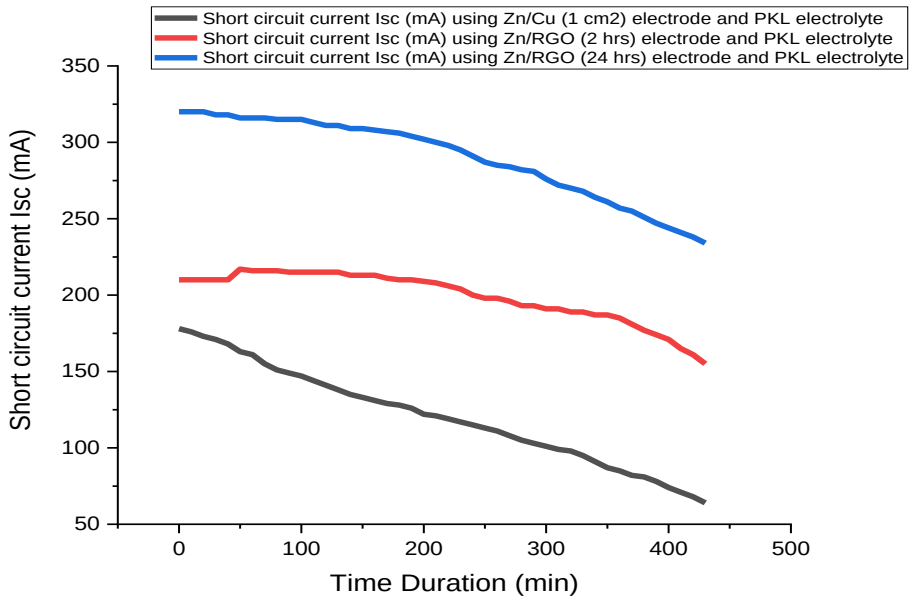

Figure 3.70: Variation of I_{sc} (mA) with time (min) among Zn/Cu (1 cm^2), Zn/ RGO (2 h) and Zn/RGO (24 h) electrode using PKL electrolyte

The figure 3.70 shows the short circuit current, I_{sc} (mA) of BVC using Zn/Cu (1 cm^2), Zn/ RGO (2 h) and Zn/ RGO (24 h) electrode with PKL electrolyte. The short circuit current, I_{sc} (mA) of

BVC using Zn/ RGO (24 h) electrode is better performer than Zn/Cu (1 cm^2) and Zn/ RGO (2 h) electrode. Because, the more the time takes to adsorbe RGO on paper electrode, the more the electrical conductivity increases which is the consistent with the published result [99,175].

The figure 3.69 shows the short circuit current, I_{sc} (mA) of BVC using Zn/ RGO (24 h) electrode with PKL electrolyte. The figure 3.70 shows the comparative performance of short circuit current, I_{sc} (mA) among Zn/Cu (1 cm^2), Zn/ RGO (2 h) & Zn/RGO (24 h) electrode using PKL electrolyte. The figure 3.70 also shows that performance of short circuit current, I_{sc} (mA) using Zn/ RGO (24 h) electrode is 32 (mA) greater than Zn/ RGO (2 h) electrode and 142 (mA) greater than Zn/Cu (1 cm^2) electrode with PKL electrolyte.

3.12.7 Effect on power (W) of BVC using Zn/Cu (1 cm^2), Zn/ RGO (2 h) and Zn/ RGO (24 h) electrode with PKL electrolyte

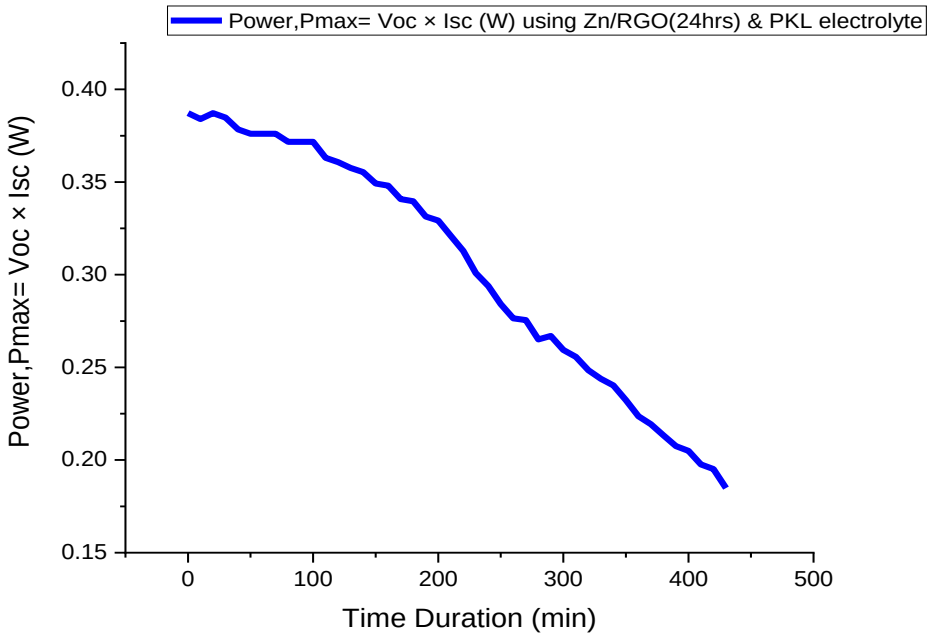

Figure 3.71: Variation of power (W) with time (min) using Zn/ RGO (24 h) electrode and PKL electrolyte

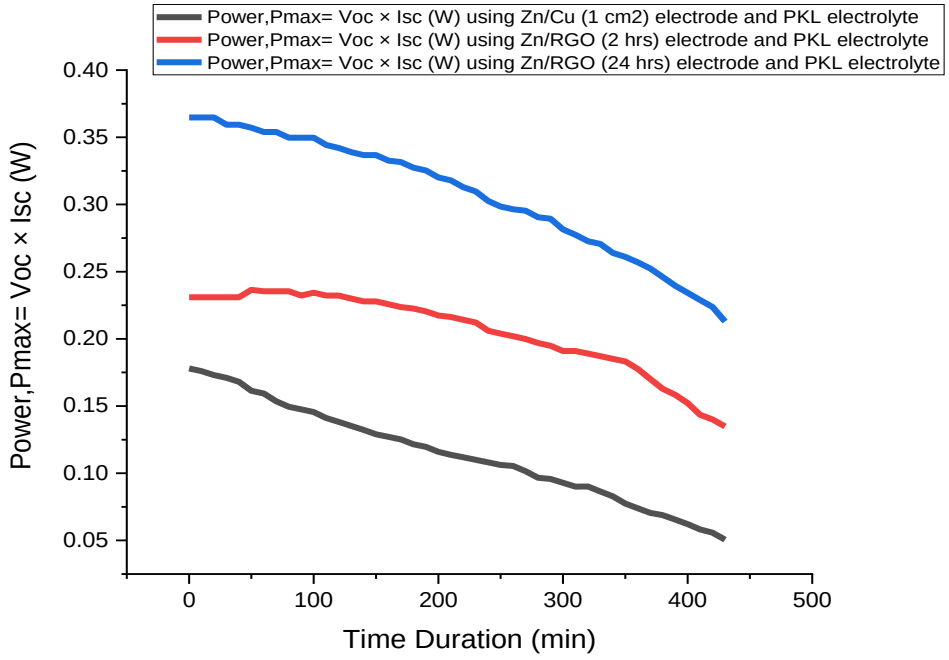

Figure 3.72: Variation of power (W) with time (min) among Zn/Cu (1 cm^2), Zn/ RGO (2 h) and Zn/RGO (24 h) electrode using PKL electrolyte

The figure 3.72 shows the power, $P_{max}= V_{oc} \times I_{sc}$ (W) of BVC using Zn/Cu (1 cm^2), Zn/ RGO (2 h) and Zn/ RGO (24 h) electrode with PKL electrolyte. The power, $P_{max}= V_{oc} \times I_{sc}$ (W) of BVC using Zn/ RGO (24 h) electrode is better performer than Zn/Cu (1 cm^2) and Zn/ RGO (2 h) electrode. Because, electrical conductivity of Zn/ RGO (24 h) is better than Zn/Cu (1 cm^2), Zn/ RGO (2 h) electrode. As a result open circuit voltage, V_{oc} (V) and short circuit current, I_{sc} (mA) as well as power, $P_{max}= V_{oc} \times I_{sc}$ (W) of Zn/ RGO (24 h) electrode are higher which is consistent with the published result [99,175].

The figure 3.71 shows the power, $P_{max}= V_{oc} \times I_{sc}$ (W) of BVC using Zn/ RGO (24 h) electrode with PKL electrolyte. The figure 3.72 shows the comparative performance of power, $P_{max}= V_{oc} \times I_{sc}$ (W) among Zn/Cu (1 cm^2), Zn/ RGO (2 h) & Zn/RGO (24 h) electrode using PKL electrolyte. The figure 3.79 also shows that performance of Power, $P_{max}= V_{oc} \times I_{sc}$ (W) using Zn/ RGO (24 h) electrode is 0.053 (W) greater than Zn/ RGO (2 h) electrode and 0.186 (W) greater than Zn/Cu (1 cm^2) electrode with PKL electrolyte.

3.12.8 Comparative study of Zn/Cu (1 cm^2), Zn/RGO (2 h) and Zn/RGO (24 h) electrode performance in BVC with PKL electrolyte

Table-3.11: Comparative performance of BVC using Zn/Cu (1 cm^2), Zn/RGO (2 h) and Zn/RGO (24 h) with PKL electrolyte

No.	Performance parameters of BVC	Type of electrolyte	Type of electrodes and highest magnitude		
			Zn/Cu (1 cm^2)	Zn/ RGO (2 h)	Zn/ RGO (24 h)
1	Open circuit voltage, V_{oc} (V)	PKL	1.00 V	1.10 V	1.14 V
2	Short circuit current, I_{sc} (mA)	PKL	178 mA	210 mA	320 mA
3	Power, $P_{max} = V_{oc} \times I_{sc}$ (W)	PKL	0.178 W	0.231 W	0.3648 W

It is clear from the above table 3.11 that BVC developed using Zn/ RGO (24 h) electrode and PKL extract electrolyte showed better performance than that of the BVC developed using Zn/Cu (1 cm^2) and Zn/ RGO (2 h) electrode and PKL extract electrolyte. Because, electrical conductivity of 24 hours RGO adsorbed paper electrode is better than Cu and 2 hours RGO adsorbed paper electrode which is the consistent with the published result [99].

3.13 Effect of RGO-Ag nanocomposite in PKL extract BVC

3.13.1 Effect of Zn/RGO (2 h)-Ag nanocomposite electrode on V_{oc} (V) in PKL extract BVC

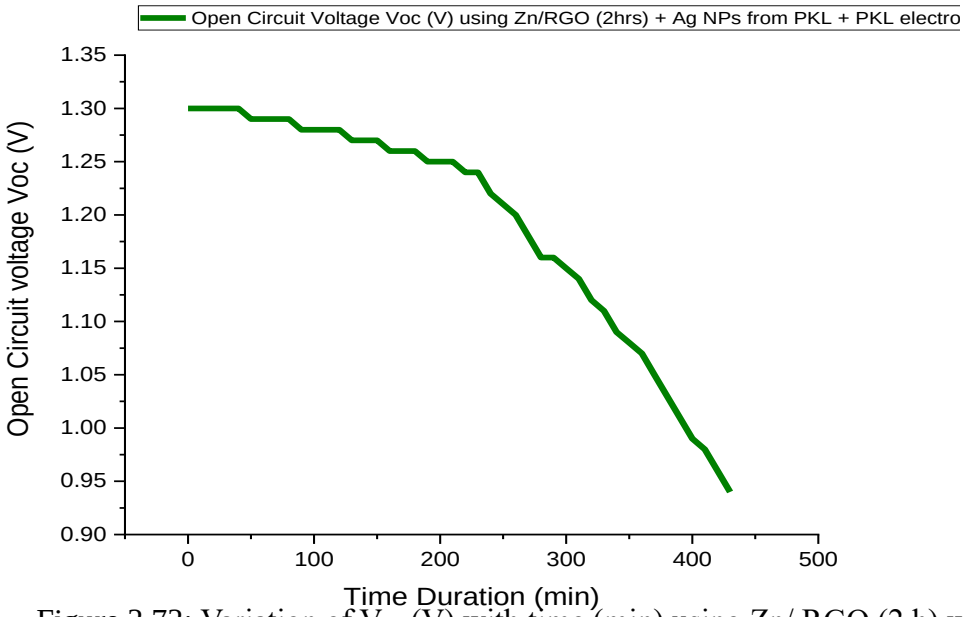

Figure 3.73: Variation of V_{oc} (V) with time (min) using Zn/ RGO (2 h) wrapped Ag NPs electrode and PKL electrolyte

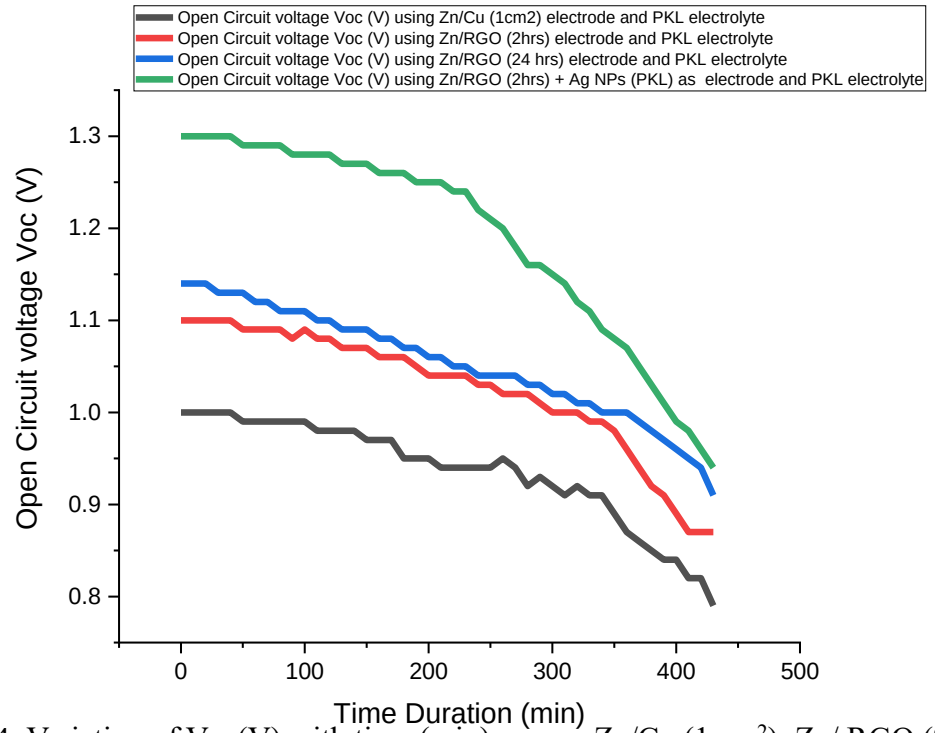

Figure 3.74: Variation of V_{oc} (V) with time (min) among Zn/Cu (1 cm^2), Zn/ RGO (2 h), Zn/ RGO (2 h) wrapped Ag NPs electrode using PKL electrolyte

The figure 3.74 shows the open circuit voltage, V_{oc} (V) of BVC using Zn/Cu (1 cm^2), Zn/ RGO (2 h), Zn/ RGO (24 h) and Zn/ RGO (2 h) wrapped Ag NPs electrode electrode with PKL electrolyte. The open circuit voltage, V_{oc} (V) of BVC using Zn/ RGO (2 h) wrapped Ag NPs electrode is better performer than Zn/Cu (1 cm^2), Zn/ RGO (2 h) and Zn/ RGO (24 h) electrode. Because, electrical conductivity of Zn/ RGO (2 h) wrapped Ag NPs electrode is better performer than Zn/Cu (1 cm^2), Zn/ RGO (2 h) and Zn/ RGO (24 h) electrode which is consistent with the published result [99,175].

The figure 3.73 shows the performance of open circuit voltage V_{oc} (V) using Zn/ RGO (2 h) wrapped Ag NPs electrode with PKL electrolyte. The figure 3.74 shows the comparative performance of open circuit voltage, V_{oc} (V) among Zn/Cu (1 cm^2), Zn/ RGO (2 h), Zn/ RGO (24 h) and Zn/ RGO (2 h) wrapped Ag NPs electrode using PKL electrolyte. The figure 3.74 also shows the open circuit voltage, V_{oc} (V) using Zn/ RGO (2 h) wrapped Ag NPs electrode is 0.16 (V) greater than Zn/ RGO (24 h) electrode 0.14 (V) greater than Zn/ RGO (2 h) and 0.10 (V) Zn/Cu (1 cm^2) electrode with PKL electrolyte.

3.13.2 Effect of Zn/RGO (2 h)-Ag nanocomposite electrode on I_{sc} (mA) in PKL extract BVC

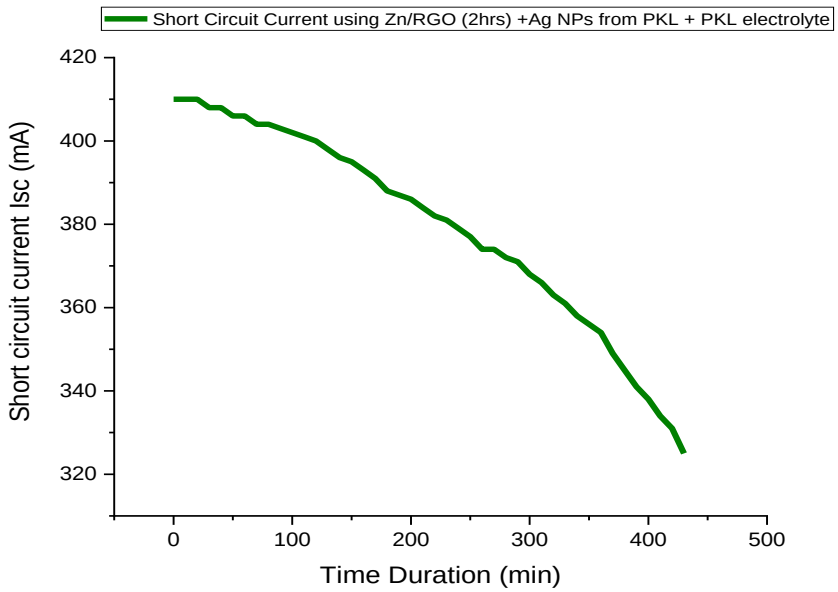

Figure 3.75: Variation of I_{sc} (mA) VS Time duration (min) using Zn/ RGO (2 h) wrapped Ag NPs electrode and PKL electrolyte

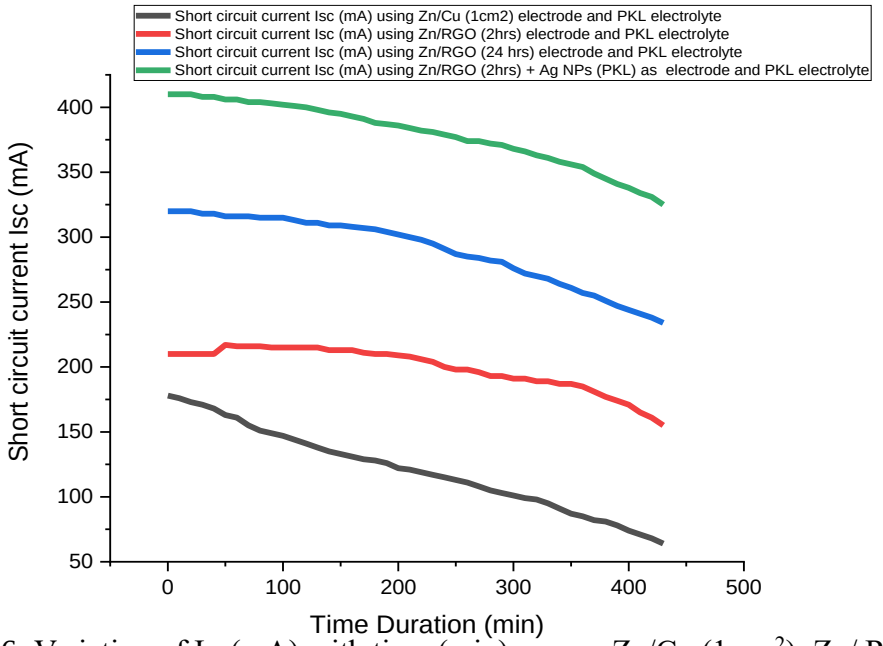

Figure 3.76: Variation of I_{sc} (mA) with time (min) among Zn/Cu (1 cm^2), Zn/ RGO (2 h), Zn/ RGO (24 h), Zn/ RGO (2 h) wrapped Ag NPs electrode using PKL electrolyte

The figure 3.76 shows the short circuit current, I_{sc} (mA) of BVC using Zn/Cu (1 cm^2), Zn/ RGO (2 h), Zn/ RGO (24 h) and Zn/ RGO (2 h) wrapped Ag NPs electrode electrode with PKL electrolyte. The short circuit current, I_{sc} (mA) of BVC using Zn/ RGO (2 h) wrapped Ag NPs electrode is better performer than Zn/Cu (1 cm^2), Zn/ RGO (2 h) and Zn/ RGO (24 h) electrode. Due to the formation of RGO and Ag NPs nanocomposite, the electrical conductivity increases which is consistent with the published result [99,175].

The figure 3.75 shows the short circuit current, Isc (mA) of BVC using Zn/ RGO (2 h) wrapped Ag NPs electrode with PKL electrolyte. The figure 3.76 shows the comparative performance of short circuit current, Isc (mA) among Zn/Cu (1 cm^2), Zn/ RGO (2 h), Zn/ RGO (24 h) and Zn/ RGO (2 h) wrapped Ag NPs electrode using PKL electrolyte. The figure 3.76 also shows that short circuit current, Isc (mA) using Zn/ RGO (2 h) wrapped Ag NPs electrode is 232 (mA) greater than Zn/ RGO (24 h) electrode, 142 (mA) greater than Zn/ RGO (2 h) and 32 (mA) greater than Zn/Cu (1 cm^2) electrode with PKL electrolyte.

3.13.3 Effect of Zn/RGO (2 h)-Ag nanocomposite electrode on power (W) in PKL extract BVC

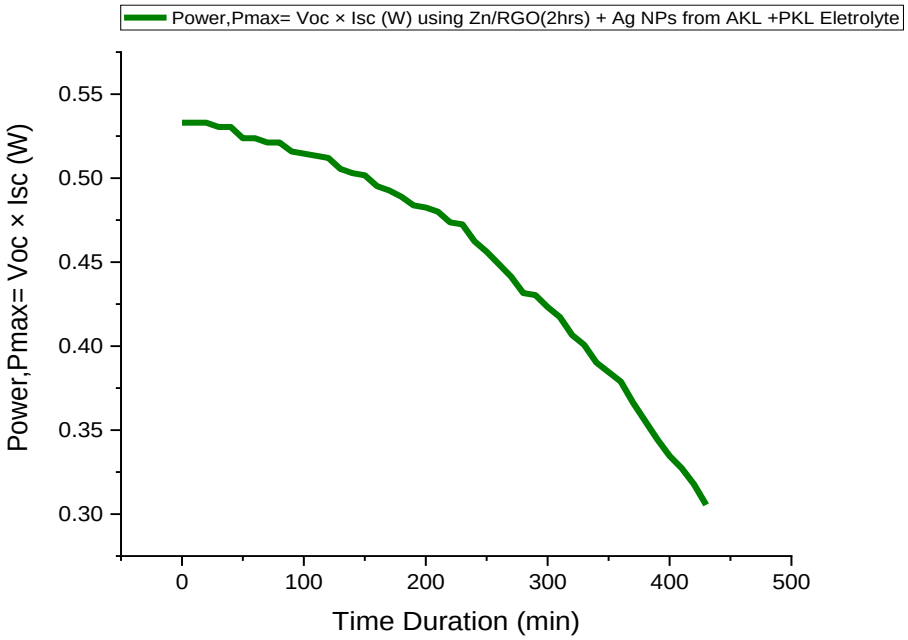

Figure 3.77: Power, $P_{max}= V_{oc} \times I_{sc}$ (W) VS Time duration (min) using Zn/ RGO (2 h) wrapped Ag NPs (from PKL) electrode & PKL electrolyte

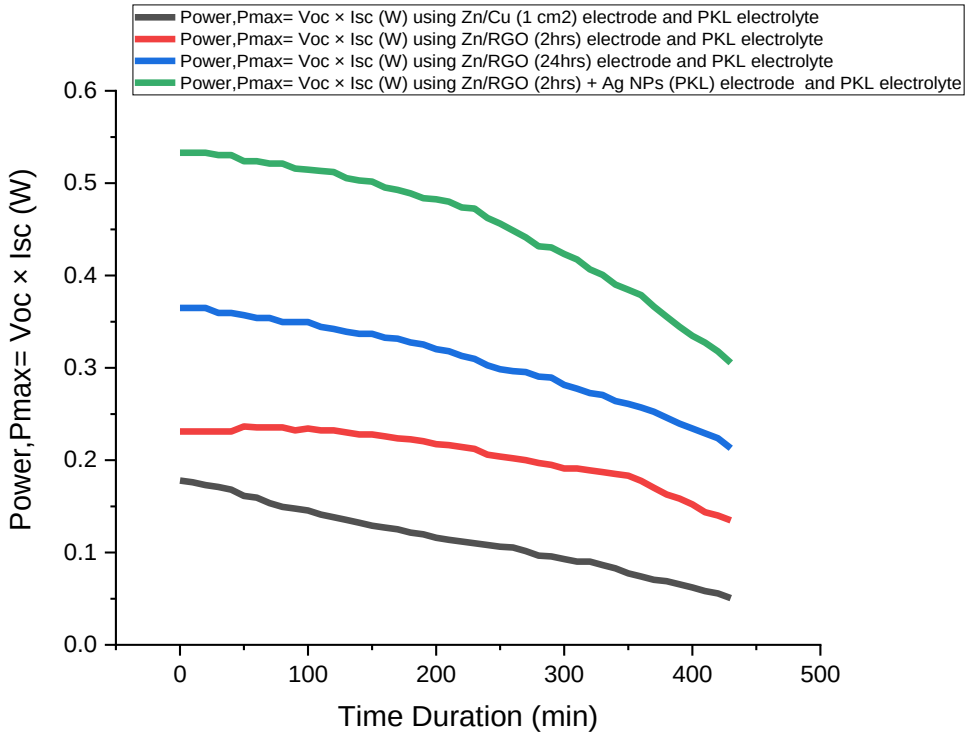

Figure 3.78: Variation of power (W) with time (min) among Zn/Cu (1 cm^2), Zn/ RGO (2 h), Zn/ RGO (2 h) wrapped Ag NPs electrode using PKL electrolyte.

The figure 3.78 shows the power, $P_{max}= V_{oc} \times I_{sc}$ (W) of BVC using Zn/Cu (1 cm^2), Zn/ RGO (2 h), Zn/ RGO (24 h) and Zn/ RGO (2 h) wrapped Ag NPs electrode electrode with PKL extract electrolyte. The power, $P_{max}= V_{oc} \times I_{sc}$ (W) of BVC using Zn/ RGO (2 h) wrapped Ag NPs electrode is better performer than Zn/Cu (1 cm^2), Zn/ RGO (2 h) and Zn/ RGO (24 h) electrode. Because, electrical conductivity as well as open circuit voltage, V_{oc} (V), short circuit current, I_{sc} (mA) and power, $P_{max}= V_{oc} \times I_{sc}$ (W) of Zn/ RGO (2 h) wrapped Ag NPs electrode is better than Zn/Cu (1 cm^2), Zn/ RGO (2 h) and Zn/ RGO (24 h) electrode which is consistent with the published result [99,175].

The figure 3.77 shows the power, $P_{max}= V_{oc} \times I_{sc}$ (W) of BVC using Zn/ RGO (2 h) wrapped Ag NPs electrode with PKL electrolyte. The figure 3.78 shows the comparative performance of power, $P_{max}= V_{oc} \times I_{sc}$ (W) among Zn/Cu (1 cm^2), Zn/ RGO (2 h), Zn/ RGO (24 h) and Zn/ RGO (2 h) wrapped Ag NPs electrode using PKL electrolyte. The figure 3.78 also shows that performance of power, $P_{max}= V_{oc} \times I_{sc}$ (W) using Zn/ RGO (2 h) wrapped Ag NPs electrode is 0.169 (W) greater than Zn/ RGO (24 h) electrode, 0.302 (W) greater than Zn/ RGO (2 h) and 0.355 (W) Zn/Cu (1 cm^2) electrode with PKL electrolyte.

3.13.4 Comparative study of Zn/Cu (1 cm^2), Zn/RGO (2 h), Zn/RGO (24 h) and Zn/RGO (2 h) wrapped Ag NPs electrode performance in BVC with PKL electrolyte

Table-3.12: Comparative performance of BVC using Zn/Cu (1 cm^2), Zn/RGO (2 h), Zn/RGO (24 h) and Zn/RGO (2 h) wrapped Ag NPs with PKL electrolyte

No.	Performance parameters of BVC	Type of electrolyte	Type of electrodes and highest magnitude			
			Zn/Cu (1 cm^2)	Zn/ RGO (2 h)	Zn/ RGO (24 h)	Zn/ RGO (2 h) wrapped Ag NPs
1	Open circuit voltage, V_{oc} (V)	PKL	1.00 V	1.10 V	1.14 V	1.16 V
2	Short circuit current, I_{sc} (mA)	PKL	178 mA	210 mA	320 mA	410 mA
3	Power, $P_{max}= V_{oc} \times I_{sc}$ (W)	PKL	0.178 W	0.231 W	0.3648 W	0.533 W

It is clear from the above table 3.8 that BVC developed using Zn/ RGO (2 h) wrapped Ag NPs electrode and PKL extract electrolyte showed better performance than that of the BVC developed

using Zn/Cu (1 cm^2), Zn/ RGO (2 h) and Zn/ RGO (24 h) electrode and PKL extract electrolyte. Because, electrical conductivity of Ag NPs wrapped 2 hours RGO adsorbed paper electrode is better than Cu, 2 hours RGO adsorbed paper electrode and 24 hours RGO adsorbed paper electrode which is the consistent with the published result [99,175].

3.13.5 Effect of Zn/RGO (24 h)-Ag nanocomposite electrode on V_{oc} (V) in PKL extract BVC

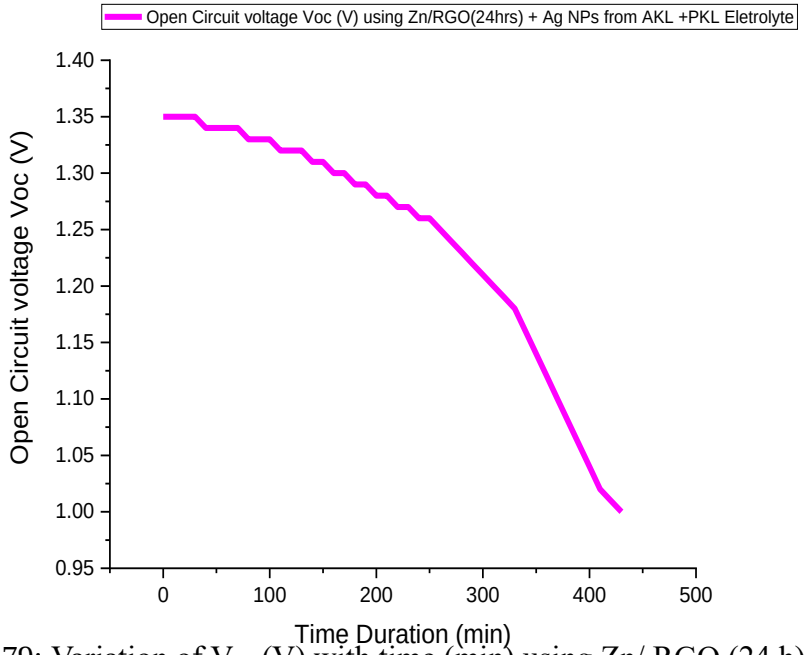

Figure 3.79: Variation of V_{oc} (V) with time (min) using Zn/ RGO (24 h) wrapped Ag NPs electrode and PKL electrolyte

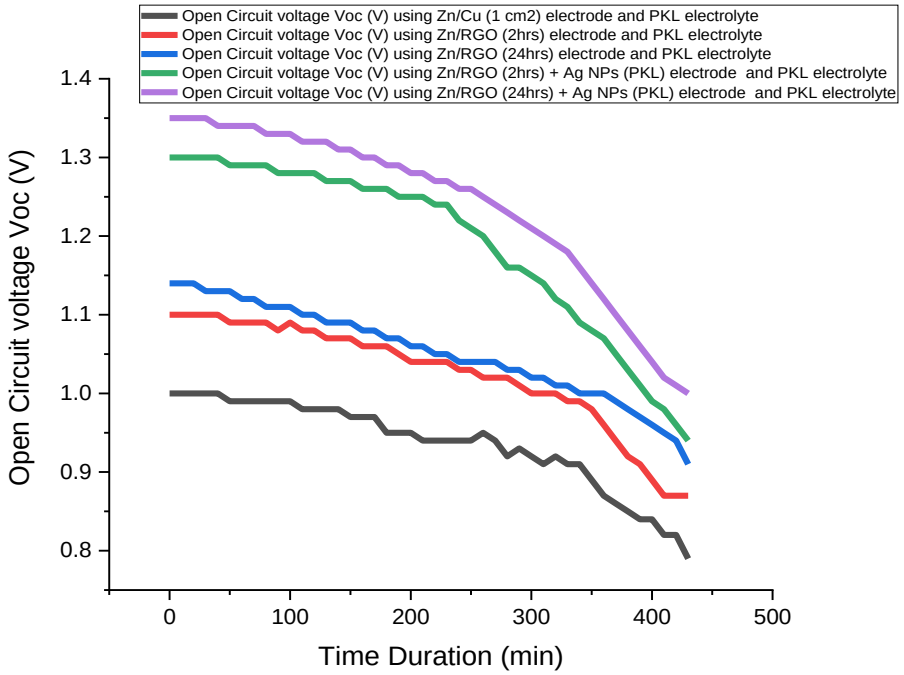

Figure 3.80: Variation of V_{oc} (V) with time (min) among Zn/Cu (1 cm^2), Zn/ RGO (2 h), Zn/ RGO (24 h), Zn/ RGO (2 h) wrapped Ag NPs and Zn/ RGO (24 h) wrapped Ag NPs electrode using PKL electrolyte

The figure 3.80 shows the open circuit voltage, V_{oc} (V) of BVC using Zn/ RGO (24 h) wrapped Ag NPs electrode and PKL extract electrolyte. The open circuit voltage, V_{oc} (V) of Zn/ RGO (24 h) wrapped Ag NPs electrode is better performer than Zn/Cu (1 cm^2), Zn/ RGO (2 h), Zn/ RGO (24 h) and Zn/ RGO (2 h) wrapped Ag NPs electrode. Because, the more the time takes to form RGO and Ag NPs nanocomposite, the more the electrical conductivity increases which is the consistent with the published result [99,175].

The figure 3.79 shows the open circuit voltage, V_{oc} (V) using Zn/ RGO (24 h) wrapped Ag NPs electrode with PKL electrolyte. The figure 3.80 shows the comparative performance of open circuit voltage, V_{oc} (V) among Zn/Cu (1 cm^2), Zn/ RGO (2 h), Zn/ RGO (24 h), Zn/ RGO (2 h) wrapped Ag NPs and Zn/ RGO (24 h) wrapped Ag NPs electrode using PKL electrolyte. The figure 3.80 also shows that performance of open circuit voltage, V_{oc} (V) using Zn/ RGO (24 h) wrapped Ag NPs electrode is 0.18 (V) greater than Zn/RGO (2 h) wrapped Ag NPs 0.20 V greater than Zn/ RGO (24 h) electrode 0.33 (V) greater than Zn/ RGO (2 h) and 0.34 (V) greater than Zn/Cu (1 cm^2) electrode with PKL electrolyte.

3.13.6 Effect of Zn/RGO (24 h)-Ag nanocomposite electrode on I_{sc} (mA) in PKL extract BVC

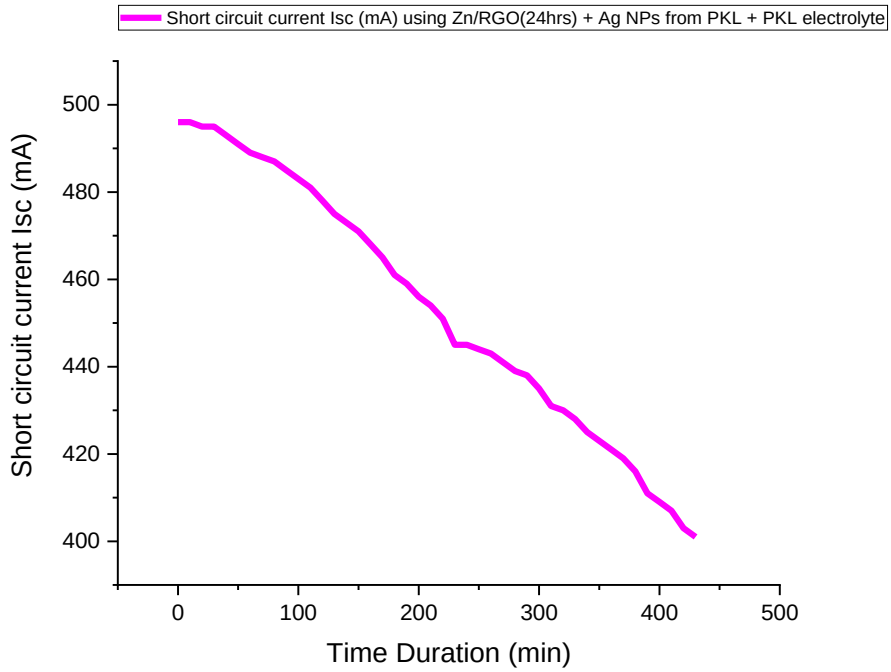

Figure 3.81: Variation of V_{oc} (V) with time (min) using Zn/ RGO (24 h) wrapped Ag NPs electrode and PKL electrolyte

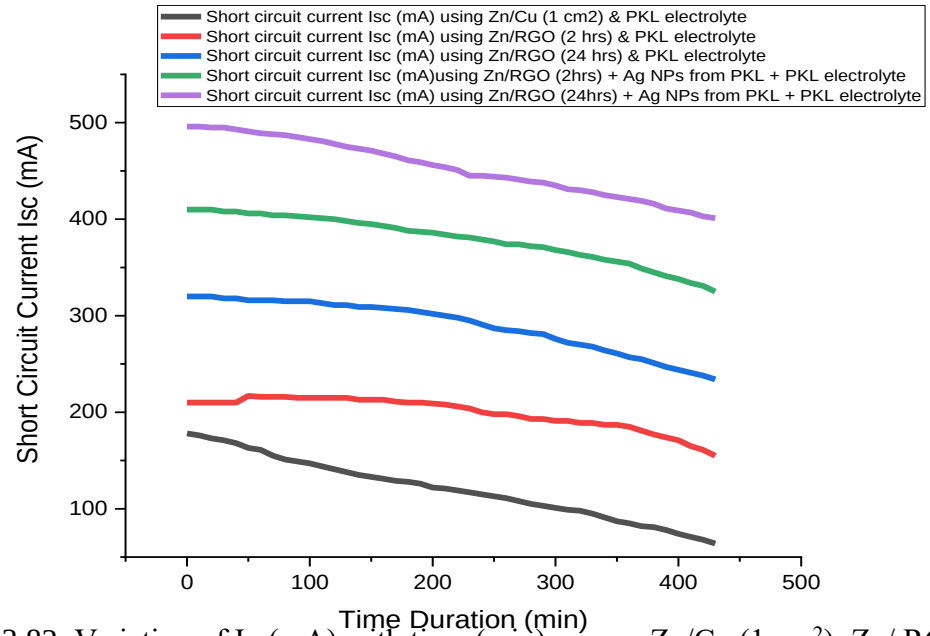

Figure 3.82: Variation of I_{sc} (mA) with time (min) among Zn/Cu (1 cm^2), Zn/ RGO (2 h), Zn/ RGO (24 h), Zn/ RGO (2 h) wrapped Ag NPs and Zn/ RGO (2 h) wrapped Ag NPs electrode using PKL electrolyte

The figure 3.82 shows the short circuit current, I_{sc} (mA) of BVC using Zn/ RGO (24 h) wrapped Ag NPs electrode and PKL extract electrolyte. The short circuit current, I_{sc} (mA) of Zn/ RGO (24 h) wrapped Ag NPs electrode is better performer than Zn/Cu (1 cm^2), Zn/ RGO (2 h), Zn/ RGO (24 h) and Zn/ RGO (2 h) wrapped Ag NPs electrode. Because, the more the time takes to form RGO and Ag NPs nanocomposite, the more the electrical conductivity increases which is the consistent with the published result [99,175].

The figure 3.81 shows the performance of short circuit current, I_{sc} (mA) of BVC using Zn/ RGO (24 h) wrapped Ag NPs electrode with PKL electrolyte. The figure 3.82 shows the comparative performance of short circuit current, I_{sc} (mA) among Zn/Cu (1 cm^2), Zn/ RGO (2 h), Zn/ RGO (24 h), Zn/ RGO (2 h) wrapped Ag NPs and Zn/ RGO (24 h) wrapped Ag NPs electrode using PKL electrolyte. The figure 3.82 also shows that short circuit current, I_{sc} (mA) using Zn/ RGO (24 h) wrapped Ag NPs electrode is 86 (mA) greater than Zn/ RGO (2 h) wrapped Ag NPs 176 (mA) greater than Zn/ RGO (24 h) electrode 286 (mA) greater than Zn/ RGO (2 h) and 318 (mA) greater than Zn/Cu (1 cm^2) electrode with PKL electrolyte.

3.13.7 Effect of Zn/RGO (24 h)-Ag nanocomposite electrode on power (W) in PKL extract BVC

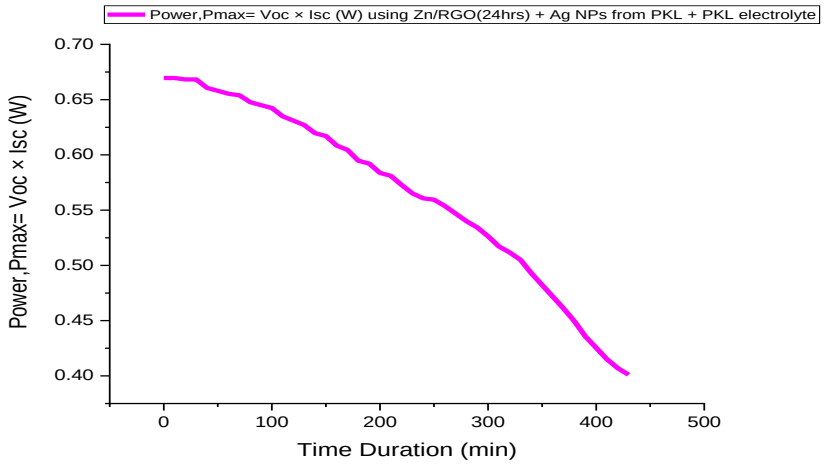

Figure 3.83: Variation of power (W) with time (min) using Zn/ RGO (24 h) wrapped Ag NPs and PKL electrolyte

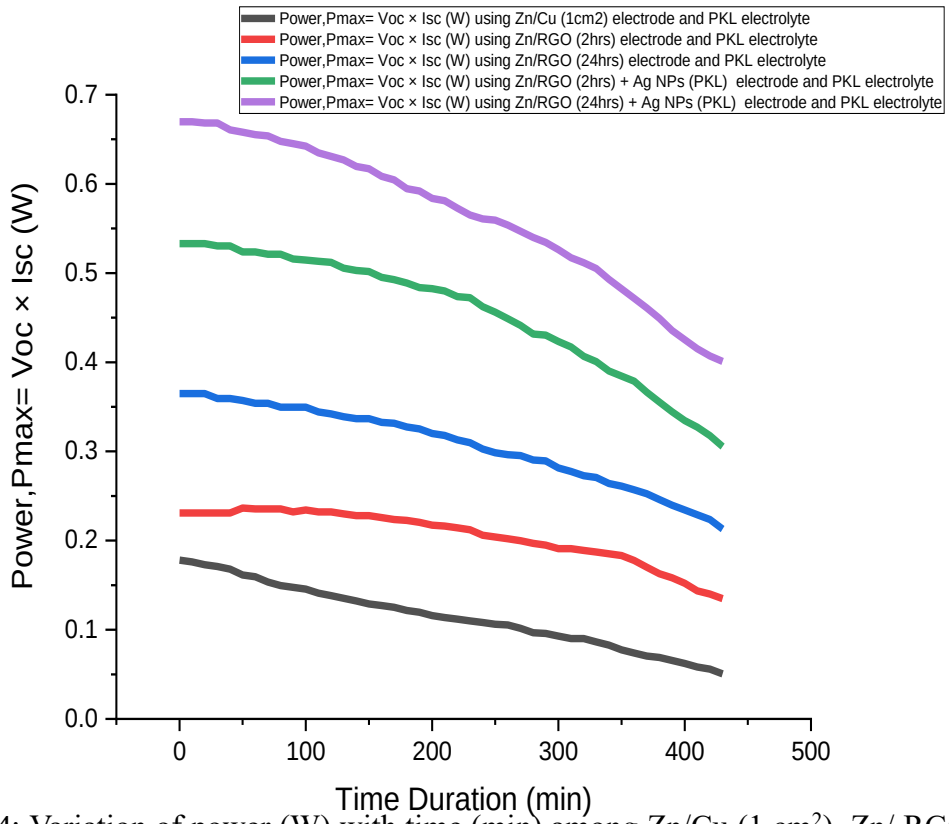

Figure 3.84: Variation of power (W) with time (min) among Zn/Cu (1 cm^2), Zn/ RGO (2 h), Zn/ RGO (24 h), Zn/ RGO (2 h) wrapped Ag NPs and Zn/ RGO (2 h) wrapped Ag NPs electrode using PKL electrolyte.

The figure 3.84 shows the power, $P_{max}= V_{oc} \times I_{sc}$ (W) of BVC using Zn/ RGO (24 h) wrapped Ag NPs electrode and PKL extract electrolyte. The power, $P_{max}= V_{oc} \times I_{sc}$ (W) of BVC using Zn/ RGO (24 h) wrapped Ag NPs electrode and PKL extract electrolyte is better performer than Zn/Cu (1 cm^2), Zn/ RGO (2 h), Zn/ RGO (24 h) and Zn/ RGO (2 h) wrapped Ag NPs electrode. Because the more the time takes to form RGO and Ag NPs nanocomposite the more open circuit voltage, V_{oc} (V), short circuit current, I_{sc} (mA) and power, $P_{max}= V_{oc} \times I_{sc}$ (W) increases which is the consistent with the published result [99,175].

The figure 3.83 shows the power, $P_{max}= V_{oc} \times I_{sc}$ (W) of BVC using Zn/ RGO (24 h) wrapped Ag NPs electrode with PKL electrolyte. The figure 3.84 shows the comparative performance of power, $P_{max}= V_{oc} \times I_{sc}$ (W) among Zn/Cu (1 cm^2), Zn/ RGO (2 h), Zn/ RGO (24 h), Zn/ RGO (2 h) wrapped Ag NPs and Zn/ RGO (24 h) wrapped Ag NPs electrode using PKL electrolyte. The figure 3.84 also shows the power, $P_{max}= V_{oc} \times I_{sc}$ (W) using Zn/ RGO (24 h) wrapped Ag NPs electrode is 0.136 (W) greater than Zn/ RGO (2 h) wrapped Ag NPs 0.305 W greater than Zn/ RGO (24 h) electrode, 0.438 (W) greater than Zn/ RGO (2 h) and 0.491 (W) greater than Zn/Cu (1 cm^2) electrode with PKL electrolyte.

3.13.8 Comparative study of Zn/Cu (1 cm^2), Zn/RGO (2 h), Zn/RGO (24 h), Zn/RGO (2 h) wrapped Ag NPs and Zn/RGO (24 h) wrapped Ag NPs electrode performance in BVC with PKL electrolyte

Table-3.13: Comparative performance of BVC using Zn/Cu (1 cm^2), Zn/RGO (2 h), Zn/RGO (24 h), Zn/RGO (2 h) wrapped Ag NPs and Zn/RGO (24 h) wrapped Ag NPs with PKL electrolyte

No.	Performance parameters of BVC	Type of electrolyte	Type of electrodes and highest magnitude				
			Zn/Cu (1 cm^2)	Zn/ RGO (2 h)	Zn/ RGO (24 h)	Zn/ RGO (2 h) wrapped Ag NPs	Zn/ RGO (24 h) wrapped Ag NPs
1	Open circuit voltage, V_{oc} (V)	PKL	1.00 V	1.10 V	1.14 V	1.16 V	1.34 V
2	Short circuit current, I_{sc} (mA)	PKL	178 mA	210 mA	320 mA	410 mA	496 mA
3	Power, P_{max}= $V_{oc} \times I_{sc}$ (W)	PKL	0.178 W	0.231 W	0.3648 W	0.533 W	0.6696 W

It is clear from the above table 3.13 that BVC developed using Zn/ RGO (24 h) wrapped Ag NPs electrode and PKL extract electrolyte showed better performance than that of the BVC developed using Zn/Cu (1 cm^2), Zn/ RGO (2 h), Zn/ RGO (24 h) and Zn/ RGO (2 h) wrapped Ag NPs electrode and PKL extract electrolyte. Because, electrical conductivity of Ag NPs wrapped 24 hours RGO adsorbed paper electrode is better than Cu, 2 hours RGO adsorbed paper electrode, 24 hours RGO adsorbed paper electrode and Zn/ RGO (2 h) wrapped Ag NPs which is the consistent with the published result [99,175].

3.14 Comparative study of RGO related various electrode in BVC using PKL and AL electrolyte

Table-3.14: Comparative performance of BVC using various electrode with AL and PKL electrolyte

No.	Performance parameters of BVC	Type of electrolyte	Type of electrodes and highest magnitude				
			Zn/Cu (1 cm^2)	Zn/ RGO (2 h)	Zn/ RGO (24 h)	Zn/ RGO (2 h) wrapped Ag NPs	Zn/ RGO (24 h) wrapped Ag NPs
1	Open circuit voltage, V_{oc} (V)	AL	0.95 V	0.99 V	1.00 V	1.12 V	1.21 V
		PKL	1.00 V	1.10 V	1.14 V	1.16 V	1.34 V
2	Short circuit current, I_{sc} (mA)	AL	110 mA	215 mA	297 mA	346 mA	423 mA
		PKL	178 mA	210 mA	320 mA	410 mA	496 mA
3	Power, P_{max}= $V_{oc} \times I_{sc}$ (W)	AL	0.10 W	0.21 W	0.29 W	0.38752 W	0.51183 W
		PKL	0.178 W	0.231 W	0.3648 W	0.533 W	0.6696 W

The table 3.14 shows that BVC developed using various electrode such as (i) Zn/Cu (1 cm^2) (ii) Zn/ RGO (2 h) (iii) Zn/ RGO (24 h) (iv) Zn/ RGO (2 h) wrapped Ag NPs (v) Zn/ RGO (24 h) wrapped Ag NPs electrode and two types of electrolyte, such as (i) PKL extract electrolyte (ii) AL extract extract electrolyte. It is also clear from the above table 3.14 that Zn/ RGO (24 h) wrapped Ag NPs electrode using PKL extract electrolyte showed better performance than any other electrode and electrolyte. Because, electrical conductivity of Ag NPs wrapped and 24 hours RGO adsorbed paper electrode is better than Cu, 2 hours RGO adsorbed paper electrode, 24 hours RGO adsorbed paper electrode as well as Ag NPs wrapped and 2 hours RGO adsorbed paper electrode which is the consistent with the published result [99,175].

3.15 Measuring cell potential of PKL and AL cell

3.15.1 Chemical reaction in PKL/AL cell

Before adding secondary Salt-

$Zn - 2e^- = Zn^{2+}$

$2H^+ + 2e^- = H_2$

$Zn + 2H^+ = Zn^{2+} + H_2$

After adding secondary salt-

$Zn - 2e^- = Zn^{2+}$

$Cu^{2+} + 2e^- = Cu$

Adding: $Zn + Cu^{2+} = Zn^{2+} + Cu$

The total chemical reaction: $2Zn + Cu^{2+} + 2H^+ \xrightarrow[or,4F]{4\ e-} 2Zn^{2+} + Cu + H_2$ ……(2.1)

Here, the reactant ions = H^+ and Cu^{2+}

And the product ions= Zn^{2+}

3.15.2 Nernst Equation in PKL/AL Cell

In the late 19th century, Josiah Willard Gibbs had formulated a theory to predict whether a chemical reaction is spontaneous based on the free energy,

$$\Delta G = \Delta G^0 + RT \ln Q \text{……(2.2)}$$

Here, ΔG is change in Gibbs free energy, ΔG° is change in standard Gibbs free energy, T is absolute temperature (Kelvin), R is the molar gas constant and Q is reaction quotient which can be found by dividing products ion concentration by reactants ion concentration. Based on Gibbs' work, Nernst extended the theory to include the contribution from electric potential on charged species [168]. The change in Gibbs free energy for an electrochemical cell can be related to the cell potential. Thus, Gibbs' theory becomes,

$$nFE = nFE^0 - RT \ln Q \text{……(2.3)}$$

Here n is the number of transport electrons during cell reaction F is the Faraday constant (coulombs/mole), and E is cell potential. Now, dividing equation (2.3) by the amount of charge transferred (nF) to arrive at a new equation which now bears his name, that is Nernst equation:

$$E = E^0 - \frac{RT}{nF} \ln Q_c \qquad (2.4)$$

Here, If Q_c =1 then $\ln Q_c$= 0 value
If Q_c >1 then $\ln Q_c$= + value
If Q_c <1 then $\ln Q_c$ = - value

ln Q_c = - value is desired. Because, increasing reactant ion increased ln Q_c = - value. As a result E_{cell} value is increased.

Assuming standard conditions (T = 25 °C) and R = 8.3145 J/K/mole, the equation above can be expressed on base-10 logarithm as shown below [168, 169]:

$$E = E^0 - \frac{0.05916V}{n} \log Q_c$$

$$E = E^0 - \frac{0.05916V}{4} \log Q_c$$

Where, n = Number of transfer electron = 4 in PKL/AL cell.

Here, Q_c = Quotient constant = [Product Ion] / [Reactant Ion]

$= [Zn^{2+}]^2/[Cu^{2+}][H^+]^2$

From cell reaction of PKL/AL cell in equation 2.1

$$E_{cell} = E^0 - \frac{0.05916V}{4} \log \frac{[Zn^{2+}]2}{[Cu^{2+}]\,[H^+]2} \qquad (2.5)$$

Here E^0 is standard cell potential. From AAS result observation $[Zn^{2+}]$ and $[Cu^{2+}]$ can be calculate.

Here, E_{cell} value can be increased increasing

1. Reactant ion
2. Concentration of extract
3. Secondary salt

3.15.3 A simple example to measure cell potential

Let us calculate the cell potential for the following system:

$Zn/ZnSO_4$ (0.1M) $\|$ $CuSO_4$ (0.05) / Cu

Where, at 25°C $E^0_{Zn^{2+}/Zn}$ = - 0.76 V and $E_{Cu^{2+}/Cu}$ = + 0.34 V

Cell reaction,

$Zn - 2e^- = Zn^{2+}$

$Cu^{2+} + 2e^- = Cu$

Adding: $Zn + Cu^{2+} \xrightarrow[or,2F]{2\ e-} Zn^{2+} + Cu$

According to Nernst equation, $E_{cell} = E^0_{cell} - \frac{2.303RT}{nF} \log Q_c$

$= E^0_{cell} - \frac{2.303\ RT}{nF} \log \frac{[Zn^{2+}]}{[Cu^{2+}]}$

Here, R= Molar gas constant = 8.314 J K^{-1} mol^{-1}

T =298 K

$[Zn^{2+}]$ = 0.10 $molL^{-1}$

$[Cu^{2+}]$ = 0.05 $molL^{-1}$

$E^0_{Zn^{2+}/Zn}$ = - 0.76 V

$E^0_{Cu^{2+}/Cu}$ = + 0.34 V

n= 2

and F= 96500 C

Now we can get from Nernst equation

E_{cell} = 0.34 V – (-0.76 V) – $\frac{2.303 \times 8.314 \times 298}{2 \times 96500} \log \frac{[0.10]}{[0.05]}$

= (1.10 – 0.008897) V

= 1.0911 V

3.15.4 Determination of [Zn^{2+}] and [Cu^{2+}] using Atomic Absorption Spectroscopy (AAS) method

The concentration of [Cu^{2+}] and [Zn^{2+}] can be estimate by applying Atomic Absorption Spectroscopy (AAS) method [231-235]. AAS is a spectro analytical process for quantitative determination of chemical element employing the absorption of optical radiation by free atoms in gaseous state. This method can be apply to determine over 70 different elements in solution [234,235]. On the other hand this AAS method can be used directly in solid samples employed in pharmacology, biophysics and toxicology research [233].

3.15.5 Effect of concentration of [Cu^{2+}] (moleL^{-1}) in BVC using PKL extract

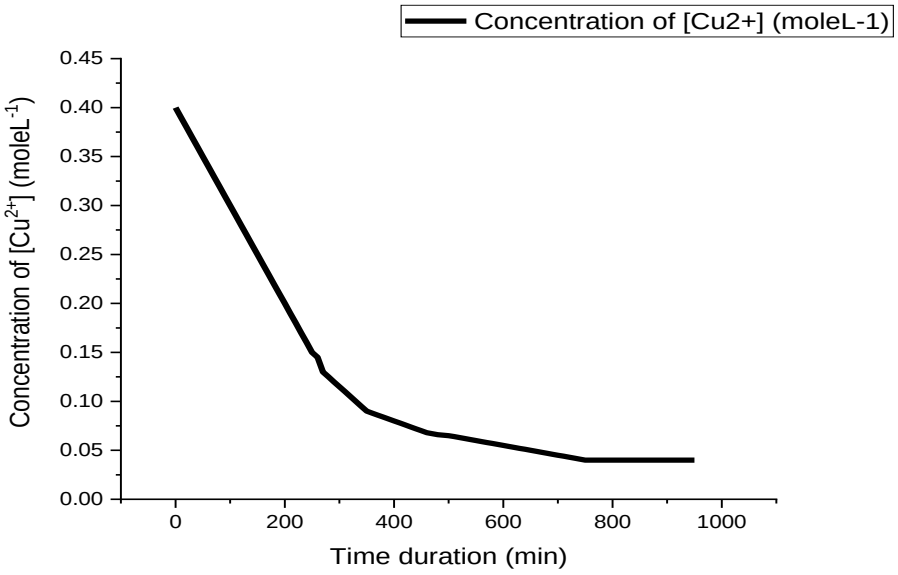

Figure 3.85: Variation of concentration of [Cu^{2+}] (moleL^{-1}) with of time (min)

The figure 3.85 shows the variation of concentration of [Cu^{2+}] (moleL^{-1}) in BVC using PKL extract electrolyte. The concentration of [Cu^{2+}] (moleL^{-1}) of PKL extract electrolyte of BVC decreased gradually. As the streangth of PKL extract reduced, the concentration of [Cu^{2+}] (moleL^{-1}) reduced gradually which is the consistent with the published result [231].

The figure 3.85 also shows that at first concentration of [Cu^{2+}] (moleL^{-1}) of PKL extract electrolyte of BVC decreased rapidly up to 300 minutes. Secondly concentration of [Cu^{2+}] (moleL^{-1}) also decrerased very slowly up to 770 minutes. Finally concentration of [Cu^{2+}] (moleL^{-1}) decreased almost linearly and very slowly covering up to 870 minutes.

3.15.6 Effect of concentration of [Cu^{2+}] ($moleL^{-1}$) on voltage of BVC

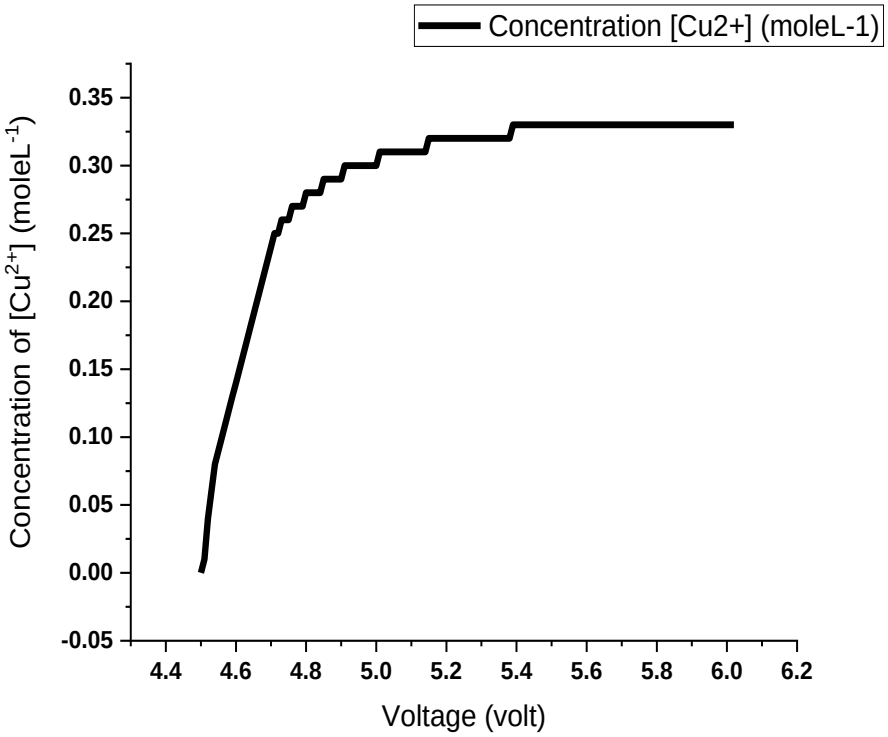

Figure 3.86: Variation of voltage with the variation of concentration of [Cu^{2+}] ($moleL^{-1}$)

The figure 3.86 shows the variation of concentration of [Cu^{2+}] ($moleL^{-1}$) with the variation of voltage using PKL extract electrolyte in BVC. The concentration of [Cu^{2+}] ($moleL^{-1}$) increased with increasing voltage. As the concentration of [Cu^{2+}] ($moleL^{-1}$) increases, the voltage of BVC increased which is the consistent with the published result [231].

The figure 3.86 also shows that at first concentration of [Cu^{2+}] ($moleL^{-1}$) increased rapidly from 0.01 to 0.25 $moleL^{-1}$ covering 0.2 Volt. Then concentration of [Cu^{2+}] ($moleL^{-1}$) increased very steadily but voltage increased very rapidly from 4.7 Volt to 5.4 Volt. Finally concentration of [Cu^{2+}] ($moleL^{-1}$) was almost constant but voltage increased very sharply from 5.4 Volt to 6.1 Volt.

3.15.7 Effect of concentration of [Zn^{2+}] (moleL^{-1}) in BVC using PKL extract

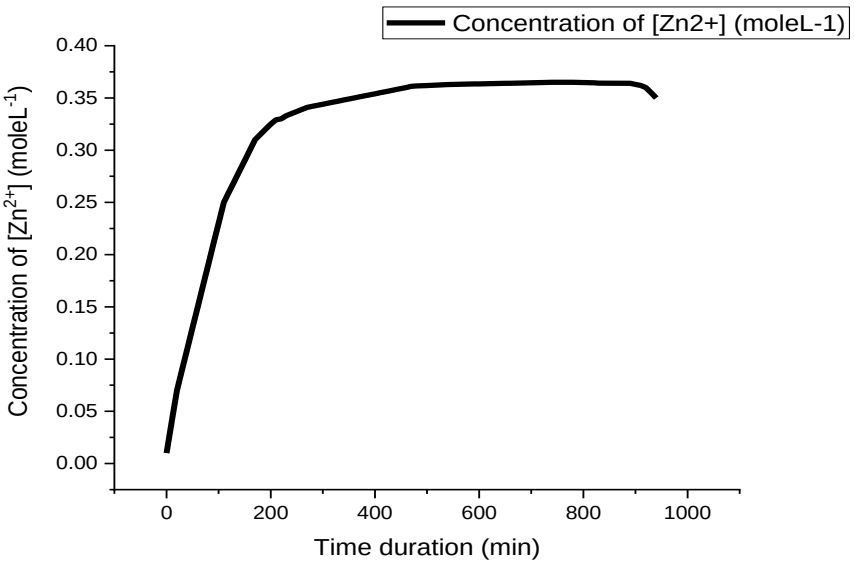

Figure 3.87: Variation of concentration of [Zn^{2+}] (moleL^{-1}) with time (min)

The figure 3.87 shows the variation of concentration of [Zn^{2+}] (moleL^{-1}) in BVC using PKL extract electrolyte. The concentration of [Zn^{2+}] (moleL^{-1}) of PKL extract electrolyte of BVC increased gradually. Bercause, the more the time passes, the more concentration of [Zn^{2+}] (moleL^{-1}) increases in BVC which is the consistent with the published result [231].

The figure 3.87 also shows that at first concentration of [Zn^{2+}] (moleL^{-1}) increased rapidly from 0.01 to 0.33 moleL^{-1} covering 180 minutes. Then concentration of [Zn^{2+}] (moleL^{-1}) increased very steadily up to 0.35 moleL^{-1} covering 720 minutes. Finally concentration of [Zn^{2+}] (moleL^{-1}) was started decreasing from 0.35 (moleL^{-1}) to 0.37 (moleL^{-1}) covering 40 minutes.

3.15.8 Effect of concentration of [Zn^{2+}] (moleL^{-1}) on voltage of BVC

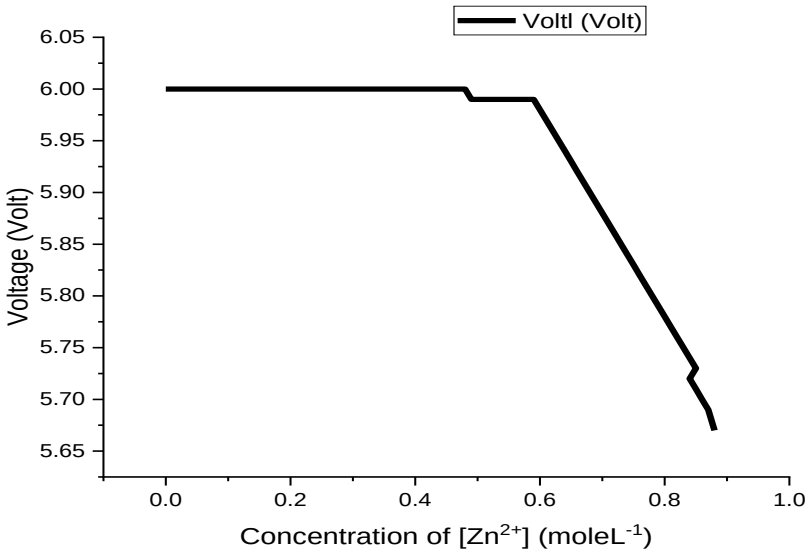

Figure 3.88: Variation of voltage with the variation of concentration of [Zn^{2+}] (moleL^{-1})

The figure 3.95 shows the concentration of [Zn^{2+}] (moleL^{-1}) increased with increasing voltage in BVC using PKL extract electrolyte. As the concentration of [Zn^{2+}] (moleL^{-1}) increases with time, voltage of BVC decreases which is the consistent with the published result [231,232,233,234].

The figure 3.93 also shows that, at first concentration of [Zn^{2+}] (moleL^{-1}) increased rapidly from 0.01 to 0.48 moleL^{-1} whereas voltage was almost constant. Then voltage decrease in two phase. At first from 6.00 Volt to 5.97 Volt secondly from 5.97 Volt to 5.96 Volt whereas concentration of [Cu^{2+}] (moleL^{-1}) increased from 0.48 moleL^{-1} to 0.6 mole$L^{-1.}$ Finally voltage decreased very rapidly in two phases. At first from 5.97 Volt to 5.72 Volt secondly from 5.72 Volt to 5.66 Volt but concentration of [Cu^{2+}] (moleL^{-1}) increased very slowly from 0.6 moleL^{-1} to 0.9 mole$L^{-1.}$

3.15.9 pH determination of AL extract

To determine pH value of AL; at first fresh AL are taken. Then it has chopped with DI water. There after digital pH meter (Hanna instruments pH - 211) set on AL paste. After every 10 minutes the pH value has been recorded.

Figure 3.89: pH determination of AL extract.

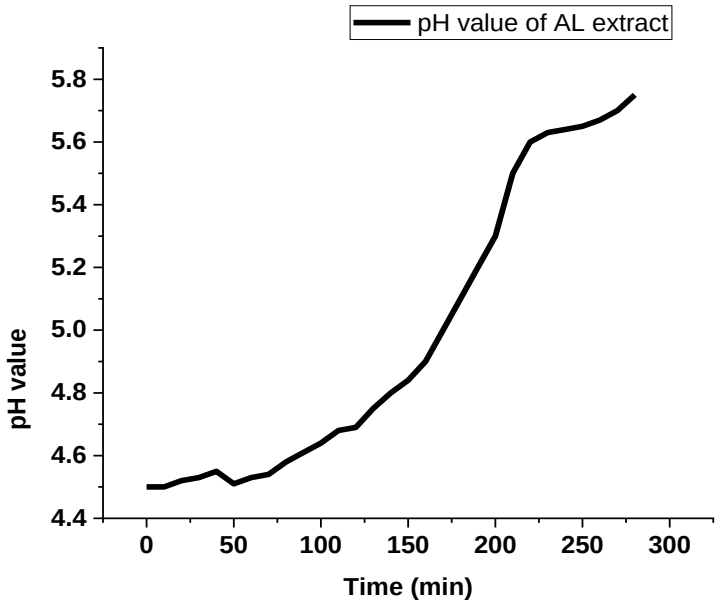

Figure 3.90: Variation of pH value with time (min).

The figure 3.11 shows the pH value of AL paste which is applied in BVC as electrolyte. The pH value of AL paste increased gradually. As the steangth of AL extract decreases, the concentration of [H^+] dcreases. As a result the pH value of AL paste increased which is consistent with the published result [4].

The figure 3.11 also shows that the pH value of AL extract increased slowly up to 40 min then decreased up to 50 min. Thereafter increased rapidly up to 220 min. Finally pH value increased very steadily up to 280 min.

3.15.10 pH determination of PKL extract

To determine pH value of PKL; at first fresh PKL are collected from Dhaka university campus. Then it has washed with DI water and chopped. There after digital pH meter (Hanna instruments pH - 211) set on PKL paste. After every 10 minutes the pH value of PKL extract has been recorded.

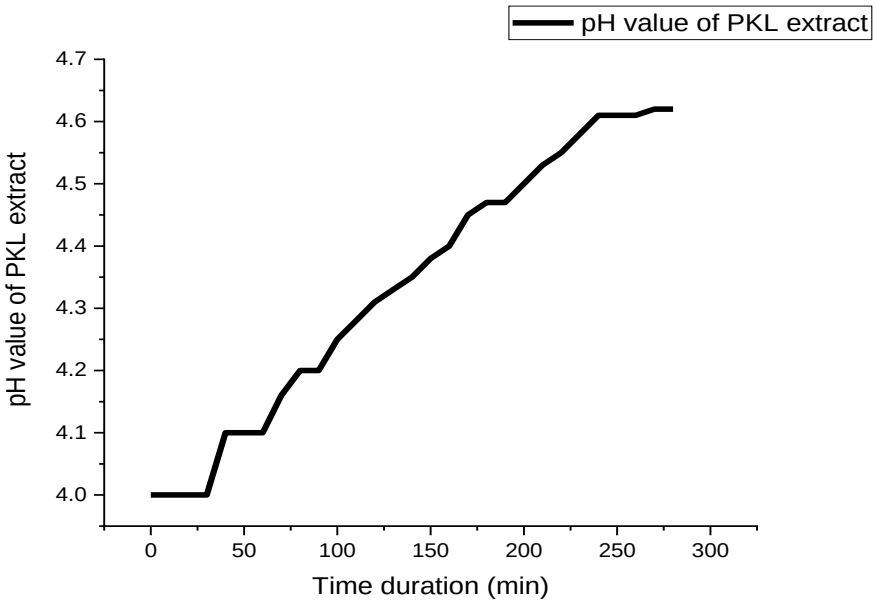

Figure 3.91: Variation of pH value with time (min).

The figure 3.12 shows the pH value of PKL paste which is applied in BVC as electrolyte. The pH value of PKL paste increased gradually. As the steangth of PKL extract decreases, the concentration of [H^+] dcreases. As a result the pH value of PKL paste increased which is consistent with the published result [85].

The figure 3.12 also shows that, the pH value of PKL extract was stable up to 40 minutes. Then increased abruptly up to 50 minutes. Then steadily increased up to 250 min. Finally pH value was very stable up to 280 minutes.

3.15.11 Effect of concentration of [H^+] (moleL^{-1}) of PKL with the variation of time (h)

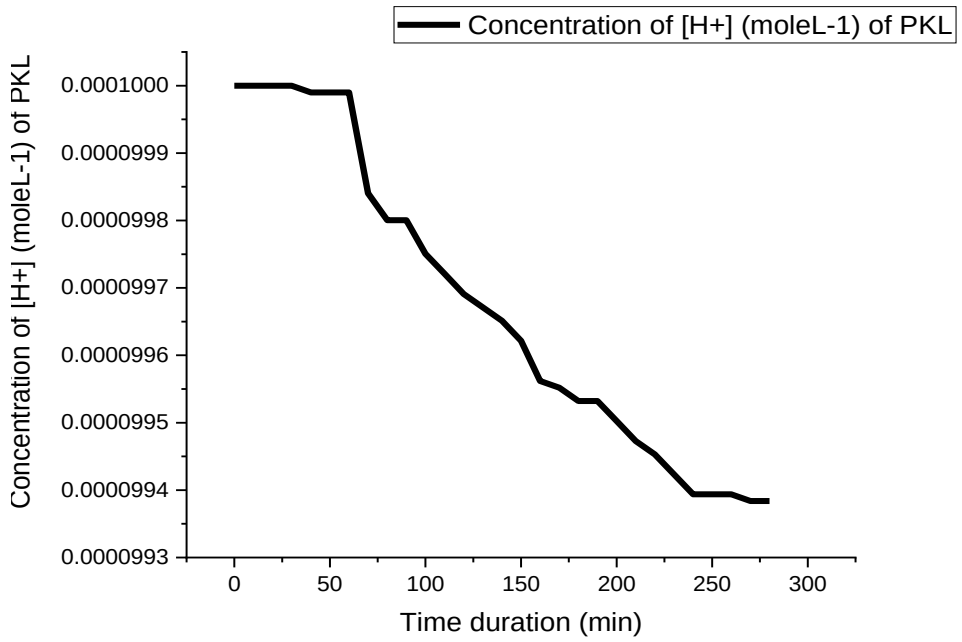

Figure 3.92: Variation of concentration of [H^+] (moleL^{-1}) of PKL with time (min)

The figure 3.92 shows the variation of concentration of [H^+] (moleL^{-1}) of PKL in BVC. The concentration of [H^+] (moleL^{-1}) of PKL in BVC decreased gradually. As the steangth of PKL extract decreases, the pH value of PKL extract increased. As a result the concentration of [H^+] dcreases which is consistent with the published result [85].

The figure 3.92 also shows that at first concentration of [H^+] (moleL^{-1}) did not decreased up to 25 minutes. Secondly concentration of [H^+] (moleL^{-1}) also decrerased very slowly up to 50 minutes. There after concentration of [H^+] (moleL^{-1}) decreased rapidly from 0.0001000 moleL^{-1} to 0.0000994 moleL^{-1} covering 180 minutes. Finally concentration of [H^+] (moleL^{-1}) decreased almost linearly and very slowly within 40 minutes.

3.15.12 Determination of concentration of [H^+] (moleL^{-1}) of AL with the variation of time (h)

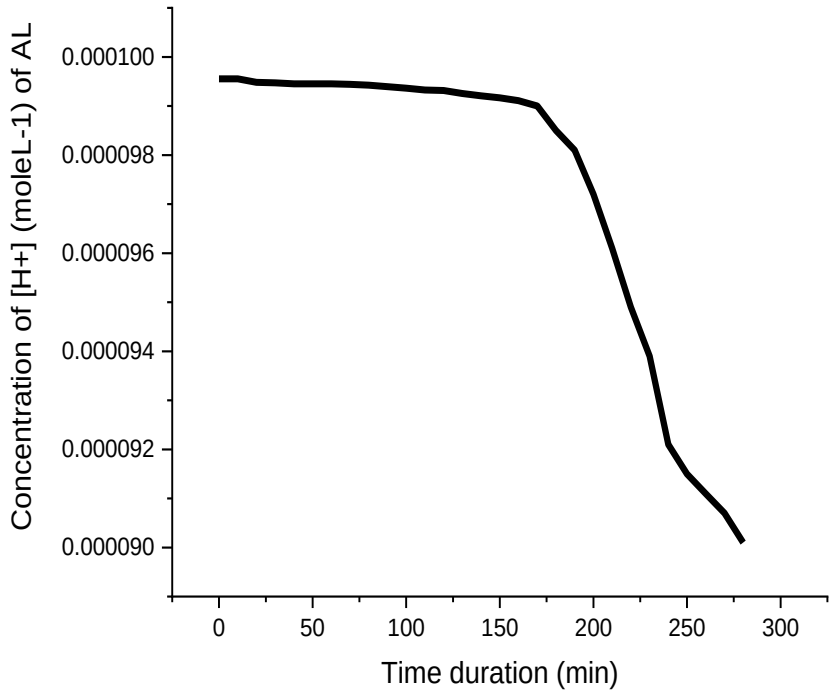

Figure 3.93: Variation of concentration of [H^+] (moleL^{-1}) of AL with time (min)

The figure 3.93 shows the variation of concentration of [H^+] (moleL^{-1}) of AL in BVC. The concentration of [H^+] (moleL^{-1}) of AL in BVC decreased gradually. As the steangth of AL extract decreases, the pH value of AL extract increased. As a result the concentration of [H^+] dcreases which is consistent with the published result [4].

The figure 3.97 also shows that at first concentration of [H^+] (moleL^{-1}) from AL extract decrerased very slowly and almost linearly up to 160 minutes. There after concentration of [H^+] (moleL^{-1}) decreased rapidly from 0.0000999 moleL^{-1} to 0.000092 moleL^{-1} covering 80 minutes. Finally concentration of [H^+] (moleL^{-1}) decreased almost slowly from 0.000092 moleL^{-1} to 0.000090 moleL^{-} covering 40 minutes.

3.15.13 Determination of cell potential (Volt) of BVC using PKL extract

Table-3.15: Concentration of $[Zn^{2+}]$, $[Cu^{2+}]$, $[H^{+}]$ ($moleL^{-1}$) and cell potential (V) of BVC using PKL extract

Time duration (min)	Concentration of $[Cu^{2+}]$ ($moleL^{-1}$)	Concentration of $[Zn^{2+}]$ ($moleL^{-1}$)	Concentration of $[H^{+}]$ ($moleL^{-1}$)	$E^0_{cell=} E^0_{Cu^{2+}/Cu} - E^0_{Zn^{2+}}/Zn$	$E_{cell} = E^0_{cell} - \frac{0.05916V}{4} \log \frac{[Zn^{2+}]2}{[Cu^{2+}][H^{+}]2}$
0	0.4	0.01	1E-4	1.10	0.9107
10	0.39	0.04	1E-4	1.10	0.8926
20	0.38	0.07	1E-4	1.10	0.885
30	0.37	0.09	1E-4	1.10	0.8815
40	0.36	0.11	9.999E-5	1.10	0.8815
50	0.35	0.13	9.999E-5	1.10	0.8785
60	0.34	0.15	9.999E-5	1.10	0.8738
70	0.33	0.17	9.98403E-5	1.10	0.8718
80	0.32	0.19	9.98004E-5	1.10	0.8699
90	0.31	0.21	9.98004E-5	1.10	0.8682
100	0.3	0.23	9.97506E-5	1.10	0.8666
110	0.29	0.25	9.97208E-5	1.10	0.865
120	0.28	0.26	9.96904E-5	1.10	0.8642
130	0.27	0.27	9.96711E-5	1.10	0.8632
140	0.26	0.28	9.96512E-5	1.10	0.8627
150	0.25	0.29	9.96214E-5	1.10	0.8613
160	0.24	0.3	9.96016E-5	1.10	0.8603

170	0.23	0.31	9.9552E-5	1.10	0.8593
Time duration (min)	Concentration of $[Cu^{2+}]$ ($moleL^{-1}$)	Concentration of $[Zn^{2+}]$ ($moleL^{-1}$)	Concentration of $[H^{+}]$ ($moleL^{-1}$)	$E^0_{cell} = E^0_{Cu^{2+}/Cu} - E^0_{Zn^{2+}/Zn}$	$E_{cell} = E^0 - \frac{0.05916V}{4} \log \frac{[Zn^{2+}]2}{[Cu^{2+}]\,[H^{+}]2}$
180	0.22	0.315	9.95322E-5	1.10	0.8697
190	0.21	0.32	9.95323E-5	1.10	0.8586
200	0.2	0.325	9.95025E-5	1.10	0.8569
210	0.19	0.329	9.94728E-5	1.10	0.8561
220	0.18	0.33	9.9453E-5	1.10	0.8554
230	0.17	0.333	9.94233E-5	1.10	0.8545
240	0.16	0.335	9.93937E-5	1.10	0.8536
250	0.15	0.337	9.93937E-5	1.10	0.8527
260	0.145	0.339	9.93937E-5	1.10	0.8522
270	0.13	0.341	9.93838E-5	1.10	0.8507
280	0.125	0.342	9.93838E-5	1.10	0.8502
290	0.12	0.343	9.938E-5	1.10	0.8496
300	0.115	0.344	9.933E-5	1.10	0.849
310	0.11	0.345	9.93E-5	1.10	0.8484
320	0.105	0.346	9.925E-5	1.10	0.8484
330	0.1	0.347	9.921E-5	1.10	0.8471
340	0.095	0.348	9.915E-5	1.10	0.8464
350	0.09	0.349	1E-5	1.10	0.8464
360	0.088	0.35	9.89E-5	1.10	0.8453
370	0.086	0.351	9.8E-5	1.10	0.8447
380	0.084	0.352	9.75E-5	1.10	0.8443

390	0.082	0.353	9.7E-5	1.10	0.8439
Time duration (min)	Concentration of $[Cu^{2+}]$ ($moleL^{-1}$)	Concentration of $[Zn^{2+}]$ ($moleL^{-1}$)	Concentration of $[H^{+}]$ ($moleL^{-1}$)	$E^0_{cell} = E^0_{Cu^{2+}/Cu} - E^0_{Zn^{2+}}/Zn$	$E_{cell} = E^0 - \frac{0.05916V}{4} \log \frac{[Zn^{2+}]2}{[Cu^{2+}]\,[H^{+}]2}$
400	0.08	0.354	9.65E-5	1.10	0.8434
410	0.078	0.355	9.6E-5	1.10	0.8429
420	0.076	0.356	9.55E-5	1.10	0.8423
430	0.074	0.357	9.5E-5	1.10	0.8418
440	0.072	0.358	9.45E-5	1.10	0.8412
450	0.07	0.359	9.4E-5	1.10	0.8407
460	0.068	0.36	9.36E-5	1.10	0.8402
470	0.067	0.3611	9.32E-5	1.10	0.8398
480	0.066	0.3615	9.29E-5	1.10	0.8396
490	0.065	0.3619	9.24E-5	1.10	0.8392
500	0.064	0.3621	9.21E-5	1.10	0.8404
510	0.063	0.3624	9.18E-5	1.10	0.8386
520	0.062	0.3626	9.15E-5	1.10	0.8383
530	0.061	0.3628	9.11E-5	1.10	0.838
540	0.06	0.363	9.07E-5	110	0.8377
550	0.059	0.3631	9.04E-5	1.10	0.8374
560	0.058	0.3632	9E-5	1.10	0.837

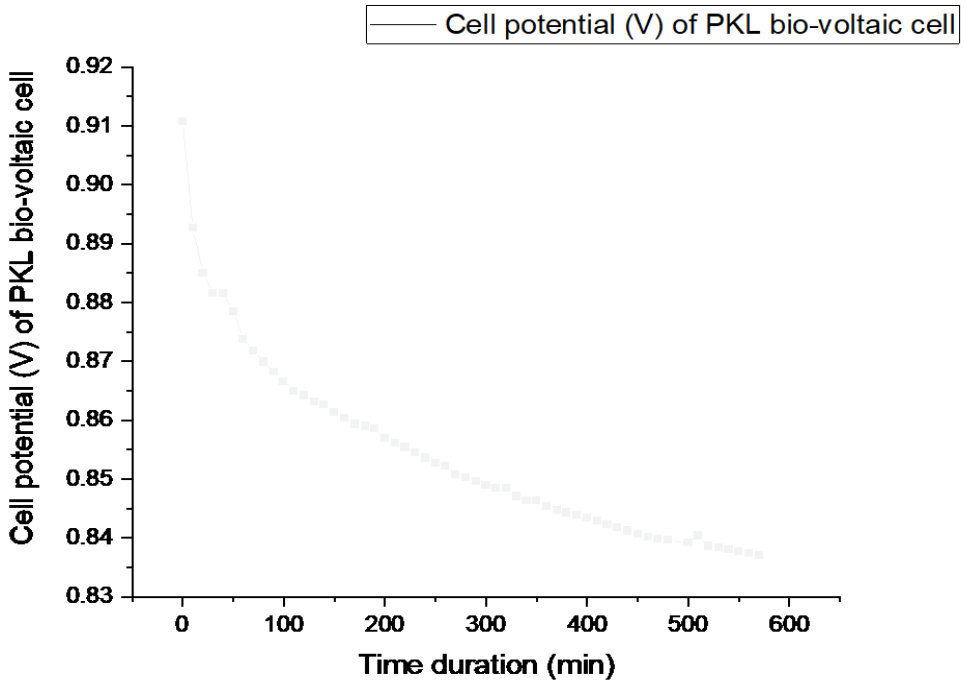

Figure 3.94: Variation of cell potential (V) with time (min)

The figure 3.94 shows the variation of cell potentials (V) of BVC using PKL extract electrolyte. The cell potentials (V) of BVC using PKL extract electrolyte decreased gradually. From eqation (2.4) we know that,

If Q_c =1 then lnQ_c= 0 value

If Q_c >1 then lnQ_c= + value

If Q_c <1 then lnQ_c = - value

ln Q_c = - value is desired. Because, increasing reactant ion increased ln Q_c = - value. As a result E_{cell} value is increased. But in this study, cell potentials (V) of BVC using PKL extract electrolyte decreased gradually. Because, reactant ion of BVC decreased gradually.

The figure 3.94 also shows that at first cell potentials (V) of BVC using PKL extract electrolyte decreased rapidly from 0.9107 Volt to 0.8815 Volt covering 40 minutes. Secondly, cell potentials (V) also decrerased up to 0.8593 Volt within 170 minutes. Finally cell potentials (V) of PKL bio-

voltaic cell decreased almost linearly and very slowly from 0.8586 Volt to 0.837 Volt up to 560 minutes.

3.16 Comparative performance between traditional voltaic cell and bio-voltaic cell

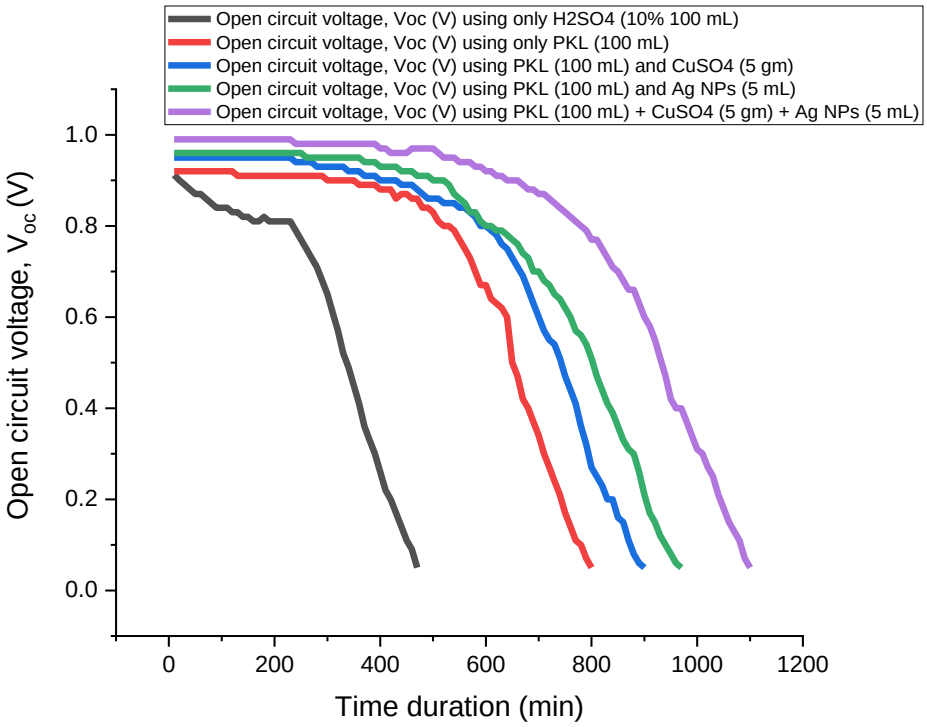

Figure 3.95: Variation of open circuit voltage, V_{oc} (V) with time (min) using traditional Voltaic cell and BVC

The figure 3.95 shows the comparative performanc of open circuit voltage, V_{oc} (V) betwwen traditional Voltaic cell and bio – voltaic cell (BVC). The graph shows that open circuit voltage, V_{oc} (V) of traditional voltaic cell shows the lowest performance wherease all of the forms of BVC show better performance than traditional voltaic cell. The figure 3.95 also shows that the highest open circuit voltage, V_{oc} (V) of traditional voltaic cell is 0.912 (V) wherease the highest value of BVC is 0.99 (V).

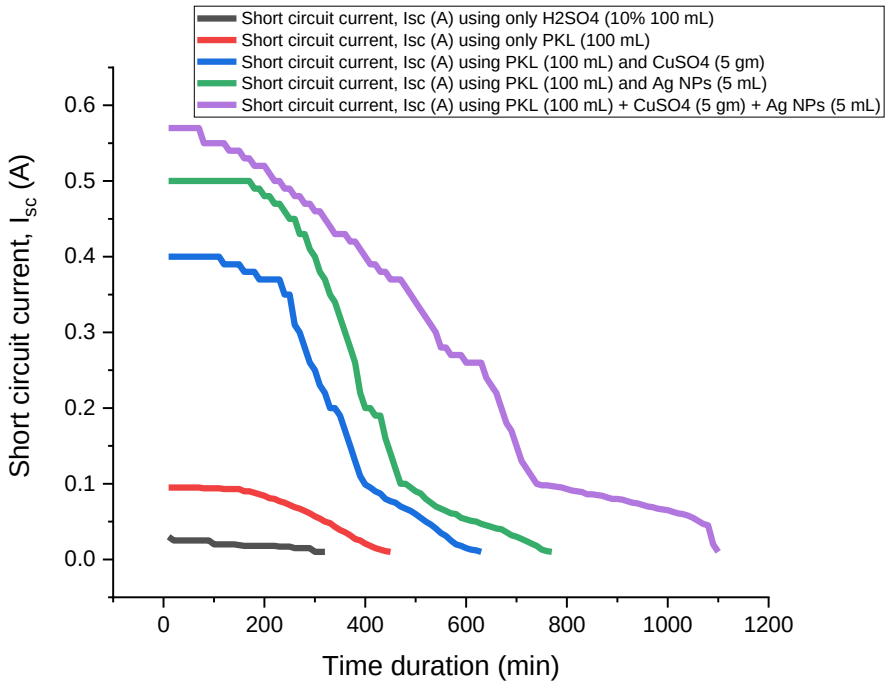

Figure 3.96: Variation of short circuit current, I_{sc} (A) with time (min) using traditional Voltaic cell and BVC

The figure 3.96 shows the comparative performanc of short circuit current, I_{sc} (A) betwwen traditional Voltaic cell and bio – voltaic cell (BVC). The graph shows that short circuit current, I_{sc} (A) of traditional voltaic cell shows the lowest performance wherease all of the forms of BVC show better performance than traditional voltaic cell. The figure 3.96 also shows that the highest short circuit current, I_{sc} (A) of traditional voltaic cell is 0.03 (A) wherease the highest value of BVC is 0.57 (A).

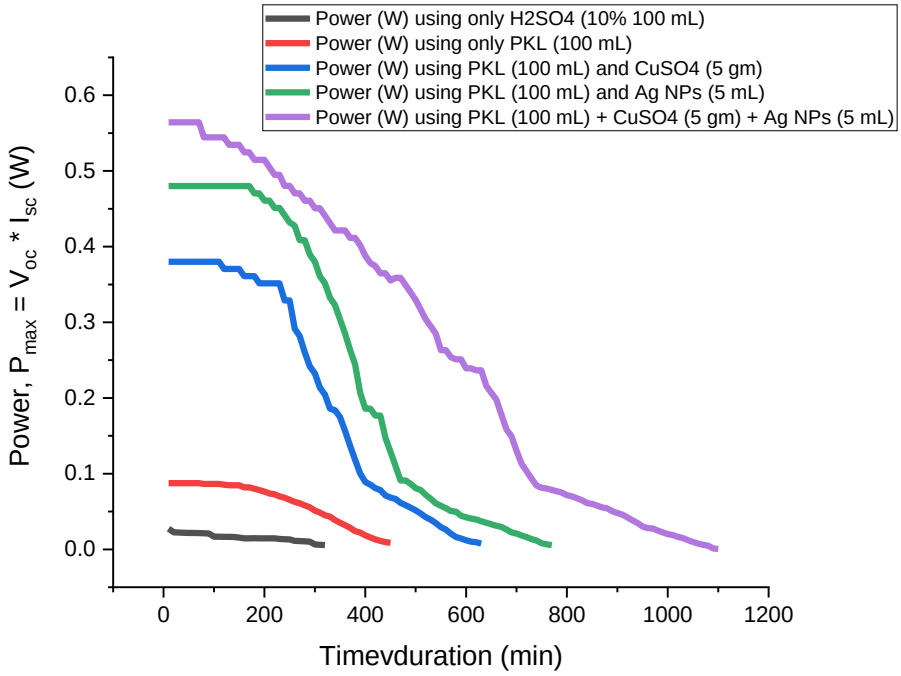

Figure 3.97: Variation of power (W) with time (min) using traditional Voltaic cell and BVC

The figure 3.97 shows the comparative performanc of power, Pmax = $V_{oc} \times I_{sc}$ (W) betwwen traditional Voltaic cell and bio – voltaic cell (BVC). The graph shows that power, Pmax = $V_{oc} \times I_{sc}$ (W) of traditional voltaic cell shows the lowest performance wherease all of the forms of BVC show better performance than traditional voltaic cell. The figure 3.97 also shows that the highest power, Pmax = $V_{oc} \times I_{sc}$ (W) of traditional voltaic cell is 0.02736 (W) wherease the highest value of BVC is 0.5643 (W).

From the above analysis, as carried out by three distinct graphs showed above, it is clearly seen that the performance of BVC is higher than that of Traditional Voltaic Cell which is consistent with the published result [220, 239].

CONCLUSION

Conclusion

The whole research is mainly focused on developing a new type of BVC (Bio-Voltaic Cell) using various electrodes and plant extract electrolytes. It was found that with the increase of electrode areas and percentage of PKL and AL extract and addition of small amound secondary salt with plant extract electrolyte can increases the performances of BVC. Besides this, the performance of BVC developed using Ag NPs and RGO and RGO wrapped Ag Nano composite paper electrode have also been investigated. On the other hand, with increase of number of electrodes and decreasing the distance between electrodes, increased the performances of BVC. In this study, effect of PKL and AL living plant as electrolyte in BVC has been investigated and it was found that PKL living plant shows better electrical performance than that of AL. The thickness and midrib area of PKL is more than that of AL and it was observed that as the exposed area of midrib of living plant increases, it can act as better electrolyte and show better performance in the BVC. As a result, open circuit voltage, V_{oc} (V), short circuit current, I_{sc} (A) and power (W) of BVC using PKL living plant were found to be higher than that of AL living plant. Ag NPs were successfully synthesized using the PKL and AL extract for the first time through an eco-friendly, cost-effective and rapid green synthesis approach. This green synthesized Ag NPs played a potential role in improving the power production of BVC. Besides this, in substitute of Cu electrode, RGO adsorbed paper electrode and RGO – Ag NPs composite adsorbed paper electrode have been applied in this BVC for the first time.

Apart from these, the BVC constructed using AL and PKL extract electrolytes with Zn/Cu ($1cm^2$) electrode, Zn/ (2 h) RGO absorbed paper electrode, Zn/ (24 h) RGO absorbed paper electrode, Zn/ (2 h) RGO wrapped Ag Nano composite paper electrode and Zn/ (24 h) RGO wrapped Ag Nano composite paper electrode and their performance have also been examined. It has been observed that PKL and Zn/ (24 h) RGO wrapped Ag Nano composite paper electrode generates enough electricity for the longest period. In addition, the developed BVC has been compared with Traditional Voltaic Cell (TVC) using various types of electrodes and electrolytes and it is observed that BVC shows better performance for longer time than that of TVC.

Finally, it has been shown that a 1 KW mini power plant can be constructed using this procedure with an affordable price. This mini power plant can be a promising issue in case of rural development by distributing electricity, where the nationwide grid is out of reach.

REFERENCES

References

1. Hossain AK, Badr O (2007) Prospects of renewable energy utilization for electricity generation in Bangladesh. Sustain Energy Rev 11(8):617–1649 (Renewable 146–152)
2. Khan and Bosu 2010) (Khan KA, Bosu R (2010) Performance study on PKL electricity for using DC fan. Int J Soc Dev Inf Syst 1(1):27–30
3. Khan and Arafat 2010) Khan KA, Arafat ME (2010) Development of portable PKL (pathor kuchi leaf) lantern. Int J Soc Dev Inf Syst 1(1):15–20}
4. Md. Afzol Hossain, Md. Kamrul Alam Khan,Md.Emran Quayum,"Performance development of bio-voltaiccell from arum leaf extract PKL extracts using zn/cu electrodes and investigation of their electrochemical performance'', International Journal of Advances in Science Engineering and Technology, ISSN: 2321-9009,Vol-5, Iss-4, Spl. Issue-1, Nov-2017.
5. S. Adeyinka Aboaba, H. Igumoye, G. Flamini, Chemical composition of the leaves and stem bark of Sterculia tragacantha, Anthocleista vogelii and leaves of Bryophyllum pinnatum, J. Essent. Oil Res. 29 (2017) 85–92, https://doi.org/ 10.1080/10412905.2016.1178182.
6. K. Fürer, M. Raith, R. Brenneisen, M. Mennet, A. Simoes-Wüst, ˜ U. von Mandach, M. Hamburger, O. Potterat, Two new flavonol glycosides and a metabolite profile of Bryophyllum pinnatum, a phytotherapeutic used in obstetrics and gynaecology, Planta Med. 79 (2013) 1565–1571, https://doi.org/10.1055/s-0033-1350808.
7. K. Fürer, A. Simoes-Wüst, ˜ U. von Mandach, M. Hamburger, O. Potterat, Bryophyllum pinnatum and related species used in anthroposophic medicine: constituents, pharmacological activities, and clinical efficacy, Planta Med. 82 (2016) 930–941, https://doi.org/10.1055/s-0042-106727.
8. K.A. Mbachu, M.G. Ibok, M.A. Adeniyi-Akee, O.E. Ajala, Chemical compositions and antioxidant activity of leaf and stem essential oils of Bryophyllum pinnatum (lam.), Kurz, GSC Biol. and Pharm. Sci. 9 (2019) 57–64, https://doi.org/10.30574/ gscbps.2019.9.2.0184.
9. Y. Obregon-Díaz, ´ A. P´erez-Colmenares, K. Obregon-Alarc ´ on, ´ R. Aparicio-Zambrano, L. Rojas-Fermín, A. Usubillaga, J. Carmona, Volatile constituents of the leaves of kalanchoe pinnata from the Venezuelan andes, Natural Product Communications 14 (2019), https://doi.org/10.1177/1934578X19842703,1934578X1984270.
10. Jain, M.S. Mehata, Medicinal plant leaf extract and pure flavonoid mediated green synthesis of silver nanoparticles and their enhanced antibacterial property, Sci. Rep. 7 (2017) 15867, https://doi.org/10.1038/s41598-017-15724-8.
11. K.A. Khan, M.H. Ali, M.A. Mamun, M.M. Haque, A.K.M.A. Ullah, M.N.I. Khan, L. Hassan, A.K.M. Obaydullah, M.A. Wadud, Bioelectrical characterization and production of nanoparticles

(NPs) using PKL extract for electricity generation, Microsyst. Technol. (2020), https://doi.org/10.1007/s00542-020-04774-0
12. K.A. Khan, M.A. Mamun, M. Ibrahim, M. Hasan, M. Ohiduzzaman, A.K. M. Obaydullah, M.A. Wadud, M. Shajahan, PKL electrochemical cell: physics and chemistry, SN Appl. Sci. 1 (2019) 1335, https://doi.org/10.1007/s42452-019- 1363-x.
13. K.A. Khan, L. Hassan, A.K.M. Obaydullah, S.M. Azharul Islam, M.A. Mamun, T. Akter, M. Hasan, MdS. Alam, M. Ibrahim, M.M. Rahman, M. Shahjahan, Bioelectricity: a new approach to provide the electrical power from vegetative and fruits at off-grid region, Microsyst. Technol. 26 (2020) 3161–3172, https://doi. org/10.1007/s00542-018-3808-3.
14. L. Lu, W. Chen, "Biocompatible composite actuator: a supramolecular structure consisting of the biopolymer chitosan, carbon nanotubes, and an ionic liquid" Adv. Mater. 2010, 22, 3745. https://doi.org/10.1002/adma.201001134.
15. G. W. Rogers, J. Z. Liu, "Graphene Actuators: Quantum-Mechanical and Electrostatic Double-Layer Effects", J. Am. Chem. Soc. 2011, 133, 10858. doi: 10.1021/ja201887r
16. L. H. Lu, J. H. Liu, Y. Hu, W. Chen, "Large volume variation of an anisotropic graphenenanosheet electrochemical–mechanical actuator under low voltage stimulation", Chem. Commun. 2012, 48, 3978.
17. X. Xie, L. Qu, C. Zhou, Y. Li, J. Zhu, H. Bai, G. Shi, L. Dai, "Synthesis, properties, and applications of graphene oxide/reduced graphene oxide and their nanocomposites", ACS Nano 2010, 4, 6050. https://doi.org/10.1016/j.nanoms.2019.02.004
18. X. Xie, H. Bai, G. Shi, L. Qu, "Load-tolerant, highly strain-responsive graphene sheets" J. Mater. Chem. 2011, 21, 2057. https://doi.org/10.1039/C0JM03926H
19. J. Kim, L. J. Cote, F. Kim, W. Yuan, K. R. Shull, J. Huang, "Graphene Oxide Sheets at Interfaces", J. Am. Chem. Soc. 2010, 132, 8180. doi: 10.1021/ja102777p
20. D. Wang , D. Choi , J. Li , Z. Yang , Z. Nie , R. Kou , D. Hu , C. Wang , L. V. Saraf, J. Zhang , I. A. Aksay , J. Liu , "Self-assembled TiO2-graphene hybrid nanostructures for enhanced Li-ion insertion", ACS Nano 2009 , 3 , 907. doi: 10.1021/nn900150y
21. C. Xu , X. Wang , "Fabrication of Flexible Metal-Nanoparticle Films Using Graphene Oxide Sheets as Substrates", Small 2009 , 5 , 2212. https://doi.org/10.1002/smll.200900548
22. Li, D., Müller, M., Gilje, S. *et al.* "Processable aqueous dispersions of graphene nanosheets". *Nature Nanotech* 3, 101–105 (2008). https://doi.org/10.1038/nnano.2007.451
23. Liu, Jinghai, et al. "Reduced graphene oxide as capturer of dyes and electrons during photocatalysis: surface wrapping and capture promoted efficiency." *Physical Chemistry Chemical Physics* 13.29 (2011): 13216-13221.

24. "Renewable energy policy of Bangladesh" Policy Documents, Power Division, Ministry of Power, Energy and Mineral resources, Government of the people's Republic in of Bangladesh, Nov. 6, 2008.

25. Dr. Md. Kamrul Alam Khan, "Electricity Generation form Pathor Kuchi Leaf (Bryophyllum pinnatum)", Int. J. Sustain. Agril. Tech. 5(4): 146-152, July 2009.

26. Pattewar,"Kalanchoe pinnata: Phytochemical and Pharmacological Profile". IJPSR, 2012; Vol.3 (4): 993-1000

27. Mandal R, Mukherjee A, Mandal N, Tarafdar J, Mukherjee A. Assessment of genetic diversity in Taro using morphometrics. Curr Agr Res J. 2013; 1:79-85

28. "Yearbook of Agricultural Statistics -2015" Bangladesh Bureau of statistics (BBS), statistics and information division (SID), Ministry of planning ,Government of the people's Republic of Bangladesh, July, 2016.

29. H.C. Teng et al. "Review on Energy Harvesting Potential from Living Plants: Future Energy Resource" International Journal of Renewable Energy Research, Vol.8, No.4, December, 2018.

30. Mehedi Hasan, Kamrul Alam Khan. "Experimental characterization and identification of cell parameters in a *B. pinnatum* electrochemical device" SN Applied Sciences (2019) 1:1008, https://doi.org/10.1007/s 42452-019-1045-8.

31. K. A. Khan, Lovelu Hassan, A. K. M. Obaydullah, S. M. Azharul Islam, M. A. Mamun, Tanjila Akter, Mehedi Hasan, Md. Shamsul Alam, M. Ibrahim, M. Mizanur Rahman, M. Shahjahan. "Bioelectricity: a new approach to provide the electrical power from vegetative and fruits at off-grid region" February 2018, DOI: 10.1007/s 00542-018-3808-

32. Bielek, B. (2014). New Classification of Renewable Energy Sources in the Development of Technology in Architecture for a Sustainable Society, Technical Transactions, Vol. 3, 1–8.

33. Volkov, A. G.; Reedus, J.; Mitchell, C. M.; Tucket, C.; Forde-Tuckett, V.; Volkova, M. I.; Markin, V. S.; Chua, L. (2014). Memristors in the electrical network of Aloe vera L., Plant Signaling & Behavior, Vol. 9, No. 7, e29056. doi:10.4161/psb.29056.

34. Volkov, A. G. (2000). Green plants: Electrochemical interfaces, Journal of Electroanalytical Chemistry, Vol. 483, No. 1, 150–156. doi: 10.1016/S0022- 0728(99)00497-0.

35. Volkov A. G.; Reedus, J.; Mitchell, C. M.; Tuckett, C.; Volkova, M. I.; Markin, V. S.; Chua, L. (2014). Memory elements in the electrical network of Mimosa pudica L, Plant Signaling and Behavior, Vol. 9, No. 10. doi:10.4161/15592324.2014.982029.

36. Volkov, A. G.; Nyasani, E. K.; Blockmon, A. L.; Volkova, M. I. (2015). Memristors: Memory elements in potato tubers, Plant Signaling and Behavior, Vol. 10, No. 10. doi:10.1080/15592324.2015.1071750.

37. By, B.; Scott, H. (1966). Electric Fields in Plants, Vol. 18, No. August, 409–418. doi: https:// doi.org/10.1146/annurev.pp.18.060167.00 2205.

38. Fensom, D. S. (1966). On measuring electrical resistance in situ in higher plants, Canadian Journal of Plant Science, Vol. 46, 169–175.

39. Ksenzhek, O.; Petrova, S.; Kolodyazhny, M. (2004). Electrical Properties of Plant Tissues. Resistance of a Maize Leaf, Bulgarian Journal of Plant Physiology, Vol. 30, Nos. 3–4, 61–67.
40. Khan KA (1998) Copper oxide coating for use in linear solar fresnel reflecting concentrating collector. J Elsevier Renew Energy Int J WREN 16(2):49–52
41. Khan KA (1999) Technical note copper oxide coatings for use in a linear solar Fresnel reflecting concentrating collector, Publication date 1999/8/1. J Renew Energy 17(4):603–608 (Publisher Pergamon)
42. S. Raj, S. Chand Mali, R. Trivedi, Green synthesis and characterization of silver nanoparticles using Enicostemma axillare (Lam.) leaf extract, Biochem. Biophys. Res. Commun. 503 (2018) 2814–2819, https: //doi.org/10.1016/j. bbrc.2018.08.045.
43. B. Khodadadi, M. Bordbar, A. Yeganeh-Faal, M. Nasrollahzadeh, Green synthesis of Ag nanoparticles/clinoptilolite using Vaccinium macrocarpon fruit extract and its excellent catalytic activity for reduction of organic dyes, J. Alloys Compd. 719 (2017) 82–88, https://doi.org/10.1016/j.jallcom.2017.05.135.
44. N. Roy, A. Gaur, A. Jain, S. Bhattacharya, V. Rani, Green synthesis of silver nanoparticles: an approach to overcome toxicity, Environ. Toxicol. Pharmacol. 36 (2013) 807–812, https://doi.org/10.1016/j.etap.2013.07.005.
45. M. Darroudi, M. Mansor Bin Ahmad, A.H. Abdullah, N.A. Ibrahim, K. Shameli, Green synthesis and characterization of gelatin-based and sugar-reduced silver nanoparticles, IJN (2011) 569, https://doi.org/10.2147/IJN.S16867.
46. M. Ahamed, M.A. Majeed Khan, M.K.J. Siddiqui, M.S. AlSalhi, S.A. Alrokayan, Green synthesis, characterization and evaluation of biocompatibility of silver nanoparticles, Phys. E Low-dimens. Syst. Nanostruct. 43 (2011) 1266–1271, https://doi.org/10.1016/j.physe.2011.02.014.
47. Y. He, F. Wei, Z. Ma, H. Zhang, Q. Yang, B. Yao, Z. Huang, J. Li, C. Zeng, Q. Zhang, Green synthesis of silver nanoparticles using seed extract of Alpinia katsumadai, and their antioxidant, cytotoxicity, and antibacterial activities, RSC Adv. 7 (2017) 39842–39851, https://doi.org/10.1039/C7RA05286C.
48. A. Danagoudar, G.K. Pratap, M. Shantaram, B. Chatterjee, K. Ghosh, S.R. Kanade, C.G. Joshi, Cancer cell specific cytotoxic potential of the silver nanoparticles synthesized using the endophytic fungus, Penicillium citrinum CGJ-C2, Mater. Today Commun. 25 (2020) 101442, https://doi.org/10.1016/j. mtcomm.2020.101442.
49. F. Gol, ¨ A. Aygün, A. Seyrankaya, T. Gür, C. Yenikaya, F. S¸ en, Green synthesis and characterization of Camellia sinensis mediated silver nanoparticles for antibacterial ceramic applications, Mater. Chem. Phys. 250 (2020) 123037, https://doi.org/10.1016/j.matchemphys.2020.123037.

50. N. Jayaprakash, J.J. Vijaya, K. Kaviyarasu, K. Kombaiah, L.J. Kennedy, R. J. Ramalingam, M.A. Munusamy, H.A. Al-Lohedan, Green synthesis of Ag nanoparticles using Tamarind fruit extract for the antibacterial studies, J. Photochem. Photobiol. B Biol. 169 (2017) 178–185, https://doi.org/10.1016/j. jphotobiol.2017.03.013.
51. S. Jain, M.S. Mehata, Medicinal plant leaf extract and pure flavonoid mediated green synthesis of silver nanoparticles and their enhanced antibacterial property, Sci. Rep. 7 (2017) 15867, https://doi.org/10.1038/s41598-017-15724-8.
52. S. Iravani, Green synthesis of metal nanoparticles using plants, Green Chem. 13 (2011) 2638, https://doi.org/10.1039/c1gc15386b.
53. M. Shahriary, H. Veisi, M. Hekmati, S. Hemmati, In situ green synthesis of Ag nanoparticles on herbal tea extract (Stachys lavandulifolia)-modified magnetic iron oxide nanoparticles as antibacterial agent and their 4-nitrophenol catalytic reduction activity, Mater. Sci. Eng. C 90 (2018) 57–66, https: //doi.org/10.1016/j. msec.2018.04.044.
54. R.R. Chavan, S.D. Bhinge, M.A. Bhutkar, D.S. Randive, G.H. Wadkar, S.S. Todkar, M.N. Urade, Characterization, antioxidant, antimicrobial and cytotoxic activities of green synthesized silver and iron nanoparticles using alcoholic Blumea eriantha DC plant extract, Mater. Today Commun. 24 (2020) 101320, https://doi.org/10.1016/ j.mtcomm.2020.101320.
55. P.V. AshaRani, G. Low Kah Mun, M.P. Hande, S. Valiyaveettil, Cytotoxicity and genotoxicity of silver nanoparticles in human cells, ACS Nano 3 (2009) 279–290, https://doi.org/10.1021/nn800596w.
56. K. Anandalakshmi, J. Venugobal, V. Ramasamy, Characterization of silver nanoparticles by green synthesis method using Pedalium murex leaf extract and their antibacterial activity, Appl. Nanosci. 6 (2016) 399–408, https://doi.org/ 10.1007/s13204-015-0449-z.
57. P. Tippayawat, N. Phromviyo, P. Boueroy, A. Chompoosor, Green synthesis of silver nanoparticles in aloe vera plant extract prepared by a hydrothermal method and their synergistic antibacterial activity, PeerJ 4 (2016) e2589, https://doi.org/ 10.7717/peerj.2589.
58. S. Jebril, R. Khanfir Ben Jenana, C. Dridi, Green synthesis of silver nanoparticles using Melia azedarach leaf extract and their antifungal activities: in vitro and in vivo, Mater. Chem. Phys. 248 (2020) 122898, https://doi.org/10.1016/j. matchemphys.2020.122898.
59. P. Rauwel, S. Küünal, S. Ferdov, E. Rauwel, A review on the green synthesis of silver nanoparticles and their morphologies studied via TEM, Advances in Materials Science and Engineering. 2015 (2015) 1–9, https://doi.org/10.1155/ 2015/682749.
60. D. Garibo, H.A. Borbon-Nu ´ nez, ˜ J.N.D. de Leon, ´ E. García Mendoza, I. Estrada, Y. Toledano-Magana, ˜ H. Tiznado, M. Ovalle-Marroquin, A.G. Soto-Ramos, A. Blanco, J.A. Rodríguez, O.A. Romo, L.A. Chavez-Almaz ´ an, ´ A. Susarrey-Arce, Green synthesis of silver nanoparticles using Lysiloma acapulcensis exhibit high antimicrobial activity, Sci. Rep. 10 (2020) 12805, https://doi.org/10.1038/ s41598-020-69606-7.

61. M. Jeyaraj, G. Sathishkumar, G. Sivanandhan, D. MubarakAli, M. Rajesh, R. Arun, G. Kapildev, M. Manickavasagam, N. Thajuddin, K. Premkumar, A. Ganapathi, Biogenic silver nanoparticles for cancer treatment: an experimental report, Colloids Surf. B Biointerfaces 106 (2013) 86–92, https: //doi.org/10.1016/j. colsurfb.2013.01.027.
62. B. Kumar, K. Smita, R. Seqqat, K. Benalcazar, M. Grijalva, L. Cumbal, In vitro evaluation of silver nanoparticles cytotoxicity on Hepatic cancer (Hep-G2) cell line and their antioxidant activity: green approach for fabrication and application, J. Photochem. Photobiol. B Biol. 159 (2016) 8–13, https: //doi.org/10.1016/j. jphotobiol.2016.03.011.
63. S. Pugazhendhi, E. Kirubha, P.K. Palanisamy, R. Gopalakrishnan, Synthesis and characterization of silver nanoparticles from Alpinia calcarata by Green approach and its applications in bactericidal and nonlinear optics, Appl. Surf. Sci. 357 (2015) 1801–1808, https://doi.org/10.1016/j.apsusc.2015.09.237.
64. H. Veisi, S. Azizi, P. Mohammadi, Green synthesis of the silver nanoparticles mediated by Thymbra spicata extract and its application as a heterogeneous and recyclable nanocatalyst for catalytic reduction of a variety of dyes in water, J. Clean. Prod. 170 (2018) 1536–1543, https://doi.org/10.1016/j. jclepro.2017.09.265.
65. U.B. Jagtap, V.A. Bapat, Green synthesis of silver nanoparticles using Artocarpus heterophyllus Lam. seed extract and its antibacterial activity, Ind. Crop. Prod. 46 (2013) 132–137, https://doi.org/10.1016/j.indcrop.2013.01.019.
66. Z. Khan, J.I. Hussain, A.A. Hashmi, Shape-directing role of cetyltrimethylammonium bromide in the green synthesis of Ag-nanoparticles using Neem (Azadirachta indica) leaf extract, Colloids Surf. B Biointerfaces 95 (2012) 229–234, https://doi.org/10.1016/j.colsurfb.2012.03.002.
67. S. Aslany, F. Tafvizi, V. Naseh, Characterization and evaluation of cytotoxic and apoptotic effects of green synthesis of silver nanoparticles using Artemisia Ciniformis on human gastric adenocarcinoma, Materials Today Communications. 24 (2020) 101011. https://doi.org/10.1016/j.mtcomm.2020.101011.
68. N. Hashim, M. Paramasivam, J.S. Tan, D. Kernain, M.H. Hussin, N. Brosse, F. Gambier, P.B. Raja, Green mode synthesis of silver nanoparticles using Vitis vinifera's tannin and screening its antimicrobial activity / apoptotic potential versus cancer cells, Materials Today Communications. 25 (2020) 101511. https://doi.org/10.1016/j.mtcomm.2020.101511.
69. R.R. Chavan, S.D. Bhinge, M.A. Bhutkar, D.S. Randive, G.H. Wadkar, S.S. Todkar, M.N. Urade, Characterization, antioxidant, antimicrobial and cytotoxic activities of green synthesized silver and iron nanoparticles using alcoholic Blumea eriantha DC plant extract, Materials Today Communications. 24 (2020) 101320. https://doi.org/10.1016/j.mtcomm.2020.101320.

70. M. Mosaviniya, T. Kikhavani, M. Tanzifi, M. Tavakkoli Yaraki, P. Tajbakhsh, A. Lajevardi, Facile green synthesis of silver nanoparticles using Crocus Haussknechtii Bois bulb extract: Catalytic activity and antibacterial properties, Colloid and Interface Science Communications. 33 (2019) 100211. https://doi.org/10.1016/j.colcom.2019.100211.
71. T.S. Alomar, N. AlMasoud, M.A. Awad, M.F. El-Tohamy, D.A. Soliman, An ecofriendly plant-mediated synthesis of silver nanoparticles: Characterization, pharmaceutical and biomedical applications, Materials Chemistry and Physics. 249 (2020) 123007. https://doi.org/10.1016/j.matchemphys.2020.123007.
72. S.O. Aisida, K. Ugwu, P.A. Akpa, A.C. Nwanya, U. Nwankwo, S.S. Botha, P.M. Ejikeme, I. Ahmad, M. Maaza, F.I. Ezema, Biosynthesis of silver nanoparticles using bitter leave (Veronica amygdalina) for antibacterial activities, Surfaces and Interfaces. 17 (2019) 100359. https://doi.org/10.1016/j.surfin.2019.100359.
73. L. Hernández-Morales, H. Espinoza-Gómez, L.Z. Flores-López, E.L. Sotelo-Barrera, A. Núñez-Rivera, R.D. Cadena-Nava, G. Alonso-Núñez, K.A. Espinoza, Study of the green synthesis of silver nanoparticles using a natural extract of dark or white Salvia hispanica L. seeds and their antibacterial application, Applied Surface Science. 489 (2019) 952–961. https://doi.org/10.1016/j.apsusc.2019.06.031.
74. A. Danagoudar, P. G K, M. Shantaram, B. Chatterjee, K. Ghosh, S.R. Kanade, C.G. Joshi, Cancer cell specific cytotoxic potential of the silver nanoparticles synthesized using the endophytic fungus, Penicillium citrinum CGJ-C2, Materials Today Communications. 25 (2020) 101442. https://doi.org/10.1016/j.mtcomm.2020.101442.
75. Y. He, F. Wei, Z. Ma, H. Zhang, Q. Yang, B. Yao, Z. Huang, J. Li, C. Zeng, Q. Zhang, Green synthesis of silver nanoparticles using seed extract of Alpinia katsumadai, and their antioxidant, cytotoxicity, and antibacterial activities, RSC Adv. 7 (2017) 39842–39851. https://doi.org/10.1039/C7RA05286C.
76. N. Jayaprakash, J.J. Vijaya, K. Kaviyarasu, K. Kombaiah, L.J. Kennedy, R.J. Ramalingam, M.A. Munusamy, H.A. Al-Lohedan, Green synthesis of Ag nanoparticles using Tamarind fruit extract for the antibacterial studies, Journal of Photochemistry and Photobiology B: Biology. 169 (2017) 178–185. https://doi.org/10.1016/j.jphotobiol.2017.03.013.

77. S. Jain, M.S. Mehata, Medicinal Plant Leaf Extract and Pure Flavonoid Mediated Green Synthesis of Silver Nanoparticles and their Enhanced Antibacterial Property, Sci Rep. 7 (2017) 15867. https://doi.org/10.1038/s41598-017-15724-8.
78. P. Rauwel, S. Küünal, S. Ferdov, E. Rauwel, A Review on the Green Synthesis of Silver Nanoparticles and Their Morphologies Studied via TEM, Advances in Materials Science and Engineering. 2015 (2015) 1–9. https://doi.org/10.1155/2015/682749.

79. D. Garibo, H.A. Borbón-Nuñez, J.N.D. de León, E. García Mendoza, I. Estrada, Y. Toledano-Magaña, H. Tiznado, M. Ovalle-Marroquin, A.G. Soto-Ramos, A. Blanco, J.A. Rodríguez, O.A. Romo, L.A. Chávez-Almazán, A. Susarrey-Arce, Green synthesis of silver nanoparticles using Lysiloma acapulcensis exhibit high-antimicrobial activity, Sci Rep. 10 (2020) 12805. https://doi.org/10.1038/s41598-020-69606-7.
80. S.K. Chandraker, M. Lal, P. Dhruve, R.P. Singh, R. Shukla, Cytotoxic, Antimitotic, DNA Binding, Photocatalytic, H2O2 Sensing, and Antioxidant Properties of Biofabricated Silver Nanoparticles Using Leaf Extract of Bryophyllum pinnatum (Lam.) Oken, Front. Mol. Biosci. 7 (2021) 593040. https://doi.org/10.3389/fmolb.2020.593040.
81. C.O. Eleazu, Characterization of the natural products in cocoyam (Colocasia esculenta) using GC–MS, Pharmaceutical Biology. 54 (2016) 2880–2885.
https://doi.org/10.1080/13880209.2016.1190383.
82. S. Agarwal, M. Gogoi, S. Talukdar, P. Bora, T.K. Basumatary, N.N. Devi, Green synthesis of silver nanoplates using the special category of plant leaves showing the lotus effect, RSC Adv. 10 (2020) 36686–36694. https://doi.org/10.1039/D0RA06533A.
83. R.K. Borah, H.J. Saikia, A. Mahanta, V.K. Das, U. Bora, A.J. Thakur, Biosynthesis of poly(ethylene glycol)-supported palladium nanoparticles using Colocasia esculenta leaf extract and their catalytic activity for Suzuki–Miyaura cross-coupling reactions, RSC Adv. 5 (2015) 72453–72457. https://doi.org/10.1039/C5RA12657F.
84. K.A. Khan, M.A. Mamun, M. Ibrahim, M. Hasan, M. Ohiduzzaman, A.K.M. Obaydullah, M.A. Wadud, M. Shajahan, PKL electrochemical cell: physics and chemistry, SN Appl. Sci. 1 (2019) 1335. https://doi.org/10.1007/s42452-019-1363-x.
85. K.A. Khan, L. Hassan, A.K.M. Obaydullah, S.M. Azharul Islam, M.A. Mamun, T. Akter, M. Hasan, Md.S. Alam, M. Ibrahim, M.M. Rahman, M. Shahjahan, Bioelectricity: a new approach to provide the electrical power from vegetative and fruits at off-grid region, Microsyst Technol. 26 (2020) 3161–3172. https://doi.org/10.1007/s00542-018-3808-3.
86. M. Hasan, K.A. Khan, Dynamic model of Bryophyllum pinnatum leaf fueled BPL cell: a possible alternate source of electricity at the off-grid region in Bangladesh, Microsyst Technol. 25 (2019) 2481–2492. https://doi.org/10.1007/s00542-018-4149-y.
87. K.A. Khan, S.R. Rasel, M. Ohiduzzaman, Homemade PKL electricity generation for use in DC fan at remote areas, Microsyst Technol. 25 (2019) 4529–4536. https://doi.org/10.1007/s00542-019-04422-2.
88. K.A. Khan, M.H. Ali, M.A. Mamun, M.M. Haque, A.K.M.A. Ullah, M.N.I. Khan, L. Hassan, A.K.M. Obaydullah, M.A. Wadud, Bioelectrical characterization and production of nanoparticles (NPs) using PKL extract for electricity generation, Microsyst Technol. (2020).
https://doi.org/10.1007/s00542-020-04774-0.

89. C. Lee, X. Wei, J.W. Kysar, J. Hone “Measurement of the elastic properties and intrinsic strength of monolayer graphene” Science, 321 (5887) (2008), pp. 385-388
DOI: 10.1126/science.1157996
90. T. Kuilla, S. Bhadra, D. Yao, N.H. Kim, S. Bose, J.H. Lee “Recent advances in graphene based polymer composites” Prog. Polym. Sci., 35 (11) (2010), pp. 1350-1375
https://doi.org/10.1016/j.progpolymsci.2010.07.005
91. Y. Cui, S.I. Kundalwal, S. Kumar “Gas Barrier Performance of Graphene/polymer Nanocomposites” Pergamon (2016), pp. 313-333 https://doi.org/10.1016/j.carbon.2015.11.018
92. L. Sun, M. Xiao, J. Liu, K. Gong “A study of the polymerization of styrene initiated by K-THF-GIC system” Eur. Polym. J., 42 (2) (2006), pp. 259-264
https://doi.org/10.1016/j.eurpolymj.2005.07.014
93. M. Xiao, L. Sun, J. Liu, Y. Li, K. Gong “Synthesis and properties of polystyrene/graphite nanocomposites” Polymer, 43 (8) (2002), pp. 2245-2248
https://doi.org/10.1016/S0032-3861(02)00022-8
94. Y. Li, J. Zhu, S. Wei, J. Ryu, Q. Wang, L. Sun, Z. Guo “Poly(propylene) nanocomposites containing various carbon nanostructures” Macromol. Chem. Phys., 212 (22) (2011), pp. 2429-2438 https://doi.org/10.1002/macp.201100364
95. Y. Li, J. Zhu, S. Wei, J. Ryu, L. Sun, Z. Guo “Poly (propylene)/Graphene nanoplatelet nanocomposites: melt rheological behavior and thermal” Electric. Electron. Prop. Macromol. Chem. Phys., 212 (18) (2011), pp. 1951-1959 https://doi.org/10.1002/macp.201100263
96. Y. Zhu, S. Murali, W. Cai, X. Li, J.W. Suk, J.R. Potts, R.S. Ruoff “Graphene and graphene oxide: synthesis, properties, and applications” Adv. Mater., 22 (35) (2010), pp. 3906-3924 https://doi.org/10.1002/adma.201001068
97. S. Niyogi, E. Bekyarova, M.E. Itkis, J.L. McWilliams, M.A. Hamon, R.C. Haddon “Solution properties of graphite and graphene” J. Am. Chem. Soc., 128 (24) (2006), pp. 7720-7721 https://doi.org/10.1021/ja060680r
98. Pendolino, Flavio, and Nerina Armata. "Graphene oxide in environmental remediation process." Springer (2017): 978-3.
99. S. Pei, H.M. Cheng “The Reduction of Graphene Oxide” (2012), pp. 3210-3228
https://doi.org/10.1016/j.carbon.2011.11.010
100. B.M. Yoo, H.J. Shin, H.W. Yoon, H.B. Park Graphene and graphene oxide and their uses in barrier polymers J. Appl. Polym. Sci., 131 (1) (2014) https://doi.org/10.1002/app.39628
101. C. Cheng, S. Li, A. Thomas, N.A. Kotov, R. Haag “Functional graphene nanomaterials based architectures: biointeractions, fabrications, and emerging biological applications” Chem. Rev., 117 (3) (2017), pp. 1826-1914 https://doi.org/10.1021/acs.chemrev.6b00520

102. B. Tan, N.L. Thomas "A review of the water barrier properties of polymer/clay and polymer/graphene nanocomposites" J. Membr. Sci., 514 (2016), pp. 595-612
https://doi.org/10.1016/j.memsci.2016.05.026
103. F.A. Ghauri, M.A. Raza, M.S. Baig, S. Ibrahim "Corrosion study of the graphene oxide and reduced graphene oxide-based epoxy coatings" Mater. Res. Express, 4 (12) (2017)
125601-125601 DOI 10.1088/2053-1591/aa9aac
104. Y.N. Singhbabu, B. Sivakumar, S.K. Choudhary, S. Das, R.K. Sahu "Corrosion-protective reduced graphene oxide coated cold rolled steel prepared using industrial setup: a study of protocol feasibility for commercial production" Surf. Coating. Technol., 349 (2018), pp. 119-132
https://doi.org/10.1016/j.surfcoat.2018.05.046
105. Luhua Lu et al "Graphene-Stabilized Silver Nanoparticle Electrochemical Electrode for Actuator Design" Adv. Mater. 2013, 25, 1270–1274 doi: 10.1002/adma.201203655.
105. K.A. Khan (2009) Community Pathor Kuchi Leaf (PKL) Electricity Generation System. Int: J. Sustain. Agril. Tech.5 (6):71-73
106. K.A. Khan and Alam MM (2010) Performance of PKL (Pathor Kuchi Leaf) Electricity and its Uses in Bangladesh. Int. J. SOC. Dev. Inf. Syst. 1(1): 15-20
107. K.A. Khan and Arafat ME (2010) Development of Portable PKL (Pathor Kuchi Leaf) Lantern. Int. J. SOC. Dev. Inf. Syst. 1(1)
108. K.A. Khan and Bosu R (2010) Performance study on PKL Electricity for Using DC Fan. Int. J. SOC. Dev. Inf. Syst. 1(1): 27-30
109. K.A. Khan and Hossain MI (2010) PKL Electricity for Switching on the Television and Radio. Int. J. SOC. Dev. Inf. Syst. 1(1): 31-36
110. Saifuddin SM & K.A. Khan (2010) Performance Study of Hybrid SPV, ST and BPL/PKL electricity Generation and storage for Practical Utilization in Bangladesh. Int: J. Eng. Tech: ISSN 1812 – 7711, 7(2)
111. K.A. Khan (2010) Organic Electricity Generation, Storage and Utilization by PKL (Bryophyllum Pinnatum). Int: Journal of Social Development and Information system (IJSDIS).1(6):
112. Sultana J, Khan KA and Ahmed MU (2011) Studies on Hybrid Pathor Kuchi Leaf (PKL)/Bryophyllum Pinnatum Leaf (BPL) and Solar Photovoltaic Electricity Generation. J. Asiat. Soc. Bangladesh. Sci. 37(2):181-188
113. Paul S, Khan KA, Islam KA, Islam B and Reza MA (2012) Modeling of a Biomass Energy based (BPL) Generating Power Plant and its features in comparison with other generating Plants. IPCBEE vol. 44 (2012) @ (2012) IACSIT Press, Singapore, doi: 10.7763/ IPCBEE. 44(3):
114. K.A. Khan, Shuva Paul, Abdullah M, Sifat SM and Yousufe MR (2013) Performance Analysis of BPL/PKL Electricity Module. Int:J. of Sci. and Eng. Research, 4(3),ISSN2229-5518

115. Hossain M, Alam S and Khan KA (2013) A study on low power generation from Pathor Kuchi Leaf (Bryophyllum) for practical utilization in Bangladesh. Int: J. of Engi. and Innovative Technology, 3660 East Bay Drive, Apartment no.116 Largo, Florida US,33771 (ISO 9001:2008 Certified)
116. Electricity Generation from Bryophyllum Pinnatum Leaf (BPL)-An Innovative approach for both Physicist and Chemist
117. Khan KA, Latif A, Alam A, Sultana J and Ali H(2014) A Study on Internal Resistance of the Pathor Kuchi Leaf (PKL) Cell. J. of Agriculture and Environment. 10(1):24-28.
118. Khan KA, Sultana J, Latif MA, Mamun MA and Saime MA (2014) A new approach of increasing the power output of Pathor Kuchi Leaf (PKL) Cell. J.ournal of Agriculture and Environment. 10(2):15-19
119. K.A. Khan, Bakshi MH, Mahmud AA (2014) Bryophyllum Pinnatum leaf (BPL) is an eternal source of renewable electrical energy for future world. J. of American Journal of Physical Chemistry 3(5):77-83, published online November 10, 2014(http://www.sciencepublishinggroup.com/j/ajpc) doi:10.11648/j.ajpc.20140305.15 ISSN: 2327-2430 (Print); ISSN: 2327-2449
120. Khan KA, Islam F, Guha B, Hassan ML and Mostofa MM (2015) Studies on Discharge Characteristics and Temperature effect of PKL (Pathor Kuchi Leaf) Cell. J. of "Bangladesh J. of Agriculture and Environment". 11(2):07-12
121. Akter T, Rubel A, Ahsan M, Mamun MA and Khan KA (2016) A Comparative study on PKL (Bryophyllum Pinnatum), Aloe Vera, Lemon and Tomato juice for Electricity Generation, Int: J. of Sci. and Eng. Research (IJSER) - ISSN 2229-5518) 7(11):
122. K.A. Khan, Paul S,Rahman MS,Kundu RK, Hasan MM, Muniruzzaman M and Mamun MA(2016) A study of performance analysis of PKL electricity generation parameters:(An experimental analysis on voltage regulation, capacity and energy efficiency of pathor kuchi leaf (PKL) electricity cell). Power India International Conference (PIICON), 7th, 25-27 Nov. 2016, IEEE , Bikaner, Rajasthan, India.
123. Khan KA, Alam MS, Mamun MA, Saime MA & Kamal MM (2016) Studies on electrochemistry for Pathor Kuchi Leaf Power System, J. of Bangladesh J. Agric. And Envirin. 12(1): 37-42
124. Khan KA, Alam MS, Rahman M, Mamun MA and Kamal MM (2017) Studies on energy efficiency for BPL power system. Bangladesh J. of Agriculture and Environment. Paper Code: BJAE/15/280

125. K.A. Khan; Rahman MS ; Das T; Ahmed MN; Saha KN; Paul S(2017) Investigation on parameters performance of Zn/Cu electrodes of BPL, AVL, Tomato and Lemon juice based electrochemical cells: A comparative study. Published in the Electrical Information and Communication Technology (EICT), 2017 3rd International Conference on IEEE Xplore: 01 February 2018, doi:10.1109/EICT.2017.8275150.
126. Hasan, M & Khan, K.A. (2019) Experimental characterization and identification of cell parametersin a PKLelectrochemical device.SN Appl.Sci.1:1008.
https://doi.org/10.1007/s42452-019-1045-8
127. K.A. Khan, M.A. Mamun, M. Ibrahim, M. Hasan, M.Ohiduzzaman, A.K.M. Obaydullah, M.A.Wadud, M. Shajahan(2019),PKL electrochemical cell: physics and chemistry,SN Applied Sciences(2019)1:1335, https://doi.org/10.1007/s42452-019-1363-x
128. M.Hazra Ali, Unesco Chakma,Debashis Howlader, M. Tawhidul Islam and K.A.Khan(2019) Studies on Performance Parametersof a Practical Transformer for Various Utilizations, Microsystem Technologies, Springer, Accepted:03 Dec 2019, doi: 10.1007/s00542-019-04711-w
129. K.A. Khan , Shahinul Islam, S. R. Rasel, M. A.Saime, Sazzad Hossain, Md. Atiqur Rahman (2020) Erformance Evaluation of BPL electricity for use in Television and Radio, Information Management and Computer Science (IMCS) 3(2) (2020) 30-37,
doi: http://doi.org/10.26480/imcs.02.2020.30.37
130. K.A. Khan, Md. Khairul Islam, Md. Alamgir Kabir, Sayed Bony Amin, Sazzad Hossain, and Md. Shahidul Islam . "A study on variation of product ion and reactant ion during BPL electricity generation" Internation Journal of Advance Research and Innovative Ideas in Education Volume 7 Issue 4 2021 Page 579-597
131. K.A. Khan, Md. Alamgir Kabir, Mustafa Mamun, Sazzad Hossain, and Md. Shahidul Islam. "BPL electricity - The Role of Physics" Internation Journal of Advance Research and Innovative Ideas in Education Volume 7 Issue 4 2021 Page 1583-1606
132. K.A. Khan, Md. Khairul Islam, Sayed Bony Amin, and Khandaker Kabir Hossain. "Leaf and vegetative extract electrochemical cells - In comparative research for capacity study" IJARIIE Volume 7 Issue 4 2021 Page 2336-2353
133. K.A. Khan, Md. Khairul Islam, Sayed Bony Amin, and Md. Abdur Rahim. "Prospects of PKL Electricity" IJARIIE Volume 7 Issue 5 2021 Page 563-582
134. K.A. Khan, Md. Alamgir Kabir, Mustafa Mamun, Mst. Sakera Khatun, and Muhammad Saiful Islam Akhand. "Effect of pH of the PKL extract during electricity production" IJARIIE Volume 7 Issue 5 2021 Page 583-600
135. K.A. Khan, Khairul Islam, Sayed Bony Amin, and Khandaker Kabir Hossain. "A study on current density for PKL electrochemical cell" Internation Journal of Advance Research and Innovative Ideas in Education" Volume 7 Issue 6 2021 Page 9-24

136. M. A. Mamun *et al*., "Electrochemistry of Green Ag Nanoparticles Modified Electrode Surface," 2022 IEEE International Conference on Semiconductor Electronics (ICSE), 2022, pp. 37-40, doi: 10.1109/ICSE56004.2022.9863176.
137. K.A.Khan, Mohammad abul kashem siddique, and Abdul Bathen Miah (2022). "Development of a LED lamp using ginger extract for practical utilization" Internation Journal of Advance Research and Innovative Ideas In Education Volume 8, Issue 5, Page 909-916
138. Kamrul Alam Khan, Salman Rahman Rasel, S.M. Zian Reza and Farhana Yesmin (March 25th 2020). Energy Efficiency and Sustainability in Outdoor Lighting - A Bet for the Future, Energy Efficiency and Sustainable Lighting - a Bet for the Future, Manuel Jesús Hermoso-Orzáez and Alfonso Gago-Calderón, Intech Open, doi: 10.5772/intechopen.89413
139. M. N. F.Rab, K. A. Khan, Salman Rahman Rasel, M.Hazrat Ali, Lovelu Hassan , M. Abu Salek , S.M.Zian Reza and M Ohiduzzaman (2020) "Voltage Cultivation from Fresh Leaves of Air Plant, Climbing Spinach, Mint, Spinach and Indian Pennywort for Practical Utilization", Energy Systems, Drives and Automations, Springer Singapore, Lecture Notes in Electrical Engineering, eBook ISBN: 978-981-15-5089-8, doi:10.1007/978-981-15-5089-8, Hardcover ISBN: 978-981-15-5088-1, Series ISSN: 1876-1100, Volume: 664,Page: 150-160
140. K. A. Khan, M. A. Saime, M.Hazrat Ali, S. M. Zian Reza, Nazmul Alam, Md. Afzol Hossain, M. N.F.Rab and Shahinul Islam (2020) "A study on PKL electrochemical cell for three different conditions ", Energy Systems, Drives and Automations, Proceedings of ESDA 2019 , Springer Singapore, Lecture Notes in Electrical Engineering, eBook ISBN: 978-981-15-5089-8, doi: 10.1007/978-981-15-5089-8, Hardcover ISBN: 978-981-15-5088-1, Series ISSN: 1876-1100, Volume: 664, Page: 374-386.
141. K A Khan Study on Development of BPL Power. In: Mandal J.K., Mukherjee I., Bakshi S., Chatterji S., Sa P.K. Computational Intelligence and Machine Learning. Advances in Intelligent Systems and Computing, vol 1276. Pp151-171, Springer, Singapore. http://doi-org-443.webvpn.fjmu.edu.cn/10.1007/978-981-15-8610-1_17
142. Pervin R., Khan K.A., Khan N.I., Atique Ullah A.K.M., Zian Reza S.M. (2021) Green Synthesis of Magnetite (Fe_3O_4) Nanoparticles using Azadirachta indica Leaf Extract and Their Characterization. In: Mukherjee M., Mandal J., Bhattacharyya S., Huck C., Biswas S. (eds) Advances in Medical Physics and Healthcare Engineering. Lecture Notes in Bioengineering. Springer, Singapore. https://doi.org/10.1007/978-981-33-6915-3_9, First Online17 June 2021, https://doi.org/10.1007/978-981-33-6915-3_9, Publisher NameSpringer, Singapore. Page: 81-90
143. Khan K.A., Sultana R., Islam S., Zian Reza S.M. (2021) A Study on Light Traps for Attracting and Killing the Insects Using BPL Electricity. In: Mukherjee M., Mandal J., Bhattacharyya S., Huck C., Biswas S. (eds) Advances in Medical Physics and Healthcare Engineering. Lecture Notes in Bioengineering. Springer, 17 June 2021, https://doi.org/10.1007/978-981-33-6915-3_14, Springer, Singapore.pp:135-143

144. Khan K.A., Rahman M.S., Rahman M.N., Khan S.A., Juel M.I., Nirjhar M.I. (2021) A Study on Electrochemical Characterizations of BPL Electricity. In: Mukherjee M., Mandal J., Bhattacharyya S., Huck C., Biswas S. (eds) Advances in Medical Physics and Healthcare Engineering. Lecture Notes in Bioengineering. Springer, Singapore. https://doi.org/10.1007/978-981-33-6915-3_54, Springer, Singapore. pp 567-581, 17 June 2021

145. Hassan L., Khan K.A. (2021) Applications of PKL Electricity for Use in DC Instruments. In: Biswas A., Saxena R., De D. (eds) Microelectronics, Circuits and Systems. Lecture Notes in Electrical Engineering, vol 755. Springer, Singapore.
https://doi.org/10.1007/978-981-16-1570-2_18, pp: 191-202

146. Khan K.A., Islam S., Delowar Hossain Munna M., Zian Reza S.M., Hazrat Ali M., Yesmin F. (2022) 3R Economy of a BPL Electrochemical Cell. In: Chanda C.K., Szymanski J.R., Sikander A., Mondal P.K., Acharjee D. (eds) Advanced Energy and Control Systems. Lecture Notes in Electrical Engineering, vol 820. Springer, pp: 137-145, Singapore.
https://doi.org/10.1007/978-981-16-7274-3_11

147. Khan K.A., Islam S., Rasel S.R., Saime M.A., Islam S., Ali M.H. (2022) PKL Backup LED Bulb-An Alternative Source of Electricity During Load Shading. In: Chanda C.K., Szymanski J.R., Sikander A., Mondal P.K., Acharjee D. Advanced Energy and Control Systems. Lecture Notes in Electrical Engineering, vol.820.pp:89-99, Springer, Singapore.
https://doi.org/10.1007/978-981-16-7274-3_7

148. Khan K.A., Mamun M.A., Adal M.I., Mia S., Ali M.H. (2022) Electrochemical Conversion of CO_2 into Useful Chemicals and PKL Electricity. In: Chanda C.K., Szymanski J.R., Sikander A., Mondal P.K., Acharjee D. Advanced Energy and Control Systems. Lecture Notes in Electrical Engineering, vol 820. Springer, pp: 55-72, Singapore.
https://doi.org/10.1007/978-981-16-7274-3_5

149. Abdul Wadud, M., Khan, K.A., Sayed Hossain, M., Rasel, S.R., Bhattacharyya, S. (2022). An Observation of Energy Density for BPL, Aloe Vera, Myrobalan, Lemon, and Tomato Electrochemical Cell. In: Mandal, J.K., Hsiung, PA., Sankar Dhar, R. Topical Drifts in Intelligent Computing. ICCTA 2021. Lecture Notes in Networks and Systems, vol 426. Springer, Singapore.
https://doi.org/10.1007/978-981-19-0745-6_60

150. Khan, K.A., Sayed Hossain, M., Rasel, S.R., Bhattacharyya, S. (2022). Comparative Studies of V_L, I_L, and P_L from Different Vegetative and Fruits Electrochemical Cells. In: Mandal, J.K., Hsiung, PA., Sankar Dhar, R. Topical Drifts in Intelligent Computing. ICCTA 2021. Lecture Notes in Networks and Systems, vol 426. Springer, Singapore.
https://doi.org/10.1007/978-981-19-0745-6_56

151. Rasel, S.R., Khan, K.A., Bhattacharyya, S. (2022). Electricity Generation Using Soil and Living PKL Tree. In: Mandal, J.K., Hsiung, PA., Sankar Dhar, R. Topical Drifts in Intelligent

Computing. ICCTA 2021. Lecture Notes in Networks and Systems, vol 426. Springer, Singapore. https://doi.org/10.1007/978-981-19-0745-6_55
152. Shuva Paul, Kamrul Alam Khan, Kazi Ahad Islam, Baishakhi Islam and Musa Ali Reza, "Modeling of a Biomass Energy based (BPL) Generating Power Plant and its features in comparison with other generating Plants ",IPCBEE vol. 44 (2012) @ (2012) IACSIT Press, Singapore doi: 10.7763/ IPCBEE. 2012. V44. 3
[153] Lovelu Hasan, Mehedi Hasan, Kamrul Alam Khan and S.M. Azharul Islam, "SEM Analysis of Electrodes and measurement of ionic pressure by AAS data to identify and compare the characteristics between different bio-fuel based electrochemical cell, " Published in the International conference on Physics-2018, Venue-Department of Physics, University of Dhaka, Dhaka-1000,Bangladesh, Organizer-Bangladesh Physical Society(BPS), 08-10 March, 2018.
[154] Mehedi Hasan and Kamrul Alam Khan, "Identification of BPL Cell Parameters to Optimize the Output Performance for the Off-grid Electricity Production, " Published in the International conference on Physics-2018, Venue-Department of Physics, University of Dhaka, Dhaka-1000,Bangladesh, Organizer-Bangladesh Physical Society(BPS), 08-10 March, 2018.
[155] K A Khan, M.S.Bhuyan, M. A. Mamun,M.Ibrahim,Lovelu Hassan and M A Wadud, "Organic electricity from Zn/Cu-PKL electrochemical cell ", Published in the Souvenir of First International Conference of Contemporary Advances in Innovative & Information Technology(ICCAIAIT) 2018,organized by KEI, In collaboration with Computer Society of India(CSI), Division-IV(Communication). The proceedings consented to be published in AISC Series of Springer, 2018
[156] M.K.A.Khan, A K M Obaydullah, M.A. Wadud and M Afzol Hossain, "Bi-Product from Bioelectricity", IJARIIE-ISSN (O)-2395-4396, Volume-4, Issue-2, Page-3136-3142, 2018
[157] M.K.A.Khan and A K M Obaydullah, "Construction and Commercial Use of PKL Cell", IJARIIE-ISSN (O)-2395-4396, Volume-4, Issue-2, Page-3563-3570, 2018
[158] Md. Kamrul Alam Khan, "Studies on Electricity Generation from Stone Chips Plant (Bryophyllum pinnatum)", International J.Eng. Tech 5(4): 393-397, December 2008.
[159] M. K. Alam Khan, "Copper Oxide Coating for use in Linear Solar Fresnel Reflecting Concentrating Collector", Published in the journal. of Elsevier, Renewable Energy, An International Journal, WREN(World Renewable Energy Network), UK, RE: 12.97/859,1998.
[160] K.A.Khan, M Afzol Hossain, A K M Obaydullah and M.A. Wadud, "PKL Electrochemical Cell and the Peukert's Law ", Vol-4 Issue-2, 2018 IJARIIE-ISSN(O)-2395-4396,Page: 4219 – 4227
[161] K.A.Khan, M.A.Wadud, M Afzol Hossain and A.K.M. Obaydullah, "Electrical Performance of PKL (Pathor Kuchi Leaf)Power", Published in the IJARIIE-ISSN(O)-2395-4396,Volume-4, Issue-2, Page-3470-3478 ,2018.

[162] K.A.Khan, M Hazrat Ali, M. A. Mamun, M. Mahbubul Haque, A.K.M. Atique Ullah, Dr. Mohammed Nazrul Islam Khan, Lovelu Hassan, A K M Obaydullah, M A Wadud, "Bioelectrical Characteristics of Zn/Cu- PKL Cell and Production of Nanoparticles (NPs) for Practical Utilization'', 5th International conference on 'Microelectronics, Circuits and Systems', Micro2018, 19th and 20th May,2018,Venue: Bhubaneswar, Odisha, India, Organizer: Applied Computer Technology, Kolkata, West Bengal, India, Page: 59-66, www.actsoft.org, ISBN: 81-85824-46-1, In Association with: International Association of Science, Technology and Management, 2018

[163] K.A.Khan, S.M.Maniruzzaman Manir, Md. Shafiqul Islam, Sifat Jahan, Lovelu Hassan, and M Hazrat Ali. "Studies on Nonconventional Energy Sources for Electricity Generation" Internation Journal of Advance Research and Innovative Ideas in Education, Volume 4 Issue 4 2018 Page 229-244

[164] K.A.Khan, Mahmudul Hasan, Mohammad Ashraful Islam, Mohammad Abdul Alim, Ummay Asma, Lovelu Hassan, and M Hazrat Ali. "A Study on Conventional Energy Sources for Power Production" Internation Journal of Advance Research and Innovative Ideas in Education, Volume 4 Issue 4 2018 Page 214-228

[165] Md. Kamrul Alam Khan ; Md. Siddikur Rahman ; Tanmoy Das ;Muhammad Najebul Ahmed ; Kaushik Nandan Saha ; Shuva Paul, Investigation on parameters performance of Zn/Cu electrodes of PKL, AVL, Tomato and Lemon juice based electrochemical cells: A comparative study, Publication Year: 2017, Page(s):1-6, Published in: 2017 3rd International Conference on Electrical Information and Communication Technology (EICT), Date of Conference: 7-9 Dec. 2017, Date Added to IEEE Xplore: 01 February 2018, ISBN Information: INSPEC AccessionNumber: 17542905, doi:10.1109/EICT.2017.8275150, Publisher: IEEE,Conference Location: Khulna, Bangladesh

[166] Sheth AK. The Herbs of Ayurveda. Ahmedabad: A.K. Sheth Publishers; 2005. p. 356.

[167] Khare CP. Indian Medicinal Plants. New Delhi: Springer; 2007. p. 167

[168] Shuva Paul, K. A. Khan, Kazi Ahad Islam, Baishakhi Islam and Musa Ali Reza, "Modeling of a Biomass Energy based (BPL) Generating Power Plant and its features in comparison with other generating Plants ",IPCBEE vol. 44 (2012) @ (2012) IACSIT Press, Singapore
doi :10.7763/ IPCBEE. 2012. V44. 3

[169] K. A. Khan, M. H. Bakshi and A. A. Mahmud, "*Bryophyllum Pinnatum* leaf (BPL) is an eternal source of renewable electrical energy for future world", American Journal of Physical Chemistry2014;3(5):7783,November10,2014, doi:10.11648/j.ajpc.20140305.15, ISSN:2327-2430 (Print); ISSN: 2327-2449

[170] David A. Bell, Electric Circuits, 6th edition, P. 50.

[171] David A. Bell, Electric Circuits, 6th edition, P. 214.

[172] Bard, A. J.; Faulkner, L. R. (2000). Electrochemical Methods: Fundamentals and Applications, 2 nd edition. New York: John Wiley & Sons. ISBN 0-471-04372-9. 59. http://batteryuniversity.com/learn/article/elevating_self_discharge
[173] Wu and White, "Self-Discharge Model of a Nickel-Hydrogen Cell." Journal of the Electrochemical Society, 2000, Vol.147 (3): P. 901-909.
[174] http://batteryuniversity.com/learn/article/elevating_self_discharge
[175] Luhua Lu et al "Graphene-Stabilized Silver Nanoparticle Electrochemical Electrode for Actuator Design" Adv. Mater. 2013, 25, 1270–1274 doi:10.1002/adma.201203655.
[176] Saptarshi Dhibar, Chapal Kumar Das "Electrochemical performances of silver nanoparticles decorated polyaniline/graphene nanocomposite in different electrolytes" Journal of Alloys and Compounds, 19 August 2015, doi: 10.1016/j.jallcom.2015.08.158.
[177] Prajapati R, Kalariya M, Umbarkar R, Parmar S, Sheth N,"Colocasia esculenta: A potent indigenous plant." Int J Nutr Pharmacol Neurol Dis 2011; 1:90- 6 doi:10.4103/2231-0738.84188
[178] J.M. Ashraf, M.A. Ansari, H.M. Khan, M.A. Alzohairy, I. Choi, Green synthesis of silver nanoparticles and characterization of their inhibitory effects on AGEs formation using biophysical techniques, Sci Rep. 6 (2016) 20414. https://doi.org/10.1038/srep20414.
[179] B. Khodadadi, M. Bordbar, A. Yeganeh-Faal, M. Nasrollahzadeh, Green synthesis of Ag nanoparticles/clinoptilolite using Vaccinium macrocarpon fruit extract and its excellent catalytic activity for reduction of organic dyes, Journal of Alloys and Compounds. 719 (2017) 82–88. https://doi.org/10.1016/j.jallcom.2017.05.135.
[180] N. Jayaprakash, J.J. Vijaya, K. Kaviyarasu, K. Kombaiah, L.J. Kennedy, R.J. Ramalingam, M.A. Munusamy, H.A. Al-Lohedan, Green synthesis of Ag nanoparticles using Tamarind fruit extract for the antibacterial studies, Journal of Photochemistry and Photobiology B: Biology. 169 (2017) 178–185. https://doi.org/10.1016/j.jphotobiol.2017.03.013.
[181] S. Raj, S. Chand Mali, R. Trivedi, Green synthesis and characterization of silver nanoparticles using Enicostemma axillare (Lam.) leaf extract, Biochemical and Biophysical Research Communications. 503 (2018) 2814–2819. https://doi.org/10.1016/j.bbrc.2018.08.045.
[182] M. Darroudi, M. Mansor Bin Ahmad, A.H. Abdullah, N.A. Ibrahim, K. Shameli, Green synthesis and characterization of gelatin-based and sugar-reduced silver nanoparticles, IJN. (2011) 569. https://doi.org/10.2147/IJN.S16867.
[183] S. Jain, M.S. Mehata, Medicinal Plant Leaf Extract and Pure Flavonoid Mediated Green Synthesis of Silver Nanoparticles and their Enhanced Antibacterial Property, Sci Rep. 7 (2017) 15867. https://doi.org/10.1038/s41598-017-15724-8.
[184] B. Khodadadi, M. Bordbar, A. Yeganeh-Faal, M. Nasrollahzadeh, Green synthesis of Ag nanoparticles/clinoptilolite using Vaccinium macrocarpon fruit extract and its excellent catalytic activity for reduction of organic dyes, Journal of Alloys and Compounds. 719 (2017) 82–88. https://doi.org/10.1016/j.jallcom.2017.05.135.

[185] M. Villanueva-Ibáñez, M.G. Yañez-Cruz, R. Álvarez-García, M.A. Hernández-Pérez, M.A. Flores-González, Aqueous corn husk extract – mediated green synthesis of AgCl and Ag nanoparticles, Materials Letters. 152 (2015) 166–169. https://doi.org/10.1016/j.matlet.2015.03.097.
[186] N. Hashim, M. Paramasivam, J.S. Tan, D. Kernain, M.H. Hussin, N. Brosse, F. Gambier, P.B. Raja, Green mode synthesis of silver nanoparticles using Vitis vinifera's tannin and screening its antimicrobial activity / apoptotic potential versus cancer cells, Materials Today Communications. 25 (2020) 101511. https://doi.org/10.1016/j.mtcomm.2020.101511.
[187] A. Danagoudar, P. G K, M. Shantaram, B. Chatterjee, K. Ghosh, S.R. Kanade, C.G. Joshi, Cancer cell specific cytotoxic potential of the silver nanoparticles synthesized using the endophytic fungus, Penicillium citrinum CGJ-C2, Materials Today Communications. 25 (2020) 101442. https://doi.org/10.1016/j.mtcomm.2020.101442.
[188] O. Velgosová, A. Mražíková, R. Marcinčáková, Influence of pH on green synthesis of Ag nanoparticles, Materials Letters. 180 (2016) 336–339. https://doi.org/10.1016/j.matlet.2016.04.045.
[189] K. Anandalakshmi, J. Venugobal, V. Ramasamy, Characterization of silver nanoparticles by green synthesis method using Pedalium murex leaf extract and their antibacterial activity, Appl Nanosci. 6 (2016) 399–408. https://doi.org/10.1007/s13204-015-0449-z.
[190] M. Ahamed, M.A. Majeed Khan, M.K.J. Siddiqui, M.S. AlSalhi, S.A. Alrokayan, Green synthesis, characterization and evaluation of biocompatibility of silver nanoparticles, Physica E: Low-Dimensional Systems and Nanostructures. 43 (2011) 1266–1271. https://doi.org/10.1016/j.physe.2011.02.014.
[191] F. Göl, A. Aygün, A. Seyrankaya, T. Gür, C. Yenikaya, F. Şen, Green synthesis and characterization of Camellia sinensis mediated silver nanoparticles for antibacterial ceramic applications, Materials Chemistry and Physics. 250 (2020) 123037. https://doi.org/10.1016/j.matchemphys.2020.123037.
[192] N. Jayaprakash, J.J. Vijaya, K. Kaviyarasu, K. Kombaiah, L.J. Kennedy, R.J. Ramalingam, M.A. Munusamy, H.A. Al-Lohedan, Green synthesis of Ag nanoparticles using Tamarind fruit extract for the antibacterial studies, Journal of Photochemistry and Photobiology B: Biology. 169 (2017) 178–185. https://doi.org/10.1016/j.jphotobiol.2017.03.013.
[193] M. Shahriary, H. Veisi, M. Hekmati, S. Hemmati, In situ green synthesis of Ag nanoparticles on herbal tea extract-modified magnetic iron oxide nanoparticles as antibacterial agent and their 4-nitrophenol catalytic reduction activity, Materials Science and Engineering: C. 90 (2018) 57–66. https://doi.org/10.1016/j.msec.2018.04.044.
[194] S. Jebril, R. Khanfir Ben Jenana, C. Dridi, Green synthesis of silver nanoparticles using Melia azedarach leaf extract and their antifungal activities: In vitro and in vivo, Materials Chemistry and Physics. 248 (2020) 122898. https://doi.org/10.1016/j.matchemphys.2020.122898.

[195] D. Garibo, H.A. Borbón-Nuñez, J.N.D. de León, E. García Mendoza, I. Estrada, Y. Toledano-Magaña, H. Tiznado, M. Ovalle-Marroquin, A.G. Soto-Ramos, A. Blanco, J.A. Rodríguez, O.A. Romo, L.A. Chávez-Almazán, A. Susarrey-Arce, Green synthesis of silver nanoparticles using Lysiloma acapulcensis exhibit high-antimicrobial activity, Sci Rep. 10 (2020) 12805. https://doi.org/10.1038/s41598-020-69606-7.

[196] S. Aslany, F. Tafvizi, V. Naseh, Characterization and evaluation of cytotoxic and apoptotic effects of green synthesis of silver nanoparticles using Artemisia Ciniformis on human gastric adenocarcinoma, Materials Today Communications. 24 (2020) 101011. https://doi.org/10.1016/j.mtcomm.2020.101011.

[197] E. Turunc, R. Binzet, I. Gumus, G. Binzet, H. Arslan, Green synthesis of silver and palladium nanoparticles using Lithodora hispidula (Sm.) Griseb and application to the electrocatalytic reduction of hydrogen peroxide, Materials Chemistry and Physics. 202 (2017) 310–319. https://doi.org/10.1016/j.matchemphys.2017.09.032.

[198] M. Mosaviniya, T. Kikhavani, M. Tanzifi, M. Tavakkoli Yaraki, P. Tajbakhsh, A. Lajevardi, Facile green synthesis of silver nanoparticles using Crocus Haussknechtii Bois bulb extract: Catalytic activity and antibacterial properties, Colloid and Interface Science Communications. 33 (2019) 100211. https://doi.org/10.1016/j.colcom.2019.100211.

[199] S.O. Aisida, K. Ugwu, P.A. Akpa, A.C. Nwanya, U. Nwankwo, S.S. Botha, P.M. Ejikeme, I. Ahmad, M. Maaza, F.I. Ezema, Biosynthesis of silver nanoparticles using bitter leave (Veronica amygdalina) for antibacterial activities, Surfaces and Interfaces. 17 (2019) 100359. https://doi.org/10.1016/j.surfin.2019.100359.

[200] P. Das, K. Ghosal, N.K. Jana, A. Mukherjee, P. Basak, Green synthesis and characterization of silver nanoparticles using belladonna mother tincture and its efficacy as a potential antibacterial and anti-inflammatory agent, Materials Chemistry and Physics. 228 (2019) 310–317. https://doi.org/10.1016/j.matchemphys.2019.02.064.

[201] R. Parameshwaran, S. Kalaiselvam, R. Jayavel, Green synthesis of silver nanoparticles using Beta vulgaris: Role of process conditions on size distribution and surface structure, Materials Chemistry and Physics. 140 (2013) 135–147. https://doi.org/10.1016/j.matchemphys.2013.03.012.

[202] B. Paul, M.A.-A. Mamun, A. Haque, M. Paul, K. Ghosh, Significant Reduction of Defect States and Surface Tailoring in ZnO Nanoparticles via Nano-Bio Interaction With Glucose for Bio-Applications, IEEE Trans.on Nanobioscience. 18 (2019) 490–497. https://doi.org/10.1109/TNB.2019.2919231.

[203] M.A. Siddiquee, M. ud din Parray, S.H. Mehdi, K.A. Alzahrani, A.A. Alshehri, M.A. Malik, R. Patel, Green synthesis of silver nanoparticles from Delonix regia leaf extracts: In-vitro cytotoxicity and interaction studies with bovine serum albumin, Materials Chemistry and Physics. 242 (2020) 122493. https://doi.org/10.1016/j.matchemphys.2019.122493.

[204] S.K. Chandraker, M. Lal, P. Dhruve, R.P. Singh, R. Shukla, Cytotoxic, Antimitotic, DNA Binding, Photocatalytic, H2O2 Sensing, and Antioxidant Properties of Biofabricated Silver Nanoparticles Using Leaf Extract of Bryophyllum pinnatum (Lam.) Oken, Front. Mol. Biosci. 7 (2021) 593040. https://doi.org/10.3389/fmolb.2020.593040.
[205] A.K.M.A. Ullah, M.M. Haque, M. Akter, A. Hossain, A.N. Tamanna, M.M. Hosen, A.K.M.F. Kibria, M.N.I. Khan, M.K.A. Khan, Green synthesis of *Bryophyllum pinnatum* aqueous leaf extract mediated bio-molecule capped dilute ferromagnetic α -MnO_2 nanoparticles, Mater. Res. Express. 7 (2020) 015088. https://doi.org/10.1088/2053-1591/ab6c20.
[206] A.K.M. Atique Ullah, A.N. Tamanna, A. Hossain, M. Akter, M.F. Kabir, A.R.M. Tareq, A.K.M. Fazle Kibria, M. Kurasaki, M.M. Rahman, M.N.I. Khan, *In vitro* cytotoxicity and antibiotic application of green route surface modified ferromagnetic TiO_2 nanoparticles, RSC Adv. 9 (2019) 13254–13262. https://doi.org/10.1039/C9RA01395D.
[207] T.S. Alomar, N. AlMasoud, M.A. Awad, M.F. El-Tohamy, D.A. Soliman, An eco-friendly plant-mediated synthesis of silver nanoparticles: Characterization, pharmaceutical and biomedical applications, Materials Chemistry and Physics. 249 (2020) 123007. https://doi.org/10.1016/j.matchemphys.2020.123007.
[208] A.D. Jadhao, S. Shende, P. Ingle, A. Gade, S.W. Hajare, R.S. Ingole, Biogenic Synthesis of Zinc Oxide Nanoparticles by BPL and its Acute Oral Toxicity Evaluation in Wistar Rats, IEEE Trans.on Nanobioscience. 19 (2020) 633–639. https://doi.org/10.1109/TNB.2020.3014023.
[209] S. M., B. K., B. M., J. S., A. S., S. A., N. P., S. R., Obtaining titanium dioxide nanoparticles with spherical shape and antimicrobial properties using M. citrifolia leaves extract by hydrothermal method, Journal of Photochemistry and Photobiology B: Biology. 171 (2017) 117–124. https://doi.org/10.1016/j.jphotobiol.2017.05.003.
[210] L. Hernández-Morales, H. Espinoza-Gómez, L.Z. Flores-López, E.L. Sotelo-Barrera, A. Núñez-Rivera, R.D. Cadena-Nava, G. Alonso-Núñez, K.A. Espinoza, Study of the green synthesis of silver nanoparticles using a natural extract of dark or white Salvia hispanica L. seeds and their antibacterial application, Applied Surface Science. 489 (2019) 952–961. https://doi.org/10.1016/j.apsusc.2019.06.031.
[211] A. Rangayasami, K. Kannan, S. Joshi, M. Subban, Bioengineered silver nanoparticles using Elytraria acaulis (L.f.) Lindau leaf extract and its biological applications, Biocatalysis and Agricultural Biotechnology. 27 (2020) 101690. https://doi.org/10.1016/j.bcab.2020.101690.
[212] P. Pawliszak, D. Malina, A. Sobczak-Kupiec, Rhodiola rosea extract mediated green synthesis of silver nanoparticles supported by nanosilica carrier, Materials Chemistry and Physics. 234 (2019) 390–402. https://doi.org/10.1016/j.matchemphys.2019.05.027.

[213] T.A. Salih, K.T. Hassan, S.R. Majeed, I.J. Ibraheem, O.M. Hassan, A.S. Obaid, In vitro scolicidal activity of synthesised silver nanoparticles from aqueous plant extract against Echinococcus granulosus, Biotechnology Reports. 28 (2020) e00545. https://doi.org/10.1016/j.btre.2020.e00545.
[214] M. Sundrarajan, K. Bama, M. Bhavani, S. Jegatheeswaran, S. Ambika, A. Sangili, P. Nithya, R. Sumathi, Obtaining titanium dioxide nanoparticles with spherical shape and antimicrobial properties using M. citrifolia leaves extract by hydrothermal method, J. Photochem. Photobiol. B Biol. 171 (2017) 117–124, https://doi.org/10.1016/j.jphotobiol.2017.05.003.
[215] A. Rautela, J. Rani, M. Debnath (Das), Green synthesis of silver nanoparticles from Tectona grandis seeds extract: characterization and mechanism of antimicrobial action on different microorganisms, J Anal Sci Technol. 10 (2019) 5. https://doi.org/10.1186/s40543-018- 0163-z.
[216] S. Raj, S. Chand Mali, R. Trivedi, Green synthesis and characterization of silver nanoparticles using Enicostemma axillare (Lam.) leaf extract, Biochemical and Biophysical Research Communications. 503 (2018) 2814–2819. https://doi.org/10.1016/j.bbrc.2018.08.045
[217] F. Eya'ane Meva, M.L. Segnou, C. Okalla Ebongue, A.A. Ntoumba, P. Belle Ebanda Kedi, V. Deli, M.-A. Etoh, E. Mpondo Mpondo, Spectroscopic synthetic optimizations monitoring of silver nanoparticles formation from Megaphrynium macrostachyum leaf extract, Revista Brasileira de Farmacognosia. 26 (2016) 640–646. https://doi.org/10.1016/j.bjp.2016.06.002.
[218] W.W. Melkamu, L.T. Bitew, Green synthesis of silver nanoparticles using Hagenia abyssinica (Bruce) J.F. Gmel plant leaf extract and their antibacterial and anti-oxidant activities, Heliyon. 7 (2021) e08459. https://doi.org/10.1016/j.heliyon.2021.e08459.
[219] S. Jain, M.S. Mehata, Medicinal Plant Leaf Extract and Pure Flavonoid Mediated Green Synthesis of Silver Nanoparticles and their Enhanced Antibacterial Property, Sci Rep. 7 (2017) 15867. https://doi.org/10.1038/s41598-017-15724-8.
[220] M.A. Hossain, B. Paul, K.A. Khan, M. Paul, M.A. Mamun, M.E. Quayum, Green synthesis and characterization of silver nanoparticles by using Bryophyllum pinnatum and the evaluation of its power generation activities on bio-electrochemical cell, Materials Chemistry and Physics. 282 (2022) 125943. https://doi.org/10.1016/j.matchemphys.2022.125943
[221] D. Kalpana, Y.S. Lee, Synthesis and characterization of bactericidal silver nanoparticles using cultural filtrate of simulated microgravity grown Klebsiella pneumoniae, Enzyme and Microbial Technology. 52 (2013) 151–156. https://doi.org/10.1016/j.enzmictec.2012.12.006.
[222] D. Kalpana, Y.S. Lee, Synthesis and characterization of bactericidal silver nanoparticles using cultural filtrate of simulated microgravity grown Klebsiella pneumoniae, Enzyme and Microbial Technology. 52 (2013) 151–156. https://doi.org/10.1016/j.enzmictec.2012.12.006.
[223] V.S. Suvith, D. Philip, Catalytic degradation of methylene blue using biosynthesized gold and silver nanoparticles, Spectrochimica Acta Part A: Molecular and Biomolecular Spectroscopy. 118 (2014) 526–532. https://doi.org/10.1016/j.saa.2013.09.016.

[224] S. Hamedi, S.A. Shojaosadati, A. Mohammadi, Evaluation of the catalytic, antibacterial and anti-biofilm activities of the Convolvulus arvensis extract functionalized silver nanoparticles, Journal of Photochemistry and Photobiology B: Biology. 167 (2017) 36–44. https://doi.org/10.1016/j.jphotobiol.2016.12.025.
[225] X. Zhao, J. Zhang, B. Wang, A. Zada, M. Humayun, Biochemical Synthesis of Ag/AgCl Nanoparticles for Visible-Light-Driven Photocatalytic Removal of Colored Dyes, Materials. 8 (2015) 2043–2053. https://doi.org/10.3390/ma8052043.
[226] S. Agarwal, M. Gogoi, S. Talukdar, P. Bora, T.K. Basumatary, N.N. Devi, Green synthesis of silver nanoplates using the special category of plant leaves showing the lotus effect, RSC Adv. 10 (2020) 36686–36694. https://doi.org/10.1039/D0RA06533A.
[227] R.K. Borah, H.J. Saikia, A. Mahanta, V.K. Das, U. Bora, A.J. Thakur, Biosynthesis of poly(ethylene glycol)-supported palladium nanoparticles using Colocasia esculenta leaf extract and their catalytic activity for Suzuki–Miyaura cross-coupling reactions, RSC Adv. 5 (2015) 72453–72457. https://doi.org/10.1039/C5RA12657F.
[228] S. Thakur, N. Karak, Green reduction of graphene oxide by aqueous phytoextracts, Carbon. 50 (2012) 5331–5339. https://doi.org/10.1016/j.carbon.2012.07.023.
[229] V.E. Manhivi, S. Venter, E.O. Amonsou, T. Kudanga, Composition, thermal and rheological properties of polysaccharides from amadumbe (Colocasia esculenta) and cactus (Opuntia spp.), Carbohydrate Polymers. 195 (2018) 163–169. https://doi.org/10.1016/j.carbpol.2018.04.062.
[230] Inamuddin, S. Kanchi, One-pot biosynthesis of silver nanoparticle using Colocasia esculenta extract: Colorimetric detection of melamine in biological samples, Journal of Photochemistry and Photobiology A: Chemistry. 391 (2020) 112310. https://doi.org/10.1016/j.jphotochem.2019.112310.
[231] K A Khan, M S Alam, M A Mamun, M A Saime & M M Kamal " Studies of Electrochemistry for Pathor Kuchi Leaf Power System" Bangladesh J. Agric. and Environ. 12 (1): 37-42, June 2016.
[232] Ghaedi M, Tavallali H, Keshavarz M and Chin. Niknam. 2009. Chem J. Vol. 27: P 2066-2072
[233] Levi S Purdy W C. 1980. Clinical Biochemistry. Vol. 13(6): P 253- 258
[234] Smith A J, Burns J C and Dahn J R. 2010. J. Electrochem.Soc. Vol. 157: P 196
[235] Douglas A, Skoog F, Holler J, Stanley R. 2007. *Principles of Instrumental Analysis (6th .ed.) Section 6D-2*
[236] Teng et al., "A Review on Energy Harvesting Potential from Living Plants: Future Energy Resource" INTERNATIONAL JOURNAL of RENEWABLE ENERGY RESEARCH H.C. Vol.8, No.4, December, 2018.
[237] Volkov, A. G.; Markin, V. S. (2014). Active and Passive Electrical Signaling in Plants, Research Gate, Vol. 194, No. 4833, 1023. doi: 10.1007/978-3-319-08807-5_6

[238] M.N.F. Rab et al. “Voltage Cultivation from Fresh Leaves of Air Plant, Climbing Spinach, Mint, Spinach And Indian Pennywort for Practical Utilization” 8th international conference on computing , Communication and sensor network- CCSN 2019.
[239] Ephraim Musa Dallatu, Rufus Sha’Ato, Ishaq Shuaibu Eneji and Adams Udoji Itodo, “Design and Construction of Compact Voltaic Cell to Perform Electrochemical Analysis” 26th March 2018. doi: 10.9734/CSJI/2018/40347

Materials Chemistry and Physics 282 (2022) 125943

Contents lists available at ScienceDirect

Materials Chemistry and Physics

journal homepage: www.elsevier.com/locate/matchemphys

Green synthesis and characterization of silver nanoparticles by using *Bryophyllum pinnatum* and the evaluation of its power generation activities on bio-electrochemical cell

Md Afzol Hossain [a], Bithi Paul [b,*], K.A. Khan [c], Monika Paul [d], M.A. Mamun [e], Md Emran Quayum [a]

[a] Department of Chemistry, University of Dhaka, Dhaka, 1000, Bangladesh
[b] Department of Physics, American International University-Bangladesh, Dhaka, Bangladesh
[c] Department of Physics, Jagannath University, Dhaka, 1100, Bangladesh
[d] Department of Zoology, National University, Bangladesh
[e] Department of Chemistry, Jagannath University, Dhaka, 1100, Bangladesh

HIGHLIGHTS

- An ecofriendly, cost-effective green synthesis of silver nanoparticles (Ag NPs) is described.
- *Bryophyllum Pinnatum* leaves extract has been used as the reducing and capping agent.
- Flavonoid compounds of plant extract are the strong functional groups to the reduction of Ag^{+} to Ag^{0}.
- A wide absorption peak is found at around 465 nm and the average particle size is 35.49 nm.
- Ag NPs play a significant role to improve the power generation system of BPL bio-electrochemical cell.

GRAPHICAL ABSTRACT

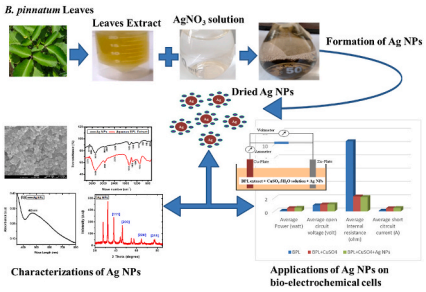

ARTICLE INFO

Keywords:
Bryophyllum pinnatum
BPL bio-Electrochemical cell
Green synthesis
Plant extract
Power generation
Silver nanoparticles

ABSTRACT

In this work, silver nanoparticles (Ag NPs) have been synthesized through an eco-friendly, cost-effective green approach by using *Bryophyllum pinnatum* leaves (BPL) extract and the power generation activity of the BPL bio-electrochemical cell has been investigated with these Ag NPs. The formation of Ag NPs was probed by X-ray diffraction (XRD), UV–visible spectroscopy, Fourier transforms infrared (FT-IR), Energy dispersion X-ray spectroscopy (EDX), and Field emission scanning electron microscopy (FESEM). The XRD studies indicated the formation of face-centered cubic (FCC) Ag NPs of an average crystallite size of about 18 nm. The FESEM images have shown spherical Ag NPs, and the average particle size was found as 35.49 nm after size distribution analysis. A significantly broad absorption peak centered at around 465 nm was revealed by the UV–visible spectra of Ag NPs, which indicated the formation of Ag^{0} from Ag^{+}. Moreover, the NPs have been applied on BPL bio-electrochemical cells to examine the power generation performance of the cell. It is observed that Ag NPs exhibited a potential role in improving open circuit voltage, short circuit current, and the power generation of BPL bio-electrochemical cells. This study demonstrates a simple, cost-effective, and eco-friendly synthesis

* Corresponding author.
E-mail address: chyabithi@gmail.com (B. Paul).

https://doi.org/10.1016/j.matchemphys.2022.125943
Received 24 April 2021; Received in revised form 10 December 2021; Accepted 27 February 2022
Available online 1 March 2022

approach of Ag NPs and the excellent performances of Ag NPs on electricity generation systems of bio-electrochemical cells. The impact of Ag NPs in the bio-electrochemical cell is a meaningful research work that may open a new platform to develop potential bio-electrochemical cells.

1. Introduction

Since the past few decades, nanomaterials have been widely investigated due to their distinguishable properties and the versatile applications in numerical fields such as electronics, optical, bioimaging, biosensor, medicines, cancer therapeutics, targeted drug delivery, agriculture, food industry, textile, renewable energy, water treatment, materials science, biotechnology [1–8]. Among all the nanomaterials, noble metal nanoparticles (eg; platinum, gold, silver) are being extensively used in interdisciplinary fields, such as physical, chemical, industrial, and biomedical applications [6,9]. Moreover, the metal nanoparticles exhibit one of the most important characteristics of surface plasmon resonance (SPR) which allows them to show unique optical properties [10]. Different shapes of nanostructures and small particle sizes with a large surface-to-volume ratio are of great interest, leading to startling differences between the chemical and physical properties of nanoparticles [11,12]. In addition, the properties of nanoparticles are switched with different synthesis approaches and depend on the size, shape, and morphology varieties of nanoparticles [5,10].

Over the few years, the promising antibacterial and anticancer activities of Ag NPs made it a potential candidate to the researchers for extensive investigations of silver nanostructures [9,13]. Along with the significant nano medicinal activities, Ag NPs have enormous applications like nonlinear optics, selective coating for solar energy absorption, intercalation materials for electrical batteries as optical receptors, catalyst in chemical reactions, antibacterial materials, and good electrical conductors [10,14,15]. Moreover, the applications of Ag NPs have been grown rapidly due to their tremendous influences on agriculture, food industries, water treatments, textile industries, targeted drug delivery [11,12].

To date, numerous chemical synthesis methods of silver nanoparticles are reported in the literature where commercially available reducing agents like sodium borohydride, ascorbic acid, trisodium citrate, and polyols have been used to reduce silver ions from the precursor solution [16]. However, most chemical and physical synthesis methods are time-consuming and expensive. They may also have harmful effects on the environment due to the toxicity of chemicals and the difficulties of removing them from NPs [12,16,17].

Nature benign, cost-effective synthesis processes of NPs are now a keen interest of the researchers. Consequently, there has been an increased emphasis on introducing the plant extract mediated synthesis (green synthesis) methods of NPs to reduce the chemical waste from the environment, which promotes non-toxic, natural, economical, and eco-friendly reducing and capping agents during the synthesis process [10]. Most of the parts of a plant such as leaves, roots, seeds, latex, bark, stem are now widely being used to synthesize the NPs, which are easily available in nature. The varieties of active functional groups of plants reduce silver ions to silver nanoparticles [18].

The use of plant and fruit extracts may be an alternative approach to eliminate the residuals toxic compounds from the synthesized NPs that can accelerate the usage of NPs in medicinal applications [12]. Plant extract contains many essential compounds (e.g., polyphenols, ascorbic acids, flavonoids, terpenoids, alkaloids, enzymes, amino acids, ascorbic acid, caffeine, linalool, and proteins), which can play a vital role in the reaction mechanism of metal ion reduction from precursor solution and NPs can be encapsulated by the bio-molecules [18,19].

For the last few years, various explorations of green synthesis of silver NPs have been reported for the promising anticancer and antibacterial activities such as Plant extracts of *Sesbania grandiflora* [20], *Rubus glaucusBenth* [21], *Alpinia calcarate* [22], *Thymbra Spicata* [23], Aloe vera leaves [16], and *Artocarpus heterophyllus* [24]. The use of *L. acapulcensis* extract is demonstrated as the suitable antimicrobial activities of Ag NPs [19], and the formation kinetics role for the shape direction of silver NPs using with Neem leaf (*Azadirachta indica*) extract has also been reported [25].

Green synthesized Ag NPs have widely been investigated for their antibacterial, anticancer activities. Nevertheless, the applications of green synthesized NPs in electricity generation still require more investigations. This study aimed to synthesize Ag NPs by using *Bryophyllum pinnatum* leaves (BPL) extract and investigate the electrical activities of Ag NPs on bio-electrochemical cells for power generation systems.

The fleshy BPL contains the herbal medicinal compound, and it is helpful as the remedy for many diseases, including hypertension, diabetes mellitus, bruises, insect bites, diarrhea, vomiting, anticancer, antitumor, antiulcer, arthritis, rheumatism, joint pains, headaches, and body pains [26–28]. The chemical constituents of *Bryophyllum. pinnatum* has been analyzed by Gas Chromatography-Mass Spectrometry (GC-MS) by many reporters [27–29]. *Bryophyllum pinnatum* contains various active bio-molecular compounds such as flavonoids, triterpenes, organic acids, alkaloids, glycosides, steroids, tannins, saponins, and minerals [27–31]. Among these, flavonoid compounds play an active role in the bio-reduction of metal ions to metal nanoparticles [10]. Several flavonoid group compounds were identified in *Bryophyllum pinnatum*, including quercetin and kaempferol, as well as a few flavone glycosides [29]. Besides the excellent medicinal activities of *Bryophyllum pinnatum*, the aqueous extract of this plant was used as a promising bio-electrolyte to generate electricity in *Bryophyllum pinnatum* leaf extract-based Zn/Cu bio-electrochemical cell [32–34].

In this study, the reduction of Ag^{+} to Ag^{0} atom was conducted by the existing functional group of BPL extract during the formation of Ag NPs, and the power development of BPL extract-based Zn/Cu electrochemical cells by using Ag NPs has been investigated for the first time. A comparative study has been performed with and without Ag NPs for a BPL bio-electrochemical cell. Different electrical parameters of the cells have been studied, and Ag NPs on the improvement of power production are examined. After implying Ag NPs on bio-electrochemical cells, the open circuit voltage and short circuit current have been increased with the duration. As a result, the power generation of the designated cells has been improved significantly. This study will enhance the use of Ag NPs in electricity generations for power development applications.

2. Materials and methods

2.1. Preparation of plant extract

20 g fresh BPL were collected from the Jagannath University Campus and washed thoroughly with tap water then with deionized (DI) water several times. Then clean leaves were crushed to make a fine paste. After that, 100 mL DI water was added to the leaves paste, and the temperature was raised at 60 °C for an hour with continuous magnetic stirring. The extract solution was cooled. After cooling, the solution was filtered twice with Whatman 41 and Whatman 42 to eliminate residual solids. Finally, the BPL extract solution was stored in the refrigerator at 4 °C for further use.

2.2. Synthesis of Ag nanoparticles

A highly pure $AgNO_3$ precursor was used in this experiment, purchased from Sigma Aldrich. 1.0 mM of 45 mL $AgNO_3$ solution was taken

onto a 100 mL conical flask, and 5 mL BPL extract was added dropwise into the above $AgNO_3$ solution. After gentle handshaking, the mixture was kept in the dark then the colorless mixture turned yellow to brown within 3 h. After a couple of days, it formed a blackish solution with some black sediments at the bottom of the flask, affirming the formation of Ag NPs. Fig. 1 shows the steps diagram of Ag NPs synthesis using BPL plant extract, and Fig. 2 represents the schematic diagram of the formation of Ag NPs.

2.3. Characterizations of biosynthesized Ag NPs

Green synthesized Ag NPs were probed by using the UV–Vis spectrometer (UV-2102, China), and the spectra of reaction solution (10 times diluted) were measured in the range of (200 nm–800 nm). The morphology of silver nanoparticles was analyzed using the field emission scanning electron microscopy (FESEM) images JSM-7610 F equipped with an energy dispersion X-ray spectroscopy (EDX) attachment at 15 KeV. Before taking the FESEM images, Ag NPs were inserted in JEC-3000FC auto fine platinum coater for 10 s. The crystalline phase of Ag NPs was investigated by the Rigaku (Ultima IV 2036E202) X-ray diffraction instrument. The CuKα radiation (λ = 1.5405 Å) source has been used for the XRD measurements in a different range of 2θ angle (20°–80°). The Fourier transforms infrared (FTIR) spectra of BPL extract and BPL extract mediated Ag NPs were recorded using the Shimadzu (IRPrestige-21) FT-IR spectrophotometer. The Gas-chromatography analysis of *Bryophyllum pinnatum* was performed GCMS QP – 2010 SE SHIMADZU, JAPAN with the helium gas carrier at 1.00 mL/min, and the injection temperature was 200 °C.

2.4. The basic principle of bio-electrochemical cell

A Zn/Cu-BPL bio-electrochemical cell was designed using Zn and Cu plates as electrodes, BPL extract as an electrolyte, and green synthesized silver nanoparticles were used as a catalyst [shown in Fig. 3]. In this cell, the zinc plate losses the electrons, the copper plate gains those electrons, and the electrons react with H^+ and Cu^{2+} ions. Eventually, ions are converted into H_2, Cu atoms respectively. Then H_2 gas is released from the cell, and copper atoms are deposited onto the Cu plate [32].

2.5. Design of bio-electrochemical cells

Three different bio-electrochemical cells were designed to investigate the influences of Ag NPs on the power generation system. For case 1, Zn and Cu plates were used as electrodes where the surface areas of both electrodes were equal. 100 mL of BPL extract and 5 mL of 0.4006 M CuSO4.5H2O solution were used as the cell's electrolyte. Then 10 mL solution of Ag NPs (1 mg) was added to the electrolyte solution of the cell. For case 2, Zn and Cu plates were used as electrodes. 100 mL of BPL extract and 5 mL of 0.4006 M CuSO4.5H2O were taken to make electrolyte for case 2. For case 3, only 100 mL of BPL extract was taken as the electrolyte. The design of three bio-electrochemical cells is shown in Fig. 3.

2.6. Power generation activities of Ag NPs

Open circuit voltage and short circuit current were monitored with the time duration for case 1, case 2, and case 3. The power of individual cells was calculated by using the formula

$$P = V_{oc} \times I_{sc}$$

And the internal resistance of the cells was also measured by the equation of

$$R_{in} = V_{oc} \div I_{sc}$$

Where P = power of the cell.

R_{in} = internal resistance of the cell
V_{oc} = open circuit voltage of the cell
I_{sc} = short circuit current of the cell

3. Result and discussions

3.1. Structural analysis of Ag NPs by XRD

The XRD measurements were carried out in the Bragg-Brentano geometry to investigate the crystal structure of as-prepared Ag NPs. Powder samples of Ag NPs were subjected to the XRD measurement, and Fig. 4a shows the XRD pattern of Ag NPs. The XRD data reveal diffraction peaks at around 38.12^0, 44.6^0, 64.56^0, and 77.36^0 that confirm the formation of face-centered cubic (FCC) silver nanoparticles which corresponds to (111), (200), (220), and (311) planes respectively (JCPDS No. 65-2871) [4,5,8,9,12,17,19,35–38].

An intense peak at 32.15 may have appeared for the cubic structure of AgK_3 [19]. The XRD pattern demonstrates naturally crystalline Ag NPs formed by the BPL extract reducing agent and capped with organic bio-molecular compounds on the surface of NPs. The average crystal size

Fig. 1. Steps diagram of green synthesis of AgNPs using *Bryophyllum pinnatum* leaves extract. (For interpretation of the references to color in this figure legend, the reader is referred to the Web version of this article.)

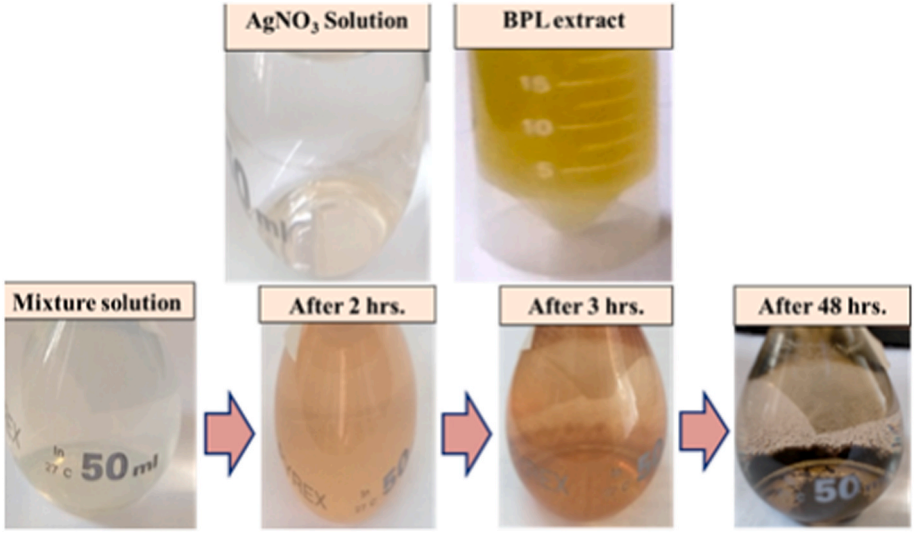

Fig. 2. Schematic diagram of color changes during the formation of Ag NPs.

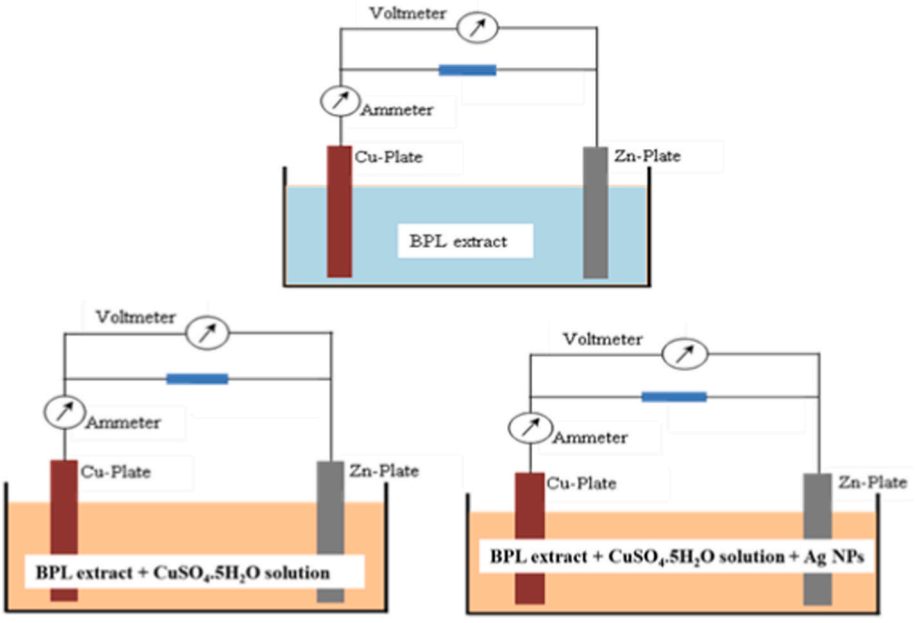

Fig. 3. Experimental set-up of the basic principle of Zn/Cu based BPL bio-electrochemical cells.

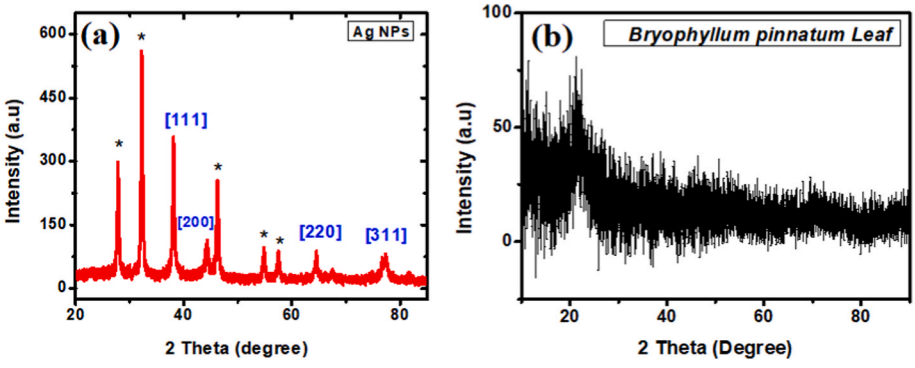

Fig. 4. XRD pattern of (a) green synthesized Ag NPs, and (b) dry *Bryophyllum pinnatum* leaf. (For interpretation of the references to color in this figure legend, the reader is referred to the Web version of this article.)

of Ag NPs is calculated from the XRD data using Debye-Scherrer formula,

$$D = 0.89\lambda/\beta\cos\theta$$

Where λ is the X-ray wavelength (λ = 1.54056 Å), θ is Bragg's diffraction angle, and β is the full width at half maximum (FWHM) [38–40]. The calculated average crystal size of the green synthesized Ag NPs is found ~18 nm. Some peaks were obvious (marked as *) in the XRD pattern, and many reports found similar results [15,41–46]. However, most of the literature reported that crystallization of various bio-compounds over the surface of green synthesized Ag NPs might be the source of these undefined peaks, but it is still controversial. In this report, XRD was carried out for dry powder of *Bryophyllum pinnatum* leaves (Fig. 4b) for the first time. Though few weak signals were found for the BPL powder, no significant peak was appeared in the dry BPL XRD pattern due to the complex bio-organic compounds. Since tap water was used several times to clean the *Bryophyllum pinnatum* leaves and leaves grinder, the Cl^- can come from these water sources. During the synthesis process of Ag NPs few Ag^+ reacted with Cl^- and AgCl crystals formed. Hence, it is concluded that these peaks appeared due to the formation of AgCl crystal structure. The peaks (*) at $2\theta = 27.5^0$, 32.1^0, 46.2^0, 54.4^0, and 57.2^0 attributed due to the corresponding planes of [111], [200], [220], [311], and [222] respectively (JCPDS No. 31-1238) for cubic structure of AgCl [47–50].

3.2. Fourier transformed infrared spectroscopy (FT-IR) analysis

Different functional groups (like flavonoids, polysaccharides, polyphenols, and triterpenoids) of biochemical compounds present in plant extract are responsible for the reduction process of metal nanoparticles from the precursor salt solution [10,51].

The reduction and capping of nanoparticles may be strongly associated with these functional groups' stretching, wagging, and bending vibrations. The FT-IR analysis investigated possible functional groups responsible for reducing, capping, and efficiently stabilizing BPL extract-mediated Ag NPs.

The FT-IR spectra revealed from the aqueous *Bryophyllum pinnatum* leaves extract and green synthesized Ag NPs are shown in Fig. 5.

In the spectrum of BPL extract, three prominent peaks appeared at the wave number values of around 3426 cm^{-1}, 1618 cm^{-1}, and 1034 cm^{-1}, corresponding to the stretching vibration bands of –OH, – C= O, and C–O–C respectively [26,52]. Some weak peaks are also found at around 3770 cm^{-1}, 2924 cm^{-1}, 2376 cm^{-1}, 1435 cm^{-1}, and 1236 cm^{-1},

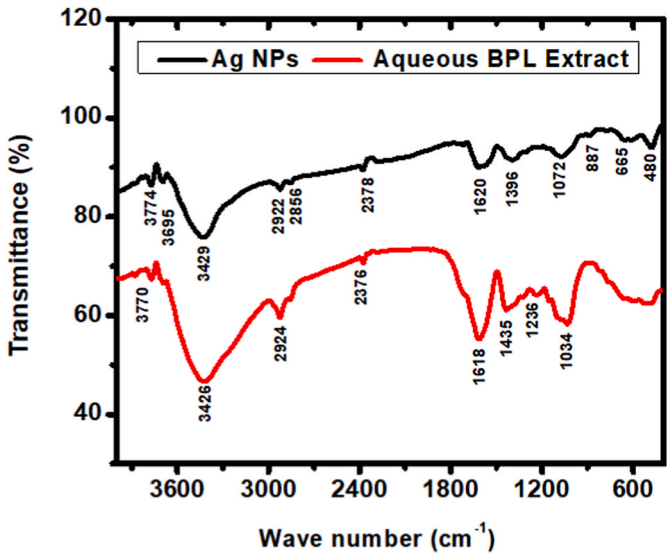

Fig. 5. FT-IR spectrum of Ag NPs and Aqueous BPL Extract.

and these peaks are obtained due to the stretching vibration bands of –OH C–H, C ≡ C, C–H of amine, C–OH respectively [26,52]. Apart from these peaks, few weak signals are found at around 3693 cm^{-1}, 2854 cm^{-1}, 887 cm^{-1}, 665 cm^{-1}. These peaks can be attributed to the stretching of –OH, alkynes, and N–H of the amide, respectively [51–53]. The functional groups may evolve due to many bio-molecules such as flavones, alkaloids, etc. presented in the aqueous leaves extract, which can be acted as the reducing and capping agents [26]. The FT-IR spectra of Ag NPs showed almost similar functional groups with some shifting wave numbers due to stretching and bending vibrations of molecular bonds in the plant extract. The similar functional groups presented in the green synthesized Ag NPs signify the encapsulation of Ag NPs with bio-molecules of BPL extract.

In FT-IR spectra of Ag NPs, all peaks of corresponding functional groups of extract were found with the shifting wavenumbers due to the interaction between plant extract and Ag NPs. The FT-IR spectra of Ag NPs revealed several peaks at around 3774 cm^{-1}, 3695.61 cm^{-1}, 3429.43 cm^{-1}, 2922 cm^{-1}, 2856 cm^{-1}, 2378 cm^{-1}, 1620 cm^{-1}, 1396 cm^{-1}, 1072 cm^{-1}, 887 cm^{-1}, 665 cm^{-1}, and 480 cm^{-1}. These shifts indicated the interaction of Ag NPs with the biomolecules such as flavonoids, alcohols, phenols, alkaloids, tannins, terpenes, and terpenoids during the reduction, capping, and stabilizing processes [35]. The bio-molecules can be attached with Ag NPs during the reduction process of Ag^+, capping, and stabilization of the Ag NPs.

The peak at around 3774 cm^{-1} may be associated with the stretching vibration of both amide and –OH bond [26,52]. The peak at around 3695 cm^{-1} is appeared due to the stretching of –OH [52]. A significant peak at 3429 cm^{-1} is commonly attributed to –OH stretching of water, H-bonded, alcohol, and phenol as a functional group [26,35,42,51–55]. Another two peaks at around 2922 cm^{-1} and 2856 $cm^{-1}$are associated due to the stretching vibration of C–H and alkynes (flavonoids). Most importantly, those strong functional groups were referred to as reducing and capping agents during the synthesis of metal nanoparticles [26,37,52,53,56,57].

Moreover, the active band of bio-molecular functional groups indicates that the surface of Ag NPs may be coated with the protein layer [37]. The peak at around 2378 cm^{-1} appeared due to C ≡ C stretching vibration, and a sharp peak at 1620 cm-1 may be associated with the stretching vibration of – C= O and C–H bands [26,58]. The bending vibration of O–H and CH_3 may be responsible for the peak at around 1396 cm^{-1} [35,51]· Another sharp peak at around 1072 cm^{-1} is originated due to the stretching vibrations of the O–C and C–N bond of aliphatic amines [26,51,53]. This sharp band indicated the presence of flavanones which are generally absorbed by the surface of metal nanoparticles [15]. The peaks at around 665 $cm^{-1}$and 887 cm^{-1} appear due to the amide group's N–H stretching [51], the wagging of N–H primary and secondary amines [53]. Moreover, the peak at around 480 cm^{-1} is found for the spectrum of Ag NPs. This peak may be appeared due to the O–Si–O stretching, the ring-opening vibration, and deforming oscillations of silica [15,54].

Eventually, it can be ascertained that the reduction of Ag^+ to Ag^0 from the $AgNO_3$ solution can be attributed due to the presence of flavonoids in the plant extract. The flavonoids compounds play an important role as the reducing agent to forming metal nanoparticles from metal ions [10,15]. The details of functional groups acting as the reducing, capping, and stabilizing agents to forming the Ag NPs are summarized in Table 1.

3.3. UV-VIS analysis of biosynthesized Ag NPs

The reduction of $AgNO_3$ solution to Ag nanoparticles was also confirmed by UV–vis spectroscopy [UV-2102, China]. Generally, Ag NPs reveal the maximum UV–visible absorption in the range of (400 nm–500 nm) due to the surface Plasmon resonance, which depends on the size of the Ag NPs [59]. Absorption at the lower band indicates a smaller particle size, whereas the higher absorption band affirms the larger

Table 1
Summary of FTIR interpretation of BPL extract mediated Ag NPs.

Peak position of Ag NPs (cm^{-1})	Active functional groups	References
3774	stretching vibration of amide and –OH bond	[26,52]
3695	stretching of –OH	[52]
3429	-OH stretching of water, H-bonded, alcohol and phenol as functional group	[26,42, 51–55]
2922	stretching vibration of C–H and alkynes (flavonoids)	[26,37,52,53, 56]
2856	stretching vibration of C–H and alkynes (flavonoids)	[26,52,53, 56]
2378	stretching vibration of C ≡ C and − C= O bonds respectively	[26]
1620	stretching vibration − C= O and C–H bands	[26,58]
1396	bending of O–H	[51]
1072	stretching vibrations of O–C and C–N bond of aliphatic amines	[26,51,53]
887	N–H stretching of amide group	[51]
665	wagging of N–H primary and secondary amines	[53]
480	O–Si–O stretching, the ring-opening, and deforming oscillations of silica	[15,54]

nanoparticles [2]. The *d*-band electrons of Ag NPs are uplifted by absorbing the incident radiation to higher electronic states in the *sp*-band, which is the main reason for fluorescence [9]. A surface Plasmon resonance absorption band is appeared due to the combined vibration of free electrons of metal nanoparticles in resonance with exposed light [1]. Ag NPs emit light between (400-700) nm, and the range varies with particle size, shape, morphology, and solvents [4,10].

Fig. 6a shows the UV–visible spectra of $AgNO_3$ solution, BPL extract, and synthesized Ag NPs. The maximum absorption is observed with a broad peak at around 465 nm [Fig. 6b] due to the transformation of Ag^0 from Ag^+, which corresponds to the surface plasmon absorption of silver nanoparticles [2]. The absorption peak at the higher wavelength (above 400 nm) is originated due to the large particle size (around 40 nm) [60,61]. The color change of the solution indicates the radiation absorption in the visible region of the electromagnetic spectrum due to the localized surface plasmon of silver nanoparticles [7,62]. During the synthesis process, adding BPL extract to $AgNO_3$ solution led to changes in the color of the solution to dark-brown, which indicates the formation of Ag^0 from the $AgNO_3$ solution.

The free electrons of Ag NPs yield a surface resonance absorption band due to the mutual vibration of electrons in resonance with light waves [15]. Hence, it is evident that the reducing agent of BPL extract played a vital role in the color change of mixture solution, which indicated the formation of Ag NPs.

3.4. Field emission scanning electron microscopy (FESEM) and EDX analysis

The particle size and the morphology of metallic nanoparticles depend on the concentration rate of the reducing, capping, and stabilizing agents present in the plant extract [63]. Fig. 7 (a,b) represent a high-resolution FESEM image of Ag NPs with different scale, and particles are found spherical. The size distribution of green synthesized Ag NPs is shown in Fig. 7d, where the particle size is in the range of 20 nm–55 nm (calculated using ImageJ software). The average particle size is to be calculated at 35.49 nm. Fig. 7c shows the concentration of green synthesized Ag NPs with other residuals elements that may appear from the environment and capping agents present in the extract.

3.5. Gas chromatography/mass spectrometry analysis

The constituents of the Bryophyllum pinnatum leaf were analyzed by the GC/MS analysis. The Acetone extract of the leaves of *Bryophyllum pinnatum* on GC/MS analysis revealed eight peaks indicating the presence of eight compounds in the plant leaves as shown in Fig. 8. The retention time, molecular weight, and percentage constituents of the compounds are shown in Table 2. The compounds of the essential oil were Acetate <butyl-> (20.722%), 3-Hexamine (28.088%),2-Propanone, 1-cyclopentyl- (12.398%),Pent-3-yne<1-hydroxy-> (7.742%), 2,5-Furandion, dihydro-3-methylene- (25.843%), 5-Decen-1-ol, acetate, (E)- (1.536%), Benzo furan, 2,3-dihydro- (2.025%), and 2-Furanone, 3,4-dihydroxxytetrahydro (1.646%).

3.6. Power generation activities of bio-electrochemical cells

The green synthesized Ag NPs have been applied in the bio-electrochemical cell to understand the role of NPs in the power development system. Three types of bio-electrochemical cells were designated to perform the electrical analysis of Ag NPs. Fig. 9 represents the impact of Ag NPs on three bio-electrochemical cells. Fig. 9a shows the open circuit voltage with the variation of time duration for different cases. It is shown that the open circuit voltages for case 1 are higher than the other two cases of case 2 and case 3. It is very interesting to say that the voltage for case 1 was almost steady up to 50hrs, whereas the open circuit voltage for case 2 was less than case 3. It is clearly shown that the open circuit voltage for case 3 is less than the other two cases but the change of voltage was almost constant up to 50 h for all the cases. The maximum voltage for the first case is 1.07 V, and the minimum is1.03 V.

For case 2, the maximum open circuit voltage is 1.046, the minimum is 0.96 V; for only BPL extract [case 1], the maximum voltage is 0.921 V, and the minimum voltage is 0.75 V. The maximum open circuit voltage difference between the first and second cases is 0.024 V. The difference of open circuit voltage between the first and third cases is 0.149 V and the difference of open circuit voltage between second and third cases is

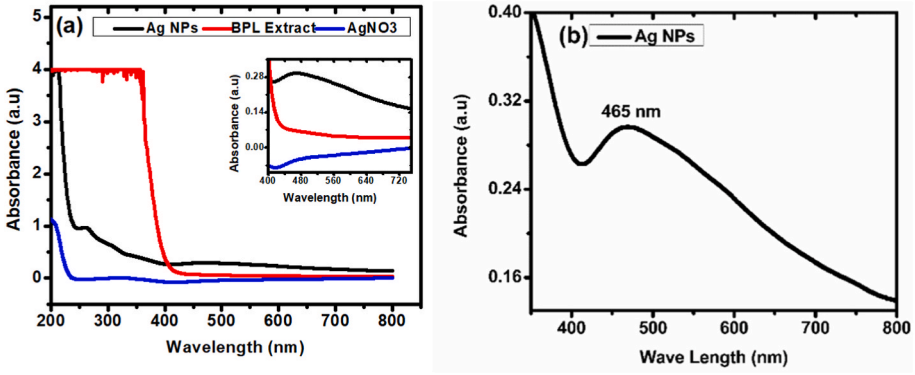

Fig. 6. UV–vis spectra of (a) Ag NPs, BPL Extract, and $AgNO_3$ (b) Ag NPs.

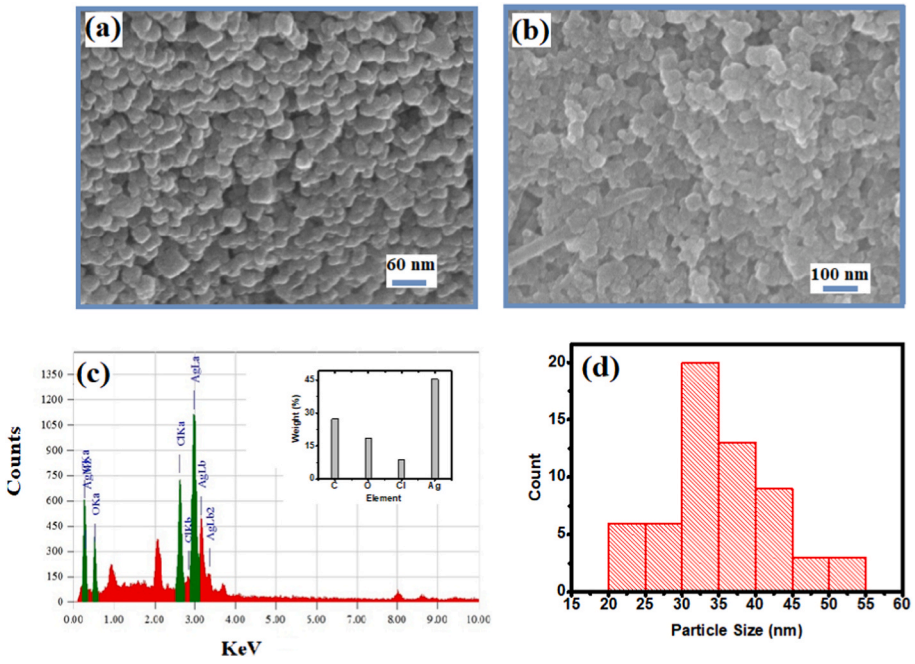

Fig. 7. (a,b) FESEM images of Ag NPs in different scales, (c) EDX data of Ag NPs, and (d) average particle size histogram of Ag NPs.

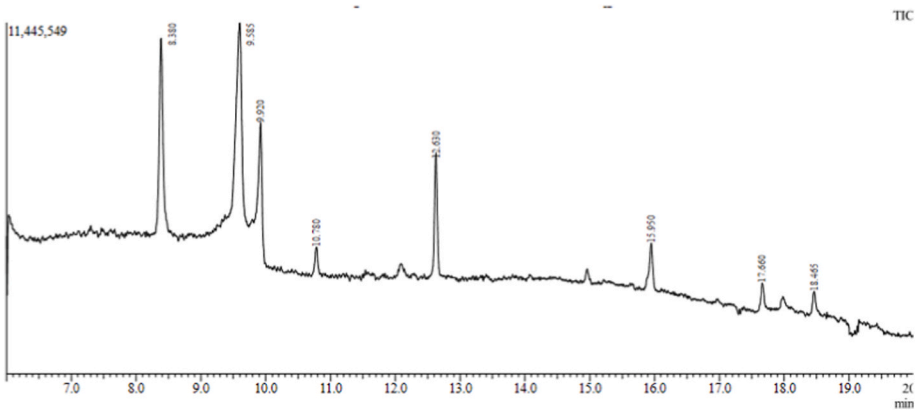

Fig. 8. Gas Chromatogram of the leaf essential oil of *Bryophyllum pinnatum*.

Table 2
Chemical compositions of Leaf of *Bryophyllum pinnatum*.

SL. No	Compounds	Retention Time (Min)	Molecular weight	Conc. (%)
1	Acetate <butyl->	8.383	56	20.722
2	3-Hexamine	9.596	72	28.088
3	2-Propanone, 1-cyclopentyl-	9.920	59	12.398
4	Pent-3-yne<1-hydroxy->	10.772	54	7.742
5	2,5-Furandion, dihydro-3-methylene-	12.625	68	25.843
6	5-Decen-1-ol, acetate, (E)-	15.950	81	1.536
7	Benzo furan, 2,3-dihydro-	17.661	120	2.025
8	2-Furanone, 3,4-dihydroxxytetrahydro	18.460	55	1.646

0.125 V. The results showed that the largest difference of open circuit voltage is found between case 1 and case 3 is 0.149 V, which indicates that the nanoparticles play a potential role in the increasing open circuit voltage of a bio-electrochemical cell.

Fig. 9b shows the short circuit current with the variation of time duration for different cases. It is clearly demonstrated that the short circuit current of case 1 is higher than those of case 2 and case 3. It can be interpreted that case 1 gives the maximum short circuit current (600 mA) compared with the other two cases, and it remained constant for 50 h. The minimum short circuit current value for case 1 is 445 mA, which is also greater than case 2 (430 mA) and case 3 (50 mA). Hence, it is evident that Ag NPs can play a significant role in increasing the short circuit current of the BPL bio-electrochemical cell with the time duration.

Fig. 9c shows the calculated power of the cells with the time duration. For case 1, the maximum power is estimated at 0.642 W, and the minimum power value is 0.457 W. For case 2 and case 3, the highest power is found at 0.575 W and 0.087 W respectively, and the lowest power for both cases is at 0.412 W, 0.035 W respectively. It is noticeable that after applying the Ag NPs on BPL bio-electrochemical cell, the maximum power is found, which is also stable for the next 50 h. Finally, the power for case 1 started to decrease after 50 h, but the minimum value is found at 0.458 W, which is even greater than the lowest values of the other two cases.

Fig. 9d represents the internal resistance for all three cases. The internal resistance for only BPL extract bio-electrochemical cells is higher than in the two other cases. The internal resistance rapidly decreased

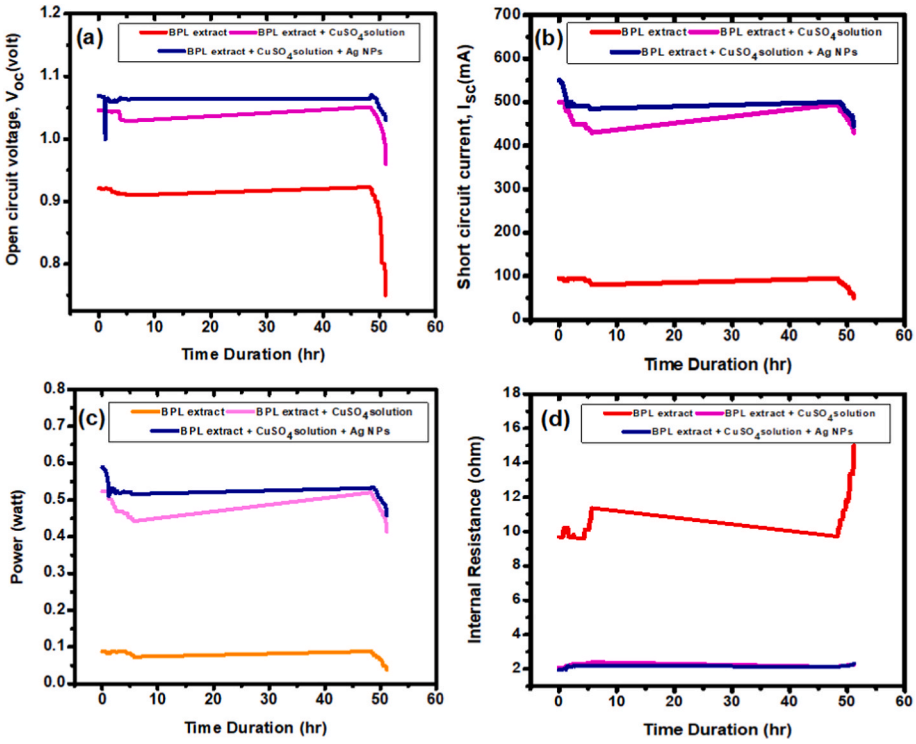

Fig. 9. Electrical activities of BPL bio-electrochemical cells (a) open circuit voltage (b) short circuit current (c) power, and (d) Internal resistance.

after using the secondary salt (CuSO4.5H2O) solution for case 2 and Ag NPs on case 1. The lowest internal resistance is found for case 1, allowing more current to flow through the bio-electrochemical cell.

Table 3 represents the values of average open circuit voltage, short circuit current, power, and internal resistance for all three bio-electrochemical cells. Fig. 10 also represents the summary of average open circuit voltage, short circuit current, power, and internal resistance of the bio-electrochemical cell.

After applying the Ag NPs on the cell, the open circuit voltage and short circuit current are rapidly increased. As a result, the power of the BPL bio-electrochemical cell is significantly increased. On the other hand, the internal resistance was found around 10.5Ω for only BPL extract, and it is surprisingly dropped at around 2.2Ω for (BPL + $CuSO_4$ solution) bio-electrochemical cell. The resistance decreased at 2.1Ω after adding NPs in the cell. It can be predicted that the influences of Ag NPs in the bio-electrochemical cell are remarkable for future power development applications.

4. Conclusion

Ag NPs were successfully synthesized using the BPL extract for the first time in this study through an eco-friendly, cost-effective, and rapid green synthesis approach. The bio reduction of Ag ions to Ag NPs was demonstrated by maximum absorption at 465 nm in the UV–vis spectra of Ag NPs, and dispersed spherical Ag NPs were found in the morphological characterization where the average particles size was found 35.49 nm. The FT-IR spectra of Ag NPs also exhibited the active functional groups responsible for the reduction process of silver nanoparticles. Though several studies were reported for the green synthesis of silver nanoparticles with different plant extracts and their antibacterial activities were investigated, Ag NPs in the development and longevity of power production of the bio-electrochemical cell is reported for the first time in this study. In a nutshell, green synthesized Ag NPs played a potential role in improving the power production of BPL bio-electrochemical cells. This study will open a new avenue for the power generation of bio-electrochemical cells.

Table 3
Average electrical performances of BPL bio-electrochemical cells.

Name of the case	Average open circuit voltage (volt)	Average short circuit current (A)	Average power (watt)	Average internal resistance (ohm)
Case 1	1.059	0.494	0.524	2.144
Case 2	1.035	0.463	0.480	2.234
Case 3	0.899	0.086	0.078	10.537

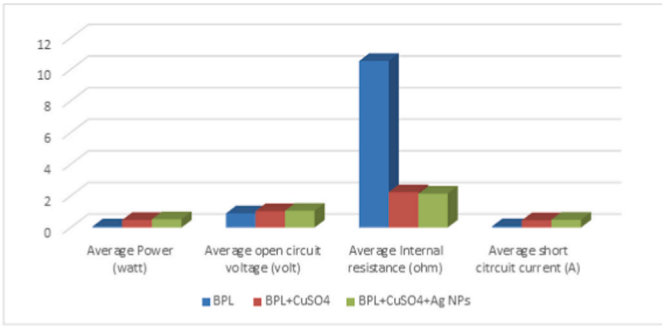

Fig. 10. Average electrical performances of BPL bio-electrochemical cells.

CRediT authorship contribution statement

Md Afzol Hossain: Conceptualization, Methodology, Validation, Investigation, Writing – review & editing. **Bithi Paul:** Conceptualization, Methodology, Validation, Investigation, Formal analysis, Data curation, Visualization, Writing – original draft. **K.A. Khan:** Conceptualization, Methodology, Supervision, Validation, Resources, Project administration, Funding acquisition, Writing – review & editing. **Monika Paul:** Investigation, Validation. **M.A. Mamun:** Writing – review & editing. **Md Emran Quayum:** Writing – review & editing.

Declaration of competing interest

The authors declare that they have no known competing financial interests or personal relationships that could have appeared to influence the work reported in this paper.

Acknowledgments

This work is supported by the GARE (Grant of Advanced Research in Education) project, Ministry of Education, Government of Bangladesh (GoB) for providing financial support during the research work (Project/User ID: PS2019949). Afzol Hossain, Bithi Paul, and Dr. Md. Kamrul Alam Khan contributed equally to this work. The authors are grateful to Professor Dr. Md. Kamrul Alam Khan, Department of Physics, Jagannath University, Dhaka, Bangladesh to his generous support during this research work.

References

[1] S. Raj, S. Chand Mali, R. Trivedi, Green synthesis and characterization of silver nanoparticles using Enicostemma axillare (Lam.) leaf extract, Biochem. Biophys. Res. Commun. 503 (2018) 2814–2819, https://doi.org/10.1016/j.bbrc.2018.08.045.

[2] B. Khodadadi, M. Bordbar, A. Yeganeh-Faal, M. Nasrollahzadeh, Green synthesis of Ag nanoparticles/clinoptilolite using Vaccinium macrocarpon fruit extract and its excellent catalytic activity for reduction of organic dyes, J. Alloys Compd. 719 (2017) 82–88, https://doi.org/10.1016/j.jallcom.2017.05.135.

[3] N. Roy, A. Gaur, A. Jain, S. Bhattacharya, V. Rani, Green synthesis of silver nanoparticles: an approach to overcome toxicity, Environ. Toxicol. Pharmacol. 36 (2013) 807–812, https://doi.org/10.1016/j.etap.2013.07.005.

[4] M. Darroudi, M. Mansor Bin Ahmad, A.H. Abdullah, N.A. Ibrahim, K. Shameli, Green synthesis and characterization of gelatin-based and sugar-reduced silver nanoparticles, IJN (2011) 569, https://doi.org/10.2147/IJN.S16867.

[5] M. Ahamed, M.A. Majeed Khan, M.K.J. Siddiqui, M.S. AlSalhi, S.A. Alrokayan, Green synthesis, characterization and evaluation of biocompatibility of silver nanoparticles, Phys. E Low-dimens. Syst. Nanostruct. 43 (2011) 1266–1271, https://doi.org/10.1016/j.physe.2011.02.014.

[6] Y. He, F. Wei, Z. Ma, H. Zhang, Q. Yang, B. Yao, Z. Huang, J. Li, C. Zeng, Q. Zhang, Green synthesis of silver nanoparticles using seed extract of Alpinia katsumadai, and their antioxidant, cytotoxicity, and antibacterial activities, RSC Adv. 7 (2017) 39842–39851, https://doi.org/10.1039/C7RA05286C.

[7] A. Danagoudar, G.K. Pratap, M. Shantaram, B. Chatterjee, K. Ghosh, S.R. Kanade, C.G. Joshi, Cancer cell specific cytotoxic potential of the silver nanoparticles synthesized using the endophytic fungus, Penicillium citrinum CGJ-C2, Mater. Today Commun. 25 (2020) 101442, https://doi.org/10.1016/j.mtcomm.2020.101442.

[8] F. Göl, A. Aygün, A. Seyrankaya, T. Gür, C. Yenikaya, F. Şen, Green synthesis and characterization of Camellia sinensis mediated silver nanoparticles for antibacterial ceramic applications, Mater. Chem. Phys. 250 (2020) 123037, https://doi.org/10.1016/j.matchemphys.2020.123037.

[9] N. Jayaprakash, J.J. Vijaya, K. Kaviyarasu, K. Kombaiah, L.J. Kennedy, R. J. Ramalingam, M.A. Munusamy, H.A. Al-Lohedan, Green synthesis of Ag nanoparticles using Tamarind fruit extract for the antibacterial studies, J. Photochem. Photobiol. B Biol. 169 (2017) 178–185, https://doi.org/10.1016/j.jphotobiol.2017.03.013.

[10] S. Jain, M.S. Mehata, Medicinal plant leaf extract and pure flavonoid mediated green synthesis of silver nanoparticles and their enhanced antibacterial property, Sci. Rep. 7 (2017) 15867, https://doi.org/10.1038/s41598-017-15724-8.

[11] S. Iravani, Green synthesis of metal nanoparticles using plants, Green Chem. 13 (2011) 2638, https://doi.org/10.1039/c1gc15386b.

[12] M. Shahriary, H. Veisi, M. Hekmati, S. Hemmati, In situ green synthesis of Ag nanoparticles on herbal tea extract (Stachys lavandulifolia)-modified magnetic iron oxide nanoparticles as antibacterial agent and their 4-nitrophenol catalytic reduction activity, Mater. Sci. Eng. C 90 (2018) 57–66, https://doi.org/10.1016/j.msec.2018.04.044.

[13] R.R. Chavan, S.D. Bhinge, M.A. Bhutkar, D.S. Randive, G.H. Wadkar, S.S. Todkar, M.N. Urade, Characterization, antioxidant, antimicrobial and cytotoxic activities of green synthesized silver and iron nanoparticles using alcoholic Blumea eriantha DC plant extract, Mater. Today Commun. 24 (2020) 101320, https://doi.org/10.1016/j.mtcomm.2020.101320.

[14] P.V. AshaRani, G. Low Kah Mun, M.P. Hande, S. Valiyaveettil, Cytotoxicity and genotoxicity of silver nanoparticles in human cells, ACS Nano 3 (2009) 279–290, https://doi.org/10.1021/nn800596w.

[15] K. Anandalakshmi, J. Venugobal, V. Ramasamy, Characterization of silver nanoparticles by green synthesis method using Pedalium murex leaf extract and their antibacterial activity, Appl. Nanosci. 6 (2016) 399–408, https://doi.org/10.1007/s13204-015-0449-z.

[16] P. Tippayawat, N. Phromviyo, P. Boueroy, A. Chompoosor, Green synthesis of silver nanoparticles in aloe vera plant extract prepared by a hydrothermal method and their synergistic antibacterial activity, PeerJ 4 (2016) e2589, https://doi.org/10.7717/peerj.2589.

[17] S. Jebril, R. Khanfir Ben Jenana, C. Dridi, Green synthesis of silver nanoparticles using Melia azedarach leaf extract and their antifungal activities: in vitro and in vivo, Mater. Chem. Phys. 248 (2020) 122898, https://doi.org/10.1016/j.matchemphys.2020.122898.

[18] P. Rauwel, S. Küünal, S. Ferdov, E. Rauwel, A review on the green synthesis of silver nanoparticles and their morphologies studied via TEM, Advances in Materials Science and Engineering. 2015 (2015) 1–9, https://doi.org/10.1155/2015/682749.

[19] D. Garibo, H.A. Borbón-Nuñez, J.N.D. de León, E. García Mendoza, I. Estrada, Y. Toledano-Magaña, H. Tiznado, M. Ovalle-Marroquin, A.G. Soto-Ramos, A. Blanco, J.A. Rodríguez, O.A. Romo, L.A. Chávez-Almazán, A. Susarrey-Arce, Green synthesis of silver nanoparticles using Lysiloma acapulcensis exhibit high-antimicrobial activity, Sci. Rep. 10 (2020) 12805, https://doi.org/10.1038/s41598-020-69606-7.

[20] M. Jeyaraj, G. Sathishkumar, G. Sivanandhan, D. MubarakAli, M. Rajesh, R. Arun, G. Kapildev, M. Manickavasagam, N. Thajuddin, K. Premkumar, A. Ganapathi, Biogenic silver nanoparticles for cancer treatment: an experimental report, Colloids Surf. B Biointerfaces 106 (2013) 86–92, https://doi.org/10.1016/j.colsurfb.2013.01.027.

[21] B. Kumar, K. Smita, R. Seqqat, K. Benalcazar, M. Grijalva, L. Cumbal, In vitro evaluation of silver nanoparticles cytotoxicity on Hepatic cancer (Hep-G2) cell line and their antioxidant activity: green approach for fabrication and application, J. Photochem. Photobiol. B Biol. 159 (2016) 8–13, https://doi.org/10.1016/j.jphotobiol.2016.03.011.

[22] S. Pugazhendhi, E. Kirubha, P.K. Palanisamy, R. Gopalakrishnan, Synthesis and characterization of silver nanoparticles from Alpinia calcarata by Green approach and its applications in bactericidal and nonlinear optics, Appl. Surf. Sci. 357 (2015) 1801–1808, https://doi.org/10.1016/j.apsusc.2015.09.237.

[23] H. Veisi, S. Azizi, P. Mohammadi, Green synthesis of the silver nanoparticles mediated by Thymbra spicata extract and its application as a heterogeneous and recyclable nanocatalyst for catalytic reduction of a variety of dyes in water, J. Clean. Prod. 170 (2018) 1536–1543, https://doi.org/10.1016/j.jclepro.2017.09.265.

[24] U.B. Jagtap, V.A. Bapat, Green synthesis of silver nanoparticles using Artocarpus heterophyllus Lam. seed extract and its antibacterial activity, Ind. Crop. Prod. 46 (2013) 132–137, https://doi.org/10.1016/j.indcrop.2013.01.019.

[25] Z. Khan, J.I. Hussain, A.A. Hashmi, Shape-directing role of cetyltrimethylammonium bromide in the green synthesis of Ag-nanoparticles using Neem (Azadirachta indica) leaf extract, Colloids Surf. B Biointerfaces 95 (2012) 229–234, https://doi.org/10.1016/j.colsurfb.2012.03.002.

[26] A.K.M.A. Ullah, M.M. Haque, M. Akter, A. Hossain, A.N. Tamanna, M.M. Hosen, A. K.M.F. Kibria, M.N.I. Khan, M.K.A. Khan, Green synthesis of *Bryophyllum pinnatum* aqueous leaf extract mediated bio-molecule capped dilute ferromagnetic α -MnO_2 nanoparticles, Mater. Res. Express 7 (2020), 015088, https://doi.org/10.1088/2053-1591/ab6c20.

[27] S. Adeyinka Aboaba, H. Igumoye, G. Flamini, Chemical composition of the leaves and stem bark of *Sterculia tragacantha* , *Anthocleista vogelii* and leaves of *Bryophyllum pinnatum*, J. Essent. Oil Res. 29 (2017) 85–92, https://doi.org/10.1080/10412905.2016.1178182.

[28] K. Fürer, M. Raith, R. Brenneisen, M. Mennet, A. Simões-Wüst, U. von Mandach, M. Hamburger, O. Potterat, Two new flavonol glycosides and a metabolite profile of Bryophyllum pinnatum, a phytotherapeutic used in obstetrics and gynaecology, Planta Med. 79 (2013) 1565–1571, https://doi.org/10.1055/s-0033-1350808.

[29] K. Fürer, A. Simões-Wüst, U. von Mandach, M. Hamburger, O. Potterat, Bryophyllum pinnatum and related species used in anthroposophic medicine: constituents, pharmacological activities, and clinical efficacy, Planta Med. 82 (2016) 930–941, https://doi.org/10.1055/s-0042-106727.

[30] K.A. Mbachu, M.G. Ibok, M.A. Adeniyi-Akee, O.E. Ajala, Chemical compositions and antioxidant activity of leaf and stem essential oils of Bryophyllum pinnatum (lam.), Kurz, GSC Biol. and Pharm. Sci. 9 (2019) 57–64, https://doi.org/10.30574/gscbps.2019.9.2.0184.

[31] Y. Obregón-Díaz, A. Pérez-Colmenares, K. Obregón-Alarcón, R. Aparicio-Zambrano, L. Rojas-Fermín, A. Usubillaga, J. Carmona, Volatile constituents of the leaves of kalanchoe pinnata from the Venezuelan andes, Natural Product Communications 14 (2019), https://doi.org/10.1177/1934578X19842703, 1934578X1984270.

[32] K.A. Khan, M.H. Ali, M.A. Mamun, M.M. Haque, A.K.M.A. Ullah, M.N.I. Khan, L. Hassan, A.K.M. Obaydullah, M.A. Wadud, Bioelectrical characterization and production of nanoparticles (NPs) using PKL extract for electricity generation, Microsyst. Technol. (2020), https://doi.org/10.1007/s00542-020-04774-0.

[33] K.A. Khan, M.A. Mamun, M. Ibrahim, M. Hasan, M. Ohiduzzaman, A.K. M. Obaydullah, M.A. Wadud, M. Shajahan, PKL electrochemical cell: physics and chemistry, SN Appl. Sci. 1 (2019) 1335, https://doi.org/10.1007/s42452-019-1363-x.

[34] K.A. Khan, L. Hassan, A.K.M. Obaydullah, S.M. Azharul Islam, M.A. Mamun, T. Akter, M. Hasan, MdS. Alam, M. Ibrahim, M.M. Rahman, M. Shahjahan, Bioelectricity: a new approach to provide the electrical power from vegetative and fruits at off-grid region, Microsyst. Technol. 26 (2020) 3161–3172, https://doi.org/10.1007/s00542-018-3808-3.

[35] S. Aslany, F. Tafvizi, V. Naseh, Characterization and evaluation of cytotoxic and apoptotic effects of green synthesis of silver nanoparticles using Artemisia Ciniformis on human gastric adenocarcinoma, Mater. Today Commun. 24 (2020) 101011, https://doi.org/10.1016/j.mtcomm.2020.101011.

[36] E. Turunc, R. Binzet, I. Gumus, G. Binzet, H. Arslan, Green synthesis of silver and palladium nanoparticles using Lithodora hispidula (Sm.) Griseb. (Boraginaceae) and application to the electrocatalytic reduction of hydrogen peroxide, Mater. Chem. Phys. 202 (2017) 310–319, https://doi.org/10.1016/j.matchemphys.2017.09.032.
[37] M. Mosaviniya, T. Kikhavani, M. Tanzifi, M. Tavakkoli Yaraki, P. Tajbakhsh, A. Lajevardi, Facile green synthesis of silver nanoparticles using Crocus Haussknechtii Bois bulb extract: catalytic activity and antibacterial properties, Colloid and Interface Science Communications 33 (2019) 100211, https://doi.org/10.1016/j.colcom.2019.100211.
[38] S.O. Aisida, K. Ugwu, P.A. Akpa, A.C. Nwanya, U. Nwankwo, S.S. Botha, P. M. Ejikeme, I. Ahmad, M. Maaza, F.I. Ezema, Biosynthesis of silver nanoparticles using bitter leave (Veronica amygdalina) for antibacterial activities, Surface. Interfac. 17 (2019) 100359, https://doi.org/10.1016/j.surfin.2019.100359.
[39] B. Paul, M.A.-A. Mamun, A. Haque, M. Paul, K. Ghosh, Significant reduction of defect states and surface tailoring in ZnO nanoparticles via nano-bio interaction with glucose for bio-applications, IEEE Trans.on Nanobioscience. 18 (2019) 490–497, https://doi.org/10.1109/TNB.2019.2919231.
[40] M.A. Siddiquee, M. ud din Parray, S.H. Mehdi, K.A. Alzahrani, A.A. Alshehri, M. A. Malik, R. Patel, Green synthesis of silver nanoparticles from Delonix regia leaf extracts: in-vitro cytotoxicity and interaction studies with bovine serum albumin, Mater. Chem. Phys. 242 (2020) 122493, https://doi.org/10.1016/j.matchemphys.2019.122493.
[41] P. Das, K. Ghosal, N.K. Jana, A. Mukherjee, P. Basak, Green synthesis and characterization of silver nanoparticles using belladonna mother tincture and its efficacy as a potential antibacterial and anti-inflammatory agent, Mater. Chem. Phys. 228 (2019) 310–317, https://doi.org/10.1016/j.matchemphys.2019.02.064.
[42] R. Parameshwaran, S. Kalaiselvam, R. Jayavel, Green synthesis of silver nanoparticles using Beta vulgaris: role of process conditions on size distribution and surface structure, Mater. Chem. Phys. 140 (2013) 135–147, https://doi.org/10.1016/j.matchemphys.2013.03.012.
[43] D. Kalpana, Y.S. Lee, Synthesis and characterization of bactericidal silver nanoparticles using cultural filtrate of simulated microgravity grown Klebsiella pneumoniae, Enzym. Microb. Technol. 52 (2013) 151–156, https://doi.org/10.1016/j.enzmictec.2012.12.006.
[44] N. Aziz, M. Faraz, R. Pandey, M. Shakir, T. Fatma, A. Varma, I. Barman, R. Prasad, Facile algae-derived route to biogenic silver nanoparticles: synthesis, antibacterial, and photocatalytic properties, Langmuir 31 (2015) 11605–11612, https://doi.org/10.1021/acs.langmuir.5b03081.
[45] V.S. Suvith, D. Philip, Catalytic degradation of methylene blue using biosynthesized gold and silver nanoparticles, Spectrochim. Acta Mol. Biomol. Spectrosc. 118 (2014) 526–532, https://doi.org/10.1016/j.saa.2013.09.016.
[46] S. Hamedi, S.A. Shojaosadati, A. Mohammadi, Evaluation of the catalytic, antibacterial and anti-biofilm activities of the Convolvulus arvensis extract functionalized silver nanoparticles, J. Photochem. Photobiol. B Biol. 167 (2017) 36–44, https://doi.org/10.1016/j.jphotobiol.2016.12.025.
[47] X. Zhao, J. Zhang, B. Wang, A. Zada, M. Humayun, Biochemical synthesis of Ag/AgCl nanoparticles for visible-light-driven photocatalytic removal of colored dyes, Materials 8 (2015) 2043–2053, https://doi.org/10.3390/ma8052043.
[48] W. Liu, S. Hu, Y. Wang, B. Zhang, R. Jin, L. Hu, Anchoring plasmonic Ag@AgCl nanocrystals onto ZnCo2O4 microspheres with enhanced visible photocatalytic activity, Nanoscale Res. Lett. 14 (2019) 108, https://doi.org/10.1186/s11671-019-2922-1.
[49] Y.-Y. Dong, Y.-H. Zhu, M.-G. Ma, Q. Liu, W.-Q. He, Synthesis and characterization of Ag@AgCl-reinforced cellulose composites with enhanced antibacterial and photocatalytic degradation properties, Sci. Rep. 11 (2021) 3366, https://doi.org/10.1038/s41598-021-82447-2.
[50] K. Okaiyeto, M.O. Ojemaye, H. Hoppe, L.V. Mabinya, A.I. Okoh, Phytofabrication of silver/silver chloride nanoparticles using aqueous leaf extract of oedera genistifolia: characterization and antibacterial potential, Molecules 24 (2019) 4382, https://doi.org/10.3390/molecules24234382.
[51] S.K. Chandraker, M. Lal, P. Dhruve, R.P. Singh, R. Shukla, Cytotoxic, antimitotic, DNA binding, photocatalytic, H2O2 sensing, and antioxidant properties of biofabricated silver nanoparticles using leaf extract of Bryophyllum pinnatum (lam.) oken, Front. Mol. Biosci. 7 (2021) 593040, https://doi.org/10.3389/fmolb.2020.593040.
[52] A.K.M. Atique Ullah, A.N. Tamanna, A. Hossain, M. Akter, M.F. Kabir, A.R. M. Tareq, A.K.M. Fazle Kibria, M. Kurasaki, M.M. Rahman, M.N.I. Khan, *In vitro* cytotoxicity and antibiotic application of green route surface modified ferromagnetic TiO $_2$ nanoparticles, RSC Adv. 9 (2019) 13254–13262, https://doi.org/10.1039/C9RA01395D.
[53] A.D. Jadhao, S. Shende, P. Ingle, A. Gade, S.W. Hajare, R.S. Ingole, Biogenic synthesis of zinc oxide nanoparticles by *Bryophyllum pinnatum* and its acute oral toxicity evaluation in wistar rats, IEEE Trans.on Nanobioscience. 19 (2020) 633–639, https://doi.org/10.1109/TNB.2020.3014023.
[54] P. Pawliszak, D. Malina, A. Sobczak-Kupiec, Rhodiola rosea extract mediated green synthesis of silver nanoparticles supported by nanosilica carrier, Mater. Chem. Phys. 234 (2019) 390–402, https://doi.org/10.1016/j.matchemphys.2019.05.027.
[55] T.S. Alomar, N. AlMasoud, M.A. Awad, M.F. El-Tohamy, D.A. Soliman, An eco-friendly plant-mediated synthesis of silver nanoparticles: characterization, pharmaceutical and biomedical applications, Mater. Chem. Phys. 249 (2020) 123007, https://doi.org/10.1016/j.matchemphys.2020.123007.
[56] M. Sundrarajan, K. Bama, M. Bhavani, S. Jegatheeswaran, S. Ambika, A. Sangili, P. Nithya, R. Sumathi, Obtaining titanium dioxide nanoparticles with spherical shape and antimicrobial properties using M. citrifolia leaves extract by hydrothermal method, J. Photochem. Photobiol. B Biol. 171 (2017) 117–124, https://doi.org/10.1016/j.jphotobiol.2017.05.003.
[57] L. Hernández-Morales, H. Espinoza-Gómez, L.Z. Flores-López, E.L. Sotelo-Barrera, A. Núñez-Rivera, R.D. Cadena-Nava, G. Alonso-Núñez, K.A. Espinoza, Study of the green synthesis of silver nanoparticles using a natural extract of dark or white Salvia hispanica L. seeds and their antibacterial application, Appl. Surf. Sci. 489 (2019) 952–961, https://doi.org/10.1016/j.apsusc.2019.06.031.
[58] A. Rangayasami, K. Kannan, S. Joshi, M. Subban, Bioengineered silver nanoparticles using Elytraria acaulis (L.f.) Lindau leaf extract and its biological applications, Biocatal. Agric. Biotechnol. 27 (2020) 101690, https://doi.org/10.1016/j.bcab.2020.101690.
[59] J.M. Ashraf, M.A. Ansari, H.M. Khan, M.A. Alzohairy, I. Choi, Green synthesis of silver nanoparticles and characterization of their inhibitory effects on AGEs formation using biophysical techniques, Sci. Rep. 6 (2016) 20414, https://doi.org/10.1038/srep20414.
[60] M. Villanueva-Ibáñez, M.G. Yañez-Cruz, R. Álvarez-García, M.A. Hernández-Pérez, M.A. Flores-González, Aqueous corn husk extract – mediated green synthesis of AgCl and Ag nanoparticles, Mater. Lett. 152 (2015) 166–169, https://doi.org/10.1016/j.matlet.2015.03.097.
[61] N. Hashim, M. Paramasivam, J.S. Tan, D. Kernain, M.H. Hussin, N. Brosse, F. Gambier, P.B. Raja, Green mode synthesis of silver nanoparticles using Vitis vinifera's tannin and screening its antimicrobial activity/apoptotic potential versus cancer cells, Mater. Today Commun. 25 (2020) 101511, https://doi.org/10.1016/j.mtcomm.2020.101511.
[62] O. Velgosová, A. Mražíková, R. Marcinčáková, Influence of pH on green synthesis of Ag nanoparticles, Mater. Lett. 180 (2016) 336–339, https://doi.org/10.1016/j.matlet.2016.04.045.
[63] T.A. Salih, K.T. Hassan, S.R. Majeed, I.J. Ibraheem, O.M. Hassan, A.S. Obaid, In vitro scolicidal activity of synthesised silver nanoparticles from aqueous plant extract against Echinococcus granulosus, Biotechnology Reports 28 (2020), e00545, https://doi.org/10.1016/j.btre.2020.e00545.

Energy Systems

The significant impact of green synthesized silver nanoparticles on a bio-voltaic cell for electricity generation

--Manuscript Draft--

Manuscript Number:	
Full Title:	The significant impact of green synthesized silver nanoparticles on a bio-voltaic cell for electricity generation
Article Type:	Original Paper
Keywords:	Green synthesis; Ag NPs; reducing agent; bio-electrochemical cell; electricity; capacity; power
Corresponding Author:	Md. Afzol Afzol Hossain, M Sc University of Dhaka Dhaka, BANGLADESH
Corresponding Author Secondary Information:	
Corresponding Author's Institution:	University of Dhaka
Corresponding Author's Secondary Institution:	
First Author:	Md. Afzol Afzol Hossain, M Sc
First Author Secondary Information:	
Order of Authors:	Md. Afzol Afzol Hossain, M Sc
	Md. Afzol Afzol Hossain, M Sc
	Md. Emran Quayum, Ph.D.
	Md. Kamrul Alam Khan, Ph.D.
Order of Authors Secondary Information:	
Funding Information:	
Abstract:	The bio-voltaic cell (BVC) is an electrochemical cell in which plant extract solution is used as an electrolyte. In this report, four types of BVC were developed by varying the electrolyte solution. The electrical performances of these cells were monitored with the time duration. Colocasia.esculenta or Aurum leaves (AL) extract, green synthesized silver nanoparticles (Ag NPs), and secondary salt (CuSO4.5H2O) were used to make different types of bio-electrolyte solutions for bio-voltaic cells. A rapid, cost-effective and eco-friendly green synthesis method was applied to synthesize the silver nanoparticles (Ag NPs) using AL extract reducing agent. The bio-reduction of Ag+ ions to Ag NPs was confirmed by the UV-visible spectrometer, where the maximum absorption peak was found at 420 nm. The functional groups that acted as reducing and capping agents were investigated by FTIR analysis. The crystal structure and morphological analysis of Ag NPs were probed by X-ray diffraction spectroscopy (XRD) and Field emission scanning electron microscopy (FESEM), respectively. Green synthesized Ag NPs have been used in the electrolyte solution, and comparative electrical performances were observed for four types of bio-electrolyte-based voltaic cells. After using Ag NPs in bio-electrolyte solution, the internal resistance was decreased, and the average power and the capacity of the BVC were significantly increased. Hence, the Ag NPs can play a vital role in the electrolyte solution to amplify the performance of a cell. This study can take a frontier forward to integrate the electrical performances of the bio-electrochemical cell by using Ag NPs.

The significant impact of green synthesized silver nanoparticles on a bio-voltaic cell for electricity generation

Md. Afzol Hossain[a], Md. Emran Quayum[b] Md. Kamrul Alam Khan[c],

[a]Department of Chemistry, University of Dhaka, Dhaka-1000, Bangladesh

[b]Department of Chemistry, University of Dhaka, Dhaka-1000, Bangladesh.

[c]Department of Physics, Jagannath University, Dhaka-1100, Bangladesh.

E-mail: [a]afzal.chemistry@gmail.com, [b]mequayum@du.ac.bd, [c]kakhan01@yahoo.com,

Abstract: The bio-voltaic cell (BVC) is an electrochemical cell in which plant extract solution is used as an electrolyte. In this report, four types of BVC were developed by varying the electrolyte solution. The electrical performances of these cells were monitored with the time duration. Colocasia.esculenta or Aurum leaves (AL) extract, green synthesized silver nanoparticles (Ag NPs), and secondary salt ($CuSO_4.5H_2O$) were used to make different types of bio-electrolyte solutions for bio-voltaic cells. A rapid, cost-effective and eco-friendly green synthesis method was applied to synthesize the silver nanoparticles (Ag NPs) using AL extract reducing agent. The bio-reduction of Ag^+ ions to Ag NPs was confirmed by the UV-visible spectrometer, where the maximum absorption peak was found at 420 nm. The functional groups that acted as reducing and capping agents were investigated by FTIR analysis. The crystal structure and morphological analysis of Ag NPs were probed by X-ray diffraction spectroscopy (XRD) and Field emission scanning electron microscopy (FESEM), respectively. Green synthesized Ag NPs have been used in the electrolyte solution, and comparative electrical performances were observed for four types of bio-electrolyte-based voltaic cells. After using Ag NPs in bio-electrolyte solution, the internal resistance was decreased, and the average power and the capacity of the BVC were significantly increased. Hence, the Ag NPs can play a vital role in the electrolyte solution to amplify the performance of a cell. This study can take a frontier forward to integrate the electrical performances of the bio-electrochemical cell by using Ag NPs.

Keywords: Green synthesis, Ag NPs, reducing agent, bio-electrochemical cell, electricity, capacity, power.

Introduction: Over this decade, green synthesis has been one of the most exciting methods of synthesizing nanomaterials. Various plant extracts such as A. ciniformis [1], Vitas vinifera [2], Blumea eriantha DC [3], Crocus Haussknechtii Boiss [4], Peganum harmala [5], Veronica amygdalina [6], Salvia hispanica L. seeds [7] have been reported to synthesis the semiconductor oxide and metal NPs (Ag, Au, ZnO, CuO, TiO_2 etc) as the reducing agent for the remarkable antibacterial and anticancer activities. The simplicity of the synthesis process has made this method very popular in the research community. The active functional groups of bio compounds

exist in the different parts of plants (polyphenols, ascorbic acids, flavonoids, terpenoids, alkaloids, enzymes, amino acids, caffeine, linalool, proteins) play an important foreword to reduce metals ion to metals NPs [11–14]. In this report, Colocasisa. esculenta or Aurum leaves (AL) extract was used to synthesize the silver nanoparticles (Ag NPs) by the green synthesis process. Colocasia.esculenta is a familiar plant available in the tropical regions, especially in Bangladesh and India. The local name of this plant is 'kochu', and the English name of this plant leaf is called Aurum Leaf (AL). The important biomolecular compounds, including flavonoids, steroids, ascorbic acid, thiamine, riboflavin, niacin, carbohydrates, and fats, are available in Colocasia.esculenta leaves, which are responsible for the bioreduction of NPs [15–17]. Different structures of nanomaterials such as Ag, Au, ZnO, CuO, and TiO_2 are the most common nanoparticles which have widely been synthesized by the green method for the last decade to be used in pharmaceutical applications (eg; targeted drug delivery, tumor therapeutic, cancer therapeutic, antifungal, antibacterial, and nanomedicines) [2,8]. Among these, Ag NPs have drawn significant attention due to their multidimensional uses in physical, chemical, industrial, agricultural, and biomedical applications [9,10]. Besides the antibacterial activities of green synthesized Ag NP, it has a significant influence on electrochemical cells as a catalyst to integrate the electrical performances. Nowadays, various plant extracts (vegetables and fruits) have been used as the electrolyte solution in an electrochemical cell to generate electricity, and such a plant extract electrolyte-based cell is called by the name of bio-electrochemical cell [18–22]. To develop the BVC, different kinds of plant exacts, fruits, and vegetable extract (such as Bryophyllum pinnatum leaf, Aloe vera, Tomato, and Lemon) are generally used as an electrolyte solution of the electrochemical cell instead of chemical electrolyte. In this study, a novel BVC is developed to generate electricity, and Ag NPs have been used to integrate the electrical performances of the cell. Four types of low-cost and portable bio-electrochemical cells have been designed by varying the electrolyte solution. Different electrical parameters have been examined to understand the impact of nanoparticles on cells. Comparative electrical performances were recorded to monitors the role of Ag NPs on electricity generation. The short circuit current and open circuit voltage were recorded for all cells with the time duration, and it was found that both the voltage and current were changing by varying the electrolyte solution of cells. The power and capacity of all bio-voltaic cells were calculated, and it is noted that after using Ag NPs in the electrolyte solution, the power and capacity of cell have been significantly integrated. This novel mini BVC power plant can be constructed by any person or even school-going students at an affordable price. Hence, this innovative renewable power plant may open a new window for low-cost electricity generation.

2. Materials and Methods

2.1. Plant extract Preparation

C.esculenta leaves were taken from the local market in Bangladesh. 20g of leaves were taken and appropriately washed with tap water to dispel the unwanted particles. After then, leaves were washed with Deionized (DI) water three times and blended to make a fine paste. 100 mL of deionized water with leaves paste were placed on a hot plate at 600 C for one hour. The hot solution

was kept aside to cool. The solution was filtered with Whatman42, and the extract was kept in a refrigerator at 40 C before use.

2.2. Biosynthesis of silver nanoparticles

A pure $AgNO_3$ precursor purchased from Sigma Aldrich has been used in this experiment. The plant extract (5 mL) was added to the 1mM $AgNO_3$ (45 mL). After an hour, the color change of the mixture solution was observed. The colorless mixture solution was becoming brownish with the time, which indicated the formation of Ag NPs. To complete the reduction of Ag^+ to Ag^0 the solution was kept at room temperature for the next couple of days in a dark chamber. The color change from light yellow to dark brown affirms the reduction of Ag^+ and the formation of Ag NPs. The fabrication steps are shown in Fig.1.

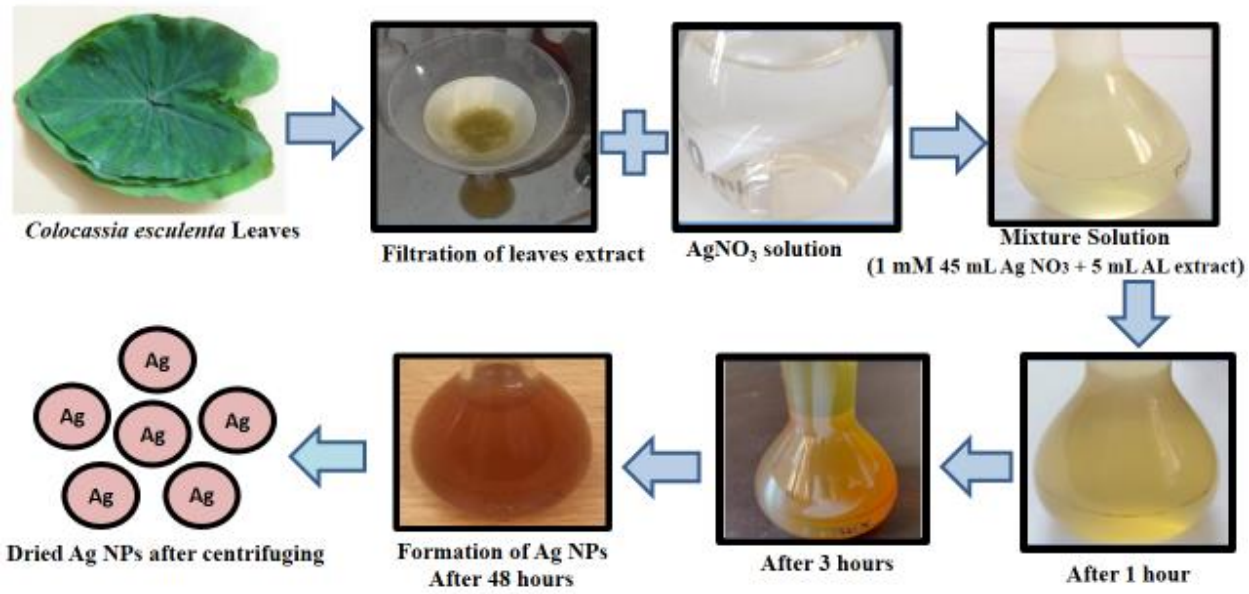

Fig.1. Steps diagram of green synthesis of silver nanoparticles.

2.3. Characterizations of biosynthesized silver nanoparticles

Ag NPs were primarily confirmed by the color change of the mixture solution from light yellow to dark brown which was further confirmed by UV-Vis spectrometer (UV-2102, China) in the range of (150 nm -900 nm). The crystalline structure of biosynthesized silver nanoparticles was probed by the X-ray diffraction instrument Rigaku (Ultima IV 2036E202) in a different range of 2θ angle (35°- 90°). The morphology of Ag NPs was observed by using the field emission scanning electron microscopy (FESEM) images (JSM-7610F) at 15 KeV. Moreover, the functional groups of plant extract were investigated by Fourier transform infrared (FTIR) measurements Shimadzu (IRPrestige-21).

2.4. Fabrication of bio-electrochemical cells

Four types of bio-electrochemical cells were constructed, namely A, B, C, and D by varying the electrolyte solutions of the cell.

In cell A, 100 mL of AL extract bio-electrolyte was used in the cell. For cell B, 10 mL of 0.4006M $CuSO_4.5H_2O$ secondary salt with 100 mL of AL extract has been taken as the electrolyte, and the influences of secondary salt in a cell have been investigated. Bio-electrolyte was made of 100 mL AL extract with 15 mL of Ag NPs (1.5 mg) and 10 mL of 0.4006M $CuSO_4.5H_2O$ for cell C.

100 mL of AL extract and 15 mL of Ag NPs (1.5mg) were mixed to prepare the bio-electrolyte for cell D. Open circuit voltages, short circuit currents, internal resistances, and maximum power were monitored for all bio-voltaic cells. Fig.2. is shown the diagram of four bio-electrochemical cells.

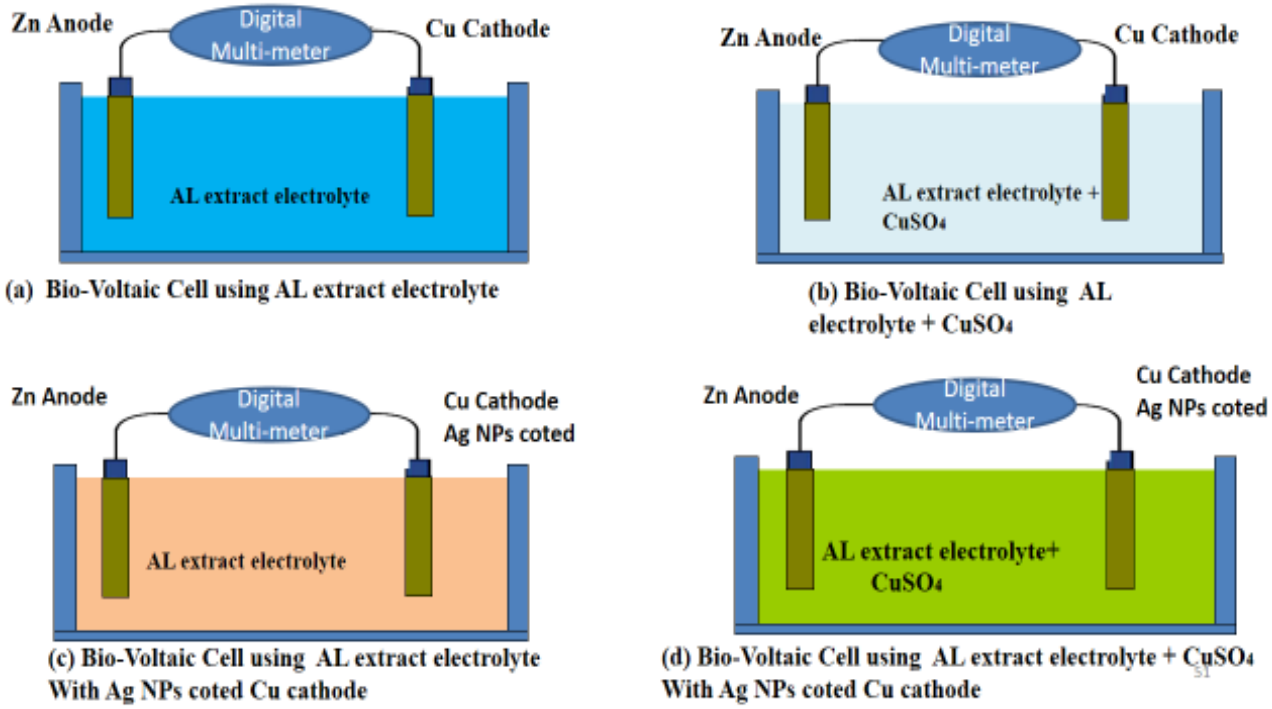

Fig. 2. Design of bio-voltaic cell with (a) AL extract bio-electrolyte, (b) (AL+ $CuSO_4$) bioelectrolyte, (c) (AL+ Ag NPs) bio-electrolyte and (d) (AL+$CuSO_4$ + Ag NPs) bio-electrolyte.

2.5. Study the impacts of bio-electrolyte on bio-electrochemical cells

To observe the significance of different bio-electrolytes on cells A, B, C, and D, the power and the internal resistance were found by using the following formulas

$$P = V_{oc} \times I_{sc}$$

$$\text{And } Rin = V_{oc} \div I_{sc}$$

And the capacity (AH) is also determined by $C = I_{sc} \times t_d$

Where P is denoted for the cell's power, R_{in} is for internal resistance, V_{oc} is for open-circuit voltage, I_{sc} represents the short circuit current, C is capacity (ampere per hour), and td is the discharge time of the cells.

3. Result and Discussions

3.1 UV-Vis analysis of green synthesized Ag NPs

Fig.3. reveals the UV-visible spectra of green synthesized Ag NPs, AgNO3 solution, and colocasia esculenta extract. Due to the formation of Ag NPs from Ag ions, the maximum absorption was appeared at 420 nm. Hence, the plant extract acted as a reducing agent to reduce the silver ions.

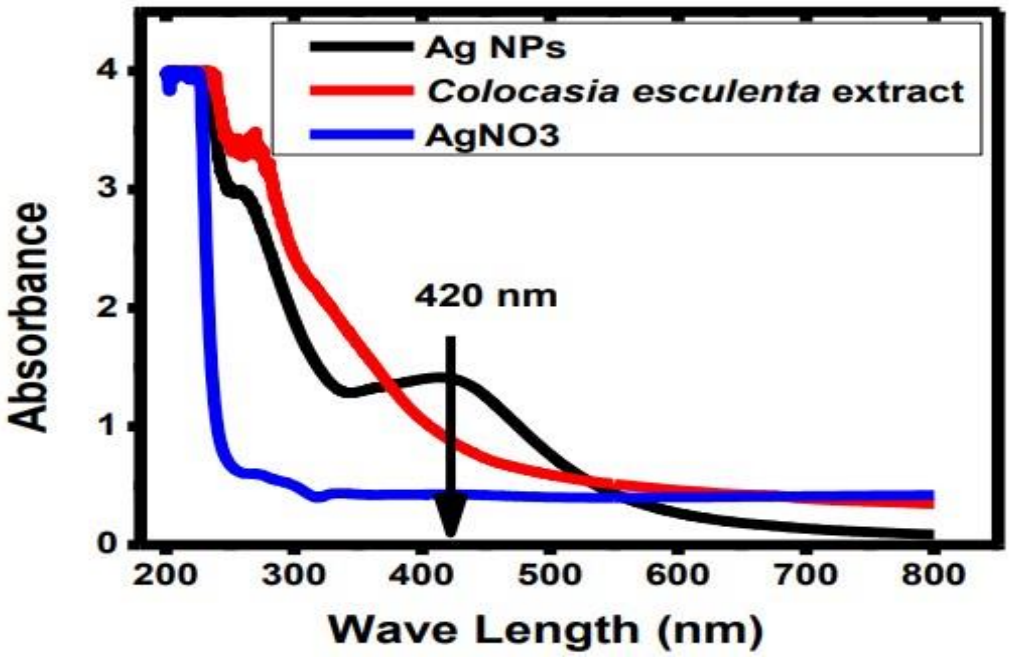

Fig.3. UV-vis spectra of AgNO3 solution (blue line), Colacasia esculenta Extract (red line), and Ag NPs (black line).

The light yellow color mixture solution became dark brown color with the time duration, which indicates the bio-reduction of Ag ions and the formation of Ag NPs. The color change of the mixture solution occurs due to the surface Plasmon vibrations, a unique optical property of novel metal nanoparticles [23]. Metal nanoparticles have free electrons, and the combined vibrations of those free electrons are responsible for a surface Plasmon resonance absorption band [24]. Silver

nanoparticles reveal a maximum absorption peak in between 400 nm to 500 nm [25–27]. The range of maximum UV-visible absorption depends on the size, shape, and type of solvent of nanoparticles [5,11,28].

3.2 XRD analysis of Ag NPs

The X-ray Diffraction measurements probed the crystal structure of green synthesized Ag NPs. Fig.4. reveals the XRD spectra of green synthesized Ag NPs. The face-centered cubic (FCC) 200 300 400 500 600 700 800 0 1 2 3 4 Absorbance Wave Length (nm) Ag NPs Colocasia esculenta extract AgNO3 420 nm structure of Ag NPs was confirmed by the diffraction peaks of at around 38.120 , 46.260 , 64.560 , and 77. 360 due to the planes of (111), (200), (220), and (311) respectively [1,10,13,28–31]. The formation of Ag Nano crystal corresponds to the JCPDS No. 04-0783 [4,6,13,28].

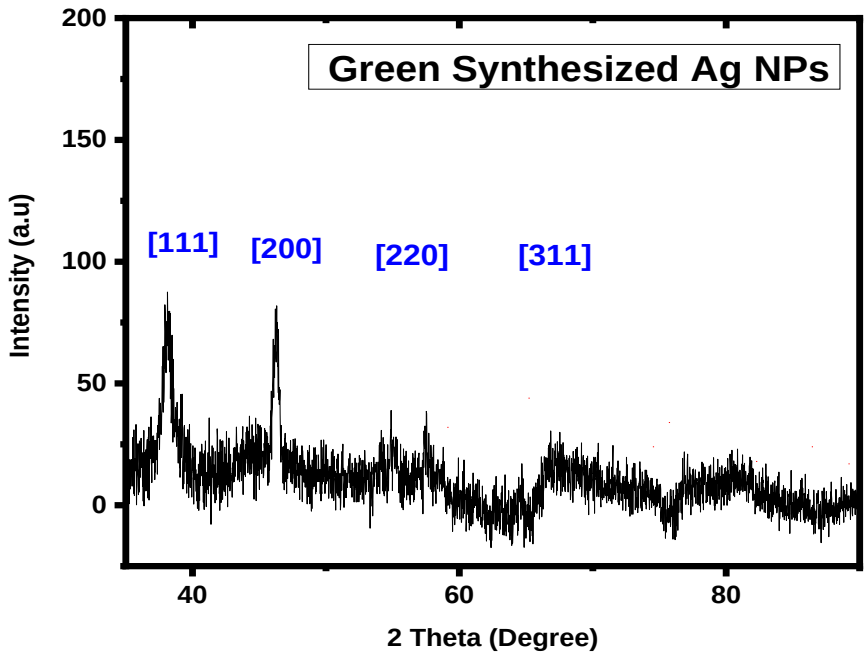

Fig.4. XRD pattern of green synthesized Ag nanoparticles from Aurum Leaf Extract.

The crystal size was estimated by using the Debye-Scherrer formula,

$$D=0.89\lambda/\beta\cos\theta$$

Here, λ represents the wavelength of X-ray (λ = 1.54056 Å), θ is represents the Bragg's diffraction angle, and the full width at half maximum (FWHM) is denoted by β [6,32,33]. The crystal size of Ag NPs is found to be around 8.0 nm. Moreover, two unassigned peaks (*) were appeared due to

the crystalline structure of biomolecular compounds on the surface of plant extract mediated Ag NPs. Similar results are reported for the green synthesized Ag NPs in a range of articles [34–39].

3.3 Fourier transformed infrared spectroscopy (FT-IR) analysis:

The bio-reduction of metal NPs is mainly associated with the active functional groups of biochemical compounds like polysaccharides, flavonoids, triterpenoids, and polyphenols present in the plants [11,40]. The stretching, wagging, and bending vibrations of functional groups are 40 50 60 70 80 90 -25 0 25 50 75 100 * [311] [220] [200] [111] Intensity (a.u) 2 Theta (Degree) Green Synthesized Ag NPs * considered the reasons for bio-reduction metal NPs. The FT-IR spectra of silver nanoparticles were carried out to investigate the possible functional groups of plant extract. Fig.5. represents the FT-IR spectra of C esculenta leaves extract mediated Ag NPs.

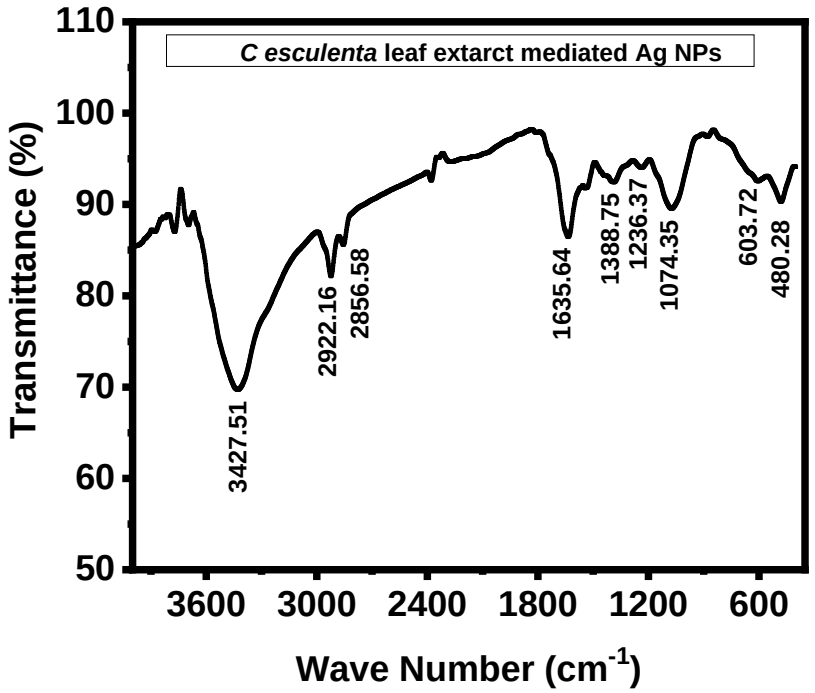

Fig.5. FT-IR spectra of Colacasia esculenta extract mediated Ag NPs.

The FTIR spectra expressed three prominent peaks at 3427.51 cm-1 , 1635.64 cm-1 , and 1074.35 cm-1 among other weak signals. The peaks at 3427.51 cm-1 and 1074.35 cm-1 mainly appeared to stretch hydroxyl groups (-OH) and the stretching of –C-O-C- bond of polyol groups on the surface of nanoparticles, respectively [1,5,16,17,41–43]. The peak at 1635.64 cm is attributed to the C=O stretching vibration of amide, peptides, flavonoid, and protein groups [44,45]. Moreover, C=C stretching vibration of ascorbic acid, –CO stretch of the amide group of plant extract are responsible for this significant peak at 1635.64 cm-1 [16,17,42]. Amide groups and polyphenol

are the effective reducing and stabilizing agent compounds of plant extract for the biosynthesis of nanoparticles [46]. Another peak at 2922 cm-1 generally appears due to the stretch of C-H bond, and the alkynes of flavonoid compounds. The alkynes and the flavonoid bio-compounds play an essential role in forming metal nanoparticles [4,47–49].

3.4 Morphology analysis of Ag NPs:

The size and shape of green synthesized NPs depend on the concentration rate of extract, P H of the solution, and reaction temperature [5,11,28,50]. Fig.6a. shows FESEM image of silver NPs, and most of the particles are found to be almost spherical. Fig.6b. represents the size distribution 3600 3000 2400 1800 1200 600 50 60 70 80 90 100 110 2922.16 2856.581236.37 3427.51 603.72 1074.35 1635.64 1388.75 Transmittance (%) Wave Number (cm-1) Plant extract mediated Ag NPs 480.28 histogram of nanoparticles. The diameter of particles is in the range of 12 nm-26 nm. The average diameter of plant extract mediated Ag NPs is ~21 nm.

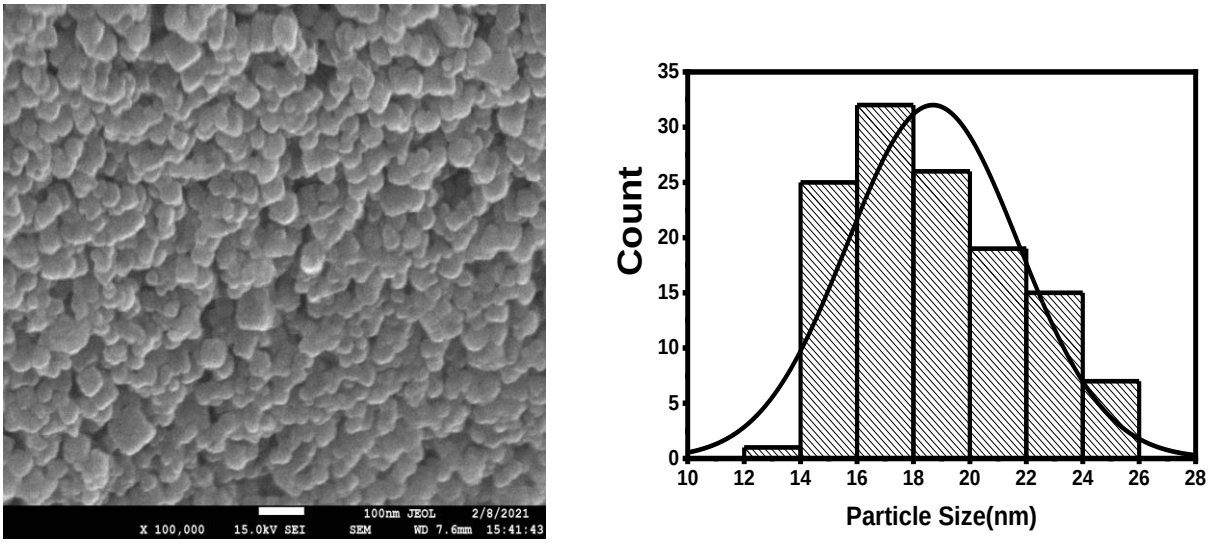

Fig.6. (a) FESEM image of green synthesized silver nanoparticles and (b) the particle size histogram of green synthesized silver nanoparticles.

3.5 Significance of silver nanoparticles on bio-electrochemical cells:

Silver nanoparticles have been used in the bio-electrochemical cell, and the impact of nanoparticles has been monitored. Four types of bio-electrochemical cells have been designated with four different bio-electrolyte solutions. Fig.7. shows the comparative analysis of electrical parameters for all cells. The open-circuit voltage and short circuit current of four cells are shown in Fig.7 (a,b). Fig.7(c,d) represents all electrochemical cells' power and internal resistance.

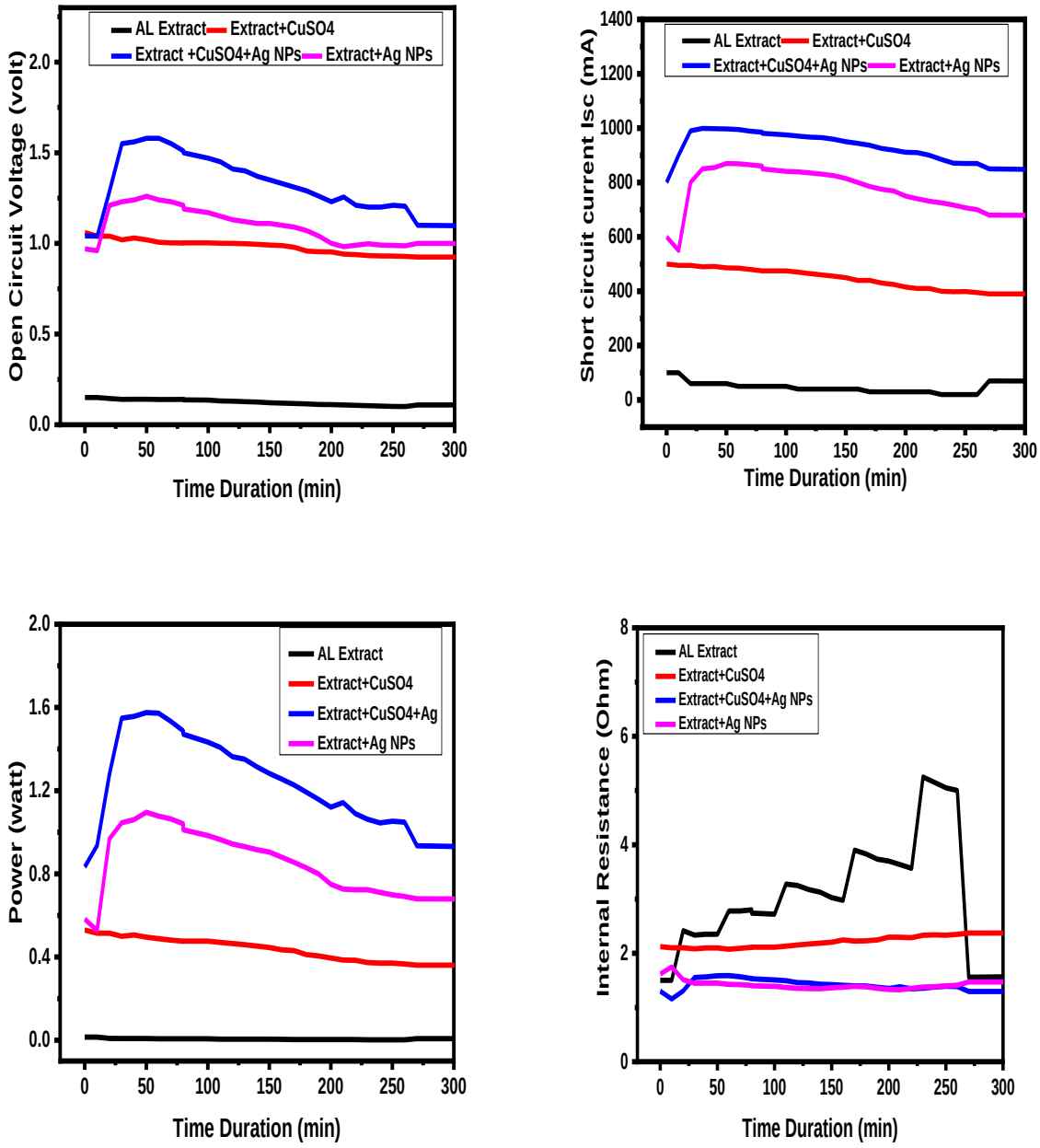

Fig.7. Comparative analysis of (a) open-circuit voltage, (b) short circuit current, (c) power, and (d) internal resistance of four bio-electrochemical cells.

The open circuit voltage and short circuit current were significantly increased after using Ag NPs to extract electrolytes. The lowest values of voltage and current were found for only plant extract electrolyte-based cells. After using CuSO4 with extract, the electrical parameters were increased due to the secondary salt effect. Moreover, the current and voltage were surprisingly increased after using silver nanoparticles in bio-electrolyte, and the maximum electrical performances were recorded for this case. Since the current and voltage were dramatically enhanced in the presence

of nanoparticles, the highest power, and the lowest internal resistance were calculated for this cell. Table.1 shows the average electrical parameters for four types of cells. Fig.8 represents the average power and the average capacity of four bio-electrochemical cells. Only AL extract electrolyte-based bio-electrochemical cell shows the minimum power and capacity, and the maximum power and capacity were recorded for the (Extract + CuSO4 + Ag NPs) bio-electrolyte based cell. It is also noticeable that the (Extract + Ag NPs) electrolyte-based cell showed the second-highest power and capacity among four cells which are even more significant than the (Extract + CuSO4) electrolyte-based cell. Hence, it is clearly demonstrated that the impact of Ag NPs on electrolyte solution is more effective than the secondary salt (CuSO4) effect.

Table1: The average power for different electrolyte-based bio-voltaic cells.

Electrolyte of cell	Average Power (watt)	Average Capacity (AH)
Extract	0.0024	0.0803
Extract + CuSO4	0.4379	0.9619
Extract + Ag NPs	0.6224	1.7208
Extract + CuSO4+ Ag NPs	0.7024	2.0630

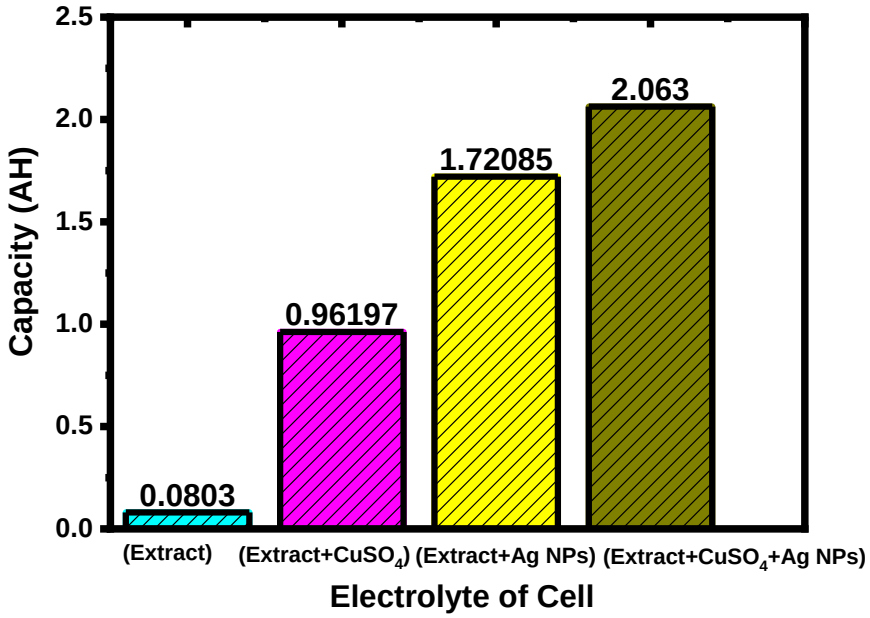

Fig.8. avarage capacity of four different electrolyte based bio-voltaic cells

Conclusion

The rising electricity demand is becoming a trend of development throughout the world in the near future. In this study, an alternative source of electricity generation has been proposed by developing a unique bio-electrochemical cell. The electrical performance of this cell is improved by incorporating green synthesized Ag NPs. The silver nanoparticles have been fabricated by a low-cost and eco-friendly method by using Colocasia esculenta leaves extract reducing agent. The antibacterial activities of green synthesized silver nanoparticles have been reported in various articles. This report introduced the impact of green synthesized silver nanoparticles on the bio-electrochemical cell. The electrical performances surprisingly increased after applying the nanoparticles in the electrolyte of cell. This new model of the bio-electrochemical cell may open a new era in supplying low-cost electricity throughout any remote area around the world.

Acknowledgments

This work is supported by the GARE (Grant of Advanced Research in Education) project, Ministry of Education, GoB for providing financial support during the research work (Project/User ID: PS2019949). The author is grateful to Dr. Md. Emran Quayum, Professor, Department of Chemistry, University of Dhaka, Bangladesh and Dr. Md. Kamrul Alam Khan Professor, Department of Physics, Jagannath University, Dhaka, Bangladesh for their generous support during this research work.

References

[1] S. Aslany, F. Tafvizi, V. Naseh, Characterization and evaluation of cytotoxic and apoptotic effects of green synthesis of silver nanoparticles using Artemisia Ciniformis on human gastric adenocarcinoma, Materials Today Communications. 24 (2020) 101011. https://doi.org/10.1016/j.mtcomm.2020.101011.

[2] N. Hashim, M. Paramasivam, J.S. Tan, D. Kernain, M.H. Hussin, N. Brosse, F. Gambier, P.B. Raja, Green mode synthesis of silver nanoparticles using Vitis vinifera's tannin and screening its antimicrobial activity / apoptotic potential versus cancer cells, Materials Today Communications. 25 (2020) 101511. https://doi.org/10.1016/j.mtcomm.2020.101511.

[3] R.R. Chavan, S.D. Bhinge, M.A. Bhutkar, D.S. Randive, G.H. Wadkar, S.S. Todkar, M.N. Urade, Characterization, antioxidant, antimicrobial and cytotoxic activities of green synthesized silver and iron nanoparticles using alcoholic Blumea eriantha DC plant extract, Materials Today Communications. 24 (2020) 101320. https://doi.org/10.1016/j.mtcomm.2020.101320.

[4] M. Mosaviniya, T. Kikhavani, M. Tanzifi, M. Tavakkoli Yaraki, P. Tajbakhsh, A. Lajevardi, Facile green synthesis of silver nanoparticles using Crocus Haussknechtii Bois bulb extract: Catalytic activity and antibacterial properties, Colloid and Interface Science Communications. 33 (2019) 100211. https://doi.org/10.1016/j.colcom.2019.100211.

[5] T.S. Alomar, N. AlMasoud, M.A. Awad, M.F. El-Tohamy, D.A. Soliman, An ecofriendly plant-mediated synthesis of silver nanoparticles: Characterization, pharmaceutical and biomedical applications, Materials Chemistry and Physics. 249 (2020) 123007. https://doi.org/10.1016/j.matchemphys.2020.123007.

[6] S.O. Aisida, K. Ugwu, P.A. Akpa, A.C. Nwanya, U. Nwankwo, S.S. Botha, P.M. Ejikeme, I. Ahmad, M. Maaza, F.I. Ezema, Biosynthesis of silver nanoparticles using bitter leave (Veronica amygdalina) for antibacterial activities, Surfaces and Interfaces. 17 (2019) 100359. https://doi.org/10.1016/j.surfin.2019.100359.

[7] L. Hernández-Morales, H. Espinoza-Gómez, L.Z. Flores-López, E.L. Sotelo-Barrera, A. Núñez-Rivera, R.D. Cadena-Nava, G. Alonso-Núñez, K.A. Espinoza, Study of the green synthesis of silver nanoparticles using a natural extract of dark or white Salvia hispanica L. seeds and their antibacterial application, Applied Surface Science. 489 (2019) 952–961. https://doi.org/10.1016/j.apsusc.2019.06.031.

[8] A. Danagoudar, P. G K, M. Shantaram, B. Chatterjee, K. Ghosh, S.R. Kanade, C.G. Joshi, Cancer cell specific cytotoxic potential of the silver nanoparticles synthesized using the endophytic fungus, Penicillium citrinum CGJ-C2, Materials Today Communications. 25 (2020) 101442. https://doi.org/10.1016/j.mtcomm.2020.101442.

[9] Y. He, F. Wei, Z. Ma, H. Zhang, Q. Yang, B. Yao, Z. Huang, J. Li, C. Zeng, Q. Zhang, Green synthesis of silver nanoparticles using seed extract of Alpinia katsumadai, and their antioxidant, cytotoxicity, and antibacterial activities, RSC Adv. 7 (2017) 39842–39851. https://doi.org/10.1039/C7RA05286C.

[10] N. Jayaprakash, J.J. Vijaya, K. Kaviyarasu, K. Kombaiah, L.J. Kennedy, R.J. Ramalingam, M.A. Munusamy, H.A. Al-Lohedan, Green synthesis of Ag nanoparticles using Tamarind fruit extract for the antibacterial studies, Journal of Photochemistry and Photobiology B: Biology. 169 (2017) 178–185. https://doi.org/10.1016/j.jphotobiol.2017.03.013.

[11] S. Jain, M.S. Mehata, Medicinal Plant Leaf Extract and Pure Flavonoid Mediated Green Synthesis of Silver Nanoparticles and their Enhanced Antibacterial Property, Sci Rep. 7 (2017) 15867. https://doi.org/10.1038/s41598-017-15724-8.

[12] P. Rauwel, S. Küünal, S. Ferdov, E. Rauwel, A Review on the Green Synthesis of Silver Nanoparticles and Their Morphologies Studied via TEM, Advances in Materials Science and Engineering. 2015 (2015) 1–9. https://doi.org/10.1155/2015/682749.

[13] D. Garibo, H.A. Borbón-Nuñez, J.N.D. de León, E. García Mendoza, I. Estrada, Y. Toledano-Magaña, H. Tiznado, M. Ovalle-Marroquin, A.G. Soto-Ramos, A. Blanco, J.A. Rodríguez, O.A. Romo, L.A. Chávez-Almazán, A. Susarrey-Arce, Green synthesis of silver nanoparticles using

Lysiloma acapulcensis exhibit high-antimicrobial activity, Sci Rep. 10 (2020) 12805. https://doi.org/10.1038/s41598-020-69606-7.

[14] S.K. Chandraker, M. Lal, P. Dhruve, R.P. Singh, R. Shukla, Cytotoxic, Antimitotic, DNA Binding, Photocatalytic, H2O2 Sensing, and Antioxidant Properties of Biofabricated Silver Nanoparticles Using Leaf Extract of Bryophyllum pinnatum (Lam.) Oken, Front. Mol. Biosci. 7 (2021) 593040. https://doi.org/10.3389/fmolb.2020.593040.

[15] C.O. Eleazu, Characterization of the natural products in cocoyam (Colocasia esculenta) using GC–MS, Pharmaceutical Biology. 54 (2016) 2880–2885. https://doi.org/10.1080/13880209.2016.1190383.

[16] S. Agarwal, M. Gogoi, S. Talukdar, P. Bora, T.K. Basumatary, N.N. Devi, Green synthesis of silver nanoplates using the special category of plant leaves showing the lotus effect, RSC Adv. 10 (2020) 36686–36694. https://doi.org/10.1039/D0RA06533A.

[17] R.K. Borah, H.J. Saikia, A. Mahanta, V.K. Das, U. Bora, A.J. Thakur, Biosynthesis of poly(ethylene glycol)-supported palladium nanoparticles using Colocasia esculenta leaf extract and their catalytic activity for Suzuki–Miyaura cross-coupling reactions, RSC Adv. 5 (2015) 72453–72457. https://doi.org/10.1039/C5RA12657F.

[18] K.A. Khan, M.A. Mamun, M. Ibrahim, M. Hasan, M. Ohiduzzaman, A.K.M. Obaydullah, M.A. Wadud, M. Shajahan, PKL electrochemical cell: physics and chemistry, SN Appl. Sci. 1 (2019) 1335. https://doi.org/10.1007/s42452-019-1363-x.

[19] K.A. Khan, L. Hassan, A.K.M. Obaydullah, S.M. Azharul Islam, M.A. Mamun, T. Akter, M. Hasan, Md.S. Alam, M. Ibrahim, M.M. Rahman, M. Shahjahan, Bioelectricity: a new approach to provide the electrical power from vegetative and fruits at off-grid region, Microsyst Technol. 26 (2020) 3161–3172. https://doi.org/10.1007/s00542-018-3808-3.

[20] M. Hasan, K.A. Khan, Dynamic model of Bryophyllum pinnatum leaf fueled BPL cell: a possible alternate source of electricity at the off-grid region in Bangladesh, Microsyst Technol. 25 (2019) 2481–2492. https://doi.org/10.1007/s00542-018-4149-y.

[21] K.A. Khan, S.R. Rasel, M. Ohiduzzaman, Homemade PKL electricity generation for use in DC fan at remote areas, Microsyst Technol. 25 (2019) 4529–4536. https://doi.org/10.1007/s00542-019-04422-2.

[22] K.A. Khan, M.H. Ali, M.A. Mamun, M.M. Haque, A.K.M.A. Ullah, M.N.I. Khan, L. Hassan, A.K.M. Obaydullah, M.A. Wadud, Bioelectrical characterization and production of nanoparticles (NPs) using PKL extract for electricity generation, Microsyst Technol. (2020). https://doi.org/10.1007/s00542-020-04774-0.

[23] A. Rautela, J. Rani, M. Debnath (Das), Green synthesis of silver nanoparticles from Tectona grandis seeds extract: characterization and mechanism of antimicrobial action on different microorganisms, J Anal Sci Technol. 10 (2019) 5. https://doi.org/10.1186/s40543-018- 0163-z.

[24] S. Raj, S. Chand Mali, R. Trivedi, Green synthesis and characterization of silver nanoparticles using Enicostemma axillare (Lam.) leaf extract, Biochemical and Biophysical Research Communications. 503 (2018) 2814–2819. https://doi.org/10.1016/j.bbrc.2018.08.045.

[25] J.M. Ashraf, M.A. Ansari, H.M. Khan, M.A. Alzohairy, I. Choi, Green synthesis of silver nanoparticles and characterization of their inhibitory effects on AGEs formation using biophysical techniques, Sci Rep. 6 (2016) 20414. https://doi.org/10.1038/srep20414.

[26] F. Eya'ane Meva, M.L. Segnou, C. Okalla Ebongue, A.A. Ntoumba, P. Belle Ebanda Kedi, V. Deli, M.-A. Etoh, E. Mpondo Mpondo, Spectroscopic synthetic optimizations monitoring of silver nanoparticles formation from Megaphrynium macrostachyum leaf extract, Revista Brasileira de Farmacognosia. 26 (2016) 640–646. https://doi.org/10.1016/j.bjp.2016.06.002.

[27] W.W. Melkamu, L.T. Bitew, Green synthesis of silver nanoparticles using Hagenia abyssinica (Bruce) J.F. Gmel plant leaf extract and their antibacterial and anti-oxidant activities, Heliyon. 7 (2021) e08459. https://doi.org/10.1016/j.heliyon.2021.e08459.

[28] M. Darroudi, M. Mansor Bin Ahmad, A.H. Abdullah, N.A. Ibrahim, K. Shameli, Green synthesis and characterization of gelatin-based and sugar-reduced silver nanoparticles, IJN. (2011) 569. https://doi.org/10.2147/IJN.S16867.

[29] M. Shahriary, H. Veisi, M. Hekmati, S. Hemmati, In situ green synthesis of Ag nanoparticles on herbal tea extract (Stachys lavandulifolia)-modified magnetic iron oxide nanoparticles as antibacterial agent and their 4-nitrophenol catalytic reduction activity, Materials Science and Engineering: C. 90 (2018) 57–66. https://doi.org/10.1016/j.msec.2018.04.044.

[30] M. Ahamed, M.A. Majeed Khan, M.K.J. Siddiqui, M.S. AlSalhi, S.A. Alrokayan, Green synthesis, characterization and evaluation of biocompatibility of silver nanoparticles, Physica E: Low-Dimensional Systems and Nanostructures. 43 (2011) 1266–1271. https://doi.org/10.1016/j.physe.2011.02.014.

[31] M.A. Hossain, B. Paul, K.A. Khan, M. Paul, M.A. Mamun, M.E. Quayum, Green synthesis and characterization of silver nanoparticles by using Bryophyllum pinnatum and the evaluation of its power generation activities on bio-electrochemical cell, Materials Chemistry and Physics. 282 (2022) 125943. https://doi.org/10.1016/j.matchemphys.2022.125943.

[32] B. Paul, M.A.-A. Mamun, A. Haque, M. Paul, K. Ghosh, Significant Reduction of Defect States and Surface Tailoring in ZnO Nanoparticles via Nano-Bio Interaction With Glucose for Bio-Applications, IEEE Trans.on Nanobioscience. 18 (2019) 490–497. https://doi.org/10.1109/TNB.2019.2919231.

[33] M.A. Siddiquee, M. ud din Parray, S.H. Mehdi, K.A. Alzahrani, A.A. Alshehri, M.A. Malik, R. Patel, Green synthesis of silver nanoparticles from Delonix regia leaf extracts: In-vitro cytotoxicity and interaction studies with bovine serum albumin, Materials Chemistry and Physics. 242 (2020) 122493. https://doi.org/10.1016/j.matchemphys.2019.122493.

[34] K. Anandalakshmi, J. Venugobal, V. Ramasamy, Characterization of silver nanoparticles by green synthesis method using Pedalium murex leaf extract and their antibacterial activity, Appl Nanosci. 6 (2016) 399–408. https://doi.org/10.1007/s13204-015-0449-z.

[35] P. Das, K. Ghosal, N.K. Jana, A. Mukherjee, P. Basak, Green synthesis and characterization of silver nanoparticles using belladonna mother tincture and its efficacy as a potential antibacterial and anti-inflammatory agent, Materials Chemistry and Physics. 228 (2019) 310–317. https://doi.org/10.1016/j.matchemphys.2019.02.064.

[36] D. Kalpana, Y.S. Lee, Synthesis and characterization of bactericidal silver nanoparticles using cultural filtrate of simulated microgravity grown Klebsiella pneumoniae, Enzyme and Microbial Technology. 52 (2013) 151–156. https://doi.org/10.1016/j.enzmictec.2012.12.006.

[37] N. Aziz, M. Faraz, R. Pandey, M. Shakir, T. Fatma, A. Varma, I. Barman, R. Prasad, Facile Algae-Derived Route to Biogenic Silver Nanoparticles: Synthesis, Antibacterial, and Photocatalytic Properties, Langmuir. 31 (2015) 11605–11612. https://doi.org/10.1021/acs.langmuir.5b03081.

[38] V.S. Suvith, D. Philip, Catalytic degradation of methylene blue using biosynthesized gold and silver nanoparticles, Spectrochimica Acta Part A: Molecular and Biomolecular Spectroscopy. 118 (2014) 526–532. https://doi.org/10.1016/j.saa.2013.09.016.

[39] S. Hamedi, S.A. Shojaosadati, A. Mohammadi, Evaluation of the catalytic, antibacterial and anti-biofilm activities of the Convolvulus arvensis extract functionalized silver nanoparticles, Journal of Photochemistry and Photobiology B: Biology. 167 (2017) 36–44. https://doi.org/10.1016/j.jphotobiol.2016.12.025.

[40] X. Zhao, J. Zhang, B. Wang, A. Zada, M. Humayun, Biochemical Synthesis of Ag/AgCl Nanoparticles for Visible-Light-Driven Photocatalytic Removal of Colored Dyes, Materials. 8 (2015) 2043–2053. https://doi.org/10.3390/ma8052043.

[41] S. Thakur, N. Karak, Green reduction of graphene oxide by aqueous phytoextracts, Carbon. 50 (2012) 5331–5339. https://doi.org/10.1016/j.carbon.2012.07.023.

[42] V.E. Manhivi, S. Venter, E.O. Amonsou, T. Kudanga, Composition, thermal and rheological properties of polysaccharides from amadumbe (Colocasia esculenta) and cactus (Opuntia spp.), Carbohydrate Polymers. 195 (2018) 163–169. https://doi.org/10.1016/j.carbpol.2018.04.062.

[43] P. Pawliszak, D. Malina, A. Sobczak-Kupiec, Rhodiola rosea extract mediated green synthesis of silver nanoparticles supported by nanosilica carrier, Materials Chemistry and Physics. 234 (2019) 390–402. https://doi.org/10.1016/j.matchemphys.2019.05.027.

[44] A. Rangayasami, K. Kannan, S. Joshi, M. Subban, Bioengineered silver nanoparticles using Elytraria acaulis (L.f.) Lindau leaf extract and its biological applications, Biocatalysis and Agricultural Biotechnology. 27 (2020) 101690. https://doi.org/10.1016/j.bcab.2020.101690.

[45] A.K.M.A. Ullah, M.M. Haque, M. Akter, A. Hossain, A.N. Tamanna, M.M. Hosen, A.K.M.F. Kibria, M.N.I. Khan, M.K.A. Khan, Green synthesis of Bryophyllum pinnatum aqueous leaf extract mediated bio-molecule capped dilute ferromagnetic α -MnO 2 nanoparticles, Mater. Res. Express. 7 (2020) 015088. https://doi.org/10.1088/2053-1591/ab6c20.

[46] Inamuddin, S. Kanchi, One-pot biosynthesis of silver nanoparticle using Colocasia esculenta extract: Colorimetric detection of melamine in biological samples, Journal of Photochemistry and Photobiology A: Chemistry. 391 (2020) 112310. https://doi.org/10.1016/j.jphotochem.2019.112310.

[47] S. M., B. K., B. M., J. S., A. S., S. A., N. P., S. R., Obtaining titanium dioxide nanoparticles with spherical shape and antimicrobial properties using M. citrifolia leaves extract by hydrothermal method, Journal of Photochemistry and Photobiology B: Biology. 171 (2017) 117–124. https://doi.org/10.1016/j.jphotobiol.2017.05.003.

[48] A.D. Jadhao, S. Shende, P. Ingle, A. Gade, S.W. Hajare, R.S. Ingole, Biogenic Synthesis of Zinc Oxide Nanoparticles by Bryophyllum pinnatum and its Acute Oral Toxicity Evaluation in Wistar Rats, IEEE Trans.on Nanobioscience. 19 (2020) 633–639. https://doi.org/10.1109/TNB.2020.3014023.

[49] A.K.M. Atique Ullah, A.N. Tamanna, A. Hossain, M. Akter, M.F. Kabir, A.R.M. Tareq, A.K.M. Fazle Kibria, M. Kurasaki, M.M. Rahman, M.N.I. Khan, In vitro cytotoxicity and antibiotic application of green route surface modified ferromagnetic TiO 2 nanoparticles, RSC Adv. 9 (2019) 13254–13262. https://doi.org/10.1039/C9RA01395D.

[50] T.A. Salih, K.T. Hassan, S.R. Majeed, I.J. Ibraheem, O.M. Hassan, A.S. Obaid, In vitro scolicidal activity of synthesised silver nanoparticles from aqueous plant extract against Echinococcus granulosus, Biotechnology Reports. 28 (2020) e00545. https://doi.org/10.1016/j.btre.2020.e00545.

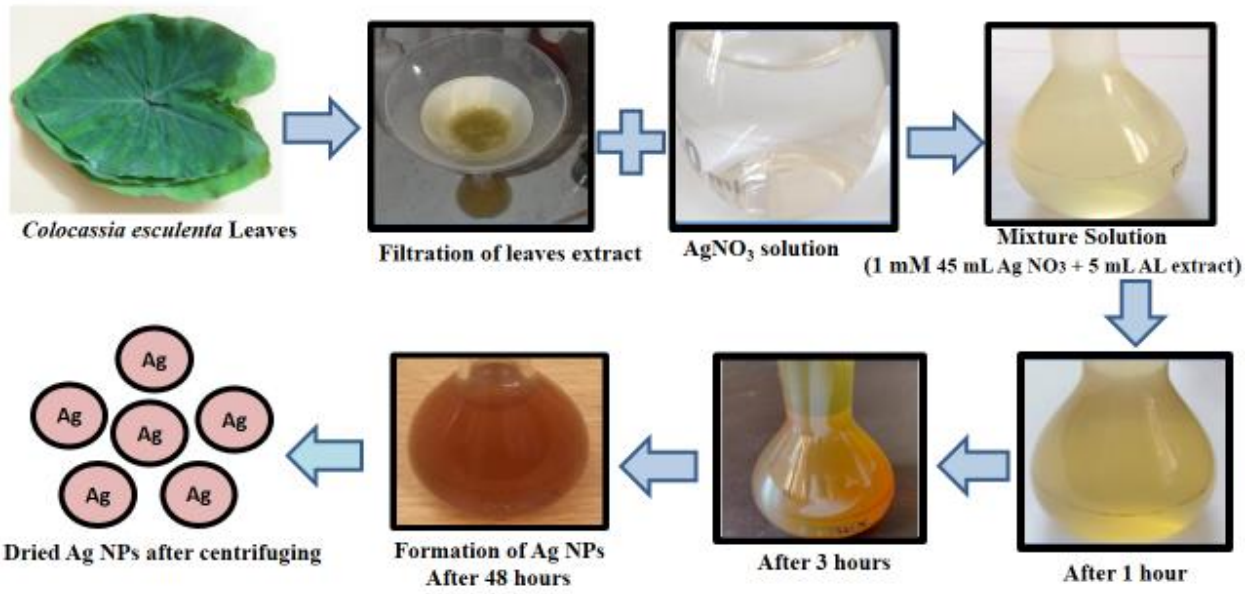

Fig.1. Steps diagram of green synthesis of silver nanoparticles.

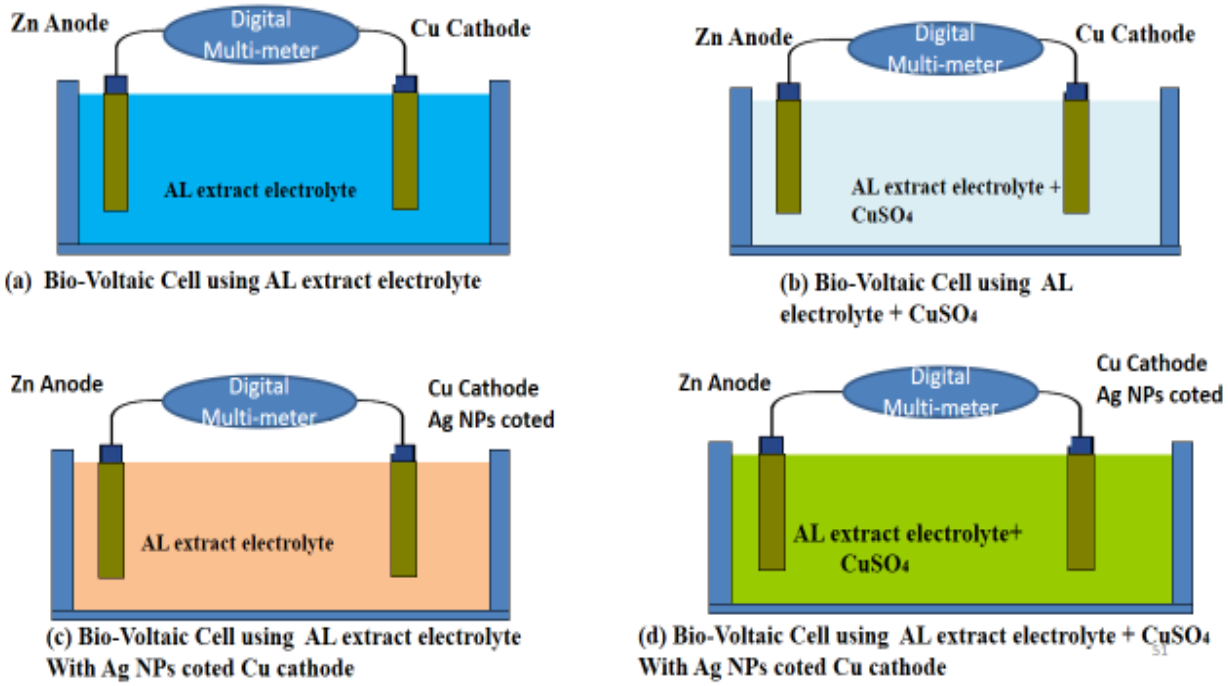

Fig. 2. Design of bio-voltaic cell with (a) AL extract bio-electrolyte, (b) (AL+ $CuSO_4$) bioelectrolyte, (c) (AL+ Ag NPs) bio-electrolyte and (d) (AL+$CuSO_4$ + Ag NPs) bio-electrolyte.

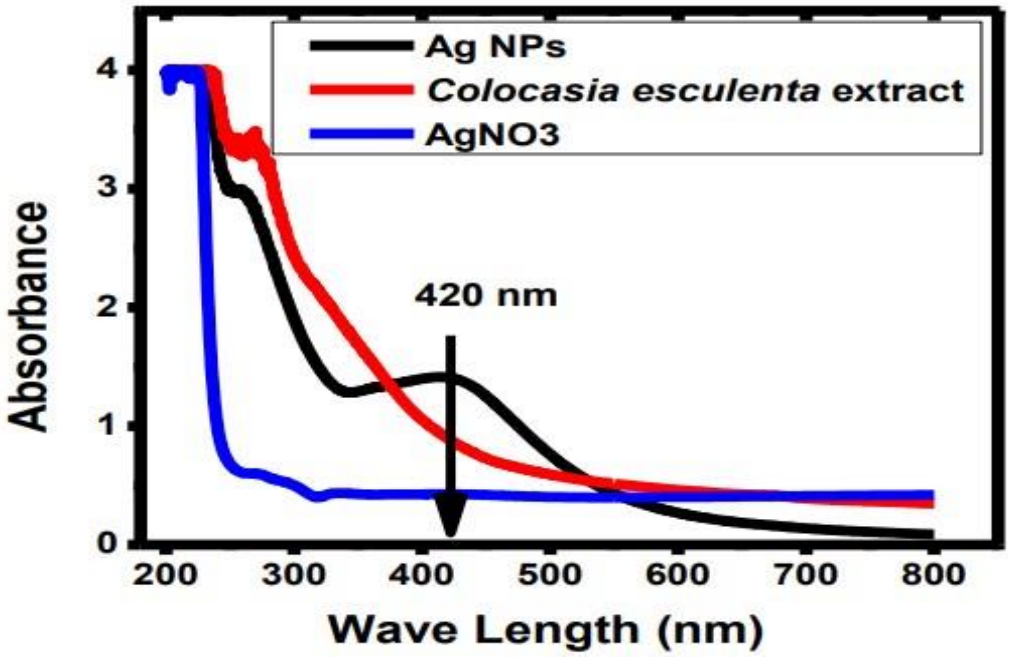

Fig.3. UV-vis spectra of AgNO3 solution (blue line), Colacasia esculenta Extract (red line), and Ag NPs (black line).

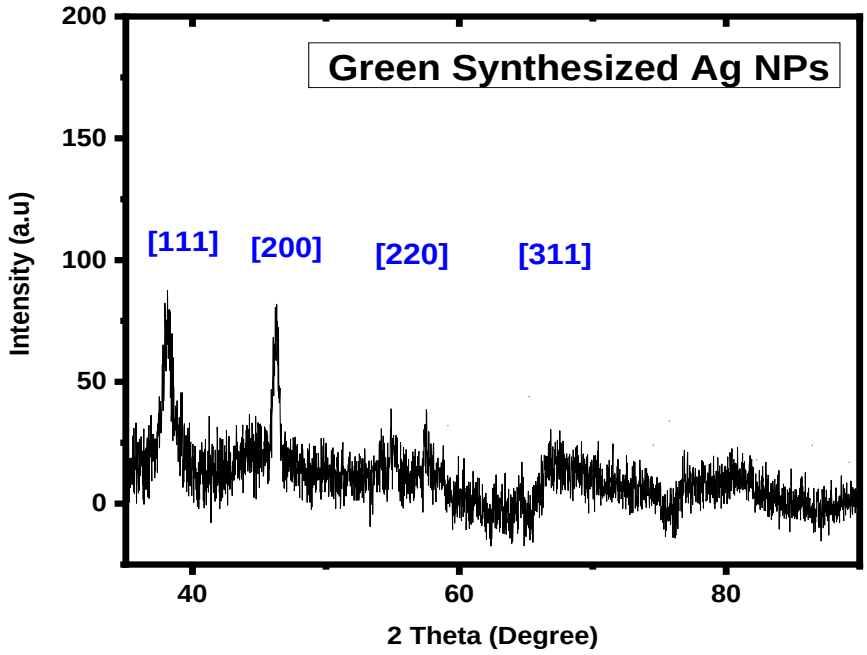

Fig.4. XRD pattern of green synthesized Ag nanoparticles from Aurum Leaf Extract.

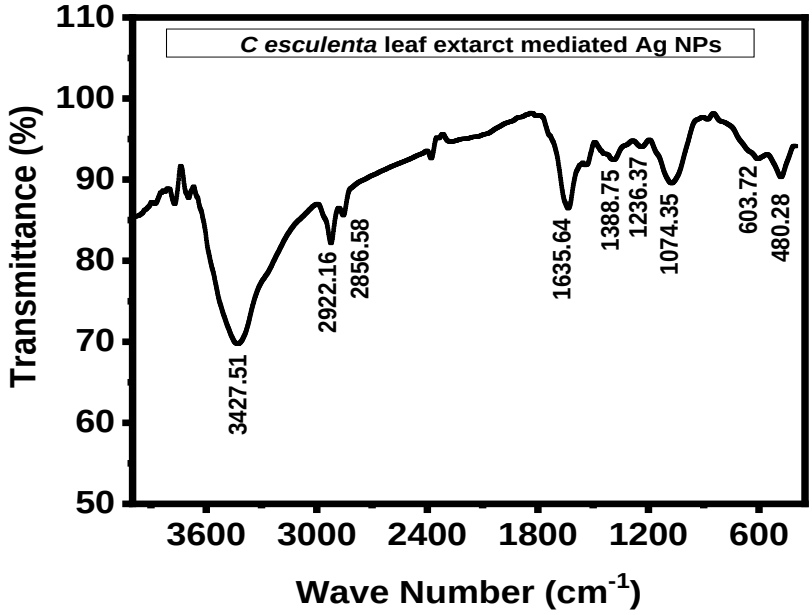

Fig.5. FT-IR spectra of Colacasia esculenta extract mediated Ag NPs.

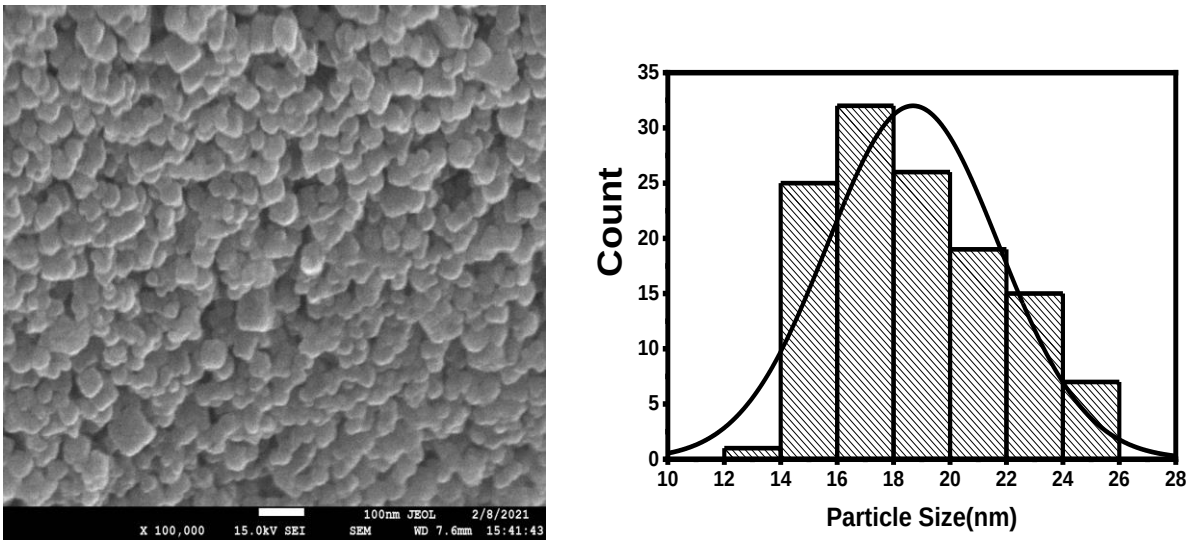

Fig.6. (a) FESEM image of green synthesized silver nanoparticles and (b) the particle size histogram of green synthesized silver nanoparticles.

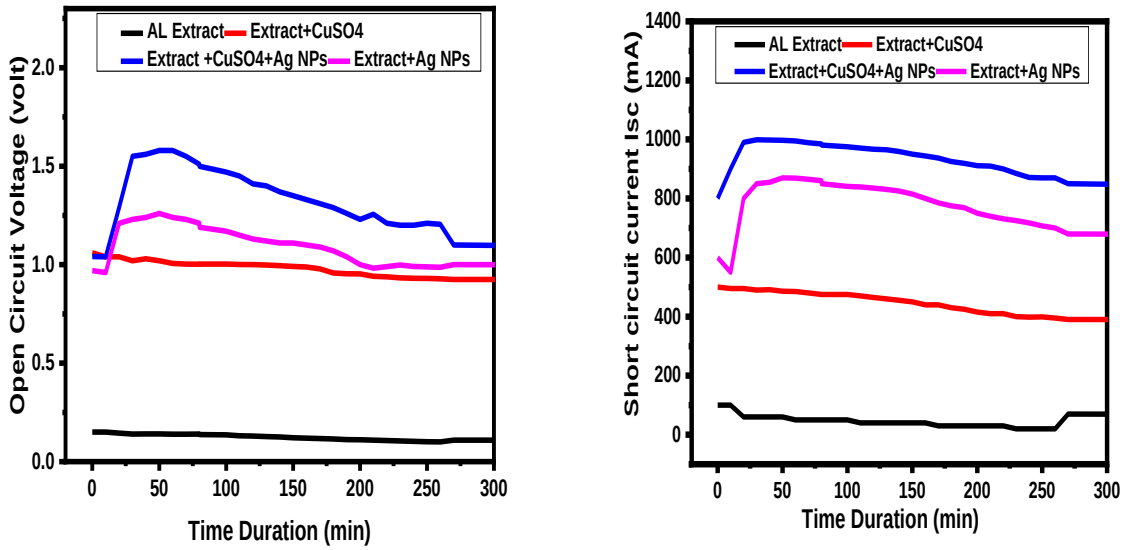

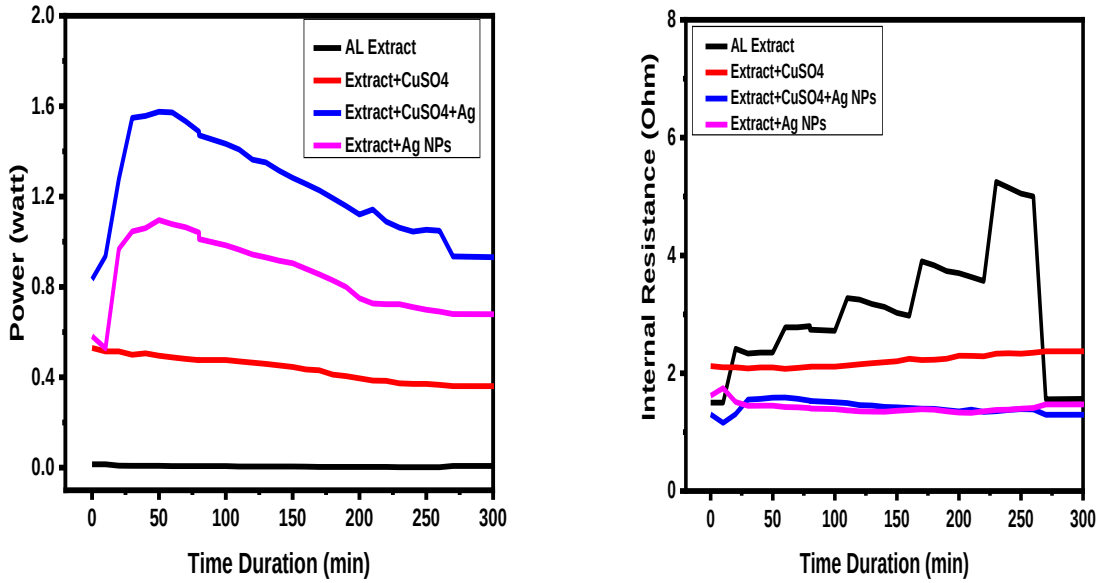

Fig.7. Comparative analysis of (a) open-circuit voltage, (b) short circuit current, (c) power, and (d) internal resistance of four bio-electrochemical cells.

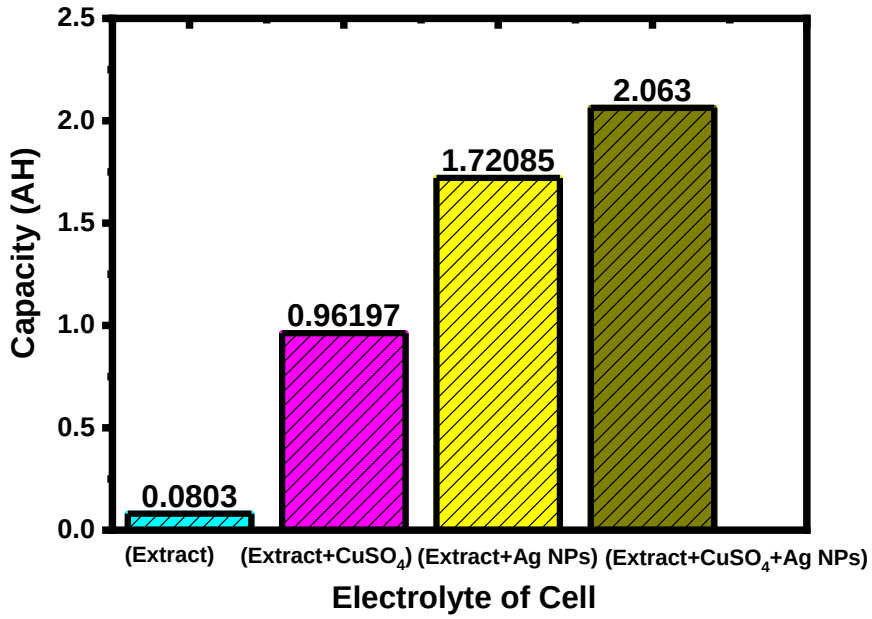

Fig.8. avarage capacity of four different electrolyte based bio-voltaic cells

Table1: The average power for different electrolyte-based bio-voltaic cells.

Electrolyte of cell	Average Power (watt)	Average Capacity (AH)
Extract	0.0024	0.0803
Extract + CuSO4	0.4379	0.9619
Extract + Ag NPs	0.6224	1.7208
Extract + CuSO4+ Ag NPs	0.7024	2.0630